Characterisation of novel mutations within heat shock protein 27 causing motor neuropathies

Amy Innes

University College London, Institute of Neurology

and

MRC Centre for Neuromuscular Diseases

PhD Supervisors:

Professor Linda Greensmith and Professor Henry Houlden

A Thesis submitted for the degree of

Doctor of Philosophy

University College London

2012

Declaration

I Amy Innes confirm that the work presented in this Thesis is my own. Where information has been derived from other sources, I confirm that this has been indicated in the Thesis.

Abstract

Charcot-Marie-Tooth disease (CMT) 2F and distal Hereditary Motor Neuropathy (dHMN) are peripheral motor axonopathies with limited sensory involvement, which usually present during the first decade of life. They are caused by mutations in heat shock protein 27 (Hsp27)/HSPB1, a highly conserved, ubiquitously expressed molecular chaperone. Hsp27 has several cytoprotective functions including the inhibition of apoptosis, protection against oxidative stress and promotion of axonal growth. In this Thesis, the effects of several pathogenic Hsp27 mutations were examined to elucidate their cellular effects *in vitro* and map these effects to different regions of the gene.

The effects of Hsp27 mutations were first investigated in neuronal-like SH-SY5Y cells *in vitro* Analysis of cell survival and cellular morphology revealed that all mutations were cytotoxic under basal conditions. However, mutations located in the α-crystallin protein domain of Hsp27 resulted in a significant increase in the vulnerability of cells to cytoskeletal stressors and decreased neurite outgrowth.

Using immunocytochemistry, interactions between mutant Hsp27 and cytoskeletal components were also examined. Mutations located in the Hsp27 α-crystallin domain increased co-localisation of Hsp27 with cytoskeletal elements. Although the mutation within the N-terminus did not have this effect it did result in the formation of distinct nuclear aggregates containing mutant Hsp27.

The functional effects of Hsp27 mutations were investigated using lentiviral delivery of mutant Hsp27 in primary motoneurons. Examination of mitochondrial function

showed that none of the Hsp27 mutants had any effect on mitochondrial membrane potential.

The results presented in this Thesis show that disease-causing Hsp27 mutations have differential effects upon protein function *in vitro* depending upon the gene position of the mutation. Therefore, although all Hsp27 mutations in CMT patients result in motoneuron degeneration, these results suggest that this process may be initiated by different pathological mechanisms and that normal Hsp27 function is essential for the maintenance of motor-axonal function.

Acknowledgments

Firstly I would like to thank my primary supervisor, Professor Linda Greensmith, who was always on hand when needed for support, guidance and spelling tutorials.

To my secondary supervisor, Professor Henry Houlden and my mentor Professor Mary Reilly who both offered me invaluable support.

I would especially like to thank Dr Virginie Bros for teaching me TMRM and for providing me with all my embryos for primary motoneuron cultures and Dr Bernadett Kalmar for her excellent teaching.

I would like to thank the MRC Centre for Neuromuscular Diseases for funding my PhD, and for the support and educational opportunities provided. Thank you to Professor Vincent Timmerman for the plasmids and to Dr Andrey Abramov and Vikki Burchell for all their help with my mitochondrial studies.

To all of my friends, especially to those of you in the Greensmith lab – Adrian, Alec, Alex, Anna, Bilal, Barney, Ching-Hua, Jim, Mhoriam, Philou, Virginie, thank you for making my time in the lab so much fun! Mhoriam, thanks for being such a good PhD and writing companion.

I couldn't have done any of this without the love and support of my family, especially Mum, Dad and KJ, thank you for everything.

Finally, this Thesis is dedicated to my Granny. Your decline and my memories of you before Alzheimer's drive me to make things better for the future. All my love x

Contents

List of Figures

List of Tables

Abbreviations

Δψm	Mitochondrial membrane potential
ALS	Amyotrophic Lateral Sclerosis
Arg	Arginine
ATP	Adenosine tri-phosphate
CMAP	Compound motor action potentials
CMT	Charcot Marie Tooth disease
CNS	Central nervous system
DAPI	4',6-diamidino-2-phenylindole
dHMN	distal Hereditary Motor Neuropathy
dHSN	distal Hereditary Sensory Neuropathy
Gly	Glycine
HSF-1	Heat shock factor 1
HSMN	Hereditary Sensory and Motor Neuropathy
HSP	Heat shock protein
HSPB1	Heat shock protein 27 gene
HSR	Heat shock response
Leu	Leucine
MAP2	Microtubule-associated protein 2
Met	Methionine
NCV	Nerve conduction velocity
NEFL	Neurofilament light chain gene
NF-200	Neurofilament-200 heavy chain
NF-L	Neurofilament light chain
PCR	Polymerase chain reaction
Phe	Phenylalanine
PMP22	Peripheral myelin protein 22
PNS	Peripheral nervous system
Pro	Proline
ROS	Reactive oxygen species
SC35	Regulator of pre-mRNA splicing
SEM	Standard error of the mean
Ser	Serine
SNAP	Sensory nerve action potential
SOD1	Cu, Zn superoxide dismutase 1

Chapter 1. General Introduction

In this Thesis, the deleterious effects of mutations in heat shock protein 27 (Hsp27), which cause Charcot-Marie-Tooth disease and distal Hereditary Motor Neuropathy, are investigated and the possibility that these pathogenic mutations, which are located in different regions of the *HSPB1* gene, have differential effects on cellular pathology is examined.

1.1. Peripheral neuropathies

Peripheral neuropathies can be sub-classified on the basis of the anatomical location of primary disease pathology. Thus, disorders can be classed as **i)** anterior horn cell diseases or neuronopathies, affecting the cell bodies in the central nervous system (CNS), for example, Amyotrophic Lateral Sclerosis (ALS) and spinal muscular atrophy (SMA) **ii)** peripheral neuropathies or axonopathies, which affect the ventral and dorsal nerve roots and peripheral nerves, **iii)** neuromuscular junction disorders that affect transmission from nerve to muscle, for example myasthenia gravis, or **iv)** myopathies, for example Duchene muscular dystrophy, primarily affecting skeletal muscle.

Peripheral neuropathies encompass a large number of diseases that are caused by damage to the nerves of the peripheral nervous system (PNS). Peripheral neuropathies can be arranged into four loose groupings based on the initial origin of the disease. Therefore, peripheral neuropathies can be inherited, diabetic, inflammatory or acquired. Although the causes of peripheral neuropathy vary across different demographics, the most common causes across the world are dependent

on socio-economic status. Thus, diabetes is the largest primary cause of peripheral neuropathy in the western world whilst leprosy is a more common cause in developing countries However, there is a wide variation in the aetiology of peripheral neuropathy (Martyn and Hughes, 1997). Diabetes predominantly presents as a distal symmetric sensory polyneuropathy, although the prognosis and time course of diabetic neuropathies differs widely (Martyn and Hughes, 1997). Inflammatory or autoimmune peripheral neuropathies include, for example, Guillain-Barré syndrome, Leprosy and chronic inflammatory demyelinating polyradiculoneuropathy (Martyn and Hughes, 1997; Lunn and Willison, 2009). Disorders of the PNS can also be acquired via physical damage or trauma to the peripheral nerves or spinal cord or exposure to toxins, including HIV treatments, solvents, heavy metals and alcohol misuse (Martyn and Hughes, 1997). Inherited neuropathies are a common group of disorders, affecting 1 in 2500 people (Reilly and Shy, 2009). Hereditary sensory and motor neuropathy (HSMN), more frequently referred to as Charcot Marie Tooth disease (CMT), has a heterogeneous presentation of clinical phenotype and genetic cause. Currently, there are approximately 50 known loci and over 40 genes with mutations associated with different forms of CMT (http://neuromuscular.wustl.edu/time/hmsn.html) (Pareyson and Marchesi, 2009). In CMT, the normally fine tuned communication between neurons and Schwann cells is perturbed by mutations in genes that play a role in the maintenance of peripheral axons.

1.2. Charcot-Marie-Tooth Disease (CMT)

CMT is defined by the presence of neuropathy as the sole or primary component of the disease (Reilly, 2007). It was first described as peroneal muscular atrophy in two papers by Charcot, Marie and Tooth in 1886 presenting as a childhood onset disorder with progressive weakness and muscle atrophy affecting feet and hands

first, followed by slow, chronic involvement of the forelimbs caused by denervation (Charcot and Marie, 1886; Tooth, 1886; Harding and Thomas, 1980).

Due to the diversity of the disease aetiology, CMT has been subdivided for ease of clinical identification and treatment. These subtypes are primarily grouped by clinical presentation and electrophysiology into demyelinating (CMT1), axonal (CMT2), intermediate (DI-CMT or CMT3), autosomal recessive (CMT4), distal Hereditary Motor Neuropathy (dHMN) and distal Hereditary Sensory Neuropathy (dHSN) (Barisic *et al*., 2008). The most common form of CMT is CMT1, formed of demyelinating neuropathies. CMT2 is the second most common group of hereditary peripheral neuropathies, and results from degeneration of the axon (Barisic *et al*., 2008). Due to the complexity and heterogeneity of CMT, a comprehensive review of all subtypes is beyond the scope of this Introduction. There are several excellent reviews on CMT (Barisic *et al*., 2008; Pareyson and Marchesi, 2009; Reilly and Shy, 2009) and a summary of the CMT subtypes is shown in Table 1.1 (CMT1), 1.2 (CMT2) and 1.3 (Other forms of CMT).

Although CMT is a highly heterogeneous disease with widely varying presentation, broadly, 'classical' CMT presents in the first or second decade of life with weakness and atrophy of distal muscles, and reduced sensation in the distal portions of the body, with proximal progression. Patients also show a distinctive foot deformity, abnormal gait and loss of tendon reflexes (Harding and Thomas, 1980).

1.2.1. Demyelinating CMT1

CMT1, a demyelinating disorder, is defined by severely reduced motor nerve conductance velocity (NCV, <38m/s) with a slow, uniform conductance, indicating a hereditary disorder. This is in contrast to acquired inflammatory neuropathies that

Table 1.1 Classification of CMT1 subtypes

Table describing the differences of CMT disease classification, including disease nomenclature, genetic cause, the function of the mutated protein and characteristic clinical features of the subtypes. Duplicated Peripheral myelin protein 22 (*PMP22*), Myelin Protein Zero (*MPZ*), Lipopolysaccharide-induced tumour necrosis factor-α factor (*LITAF*), small integral membrane protein of lysosome/ late endosome (*SIMPLE*), Early growth response protein 2 (*EGR2*), Neurofilament light (*NEFL*).

Table 1.1 Classification of demyelinating CMT1 subtypes.

CMT subtype	Genetic cause	Protein function	Specific characteristic clinical features	References
CMT1	Primary demyelinating disease; Autosomal dominant Slow nerve conduction velocities (NCV) < 38m/s Distal muscle weakness and atrophy, sensory loss, hyporeflexia, classical skeletal deformity Nerve biopsy pathology shows demyelination, onion bulb formation and secondary axonal degeneration			
CMT 1A	*PMP22* Point mutation *PMP22*	Integral membrane protein of myelin expressed by Schwann cells	'Classical' CMT1 Duplication is the most common form of CMT found in 70% of all CMT cases Point mutations give a more severe phenotype Point mutations can be dominant or recessive	(Matsunami *et al*., 1992)(Patel *et al*., 1992)(Timmerman *et al*., 1992)(Valentijn *et al*., 1992)(Szigeti *et al*., 2006)
CMT 1B	*MPZ*	Most abundant protein in myelin Adhesion molecule required for formation and maintenance of myelin	Dejerine-Sottas syndrome Congenital hypomyelinating neuropathy Can cause axonal neuropathy	(McMillan *et al*., 2010)(Su *et al*., 1993)
CMT 1C	*LITAF* *SIMPLE*	Nuclear transcription factor involved in tumor necrosis factor-α gene regulation Involved in lysosomal sorting and protein degradation	Classic CMT1	(Shirk *et al*., 2005) (Street *et al*., 2003)
CMT 1D	*EGR2*	Required for myelination of axons by Schwann cells	Also causes autosomal recessive CMT 4E	(Kamholz *et al*., 1999)(Warner *et al*., 1998)
CMT 1F and CMT 2E	*NEFL*	Light chain component of neurofilaments which are part of the cytoskeleton. Involved in axonal maintenance and axonal transport	Early onset, also causes CMT 2E	(Jordanova *et al*., 2003a)(Fabrizi *et al*., 2007)
Currently, approximately 10% of all CMT1 has no known genetic linkage				(Pareyson and Marchesi, 2009)

Table 1.2 Classification of CMT2 subtypes

Table describing the differences of CMT disease classification, including disease nomenclature, genetic cause, the function of the mutated protein and characteristic clinical features of the subtypes. Mitofusin-2 (*MFN2*), Kinesin family member 1B (*KIF1B*), RAS-associated protein Rab7 (*RAB7*), Transient receptor potential vanilloid 4 (*TRPV4*), Glycyl-tRNA synthetase (*GARS*), Neurofilament light (*NEFL*), Heat shock protein 27 (*HSPB1*), Ganglioside-induced differentiation-associated protein 1 (*GDAP1*), Lamin A/C (*LMNA*), Heat shock protein 22 (*HSPB8*), Dynamin 2 (*DNM2*), Alanyl-tRNA synthetase (*AARS*), Dynein, cytoplasmic 1, heavy chain 1 (*DYNC1H1*).

Table 1.2 Classification of axonal CMT2 subtypes.

CMT subtype	Genetic cause	Protein function	Specific characteristic clinical features	References
CMT2	Primary axonal disease; Autosomal dominant Normal or slightly reduced NCVs with decreased amplitudes Distal muscle weakness and atrophy, sensory loss, hyporeflexia, classical skeletal deformity Later age of onset than classical CMT 1 Nerve biopsy pathology shows chronic axonal changes without specific diagnostic features			
CMT 2A	*MFN2* *KIF1B*	A GTPase which regulates mitochondrial fusion Motor protein involved in axonal transport	Severe CMT2	(Kijima *et al*., 2005b)(Zhao *et al*., 2001)
CMT 2B and HSAN	*RAB7*	Multiple regulation mechanisms in endosomal sorting, biogenesis of lysosomes and phagocytosis	Predominantly sensory phenotype, very limited motor involvement	(Verhoeven *et al*., 2003)(Zhang *et al*., 2009)
CMT 2C	*TRPV4*	Nonselective cation channel responding to environmental stimuli	More pronounced motor phenotype, deafness, incontinence Skeletal dysplasia	(Landouré *et al*., 2010)
CMT 2D and HMN V	*GARS*	Add amino acid groups onto tRNA during translation, essential role in protein biogenesis	Predominantly motor phenotype with primary upper limb involvement	(Stum *et al*., 2011)(Del Bo *et al*., 2006)
CMT 2E and CMT 1F	*NEFL*	Light chain component of neurofilaments that are part of the cytoskeleton. Involved in axonal maintenance and axonal transport	Early onset	(Jordanova *et al*., 2003a)(Fabrizi *et al*., 2007)
CMT 2F and dHMN II	*HSPB1*	Small heat shock protein involved in protein folding, cytoskeletal maintenance and apoptosis	Predominantly motor phenotype dHMN II with no sensory involvement	(Evgrafov *et al*., 2004)(Houlden *et al*., 2008)
CMT 2K	*GDAP1* *LMNA*	Mitochondrial fission Nuclear envelope protein	Autosomal recessive Early-onset with diaphragm and vocal cord involvement Autosomal recessive	(Cassereau *et al*., 2009)(De Sandre-Giovannoli *et al*.,

			Rapid progression, also causes muscular dystrophy, cardiomyopathy	2002)
CMT 2L	*HSPB8*	Small heat shock protein involved in protein folding and apoptosis	Predominantly motor phenotype dHMN II with no sensory involvement	(Irobi *et al*., 2004)
CMT 2M	*DNM2*	Endosomal trafficking	DI-CMT 2B Centronuclear myopathy	(Pareyson *et al*., 2009)(Hanisch *et al*., 2011)(Züchner *et al*., 2005)
CMT 2N	*AARS*	Add amino acid groups onto tRNA during translation, essential role in protein biogenesis	Mild asymmetric CMT	(Latour *et al*., 2010)
CMT 2O and HMN	*DYNC1H1*	Core of dynein complex; Responsible for protein complex binding to and moving along microtubules	Childhood onset with some displaying delayed motor milestones	(Weedon *et al*., 2011)
Currently, approximately 70% of all CMT2 has no known genetic linkage				(Pareyson and Marchesi, 2009)

Table 1.3 Classification of other CMT subtypes

Table describing the differences of CMT disease classification, including disease nomenclature, genetic cause, the function of the mutated protein and characteristic clinical features of the subtypes. Ganglioside-induced differentiation-associated protein 1 (*GDAP1*), Myotubularin-related protein 2 (*MTMR2*), Myotubularin-related protein 13 (*MTMR13*), SH3 domain and tetratricopeptide repeats 2 (*KIAA1985, SH3TC2*), N-myc downstream-regulated gene-1 (*NDRG1*), Periaxin (*PRX*), Frabin (*FGD4*), FIG4 (*FIG4*), RNA polymerase II subunit A C-terminal domain phosphatase, FCP1 (*CTDP1*), Gap junction β-1 (*GJB1*)/ Connexin 32 (*Cx32*), Phosphoribosylpyrophosphate synthetase 1 (*PRPS1*), Dynamin 2 (*DNM2*), Tyrosyl-tRNA synthetase (*YARS*), Myelin Protein Zero (*MPZ*), Heat shock protein 27 (*HSPB1*), Heat shock protein 22 (*HSPB8*), Glycyl-tRNA synthetase (*GARS*), Berardinelli-Seip congenital lipodystrophy (*BSCL2*), Immunoglobulin μ-binding protein 2 (*IGHMBP2*), Dynein, cytoplasmic 1, heavy chain 1 (*DYNC1H1*), Serine palmitoyltransferase, long chain base subunit 1 (*SPTLC1*), WNK lysine deficient protein kinase 1 (*WNK1*), Inhibitor of kappa light polypeptide gene enhancer in B-cells (*IKBKAP*), Nerve growth factor, β-polypeptide (*NGFβ*), Chaperonin containing TCP1, subunit 5 (*CCT5*)

Table 1.3 Classification of other CMT subtypes.

CMT subtype	Genetic cause	Protein function	Specific characteristic clinical features	References
CMT4	Autosomal recessive, primarily demyelinating CMT 1 with fewer cases of axonal CMT 2 Early-onset CMT1 phenotype More severe distal muscle weakness and atrophy, sensory loss, hyporeflexia, classical skeletal deformity			
CMT 4A	*GDAP1*	Mitochondrial fission	Vocal cord and diaphragm involvement	(Cuesta *et al*., 2002)(Casserea u *et al*., 2009)
CMT 4B1	*MTMR2*	Phosphatase that acts on lipids	Abnormal folding of myelin sheaths Facial and bulbar involvement	(Bolino *et al*., 2000)(Kim *et al*., 2003)
CMT 4B2	*MTMR13*	Phosphotase interacting with MTMR2	Abnormal folding of myelin sheaths	(Conforti *et al*., 2004)
CMT 4C	*KIAA1985, SH3TC2*	Unknown protein function Expressed in Schwann cells May interact with Rab11 affecting endosomal recycling and myelin formation	Severe, early-onset scoliosis	(Senderek *et al*., 2003)(Roberts *et al*., 2010)(Stendel *et al*., 2010)
CMT 4D (HMSN-Lom)	*NDRG1*	Cytoplasmic protein involved in stress responses, hormone responses, cell growth, and differentiation. Necessary for p53-mediated caspase activation and apoptosis	Deafness	(Kalaydjieva *et al*., 1996)(Kalaydjiev a *et al*., 1998)
CMT 4F	*PRX*	Myelin sheath development	Dejerine-Sottas syndrome More sensory involvement	(Scherer *et al*., 1995)(Marchesi *et al*., 2010)
CMT 4H	*FGD4*	GDP/GTP exchange factor for the Rho	Classic CMT1	(Stendel *et al*.,

		GTPase cell-division cycle 42 F-actin-filament binding protein		2007)(Fabrizi *et al*., 2009)
CMT 4J	*FIG4*	Phosphatase that acts on lipids Role in regulation of endosomal vesicles	Classic CMT1	(Chow *et al*., 2007)
CCFDN	*CTDP1*	Regulation of transcription initiation via RNA polymerase II	Congenital cataracts, facial dysmorphism, and neuropathy	(Varon *et al*., 2003)
CMT Other	(X-linked and intermediate)			
CMT X1	*GJB1*, *Cx32*	Gap junction structural proteins	Dominant X-linked mutation Men more severely affected 7-12% of all CMT CNS involvement Axonal and demyelinating pathology	(Ionasescu *et al*., 1994)(Pareyson *et al*., 2009)
CMT X5	*PRPS1*	Essential for the *de novo* synthesis of purine, pyrimidine, and pyridine nucleotides	Recessive X-linked mutation Also causes Arts syndrome, and X-linked nonsyndromic sensorineural Deafness	(Pareyson *et al*., 2009)(de Brouwer *et al*., 2007)(de Brouwer *et al*., 2010)
DI-CMTB	*DNM2*	Large GTPase, part of the cellular fusion-fission apparatus	Dominant intermediate (DI) CMT; mild to moderate severity and pathological features of both CMT1 and CMT2 Also causes centronuclear myopathy	(Pareyson *et al*., 2009)(Hanisch *et al*., 2011)(Züchner *et al*., 2005)
DI-CMTC	*YARS*	Add amino acid groups onto tRNA during translation, essential role in protein biogenesis	DI-CMT	(Jordanova *et al*., 2006)
DI-CMTD	*MPZ*	Most abundant protein in myelin Adhesion molecule required for formation and	DI-CMT	(Banchs *et al*., 2010)

		maintenance of myelin		
HNPP	*PMP22*	Integral membrane protein of myelin expressed by Schwann cells	Deleted - Hereditary neuropathy with liability to pressure palsies Point mutation - Autosomal dominant	(Chance *et al*., 1993)(Nicholson *et al*., 1994)
distal Hereditary Motor Neuropathy				
dHMN II	*HSPB1* *HSPB8*	Small heat shock proteins involved in protein folding, cytoskeletal maintenance and apoptosis	Typical distal Hereditary Motor Neuropathy and CMT2	(Evgrafov *et al*., 2004)(Irobi *et al*., 2004)
HMN V (HMN5A)	*GARS*	Add amino acid groups onto tRNA during translation, essential role in protein biogenesis	dHMN phenotype with primary upper limb involvement	(Stum *et al*., 2011)(Del Bo *et al*., 2006)
HMN V (HMN5B)	*BSCL2*	Seipin is an integral membrane protein of the endoplasmic reticulum	dHMN phenotype with primary upper limb involvement and Silver syndrome	(Windpassinger *et al*., 2004)
HMN VI	*IGHMBP2*	Involved in pre-mRNA processing and regulation of transcription by DNA binding	Autosomal recessive Spinal muscular atrophy with respiratory distress (SMARD1)	(Grohmann *et al*., 2001)(Pitt *et al*., 2003)
HMN and CMT 2O	*DYNC1H1*	Core of dynein complex; Responsible for protein complex binding to and moving along microtubules	Childhood onset with some displaying delayed motor milestones	(Weedon *et al*., 2011)
distal Hereditary Sensory Neuropathy				
HSAN I	*SPTLC1*	Catalyzes the first step of biosynthesis of sphingolipids	Autosomal dominant Loss of pain and temperature sensation	(Bejaoui *et al*., 2001)(Dawkins *et al*., 2001)
HSAN II	*WNK1*	Serine/threonine protein kinase, aids in the regulation of salt transport and blood pressure	Autosomal recessive Childhood onset, Prominent sensory loss and mutilations in hands and feet, acropathy	(Lafreniere *et al*., 2004)
HSAN III	*IKBKAP*	Scaffold protein, assembles active kinase	Autosomal recessive	(Slaugenhaupt

(Riley-Day syndrome)		complexes	Congenital, Familial dysautonomia, prominent autonomic disturbances and complications, absence of fungiform papillae of the tongue, alacrimia, excessive sweating	*et al*., 2001)
HSAN IV	*NTRK*	Binds neurotrophins and phosphorylates member of the MAPK pathway. Cell differentiation	Autosomal recessive No or reduced response to painful stimuli, anhidrosis, episodic fever, mild mental retardation, skin and cornea lesions, joint deformities	(Indo *et al*., 1996)
HSAN V	*NGFβ*	Development of the nervous system	Autosomal recessive Congenital insensitivity to pain, severe loss of deep pain perception, painless fractures, joint deformities, normal intelligence	(Einarsdottir *et al*., 2004)
HSAN with spastic paraplegia	*CCT5*	Member of chaperonin complex TRiC, folds polypeptides through 2 stacked rings in an ATP-dependent manner	Autosomal recessive Prominent sensory neuropathy with sensory loss of all qualities, mutilating acropathy, spastic paraplegia	(Bouhouche *et al*., 2006)

show multifocal slowing of nerve conduction and conduction block (Lewis and Sumner, 1982). NCV is an indication of myelin disruption while the degree of axonal damage and nerve fibre loss can be measured using compound motor action potentials (CMAPs) and sensory nerve action potentials (SNAPs) (Pareyson *et al*., 2006). Classically, CMT1 patients also have reduced or absent sensory action potentials (Reilly, 2007). The severity of the balance deficit present in CMT1 correlates with a decrease in CMAPs and SNAPs rather than NCV (Barisic *et al*., 2008). This suggests that even though demyelination maybe the primary pathology of the neuropathy, the severity of the disease is directly linked to the degeneration of the nerve axon. Nerve biopsies show classical signs of demyelination, which include a reduced density in myelinated nerve fibres, variations in intermodal length and diameter, onion bulb formation (resulting from continuous segmental demyelination and remyelination) and tomacula formation (small focal myelin thickenings) with secondary axonal atrophy (Gabreëls-Festen *et al*., 1992).

Although CMT1 patients usually present with the classical phenotype described above, there are clinical variations and intermediate presentations between categories, as listed in Tables 1.1 and 1.3. These have been further sub-classified into groups that may correspond to known genetic mutations. Genetically, CMT1 is the most well characterised hereditary neuropathy and the most common type of CMT has been sub-classified as CMT 1A, which accounts for approximately 70% of all CMT1 and around 50% of all CMT cases (Pareyson and Marchesi, 2009). It is caused by duplications or point mutations in the peripheral myelin protein 22 (*PMP22*) gene (Table 1.1), the most abundant protein in the peripheral myelin sheath (Keller and Chance, 1999).

1.2.2. Axonal CMT2

Approximately 20% of all CMT can be classified as the axonal form of CMT, or CMT2 (Barisic *et al*., 2008) and to date only 25-35% of identified CMT2 have been genetically classified (Patzkó and Shy, 2011). These different genetic causes form the basis of further sub-classification of CMT2 (See Table 1.2). Electrophysiologically, CMT2 is characterised by reduced CMAPs and SNAPs but nearly normal MCV showing axonal degeneration, but limited disruption of the myelin sheath (Reilly, 2007; Reilly and Shy, 2009). Nerve biopsies of CMT2 also show markedly different degenerative patterns to those of CMT1 with a loss of large myelinated fibres, axonal atrophy, axonal swellings, regenerative axonal sprouting shown by closely adjacent fibres and occasional onion bulb formation (Berciano *et al*., 1986; Senderek *et al*., 1998; Gemignani and Marbini, 2001; Schröder, 2006). Together, electrophysiology and pathology indicate an axonal degeneration disorder rather than a myelinopathy. Pronounced differences between the two main subtypes of CMT can also be observed in the muscle. CMT1 muscle examples exhibit angular, atrophic fibres scattered throughout biopsies while CMT2 muscle shows hypertrophic muscle fibres, central nuclei, fibre splitting, and other signs of degeneration and regeneration suggesting different aetiologies of nerve dysfunction (Ericson *et al*., 1998; Borg and Ericson-Gripenstedt, 2002). Due to the lack of knowledge of the genetic causes and pathophysiology of axonal neuropathies, the pathological findings from nerve biopsies are relatively unhelpful for both clinical diagnosis and elucidating the pathophysiology as all these features are indicators of general degenerative characteristics and are all common in the latter stages of axonal disease (Gemignani and Marbini, 2001).

1.2.3. Intermediate and X-linked CMT

In total, over 30 genetic causes of CMT have been described to date (Reilly and Shy, 2009). The majority of these are the autosomal dominant causes of CMT 1 and 2, but CMT is a highly heterogeneous disorder and there are many forms of CMT that segregate between the demyelinating and axonal clinical and pathological features without a classical CMT phenotype; these are classified as Intermediate CMT or DI-CMT (See Table 1.3). A full discussion of these less common types of CMT is outside the scope of this study but they are briefly outlined in Table 1.3. For reviews see (Bernard *et al*., 2006; Nicholson and Myers, 2006; Kleopa and Scherer, 2006). These forms of CMT include those with genetic causes other than autosomal dominant, including sporadic dominant mutations where no family history can be recorded, X-linked mutations, of which 2 has been identified and 3 have been mapped to chromosomal regions and autosomal recessive mutations (CMT4, Table 1.1C)(Bernard *et al*., 2006; Kleopa and Scherer, 2006; Pareyson and Marchesi, 2009). Autosomal recessive mutations are found in less than 10% of European and North American populations, but cause between 30-50% of cases in the Mediterranean Basin and Middle East (Patzkó and Shy, 2011).

1.2.4. Penetrance differences and overlapping phenotypes in CMT

Mutations in over 30 genes have now been shown to be causative of CMT (Reilly and Shy, 2009). CMT patients display varying degrees of penetrance of the disease, to give a spectrum of clinical severity within genetic subtypes. For example mutations in PMP22, causing CMT1A, can display varying levels of severity from patients being almost asymptomatic to having delayed motor milestones and severe skeletal deformities (Birouk *et al*., 1997; Thomas *et al*., 1997). The same genetic mutations within PMP22 in monozygotic twins can also give different levels of disease severity (Garcia *et al*., 1995), perhaps illustrating the importance of gene

penetrance, epigenetic factors and environmental modulation on the course and severity of the disease. To this end, mutations in the same gene can also cause different clinical subtypes of CMT, for example, mutations in neurofilament light chain (*NEFL*) can cause both demyelinating CMT 1F and axonal CMT 2E, while Ganglioside-induced differentiation-associated protein 1 (*GDAP1*) causes early onset CMT 4A and axonal CMT 2K (Jordanova *et al*., 2003; Fabrizi *et al*., 2007; Cassereau *et al*., 2009).

1.3. Why does CMT affect the peripheral nervous system?

Despite the heterogeneity of CMT, it remains a PNS disorder, with few CNS exceptions (Amato and Barohn, 1996; Bähr *et al*., 1999; Wakerley *et al*., 2011). This is unusual as many of the genes affected in CMT code for proteins that are essential to neurons and glial cells and are ubiquitously expressed throughout the nervous system or indeed the whole organism. When the different CMT subtypes are examined for a link between the mutation types and pathomechanisms, affected genes can be divided into 5 groups affecting: **i)** Myelination; **ii)** protein homeostasis; **iii)** the cytoskeleton and axonal transport; **iv)** mitochondrial function and **v)** gene regulation (See Figure 1.1), which may all contribute to increased vulnerability of motoneurons.

The first and most common group of CMT genes affect different aspects of **myelination**, causing subtypes of CMT1 and CMT4 (Table 1.1 and 1.3). This group includes mutations in components of myelin, for example PMP22 and myelin protein zero, and genes coding for proteins involved in regulation of myelin protein transcription, synthesis and transport, including early growth response protein 2 and myotubularin-related lipid phosphatase (Berger *et al*., 2006). Demyelinating

Figure 1.1

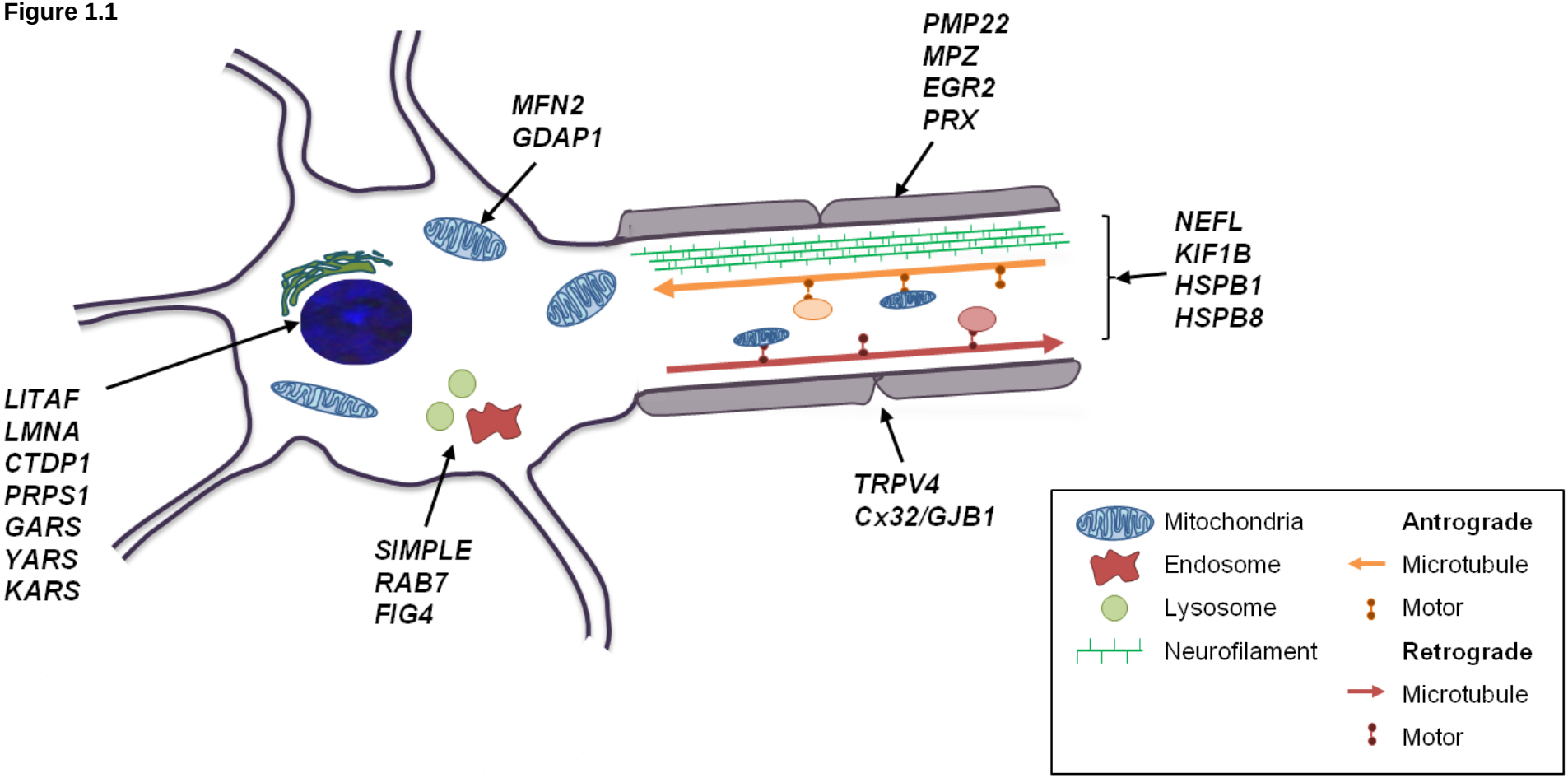

Figure 1.1 Schematic overview highlighting CMT mutations in motoneurons.

This schematic diagram highlights the subcellular localisation of proteins mutated in CMT, dHMN and HSN.

neuropathies cause a slowing of conduction velocities, but the chronic disease progression, including muscle weakness and wasting seen in CMT1, correlates with pathological hallmarks of neuronal degeneration (Hattori *et al*., 2003).

The second group of genes code for proteins involved in metabolic functions linked to **protein synthesis and maintenance** such as mutations in *YARS, GARS, AARS* and *KARS* encoding aminoacyl-tRNA synthases (ARS), which have been associated with axonal CMT (Antonellis *et al*., 2003; Jordanova *et al*., 2006; Latour *et al*., 2010; McLaughlin *et al*., 2010). The ARS enzymes charge transfer RNA (tRNA) with cognate amino acids in an ATP-dependent manner before the tRNA is used for protein synthesis at the ribosome (Motley *et al*., 2010). ARSs are ubiquitously expressed and essential for protein synthesis, and yet they are implicated in peripheral neuropathy, seemingly affecting only a subtype of neurons. Other CMT mutations that affect cell metabolism are FIG4 and SIMPLE, a phosphatase and a membrane protein respectively, which have roles in the trafficking and regulation of endosomal vesicles and lysosomes for protein degradation (Street *et al*., 2003; Chow *et al*., 2007).

Several mutations causing CMT affect proteins involved in the **structure of the cell and axonal transport**. For example, mutations in neurofilament light chain protein (*NEFL*), a major structural component of neurofilaments essential to all neurons predominantly cause CMT 2L, an axonal form of CMT affecting peripheral sensory and motor nerves with varying age of onset (Jordanova *et al*., 2003). Mutations in this gene can also cause CMT 1F, an early-onset demyelinating peripheral neuropathy (Fabrizi *et al*., 2007). Mutations in kinesin family member 1B, a motor protein involved in axonal transport along microtubules cause CMT 2A, result in a severe form of axonal CMT (Zhao *et al*., 2001). This group also includes mutations in Hsp27 as it interacts with various pathways controlling cell integrity and axonal

transport and for example, Hsp27 acts as an actin-capping protein during cell stress (Mounier and Arrigo, 2002).

The fourth group of genes in which mutations cause various forms of CMT are integral to the function of **mitochondria**. Mitochondrial mutations give rise to both axonal and demyelinating phenotypes, with some proximal muscle involvement (Table 1.2 and 1.3). Mitofusin-2 works as a transmembrane GTPase, regulating mitochondrial fusion (Chen *et al*., 2003; Kijima *et al*., 2005b) and ganglioside-induced differentiation-associated protein 1 promotes mitochondrial fission (Cassereau *et al*., 2009). Mitochondrial fission and fusion work to maintain mitochondrial integrity and turnover, and are the basis of mitochondrial dynamics. A lack of fusion leads to fragmentation, while a lack of fission the mitochondrial population becomes excessively large and interconnects (Chen and Chan, 2009). Both of these states lead to a lack of effective mitochondrial transport in the periphery (Chen and Chan, 2009). Fusion and fisson are vital for the maintenance of mitochondrial morphology, which in turn affects mitochondrial membrane potential, respiration, cell growth and functions of the apoptotic pathway (Chen, 2005).

The final group of effected genes in CMT discovered so far affect different aspects of **gene regulation** and mRNA sysnthesis, a highly complex and tightly regulated system. Mutations in this group of genes cause a more severe and wider phenotypic variation that affects regions of the CNS as well as causing severe peripheral neuropathies. These mutations affect different areas of the gene regulation pathway, from phosphoribosylpyrophosphate synthase 1, an enzyme essential for the *de novo* synthesis of nucleotides and therefore essential for nucleic acid synthesis and cellular signalling, to RNA polymerase II subunit A C-terminal domain, which works as a second messenger, regulating transcription initiation via RNA

polymerase II and the recruitment of pre-mRNA splicing factors during transcription (Licciardo *et al*., 2003; Varon *et al*., 2003; de Brouwer *et al*., 2010).

Although it is easy to understand why mutations in neuron-specific proteins will result in a neuronal phenotype, for example, mutations in proteins involved in axonal transport, it is not clear why these mutations may affect specific subpopulations of neurons, e.g. motor rather than sensory. Furthermore, many CMT-causing mutations are in ubiquitously expressed proteins, so the reasons for their deleterious effects in neurons alone are less easy to understand. However, when the proteins are considered in terms of their biological role, it becomes clear that they play key roles in pathways which are particularly important for neurons. Thus, CMT-causing mutations can be found in proteins that are important for myelin maintenance, fast metabolism, high protein turnover and axonal transport. So what are the specific characterisations of neurons and their axons that make them more vulnerable to these genetic mutations? It is possible that the specific requirements of motor and sensory neurons based on their unique anatomy that has evolved and adapted to carry out functions that require high metabolic demands, rapid protein synthesis and degradation, a complex structure and increased axonal transport may render neurons particularly vulnerable to CMT mutations (Shaw and Eggett, 2000).

1.4. Anatomy of the peripheral nervous system

The PNS is a complex network of highly specialised neurons and supporting cells. The PNS transmits sensory and motor information from the CNS higher centres in the brain and spinal cord to the muscle and back. Information is sent and received via ascending and descending tracts that run between centres in the brain and the peripheral nerves along the spinal cord.

1.4.1. Sensory nerves

Sensory impulses are sent to the brain via afferent pathways leading from peripheral sensory neurons that detect all sensation including, but not limited to, mechanosensation, nocioception and proprioception. The sensory neurons in the PNS are also termed 'primary afferents'. The cell soma for these neurons lies outside of the CNS in the dorsal root ganglion. They have one axon projecting peripherally, and axons that project to regions of the dorsal horn of the spinal cord (Snell, 2009). There they either ascend the spinal cord via several tracts, or they synapse onto second-order sensory neurons in the dorsal horn, eventually travelling to the somatosensory cortices within the brain. There are 4 main subgroups of primary afferent sensory neurons in the PNS (Bear *et al*., 2007):

- Aα neurons have an axonal diameter of 13-20μm and a conduction velocity of 80-120m/sec. They act as proprioceptors of skeletal muscle and are heavily myelinated. Aα neurons are essential for the stretch reflex; by associating with muscle spindles in the periphery and synapsing on intermediate and alpha motoneurons they are responsible for the myotatic reflex, which is a measure of the stretch and position of the muscle. By synapsing on alpha motoneurons in the spinal cord and directly illiciting a motor response and the generation of force, the Aα sensory neuron forms a reflex arc which is independent of the brain.
- Aβ neurons are responsible for mechanoreception (touch) from the skin. They are myelinated neurons with an axonal diameter of 6-12μm and a conduction velocity of 35-75m/sec.
- Aδ neurons have an axonal diameter of 1-5μm and a conduction velocity of 5-30m/sec. They are thinly myelinated and respond to low-threshold nocioception and cold temperatures.

- C fibres are unmyelinated neurons with an axonal diameter of between 0.2-1.5μm and a conduction velocity of 0.5-2m/sec. C fibres respond to heat over 43°C and high-threshold nocioception.

1.4.2. Motor nerves

The motor system, consisting of muscles and their innervating motoneurons is extremely complex and only a brief overview will be presented here, focusing on the lower motoneurons that innervate skeletal muscle. The main control of the motor system and lower motoneurons commences in the neocortex where the corticospinal tract, the largest CNS tract originates. Information processed in the motor and somatosensory cortices are transported along axons of upper motoneurons through the internal capsule across the telencephalon and thalamus, through the midbrain and pons before forming the pyramidal tract at the base of the medulla. At the spinal cord level, this information decussates and terminates in the dorsolateral region of the ventral horn of the spinal cord. Here, upper motoneurons synapse onto lower motoneurons where, after summation of multiple inputs from upper motoneurons with interneurons, action potentials are generated. Action potentials generated in lower motoneurons travel out of the spinal cord via spinal nerve roots down motor axons to the muscle (Bear *et al*., 2007; Snell, 2009).

Each muscle fibre is innervated by an individual axon branch derived from a lower motoneuron forming the 'Motor Unit'. One motoneuron can innervate up to 1700 muscle fibres in man (Feinstein *et al*., 1955; Beardwell, 1967). There are three types of lower motoneuron:

- Alpha motoneurons are the largest subtype of lower motoneuron and they innervate both slow and fast extrafusal muscle fibres.

- Beta motoneurons, the smallest sub-population of motoneurons mostly innervates slow-twitch muscle.
- Gamma motoneurons innervate intrafusal muscle fibres within the muscle spindle.

Motoneurons, like sensory neurons, are anatomically suited for purpose. They are large cells with long axonal processes, sometimes over a metre in length (Beardwell, 1967), and with axonal diameters that range from 2μm to more than 20μm (Henneman *et al*., 1965). This size difference in axonal diameter is the determinant of how many motor fibres the motoneuron innervates, i.e. Motor Unit size (Wuerker *et al*., 1965; McPhedran *et al*., 1965).

1.5. Why are some neuron populations differentially vulnerable to environmental stressors and disease?

Neuronal populations differ substantially in anatomy and function. This means that different neuronal populations can be more or less reliant on certain cellular processes to maintain homeostasis, altering the vulnerability of subpopulations of neurons to different cellular stresses. The Fig4-deficient pale tremor mouse (plt), a model of CMT 4J (Table 1.3) is an example of one genetic mutation differentially affecting different types of neurons. CMT 4J is a demyelinating peripheral neuropathy that gives both a motor and sensory phenotype (Chow *et al*., 2007). Katona *et al*. demonstrate, using ultrastructural techniques in young plt mice, that a deficiency in Fig4 gave distinct pathogenic processes in motor and sensory neurons creating different cellular deficits early in the disease progression (Katona *et al*., 2011). Below, I will discuss specific examples of cellular processes which are particularly vulnerable to stress in neurons, with an emphasis on the specific properties of motoneurons that may be influential in leading to specific cellular

responses to disease-causing mutations: **i)** mitochondrial function; **ii)** the cytoskeleton and axonal transport; **iii)** the stress response.

1.5.1. Motoneurons and mitochondria

Motoneurons are highly polarised, excitable cells that have the ability to send transient electrical signals rapidly over long distances or in localised areas of the membrane. In order to be available to transmit an action potential at any time, the motoneuron has a relatively low threshold for initiation of action potentials and therefore must actively maintain a membrane resting potential of -70mV, as small changes of membrane voltage can trigger an all-or-none action potential (Kandel *et al*., 2000). The active maintenance of the membrane potential requires a high level of energy. It is estimated that 10% of resting energy in a human is expended on maintenance of the ionic concentration gradients in resting neurons (Laughlin *et al*., 1998). Thus, in cells such as motoneurons which have a particularly high membrane surface area to volume ratio and where the axon of the cell can contain >99% of the cell cytoplasm, this estimate of the energy requirements of motoneurons is likely to be conservative (Hurd and Saxton, 1996).

As neurons are cells that require a very high level of energy just to actively maintain a resting state, they contain very large numbers of mitochondria. Mitochondria are very sensitive to changes in the cellular environment and changes in mitochondrial function are one of the first signs of motoneuron pathology in Cu, Zn superoxide dismutase 1 (SOD1) mice that model ALS (Bilsland *et al*., 2008). Mutations reported in mitochondrial proteins, either from mitochondrial or nuclear DNA always lead to disorders that have neuropathic and/or muscular involvement (Chinnery, 2000; Finsterer, 2004). These disorders range in severity and phenotype. For example, mutations in OPA1, a GTPase inner membrane protein, and mitofusin 2, a GTPase

transmembrane protein localised on the outer membrane, are both proteins involved in the process of mitochondrial fusion, but cause dominant optic atrophy and CMT 2A respectively (Chen and Chan, 2006), disorders which affect completely different subpopulations of neurons.

Work by Vande Velde *et al*. (2011) shows that there is an alteration in mitochondrial shape before disease onset in SOD1 mice, with the presence of mutant SOD1 resulting in smaller and rounder mitochondria and a shortening of mitochondrial length in comparison to mitochondria in wild type mice. This finding suggests aberrant functioning of mitochondrial fusion or fission in motoneurons of SOD1 mice (Vande Velde *et al*., 2011). The mitochondrial pathways of fission and fusion are vital for the maintenance of mitochondrial morphology, which in turn affects mitochondrial membrane potential, respiration, cell growth as well as the apoptotic pathway. Motoneurons are particularly vulnerable to deficits in these pathways and several of the CMT-causing mutations involve proteins that play key roles in several of these pathways (See Section 1.3) (Chen *et al*., 2003; Chen, 2005; Kijima *et al*., 2005; Cassereau *et al*., 2009). The control of mitochondrial autophagy, or mitophagy, also ensures maintenance of the mitochondrial membrane potential and ATP production by maintaining a high turnover of mitochondria to produce a consistently high quality of mitochondria (Chen and Chan, 2009; Twig and Shirihai, 2011).

Ultrastructural studies on neurons reveal that there is a high concentration of mitochondria in nerve synapses, around nodes of Ranvier and in the cell soma (Palay, 1958; Fabricius *et al*., 1993; Li *et al*., 2004), suggesting that the position of mitochondria and their transport is likely to be particularly important for neurons. The importance of mitochondrial distribution throughout motoneurons is highlighted in

the mutant SOD1 mouse model of ALS, in which there is a disruption in the normal distribution of mitochondria throughout the motor axon prior to onset of disease phenotype (Vande Velde *et al*., 2011) The importance of axonal trafficking of mitochondria in motoneurons is discussed below in detail in Section *1.5.4.2.*

1.5.2. Motoneurons, reactive oxygen species and calcium vulnerability

Studies have demonstrated that motoneurons are selectively more vulnerable to mitochondrial dysregulation in comparison to other types of neuron (Kaal *et al*., 2000). Mitochondria function to provide energy in the form of ATP for the cell, but they also regulate apoptosis and buffer intracellular calcium (Chance, 1965; Chan *et al*., 2009; Russell H., 2011). Mitochondria are also a source of reactive oxygen species (ROS) and produce it as a by-product of oxidative phosphorylation, where unpaired electrons from the electron transport chain are donated directly to molecular oxygen to generate superoxide (Cozzolino and Carri, 2011). The high energy demands of motoneurons means that cells contain higher amounts of mitochondria and therefore will be exposed to increased levels of intracellular oxidative stress over time. This becomes a problem when the cellular antioxidant defences, which include enzymatic defences such as Cu, Zn-superoxide dismutase and smaller molecules such as glutathione, are insufficient to hold levels of ROS below a toxic threshold (Schulz *et al*., 2000; Lewinski and Keller, 2005). This suggests that motoneurons are more susceptible than other cells to a build up of ROS leading to oxidative stress over time.

The high number of mitochondria also lead to an increased vulnerability of motoneurons to changes in intracellular calcium homeostasis (Lewinski and Keller, 2005). When different subtypes of motoneurons were compared for vulnerability to hypoxic states, by the addition of sodium cyanide as a pharmacological inhibitor of

complex IV of the mitochondrial respiratory chain, differences in mitochondrial release and uptake of calcium were observed (Lewinski and Keller, 2005). More vulnerable motoneurons displayed increased excitotoxicity and a decreased capability to buffer increased intracellular calcium (Bergmann and Keller, 2004). This relatively low threshold and weak buffering of calcium ions may be useful in physiological conditions to aid the rapid transient levels of calcium ions need for the high level of motoneuron firing rate (Lewinski and Keller, 2005). However, this property of motoneurons renders them more vulnerable to changes in calcium homeostasis in comparison to other neuronal subtypes (Carriedo *et al*., 1996).

The low threshold of motoneurons to calcium ions is, in part, due to a relative deficiency of GluR2, a subunit of the AMPA glutamate receptor complex, which determines the permeability of the AMPA receptor to calcium ions, and therefore the permeability of the motoneuron. Receptors lacking GluR2 have higher calcium ion permeability in comparison to AMPA receptors containing the GluR2 subunit (Hollmann *et al*., 1991). This lack of specificity makes selective motoneurons less able to withstand excitotoxic insults. Thus, studies of GluR2 knock-out mice showed no signs of motoneuron deficit (Jia *et al*., 1996), while transgenic mice over-expressing the GluR2 subunit developed a late-onset motoneuron deficit (Feldmeyer *et al*., 1999). Taken together, the evidence presented suggests that motoneurons are more susceptible to a build up of ROS leading to oxidative stress and have an increased permeability to calcium ions and are therefore selectively more vulnerable to excitotoxicity from pathogenic insults (Van Damme *et al*., 2002).

1.5.3. The cytoskeleton and axonal trafficking in motoneurons

The anatomy of a neuron is shaped by its plasticity and function, with long axons and varying numbers of dendrites and axonal branches creating variations in

anatomical structure (Kandel *et al*., 2000). Motoneurons are a good example of this extreme morphology as they can be the largest cells in the body, with axonal processes that can reach well over a metre in length and with varying diameters (Henneman *et al*., 1965; Wuerker *et al*., 1965; McPhedran *et al*., 1965; Beardwell, 1967). This unique length and diameter leading to a large axonal size, places a heavy reliance on the stability of the cytoskeleton and axonal transport along the cytoskeleton. The cytoskeleton of a neuron consists of three structural components, which are, in turn, complex arrangements of proteins that act dynamically to not only facilitate axonal transport, cell growth and motility, but also maintain cell structure and homeostasis. Microtubules, the largest component of the cytoskeleton, consist of tubulin and are hollow cylinders with a diameter of ~24nm. Intermediate filaments, which also include neuron-specific filament proteins, form a core filament of ~10nm diameter and thinner projections of 4-5nm which form cross bridges between the core filaments. Finally, microfilaments, asymmetric two-stranded helical filaments consisting of actin only, form the thinnest components of the cytoskeleton and provide flexibility to the cell structure (Kandel *et al*., 2000).

1.5.3.1. Microtubules

Found in all types of cells, microtubules are polymers made up of isomers of α, β and γ-tubulin and are involved in many neuronal processes including mitosis, cell growth, motility, axonal transport, cell integrity and polarisation. Following polymerisation, microtubules are subject to many different types of post-translational modifications including acetylation, phosphorylation and polyglycylation, which differentially affect the stability and spatial distribution of the microtubules (Conde and Cáceres, 2009). Within the cytoplasm there is equilibrium between tubulin monomers and polymers, with tubulin constantly polymerising and depolymerising, leading to a characteristic property of dynamic instability, so that they have the

ability to undergo rapid growth and disassembly. Microtubules form dense parallel bundles stabilised by intermediate filaments and an array of microtubule-associated proteins, including MAP2 and tau (Kobayashi and Mundel, 1998). Microtubule-associated proteins are important in disease and disruptions in tau, or neurofibrillary tangles, are a major or primary pathological feature of many neurodegenerative diseases including Alzheimer's disease and progressive supranuclear palsy (Iqbal *et al*., 2010). Defects of neuronal migration resulting in severe neurological deficits have also been linked to microtubule dysfunction and dysregulation (Liu, 2011), further demonstrating how important the regulation of microtubules is for axonal functions. In neurons, microtubule density increases with axonal diameter and there are no differences in microtubule numbers between sensory and motor axons (Pannese *et al*., 1984). However, microtubule density was seen to be higher in peripheral axons than central axons, which may correlate with the role of microtubules in fast axonal transport (Pannese *et al*., 1984).

Microtubules are central to axonal transport in neurons, acting as rails for fast, slow and intermediate long range travel along the axon. Microtubules are highly polarised, and it is this feature which makes them integral to axonal transport, with a plus end at the distal end of the axon, and the minus end at the cell soma. This polarity informs the specificity of the molecular motors which carry cargoes along the cell, with anterograde motors always travelling away from the cell body towards the plus end of the microtubule, and retrograde motors transporting cargoes back to the cell body towards the minus end of the microtubule.

1.5.3.2. Anterograde axonal transport motors

Kinesins are the largest superfamily of motors and the most abundant motor in many cell types. Currently, over 45 kinesins have been identified, although multiple

isoforms increase the diversity of this superfamily (Miki *et al*., 2001). Kinesins are ATP-dependent microtubule motors, using microtubules as 'rails' to transport cargo in a mostly anterograde manner away from the cell soma (Hirokawa, 1998; Hirokawa and Noda, 2008). The kinesin superfamily can be further organised into 3 different types of kinesin in which the position of the motor domain, at the amino-terminus, in the middle portion and at the carboxyl-terminus (N-kinesin, M-kinesin and C-kinesin, respectively) affects the cellular role of the protein. Typically, kinesin motors associate with scaffold and adaptor proteins to bind different cargoes, but they can also specifically bind cargo directly (Hirokawa *et al*., 2009). Illustrating the importance of axonal transport and molecular motors in motoneurons in particular is the fact that mutations in members of the kinesin family lead to various forms of neuronal degeneration with a predominantly peripheral phenotype. Mutations in KIF5A, a motor linked to the slow transport of neurofilaments, cause hereditary spastic paraplegia (Reid *et al*., 2002; Xia *et al*., 2003), and mutations in KIF1B lead to CMT 2A (Table 1.1B)(Zhao *et al*., 2001).

1.5.3.3. Retrograde axonal transport motors

Dynein molecular motors, the major retrograde motors, are multimeric complexes of two dynein heavy chains, two intermediate chains, four light intermediate chains and a number of light dynein chains (Gunawardena and Goldstein, 2004). The specificity of cargo binding is partly due to the composition of the dynein complex, but is also due to indirect mediation by the dynactin complex that acts as a receptor to link the dynein to cargo and activate dynein transport (Waterman-Storer *et al*., 1997; King and Schroer, 2000). The dynactin complex is a large composite of proteins including p50, p150glued, which binds to both microtubules and the intermediate chain of dynein, and various actin interacting proteins (Holleran *et al*., 1998). Mutations in the p150glued subunit of dynactin that cause motoneuron disease illustrate the

importance of axonal transport in the proper functioning of long lower motoneurons (Puls *et al*., 2003; Lai *et al*., 2007).

1.5.3.4. Intermediate filaments

Intermediate filaments consist of many different forms of filament protein of which there are at least 65 types in humans, including vimentin, keratin and neuron-specific intermediate filaments that are abundant in axons and form a major cytoskeletal component (Hirokawa *et al*., 1984; Gotow, 2000; Herrmann and Aebi, 2004). There are three subunits of neurofilaments that are classified according to their molecular weight in relation to each other, neurofilament light, medium and heavy NF-L, NF-M and NF-H, respectively. These subunits come together to form neurofilaments comprising of a core filament of ~10nm diameter and thinner projections of 4-5nm which form cross bridges between the core filaments (Gotow *et al*., 1992). In axons, neurofilaments are highly organised and arranged in parallel bundles in all cytoplasmic compartments. The organisation of neurofilaments is dependent on phosphorylation (Gotow, 2000). Neurofilaments are important in neurons as they influence the degree of stability of the cytoskeleton in mature cells (Morris and Lasek, 1982) and maintain axonal calibre (Hoffman *et al*., 1984). The calibre of neuronal axons is directly proportional to the number of neurofilaments present (Friede and Samorajski, 1970). In disease states neurofilaments are often affected, for example in CMT1, neurofilament numbers are reduced (Nukada and Dyck, 1984) while in other subtypes of CMT neurofilaments increase or aggregate into bundles of protein (Benedetti *et al*., 2010a). Mutations in NF-L also lead to CMT 2E and CMT 1F (Jordanova *et al*., 2003; Fabrizi *et al*., 2007).

1.5.3.5. Microfilaments

Neuronal actin filaments are the thinnest (~8nm) and most flexible components of the cytoskeleton and are composed of monomers of two distinct types of actin, β-actin and γ-actin of approximately 42kDa (Choo and Bray, 1978). Actin is present in the cell in 2 states: monomeric G-actin (globular actin) and F-actin (filamentous actin) bound in asymmetric two-stranded helical filaments composed of G-actin. Actin filaments are made of G-actin bound by weak non-covelent bonds with preferential polymerisation of F-actin at the barbed end of the filament and release of G-actin at the pointed end (Cingolani and Goda, 2008). Actin filaments are present in the nucleus, cytoplasm and on the surface of cells and play a significant role in stabilising the cellular structure. Actin filaments anchor the cytoskeleton to the cellular membrane, playing a role in cell division, drive cell motility and are important for axon and dendritic growth and synaptic development through the formation of growth cones. Actin filaments are also base structures along which myosins, which are actin motors that mostly participate in contractile force and short-range axonal transport, trafficking cargoes locally along neural projections (Ligon and Steward, 2000).

The spatial organisation of cytoskeletal components is vital for cells and is controlled and modified by many different pathways through processes of cell development and maintenance. In neurodegenerative disease, as discussed above, the cytoskeleton is often disrupted, for example, the appearance of neurofibrillary tangles in tauopathies, the disruption of neurofilaments in CMT and ALS and mutations in neurofilament light chain which lead to CMT 2E/1F (Jordanova *et al*., 2003; Fabrizi *et al*., 2007; Benedetti *et al*., 2010; Iqbal *et al*., 2010).

1.5.4. Axonal transport in motoneurons

In neurons there are significant distances between sites of organelle and protein biosynthesis, function, recycling and degradation. Therefore the molecules and organelles required for these processes need to be transported from the cell body where the majority of proteins required for cell homeostasis are synthesised (Shah and Cleveland, 2002). This is especially important for cells such as motoneurons which can contain >99% of the cell cytoplasm in the peripheral axon (Hurd and Saxton, 1996). Axonal trafficking is a multifaceted process where transport can take from seconds to days to traverse the full length of the axon. Transport is required for the trafficking of a variety of cargoes including proteins, mRNA, neurofilaments and mitochondria, which will be used in processes ranging from local protein synthesis, energy production and cytoskeletal remodelling (Sau *et al*., 2011). Axonal transport involves motor protein complexes carrying cargo via microtubule networks (Gunawardena and Goldstein, 2004). Within the axon, transport can be divided into two classes, fast (20 to 400mm/day) and slow (0.1 to 20 mm/day) (Miller and Heidemann, 2008).

Long distance fast and slow axonal transport of mitochondria takes place along microtubules. In contrast, short-range transport of mitochondria occurs by myosin motor transportation along actin filaments in neurons (Kuznetsov *et al*., 1992; Ligon and Steward, 2000; Langford, 2002; Hollenbeck and Saxton, 2005). The direction and organisation of long-distance axonal transport is dependent on microtubule orientation and type of motor protein that are classed as unidirectional as they travel towards the charged ends of microtubules. Kinesin motors travel in an anterograde direction towards the plus ends of microtubules at the distal end of the axon and dyenin motors travel retrogradely towards the minus end of the microtubule at the cell soma. Molecular motors, discussed above, primarily consist of two functional

structures; a motor domain that interacts with cytoskeletal filaments along which the motors move and tail domains which interact with the cargo. It is the diversity within the tail domains or through association with accessory light chains which allows for such a wide range of cargo to be transported (Gunawardena and Goldstein, 2004).

1.5.4.1. Fast and slow axonal transport

As mentioned above, axonal transport can be roughly grouped by speed into fast (20 to 400mm/day) and slow (0.1 to 20 mm/day) trafficking (Miller and Heidemann, 2008). Mitochondria, polyribosomes, membrane-bound organelles and synaptic vesicles typically traverse the cell by fast axonal transport. To illustrate the importance of fast transport in motoneurons, mitochondrial transport shall be used here as an example. As discussed above in Section 1.5.1., mitochondria are particularly important in cells such as motoneurons, which have high energy demands, even in a resting state, and an increased reliance on transport along long axons for correct local distribution of mitochondria. Anterograde transport of mitochondria is associated with specific forms of kinesin, including a kinesin-1 and a kinesin-3, while retrograde transport relies on the dynein complex, with kinesin-1 also critical for retrograde movement (Nangaku *et al*., 1994; Tanaka *et al*., 1998; Pilling *et al*., 2006). The mitochondria attach to these motor complexes by a variety of different adaptor proteins, which link the mitochondria via receptors, for example, milton and miro, respectively (Fransson *et al*., 2006; Glater *et al*., 2006; Frederick and Shaw, 2007). Although the basic mechanism of mitochondrial transport is presented here, the full breadth of complexity of these organelle movements is complicated and not yet fully understood. What is apparent is the importance of the correct movements of mitochondria for the homeostatic balance of the cell, with deficits in fast mitochondrial transport being reported in mouse models of ALS,

reducing axonal mitochondria content, and thus compromising mitochondrial and axonal functioning (Kieran *et al*., 2005; De Vos *et al*., 2007; Bilsland *et al*., 2010).

Slow transport works in both an anterograde and retrograde direction with a net direction of anterograde, away from the cell body transporting many cargoes, including cytoskeletal components (Hoffman and Lasek, 1975; Lasek *et al*., 1984). Slow axonal transport is thought to be the more common pathway of axonal trafficking even though many of its proposed cargoes have not yet been identified, and the actual mechanism of slow transport is yet to be sufficiently elucidated. Although it is proposed to be a transport mechanism with many long pauses in movement across the axon contributing to an overall average slower speed of transport of 0.6-0.7μm/sec, for example, neurofilaments spend only 20% of time in transit moving, with the rest of the time paused (Roy *et al*., 2000; Miller and Heidemann, 2008). Slow transport can be further sub-classified by speed, and these sub-classifications correspond to certain groups of cargo, with some elements of the cytoskeleton, most notably neurofilaments and microtubule subunits transported at slower speeds than subunits of actin, actin-associated proteins such as clathrin and glycolysis enzymes which are transported in the faster sub-compartment (McQuarrie *et al*., 1986; Shah and Cleveland, 2002). There is also thought to be neuronal variations in the transport of identified proteins across the axon with significant variations in average speed of movement and levels of different proteins measured in comparable neuronal types (McQuarrie *et al*., 1986). For example, when measured in retinal ganglion cells and spinal motor axons, tubulin displayed peak advancement of 0.36mm/day and 1.3mm/day respectively (McQuarrie *et al*., 1986). As the neuron ages, there is a gradual decline in the rate of slow transport, possibly leading to the increased vulnerability of aged neurons to neurodegenerative diseases (McQuarrie *et al*., 1989). Slow transport is also affected in

neurodegenerative disease before phenotypic onset, with selective cargoes, including tubulin, affected as an early feature of ALS in mutant SOD1 mice (Williamson and Cleveland, 1999).

Thus, axonal transport is a finely regulated process which is differentially regulated in different subpopulations of neurons in which disruptions, for example caused by genetic mutations in essential proteins or blockages in the axon caused by aberrant proteins, can result in axonal degeneration (Gunawardena and Goldstein, 2004; Sinadinos *et al*., 2009).

1.5.5. Motoneurons have a high threshold for activation of the heat shock response

In addition to the cellular vulnerabilities that are exacerbated by anatomical features, motoneurons also have intrinsically reduced capacity to respond to stress. Thus, motoneurons have an innate high threshold for activation of the heat shock response (HSR), the integral pathway that responds to cell stress (Batulan *et al*., 2003), which is described at length below in Section 1.6. The reason for this higher threshold is not yet understood, but it may be a mechanism to stop whole cell HSR response to local fluctuations in the cell environment. As described above, motoneurons are excitable cells which have very fast and intense local changes in homeostasis which can happen at long distances from the cell body, and which should not induce the HSR. The higher threshold of the HSR is another likely contributor to the preferential vulnerability of motoneurons to mutations in a ubiquitously expressed protein. Demonstrated by the lack of significant increase in Hsp70 in motor and sensory neurons after axotomy (Tidwell *et al*., 2004).

There are many cellular pathways that can be impaired in stress and lead to motoneuron damage and activation of the HSR. These can include protein unfolding, increase in ROS and changes in calcium homeostasis which can lead to damaging cellular changes including the misfolding of proteins and protein aggregation, cytoskeletal abnormalities, oxidative stress, impaired mitochondrial function and defective axonal transport, all of which are particularly important to neurons (Der Perng and Quinlan, 2004).

Thus, not only do motoneurons have an increased metabolic load, an active balance of ions and increased axonal transport which all increase cellular vulnerability to environmental stressors, they also have the additional problem of a higher activation level of the protective HSR than in other cells (Batulan *et al*., 2003). This is possibly due to local homeostasis imbalances caused by the large, transient local changes in ion balances and localisation of higher levels of ROS around areas of high mitochondrial density, such as the Nodes of Ranvier which would normally trigger a HSR in cells with a lower threshold, but in motoneurons are not significant enough to trigger a global response (Palay, 1958; Fabricius *et al*., 1993; Li *et al*., 2004).

1.6. The heat shock response

The heat shock response is a ubiquitously expressed cytoprotective response to cell stress and unfolded proteins, that exists in all organisms, suggesting that the process is an ancient, evolutionarily conserved response (Lindquist, 1986). The HSR can be initiated by diverse stimuli, such as heat stress, oxidative stress and toxic substances, which result in shifted homeostasis and increased protein misfolding and aggregation, degradation and improper protein trafficking (Morimoto, 2008; Shamovsky and Nudler, 2008) which can lead to programmed cell death (apoptosis) if not reversed (Welch and Suhan, 1985; Richter *et al*., 2010). Thus, the

HSR is a vital cellular response and essential for cell survival. The HSR is an acute response that induces a massive, and rapid increase in the expression of genes that code for a family of protein chaperones, the heat shock proteins (HSPs) (Shamovsky and Nudler, 2008). The activation of the HSR is well characterised, although not all of the regulatory mechanisms of the HSR are well understood. The HSR is activated by translocation of heat shock factor 1 (HSF1) from the cytoplasm to the nucleus where it binds to the heat shock element (HSE), initiating transcription and thereby up-regulating a cascade of molecules that form the HSR (Richter *et al*., 2010). This mechanism will be briefly described here, and is illustrated in Figure 1.2.

Under normal cell conditions, HSF1 exists as a monomer in complexes with heat shock protein 70 (Hsp70) (Abravaya *et al*., 1992), heat shock protein 40 (Hsp40) and heat shock protein 90 (Hsp90) (Zou *et al*., 1998). On detection of unfolded or misfolded proteins, HSF1 is released from these complexes and can trimerize spontaneously (Zhong *et al*., 1998), or by interactions with cellular factors, for example with heat shock RNA 1 (HSR1) which may assist trimer assembly or enhance the stability of the HSF1 complex (Shamovsky *et al*., 2006). Trimerized HSF1 then relocates to the nucleus where it binds to the HSE (Wu, 1984), a consensus DNA sequence with conserved homology that is found in the promoter site of all HSPs (Zimarino *et al*., 1990). From this point, protein chaperones and co-chaperones are upregulated and cellular pathways in response to cellular stress are initiated. During cell stress, cellular structures and organelles are disturbed, including components of the cytoskeleton, which firstly undergo reorganisation of actin filaments to stress fibres (Ke *et al*., 2011) before structural collapse is caused by the aggregation of filamentous proteins including vimentin (Welch and Suhan, 1985). The mitochondria in the cell swell and change location to the cell soma

Figure 1.2

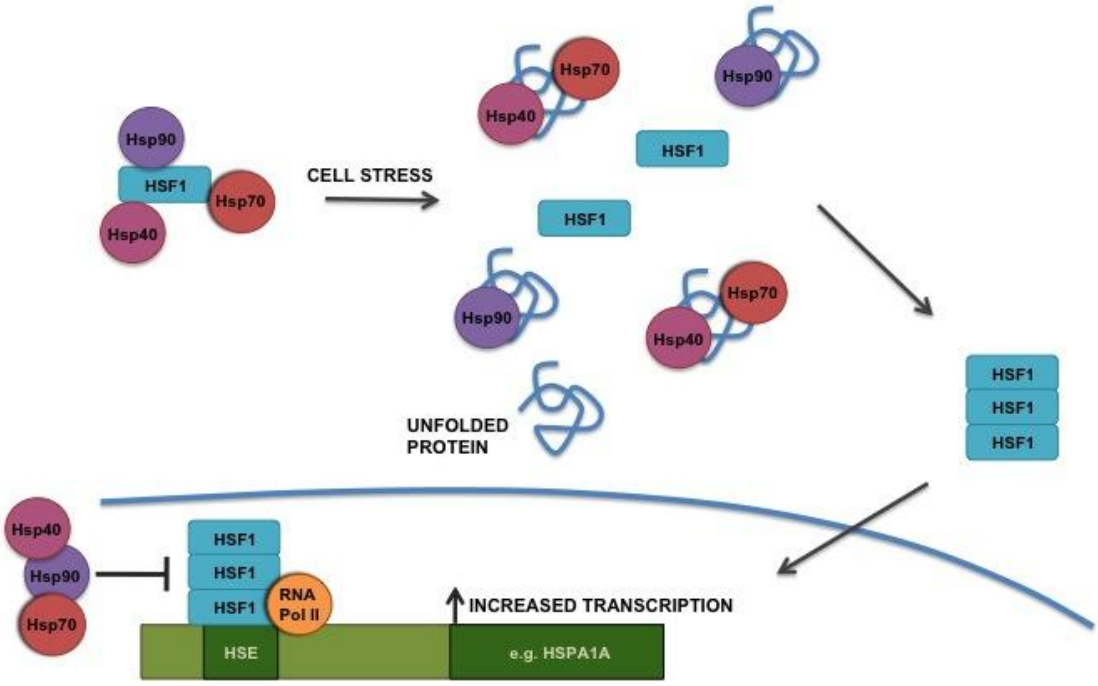

Figure 1.2 Diagrammatic representation of activation and translocation of heat shock transcription factor 1 (HSF1).

In unstressed conditions HSF1 is bound in an inactive state in the cytoplasm in complexes with heat shock proteins (Hsp) 40, 70 and 90. Under conditions of cell stress, proteins become misfolded, triggering a chaperoning response from Hsp40, 70 and 90 and activating monomeric HSF1 which then trimerizes and translocates to the cell nucleus when it binds to the heat shock element (HSE) with RNA polymerase II (RNA pol II) in the promoter region of heat shock genes and increases transcription.

On conclusion of cell stress, HSPs negatively regulate transcription by inhibition of HSF1.

surrounding the nucleus (Welch and Suhan, 1985), possibly causing rapid declines in intracellular ATP production (Lambowitz *et al*., 1983; Patriarca and Maresca, 1990) while mRNA of housekeeping and non-important genes are sequestered in stress granules as a protective measure (Thomas *et al*., 2011) and the golgi and ER fragment, all leading to a decrease in protein production (Welch and Suhan, 1985).

HSF-1 trimerization and activation is regulated by the negative feedback of HSPs produced by the HSR. When HSP levels are sufficiently elevated, free HSPs, including, but not limited to Hsp90, Hsp70, Hsp27 and Hsp40, bind to and modulate HSF-1 to make it inactive (Åkerfelt *et al*., 2010).

1.7. Heat shock proteins

Of the proteins upregulated following HSF1 activation, HSPs, which target unfolded or misfolded proteins to prevent protein aggregation by protein refolding or degradation, are the most significant, although many of these proteins require co-factors for their cellular actions (Pratt and Toft, 2003). As well as being induced under conditions of cellular stress, HSPs are ubiquitously present in unstressed cells where they work in different cellular compartments to maintain protein homeostasis by facilitating protein folding, degradation through the proteosome, clearance and transport (Arya *et al*., 2007; Morimoto, 2008; Kalmar and Greensmith, 2009).

The nomenclature of molecular chaperones is based on their weight (kDa) and from here they can be grouped accordingly; Hsp90, Hsp70, Hsp60, Hsp40 and the small heat shock proteins (sHSPs). A Table listing HSPs is shown in Table 1.4, and catalogues some of the basic functions of the HSPs. It is also becoming increasingly common to name some HSPs by their gene name as multiple genetic forms of

Table 1.4 Heat shock proteins

The Table describes the different classes of HSP, including gene name, protein name, tissue location, subcellular location, known functions and diseases caused by genetic mutations.

Table 1.4. Heat shock proteins

Gene name	Protein name	Tissue location	Subcellular localisation	Known functions	Genetic involvement of disease	References
HSPA1A	Hsp70, Hsp72	Ubiquitous	Cytoplasm	ATP-dependant molecular chaperone, upregulated on heat stress	_	(Mayer and Bukau, 2005)
HSPA5	BIP, GRP78, MIF2	Ubiquitous	ER	Molecular chaperone at the ER, initiates unfolded protein response (UPR)	_	(Vembar and Brodsky, 2008)(Lai *et al*., 2010)
HSPA8	Hsc70, Hsc(p)71, Hsp73	Ubiquitous	Cytoplasm	ATP-dependant molecular chaperone	Genetic variants contribute to coronary heart disease	(He *et al*., 2010)
HSPB1	Hsp27	Ubiquitous	Cytoplasm/ nucleus	Stabilises cytoskeleton, inhibits apoptosis, acts as a co-chaperone of Hsp70	CMT 2F, dHMN II	(Rogalla *et al*., 1999) (Evgrafov *et al*., 2004)
HSPB2	Hsp27/ MKBP	Heart, skeletal muscle, cortex, hippocampus	Cytoplasmic granules/ mitochondria	Binds and activates myotonic dystrophy protein kinase, forms complexes with HSPB3	_	(Suzuki *et al*., 1998) (Sugiyama *et al*., 2000) (Kirbach and Golenhofen, 2011)
HSPB3	HSPL27	Muscle, cortex, cerebellum, nerve	Cytoplasm	Forms complexes with HSPB2	Asymmetric axonal motor neuropathy	(Sugiyama *et al*., 2000) (Kolb *et al*., 2010) (Kirbach and Golenhofen, 2011)
HSPB4/ CRYAA	α A-crystallin	Eye lens	Cytoplasm	Holdase, inhibits apoptosis, regulates cell growth, structural protein, gene activator, major	Cataracts	(Horwitz, 2003)(Graw, 2009)

				component of the eye-lens		
HSPB5	α B-crystallin	Ubiquitous	Cytoplasm/ nucleus	Inhibits apoptosis, interacts with cytoskeletal components	Desmin-related cardiomyopathy, cataracts, myofibrillar myopathy	(Bennardini *et al*., 1992) (Vicart *et al*., 1998) (Berry *et al*., 2001) (Graw, 2009)
HSPB6	Hsp20	Heart, muscle, brain	Cytoplasm	Inhibits apoptosis, works as an anti-ischaemic protein, actin-binding protein	Protective mediator in neuro-degenerative and cardiovascular diseases	(Brophy *et al*., 1999) (Edwards *et al*., n.d.)
HSPB7	cvHSP	Heart, skeletal muscle	Cytoplasm/ nucleus	Interacts with cytoskeletal components	_	(Krief *et al*., 1999)
HSPB8	Hsp22	Muscle, brain, keratinocytes, placenta	Cytoplasm/ plasma membrane	Complexes with HSPB1, chaperone activities and apoptotic effects	CMT 2L, dHMN II	(Benndorf *et al*., 2001a)(Irobi *et al*., 2004) (Shemetov *et al*., 2008)
HSPB9	HSPB9	Testis	Cytoplasm/ nucleus	May interact with dynein	_	(Kappé *et al*., 2001)(de Wit *et al*., 2004)
HSPB10	ODF1	Testis	Spermatozoa tails	_	_	(Fontaine *et al*., 2003)
HSPB11	Hsp16.2	Unknown	Cytoplasm/ nucleus	May inhibit apoptosis and effect mitochondrial membrane	_	(Bellyei *et al*., 2007)
HSPD1	Hsp60	Ubiquitous	Mitochondria/ cytoplasm, cell surface	Chaperone activities in mitochondria, immune trigger at cell surface	Implicated in hereditary spastic paraplegia and hypomyelinating leukodystrophy	(Magen *et al*., 2008) (Christensen *et al*., 2010)(Grundtman *et al*., 2011)
HSPH1	Hsp105	Ubiquitous	Cytoplasm/	Induces and interacts with Hsp70 to reduce protein	_	(Saito *et al*., 2007)

			nucleus	aggregation		(Yamagishi *et al*., 2009)
HSPH2	Hsp110, APG-2	Ubiquitous	Cytoplasm/ nucleus	Interacts with Hsp70 and Hsp90, target proteins for degradation	_	(Mandal *et al*., 2010)
DNAJB1	Hsp40	Ubiquitous	Cytoplasm	Inactivates HSF1, co-chaperones Hsp70	_	(Zou *et al*., 1998) (Kampinga and Craig, 2010)
DNAJB2	HSJ1	Heart, muscle, brain	Cytoplasm/ ER	Co-chaperones Hsp70, target proteins for proteosome	autosomal recessive dHMN	(Westhoff *et al*., 2005) (Blumen *et al*., 2008) (Kampinga and Craig, 2010)
HSP90A	Hsp90	Ubiquitous	Cytoplasm	ATP-dependent protein chaperone with many co-chaperones	_	(Zhao and Houry, 2005)

similar proteins are discovered. For example, Hsp27 is the common protein name for the *HSPB1* gene. However, *HSPB3* and *HSPB7* are genes coding for sHSPs with the same molecular weight of 27kDa, but different tissue locations and varying cellular functions (Kappé *et al*., 2003). HSPs can also be grouped according to their reliance on energy. Large molecular chaperones are generally ATP-dependent, including proteins such as Hsp70 and Hsp90 which actively chaperone proteins, whereas smaller HSPs, such as Hsp20 and Hsp27 are ATP-independent and act mainly as co-chaperones to the larger, energy-dependent chaperones.

1.7.1. Heat shock protein 90

Hsp90 chaperones are essential components of the eukaryotic cell. The Hsp90 family is one of the most highly conserved HSPs across all species and highly abundant in non-stressed cells as well as being an essential component of the HSR. In unstressed cells, Hsp90 chaperones client proteins in an ATP-dependent manner to fold proteins into a final, functional conformation. The client proteins of Hsp90 depend on the chaperone to acquire active conformation, and include protein kinases, eNOS, chromatin proteins and nuclear steroid receptors, indicating that Hsp90 has a vital and possibly modulatory role in many regulatory processes (Taipale *et al*., 2010). Hsp90 interacts with over 20 co-chaperones that aid Hsp90 by guiding its recognition of client proteins, therefore modulating Hsp90 activity and to reach attainment of the clients' active conformation (Taipale *et al*., 2010). As well as its role in maintaining active conformation, Hsp90 has also been shown to disassemble and down-regulate macromolecular complexes and, for example, is involved in the reversible disassembly of transcriptional regulatory complexes of intracellular receptors, thereby influencing receptor activity (Freeman and Yamamoto, 2002). Hsp90 also works in partnership with other HSPs to achieve protein maturation. For example, Hsp90, working with the co-chaperones, HOP and

p23, binds to the progesterone receptor after HSPs 40 and 70 (Cintron and Toft, 2006).

1.7.2. Heat shock protein 70

Hsp70 is a subgroup of HSPs with a molecular weight of 70kDa, and is the most ubiquitous of all HSP subgroups with at least 8 members (Daugaard *et al*., 2007). Hsp70 is expressed in two different forms, as cognate proteins (Hsc70) which are constantly expressed in the cell and perform housekeeping functions to maintain homeostasis, and inducible forms (Hsp72) which are up regulated by activation of HSF1 as part of the HSR (Morimoto, 2008). Hsc70, under normal physiological conditions, binds to hydrophobic surfaces of substrates to prevent protein aggregation and misfolding of proteins (Lu *et al*., 2010). This ATP-dependent function of protein chaperone is the primary task of all Hsp70s, and during times of cell stress the chaperone roles of Hsp70 is critical to the HSR and therefore the survival of the cell. Upregulation of Hsp70 has been shown to increase cell survival in sensory and motoneurons (Tidwell *et al*., 2004). No mutations have been described in Hsp70, although genetic variations in the gene coding for Hsc70, *HSPA8* are associated with coronary heart disease (He *et al*., 2010). Mouse models containing a knockout of individual stress-induced Hsp70 proteins are viable, although they demonstrate increased sensitivity to external stresses including heat, ischemia, genomic instability, osmotic stress and pancreatitis, with a reduced capacity to acquire pre-conditioned stress resistance (Huang *et al*., 2001; Lee *et al*., 2001; Kwon *et al*., 2002; Shim *et al*., 2002; Hunt *et al*., 2004). Together, this data shows the importance of individual Hsp70 proteins to the cells innate stress response.

1.7.3. Small heat shock proteins

sHSPs, described in more detail in Table 1.2, are a ubiquitous family of molecular chaperones classified by having a molecular weight of less than 43kDa and a shared, highly conserved α-crystallin domain (Ganea, 2001; Kappé *et al*., 2003). The sHSPs are conserved in all organisms. In the human genome, sHSPs are dispersed across 9 chromosomes, observing the ancient duplications that have formed the gene family (Kappé *et al*., 2003; Li *et al*., 2009). sHSPs are ATP-independent chaperones, and they do not exist in a cognate and inducible form, therefore during times of cell stress, the protein which is expressed normally is upregulated. sHSPs exist in the cell as monomers or complexes that can range in size from 2 to 40 units, and although ubiquitously expressed in all tissues, the expression levels can vary between both tissue and cell types (Table 1.2) (Kappé *et al*., 2003; Kirbach and Golenhofen, 2011). As well as forming large homomeric complexes, sHSPs can also interact to form heterologous oligomeric complexes within the cell, demonstrating protein interactions within the sHSP family (Sugiyama *et al*., 2000; Bova *et al*., 2000). All members of the sHSP family demonstrate an ATP-independent chaperone function, protecting proteins from irreversible aggregation during physiological cell stress and acting as co-chaperones to ATP-dependent chaperones including Hsp70 and Hsp90 (Narberhaus, 2002; Sun and MacRae, 2005). As well as having common functions shared by sHSPs, they can play different and more varied roles as described in Table 1.2, including inhibition of apoptosis, cytoskeletal stabilisation, redox state regulation, activation of autophagy, as a structural protein and in the regulation of cell growth (Kappé *et al*., 2003).

Mutations discovered in 5 different sHSPs have been shown to cause neuropathies, cataracts and myopathies, where sHSPs have highly specialised functions specific to those cells or a higher level of expression (Berry *et al*., 2001; Horwitz, 2003;

Evgrafov *et al*., 2004; Irobi *et al*., 2004; Kolb *et al*., 2010). Some sHSPs such as α B-crystallin, Hsp22 and Hsp27 have also been seen as components of protein aggregates, which are associated with protein misfolding diseases, such at Alzheimer's and Parkinson's disease (Smith *et al*., 2005; Laskowska *et al*., 2010). Mutations in Hsp27, a ubiquitous, and well-studied sHSP with a number of cytoprotective functions, cause CMT 2F and dHMN II, neuropathies with a specific clinical presentation (Evgrafov *et al*., 2004). Therefore the functions of Hsp27, and the possible reasons for the cell-type specificity of mutations in this ubiquitous protein are discussed next.

1.8. Hsp27

Hsp27 is a small heat shock protein with a molecular weight of 27kDa and corresponding rodent homolog of 25kDa (Hsp25). Hsp27 corresponds to the *HSPB1* gene, which is located on chromosome 7 and consists of 3 exons and 737 base pairs (Hickey *et al*., 1986; Carper *et al*., 1990). Hsp27 consists of a highly conserved α-crystallin domain, a poorly conserved N-terminus containing a hydrophobic WDPF motif required for protein binding and oligomerization, and a highly flexible, variable C-terminus (Kostenko and Moens, 2009). The presence of the 80-100 amino acid a-crystallin domain is a characteristic feature of the structurally divergent small heat shock protein family members discussed above and its presence is conserved across species (Kappé *et al*., 2003). Hsp27 is ubiquitously expressed in all cells to different expression levels, and it has a number of housekeeping and cytoprotective functions including in protein handling and folding, inhibition of apoptosis, protection against oxidative stress and promotion of axonal growth, all of which make Hsp27 essential for motoneuron growth and survival (Kalmar *et al*., 2002; Franklin *et al*., 2005).

1.8.1. Hsp27 expression in animal models

Analysis of animal models of Hsp27 disruption and over expression clearly demonstrates the importance of Hsp27. Currently; only two studies have examined the effects of reduced Hsp27 expression. Brown *et al*., (2007) used morpholino injections in *Xenopus laevis* embryos to inhibit endogenous *HSPB1* translation (Brown *et al*., 2007). In this model, defects in heart tube fusion were observed, with actin filament disorganisation and partial cardia bifida (Brown *et al*., 2007). However, in a zebrafish model of Hsp27 mRNA knockdown, there was no effect on either the structure of muscle myotomes in development or in motility overall (Tucker *et al*., 2009). Furthermore, in a mouse model with targeted disruption of *HSPB1* by the replacement of 60% of the *HSPB1* start coding sequence with a *lacZ* reporter gene, there were no developmental disruptions and no reported change in tissue function under normal physiological conditions, although transgenic mice in this study did exhibit higher levels of apoptosis after heat challenge, suggesting a significant disruption of the HSR (Huang *et al*., 2007).

Conversely, over-expression of Hsp27 in mouse models demonstrates the neuroprotective effects of Hsp27, accelerating axonal growth after injury, decreasing neurotoxicity, decreasing severity of induced seizures and neuronal death (Akbar *et al*., 2003, Ma *et al*., 2011). Furthermore, over-expression of human Hsp27 in a second mouse model conferred protection against spinal cord ischemia, demonstrating the importance of Hsp27 in motoneurons (Krishnan *et al*., 2008). Also, when the Hsp27 over-expressing mouse was crossed with transgenic mice containing the mutant ALS gene, SOD1, there was a delay of disease onset, however, there was no overall rescue of disease phenotype (Krishnan *et al*., 2008; Sharp *et al*., 2008).

1.8.2. Phosphorylation of Hsp27

Hsp27 has many functions within the cell arising from different cellular interactions. These are facilitated by the conformation of Hsp27, which is modified post-translationally by individual phosphorylation at three Serine residues, 15, 78 and 82 and at two Serine residues, 15 and 86 in Hsp25 (Chrétien and Landry, 1988; Landry *et al*., 1992; Kostenko and Moens, 2009). When phosphorylated, Hsp27 exists within the cell as monomers and dimers (27-54kDa), but when unphosphorylated, it exists as large multimers of ~500-800kDa in size (Lambert *et al*., 1999). It can also form large heteromeric structures with other members of the small heat shock family, for example, Hsp20 and Hsp22 (Bukach *et al*., 2009; Benndorf *et al*., 2001). Modification of Hsp27 is essential for the divergent roles it has within the cell, and this is achieved by a cascade of several kinases *in vitro* that is described below, and illustrated in Figure 1.3. A tightly regulated intracellular signalling pathway of mitogen-activated protein kinases (MAPK) phosphorylates Hsp27 (Dorion and Landry, 2002). Hsp27 is directly phosphorylated by a serine-protein kinase MAPK-activated protein kinase 2 (MAPKAP2) *in vivo* (Stokoe *et al*., 1992; Huot *et al*., 1995), and has also been shown to be activated by MAPK-activated protein kinase 3 (MAPKAP3), but only in the absence of, and with weaker interactions than MAPKAP2. MAPKAP2 is most likely the dominant phosphorylator of Hsp27, suggesting that MAPKAP3 plays a less common role within the cell *in vivo* (Dorion *et al*., 2002). There is also evidence indicating a role for MAPK-activated protein kinase 5 (MAPKAP5) that phosphorylates Hsp27 when induced, at serine positions 78 and 82 *in vivo* when induced (Kostenko *et al*., 2009a). MAPKAP2 is phosphorylated *in vivo* by the mitogen-activated protein kinase p38 which is in turn, itself phosphorylated and activated by specific upstream kinases, MAPK-kinase 3/6 (MKK3/6) (Zanke *et al*., 1996; Pietersma *et al*., 1997). MKK3/6 are phosphorylated by MAPK-kinase-kinase apoptosis signal-regulating kinase-1 (ASK1), one of the

Figure 1.3

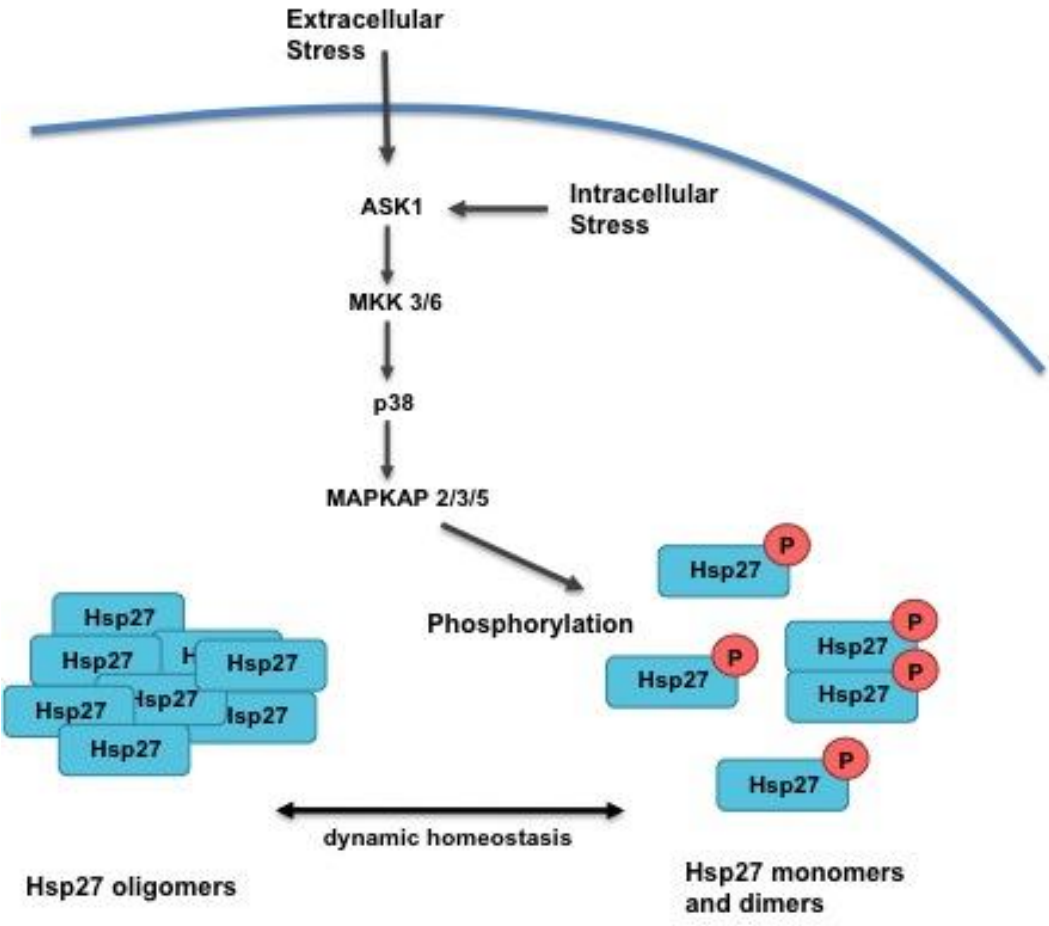

three

Figure 1.3 Diagrammatic representation of the Hsp27 phosphorylation pathway

Hsp27 is naturally found in cells as monomers, dimers and small and large multimers, with a dynamic equilibrium of size depending on cell homeostasis. Hsp27 oligomerization is dependent on Hsp27 phosphorylation, which is tightly regulated by MAP kinase pathways. Here, the most common *in vivo* pathway is described. ASK1 is activated by various forms of stress including cytokines, heat shock, chemical and oxidative stress and then phosphorylates MAPK-kinase 3/6 (MKK3/6) which, in turn, phosphorylates and activates p38, a mitogen-activated protein kinase that phosphorylates several MAPK-activated protein kinases; 2, 3 and 5 which directly phosphorylate Hsp27 at different sites to modulate Hsp27 conformation and function.

conserved mitogen-activated protein kinase pathways activated by various forms of stress including cytokines, heat shock, chemical and oxidative stress (Widmann *et al*., 1999; Nagai *et al*., 2007; Hattori *et al*., 2009). The ASK1 kinase pathway has been shown to be modulated via different MAP-kinases, and these different pathways can be induced by different cell stressors by indirectly phosphorylating Hsp27, leading to specific functions, for example, the protein kinases B and D (PKB and PKD respectively). PKB, or Akt is most likely a molecule which works upstream, and therefore indirectly on Hsp27 to phosphorylate Ser-82 preferentially (Rane *et al*., 2003).

Although several different kinase pathways have been described both *in vivo* and *in vitro* to have seemingly differential effects on the rate of Hsp27 phosphorylation at different sites and therefore different cellular patterns of action, there is little evidence from *in vivo* studies to confirm that all the pathways described have roles within the stressed cell. It is clear therefore that the pathways involved in the phosphorylation of Hsp27 are still far from understood.

1.8.3. The role of phosphorylation in Hsp27 function in conditions of cell stress

Hsp27 is naturally found in cells as monomers, dimers and small and large multimers, depending on its state of phosphorylation at three Serine residues (Kostenko and Moens, 2009). The equilibrium of size is very dynamic and depends on not only the homeostatic state of the cell (normal or stressed) but also the type of stress the cell may be under (chemical, thermal etc) (Garrido 2002). For example, PKD may indirectly mediate the phosphorylation of Hsp27 at ser-82 only in response to vascular endothelial growth factor (VEGF), and it is these different

initiation pathways that will activate the different functions of Hsp27 (Döppler *et al*., 2005).

The actions of Hsp27 in the cell are varied and include primary actions on molecules and pathways, and secondary, downstream effects where Hsp27 has a more modulatory effect. All these functions are, in some way, dependent on the level of Hsp27 phosphorylation. When phosphorylated, Hsp27 present in the cell as monomers and dimers, acts as an actin-capping protein, stabilising the actin cytoskeleton during cellular stress (Lavoie *et al*., 1995). In this state, Hsp27 also has anti-apoptotic properties, binding and inhibiting a pro-apoptotic protein, Daxx (Charette *et al*., 2000). Whereas non-phosphorylated large oligomers of Hsp27 demonstrate the ability to act as a holdase, an ATP-independent co-chaperone to Hsp70, preventing aggregation of misfolded proteins (Rogalla *et al*., 1999). Large oligomers have also been shown to be the active form responsible for the caspase-dependent, anti-apoptotic properties of Hsp27, as well as its ability to reduce reactive oxygen species levels by modulation of the intracellular level of glutathione in the cell (Mehlen *et al*., 1997; Rogalla *et al*., 1999; Bruey *et al*., 2000b). For example, a study by Abisambra *et al*., (2010) demonstrated the fundamental importance of the ability of Hsp27 to be phosphorylated by analysing pseudo-phosphorylated Hsp27 in hippocampal neurons. This study showed a decrease in long-term potentiation and an increase in soluble tau intermediates, suggesting that the dynamic phosphorylation of Hsp27 is vital to its role in tau regulation in neurodegenerative diseases (Abisambra *et al*., 2010).

1.8.4. Chaperoning activity of Hsp27

The classic chaperoning action of Hsp27 is possibly the most documented of the cellular roles of Hsp27. When organised into large oligomers of up to 800kDa,

Hsp27 acts as a co-chaperone to Hsp70, an ATP-dependent chaperone which re-folds misfolded proteins or sends them for degradation by the proteosome (Parcellier 2006). Hsp27 is an ATP-independent holdase, binding mis-folded or unfolded proteins via the Hsp27 α-crystallin domain, securing the protein to prevent aggregation and presenting the proteins to Hsp70 (Rogalla *et al*., 1999). Thus, Hsp27 does not have an ATPase domain, making its chaperoning activity reliant on the presence of Hsp70 as Hsp27 cannot actively refold proteins. As a chaperone holdase, and independent of Hsp70, Hsp27 has been shown to abolish the toxicity of Aβ aggregates in mouse models of Alzheimer's disease, possibly by sequestering toxic oligomers into large, non-toxic aggregates, or plaques (Ojha *et al*., 2011). The cytoprotective effects of Hsp27 and Hsp70 are vital for in the cellular response to stress, and inducing levels of the two proteins protects against injury-induced apoptosis in neuronal studies (Franklin *et al*., 2005; Latchman, 2005; Kong *et al*., 2011). Although Hsp27 functions separately from Hsp70 in many of its roles, the maximal cytoprotective effect of Hsp27 is dependent on Hsp70 (Sreedharan *et al*., 2011).

1.8.5. Hsp27 can act as an inhibitor of apoptosis

Hsp27 has an active role in the modulation of apoptotic pathways by interacting with components of the intrinsic pathway of the apoptotic cascade at several points. The intrinsic, mitochondrial pathway of apoptosis involves the activation of the caspase cascade through mitochondria. Hsp27 mediates the release and action of cytochrome *c* via N-terminus binding, inhibiting the formation of the apoptosome and activation of procaspase-9 (Bruey *et al*., 2000; Garrido *et al*., 1999). Hsp27 also inhibits the extrinsic apoptotic pathway mediated by Daxx (Charette *et al*., 2000). Daxx, a death-domain associated protein, interacts with Fas, an apoptosis antigen and a key regulator of cell death, initiating the extrinsic pathway leading to activation

of caspase-8, which in turn activates downstream caspases (Charette *et al*., 2000). Daxx is only inhibited by phosphorylated Hsp27, which suggests that this is a protective function of Hsp27 during stress and cellular differentiation (Charette *et al*., 2000). The inhibitory effects of Hsp27 on apoptotic pathways demonstrate its importance in cell survival.

1.8.6. Hsp27 contributes to the maintenance of the normal redox balance

Hsp27 can be protective in conditions of oxidative stress, both directly and indirectly, and has been shown to decrease the basal levels of reactive oxygen species (ROS) and up regulate glutathione (Arrigo *et al*., 2005). This is particularly important in peripheral neurons, as the high-energy demands of motoneurons means that cells will be exposed to increased levels of intracellular oxidative stress over time (Lewinski and Keller, 2005). The actions of Hsp27 on levels of glutathione are thought to be mediated through the modulation of several pathways, both as a downstream effect of Hsp27 action on other cellular functions and through direct interactions with redox modulators such as Glucose-6-phosphate dehydrogenase, a key enzyme in the reducing state of glutathione (Pandolfi *et al*., 1995; Préville *et al*., 1999). When ROS increases, Hsp27 keeps glutathione in a reduced state, maintaining intracellular glutathione balance (Arrigo *et al*., 2005). Thus, impairments in Hsp27 can also lead to accumulations of toxic ROS products.

1.8.7. Hsp27 aids mitochondrial function

As already discussed, Hsp27 plays an important role in the reduction of harmful ROS and the inhibition of apoptotic signals, but Hsp27 also aids in the maintenance of mitochondrial function and morphology, where a decrease in Hsp27 expression leads to reduced ATP production and increased mitochondrial fragmentation (Tang *et al*., 2011). Hsp27 acts as a downstream mediator of High-mobility group box-1

(HMGB1), an essential regulator of mitochondrial autophagy (Tang *et al*., 2011). Knockdown of either HMGB1 or Hsp27 results in a cellular phenotype consistent with a decrease in mitophagy, as demonstrated by increased mitochondrial fragmentation and loss of ATP production (Tang *et al*., 2011). These authors suggest that the role of phosphorylated Hsp27 as a cytoskeletal regulator maybe critical for the trafficking which takes place during mitophagy as actin and mitochondria co-localise during stress. Furthermore, Hsp27 phosphorylation is also necessary for Hsp27-mediated autophagy (Tang *et al*., 2011).

Mitochondria are very sensitive to changes in the cellular environment and changes in mitochondrial function are one of the first signs of motoneuron distress in models of ALS (Bilsland *et al*., 2008). Thus the role Hsp27 plays in the maintenance of mitochondria maybe of particular importance in high-energy cells such as motoneurons.

1.8.8. Hsp27 protects the cytoskeleton during cell stress and has a putative role in axonal transport

Motoneurons differ from other cell types in length and unique large size, placing a heavy reliance on the cytoskeleton and axonal transport (Sau *et al*., 2011). The axonal cytoskeleton and transport are finely regulated and disruptions, for example caused by genetic mutations in essential proteins, can result in axonal degeneration (Gunawardena and Goldstein, 2004). The phosphorylated form of Hsp27 also plays a role in the survival of injured motor and sensory neurons (Benn *et al*., 2002; Kalmar *et al*., 2002). This may be due, in part, to the actions and effects of phosphorylated Hsp27 on components of the cytoskeleton which may then impact on axonal outgrowth and cellular transport (Benn *et al*., 2002; Mounier and Arrigo, 2002; Williams *et al*., 2005).

1.8.8.1. Hsp27 interacts with cytoskeletal elements

Miron *et al*. first described a functional link between Hsp27 and actin in 1991, demonstrating that Hsp27 inhibited actin polymerisation *in vitro* (Miron *et al*., 1991). Then, in 1994, Benndorf *et al*., showed that Hsp27 played a role as an actin-capping protein when phosphorylated, monomeric Hsp27 inhibits actin polymerisation by binding to the barbed end of the actin filament, decreasing the activity of the actin binding, inhibiting polymerisation and promoting stability of actin microfilaments during heat-shock and other cell stressors (Lavoie *et al*., 1993b)(Benndorf 1994). Hsp27 has also been shown to protect against aggregation of heat-denatured F-actin, binding the dissociated oligomers into highly soluble complexes during heat shock (Pivovarova *et al*., 2005; Pivovarova *et al*., 2007). Under normal physiological conditions in *in vitro* cell development, Hsp27 co-localises with actin in lamellipodia, processes and growth cones, with atypical growth patterns in cells with inhibited Hsp27 phosphorylation, suggesting an important role in modulation of actin dynamics and neurite outgrowth under normal conditions (Williams *et al*., 2005; Williams *et al*., 2006).

As well as the functional interaction of Hsp27 with actin described above, the small heat shock protein has also been found to co localise with other elements of the cytoskeleton *in vitro*, including possible interactions between Hsp27 and glial fibrillary acidic protein and vimentin intermediate filament networks (Perng *et al*., 1999). Hsp27 has been linked with the management of some interactions between intermediate filaments and their binding partners, maintaining cytoskeletal integrity (Perng *et al*., 1999). Hsp27 also co localises with β-tubulin, although the proteins have not been seen to functionally interact, at least *in vitro* (Hino *et al*., 2000; Williams *et al*., 2006).

1.8.8.2. Hsp27 and axonal transport

A link between the disruption in axonal transport and mutations in Hsp27 has been shown by the mislocalisation and aggregation of p150, a dynactin subunit which is integral in retrograde transport, in cells transfected with mutant Hsp27 (Ackerley *et al*., 2006). Transgenic mice expressing disease-causing Hsp27 mutations also display significant defects in mitochondrial transport, at least in sensory neurons (d' Ydewalle *et al*., 2011). The integrity of the cytoskeleton and axonal transport is dependent on actin, which functionally interacts with Hsp27 both in basal and stressed conditions (Williams *et al*., 2005). For example, during cell stress, Hsp27 acts as an actin-capping protein increasing the stability of actin microfilaments (Benndorf *et al*., 1994). The length and calibre of motoneurons, and therefore axonal transport, is dependent on the cytoskeleton, which not only maintains spatial organisation, but also drives axonal growth and is fundamental for axonal transport (Chevalier-Larsen and Holzbaur, 2006). Taken together, this suggests that mutations in Hsp27 would have a significant impact on the cytoskeleton and axonal transport, two cellular features where motoneurons are particularly vulnerable to disruptions (Shaw and Eggett, 2000).

1.8.9. The role of Hsp27 in the nucleus

During stress, Hsp27 translocates to the nucleus, where its role is unclear, although it is thought to act by targeting proteins for degradation (Bryantsev *et al*., 2002; Bryantsev *et al*., 2007a). This is due the role phosphorylated Hsp27 plays in mediating mRNA decay by stabilising AU-rich element (ARE) mRNA via modulation of ARE-binding protein (AUF1) levels, as well as the localisation of Hsp27 in the nucleus into granules, which localise with chromatin and the 20S proteosomes, thereby suggesting storage of misfolded proteins for degradation rather than refolding via Hsp70 (Bryantsev *et al*., 2007; Knapinska *et al*., 2011). These nuclear

granules are more commonly called nuclear splicing speckles or SC35-positive speckles as they contain SC35, a member of the serine/arginine rich (SR) family of mRNA splicing proteins (Graveley, 2000). Hsp27 has been shown to translocate to SC35-positive speckles *in vitro* and may be driven by the N-terminus of Hsp27 (Bryantsev *et al*., 2007; Vos *et al*., 2009). Other small heat shock proteins also translocate into the nucleus to SC35-positive speckles, including HSPB7 and αB-crystallin (van den IJssel *et al*., 2003; Vos *et al*., 2009). The nuclear speckle localisation of αB-crystallin is inhibited by mutations that cause cardiomyopathy (van den IJssel *et al*., 2003).

As well as its association with nuclear speckles, Hsp27 has also been linked to activation of gene transcription of neurotrophic receptor genes by interaction with SP1, a gene transcription factor, modulating SP1-dependent transcriptional activity and promoting neuronal protection via upregulation of neurotrophic receptors in a mouse model of spinocerebellar ataxia 17 (Friedman *et al*., 2009). In the nucleus, Hsp27 has also been implicated in the modulation of HSF1 activity by sumoylation, blocking HSF1s transactivation capacity and therefore inhibiting and modulating processes of the HSR (Brunet Simioni *et al*., 2009). Clearly, the roles of Hsp27 in the nucleus are not fully elucidated, and there is an interesting overlap of localisation with other small heat shock proteins, but not with Hsp70, suggesting that the nuclear role of Hsp27 is not a traditional chaperoning role (van den IJssel *et al*., 2003; Bryantsev *et al*., 2007; Vos *et al*., 2009).

1.8.10. Hsp27 in neurodegenerative disease

Hsp27 has been implicated in several neurodegenerative diseases as a protein which may contribute to disease pathogenesis as it is a member of the HSR and is affected downstream of many pathological processes. For example, Hsp27

expression is decreased in neurodegenerative diseases such as Amyotrophic Lateral Sclerosis (ALS) and Spinocerebellar ataxia (Sharp *et al*., 2008; Okado-Matsumoto and Fridovich, 2002; Tsai *et al*., 2005). Hsp27 is also associated with many pathological hallmarks of neurodegenerative diseases such as amyloid-β plaques in Alzheimer's disease (Smith *et al*., 2005). Due to the versatility of Hsp27 functions, its importance in the HSR and its ubiquitous presence in all cell types, it is surprising that mutations appear to only result in a peripheral axon-specific clinical phenotype and affects motoneurons to a greater extent than other neurons.

1.9. Hsp27 mutations cause CMT 2F and dHMN II

As described in Section 1.2, hereditary peripheral neuropathies can be classified into several subgroups according to clinical phenotype, neurophysiology and genetic cause. CMT 2F was first described in 2001 when Ismailov *et al.* linked a novel locus on chromosome 7q11-q21 to an autosomal dominant Russian CMT2 family of 6 generations (Ismailov *et al*., 2001). Affected members of the family showed a similar clinical presentation, with an age of disease onset ranging between 15 and 25 years. A symmetrical, slowly progressive muscle weakness and atrophy was described, starting in the lower limbs and advancing to the upper limbs after several years, resulting in significant disability within 15 to 30 years of onset. The disease was predominantly of a motor presentation (Ismailov *et al*., 2001). Three years later in 2004, Evgrafov *et al.* reported a missense mutation in the *HSPB1* gene coding for Hsp27 in this family, and 4 other novel mutations within *HSPB1* causing CMT 2F or dHMN in 6 unrelated families from different populations (Evgrafov *et al*., 2004).

Since the initial description of these Hsp27 mutations, several more mutations have been identified in patients with CMT from different populations (See Table 1.5). The Arg127Trp mutation, discovered in a Belgian family by Evgrafov *et al.* (Evgrafov *et*

al., 2004) has also been identified in Chinese patients (Tang *et al*., 2005), and novel mutations have been found in Japanese, Italian, English, Korean, Indian and Pakistani families (Ikeda *et al*., 2009; James *et al*., 2008; Kijima *et al*., 2005; Solla *et al*., 2010; Chung *et al*., 2008; Benedetti *et al*., 2010; Luigetti *et al*., 2010; Mandich *et al*., 2010). In 2008, Houlden *et al.* discovered a wide range of novel Hsp27 mutations in different families that give rise to dHMN and CMT 2F (Houlden *et al*., 2008). The disease-causing Hsp27 mutations identified to date are shown in Table 1.3. The disorder caused by Hsp27 mutations is classified as either dHMN or CMT 2F depending on the level of sensory disturbance detected on clinical examination. When first described, it was thought that these were two separate disorders caused by mutations within the same gene. However, in 2010, Solla *et al.* reported a family carrying the autosomal dominant mutation Arg127Trp, which showed a varied amount of sensory involvement but comparable ages of onset and motor signs (Solla *et al*., 2010). This suggests that the sensory deficits in CMT 2F are part of a disease spectrum, with no or minimal to moderate sensory involvement.

1.10. The cellular effects of Hsp27 mutations

Since the discovery of the first disease-causing Hsp27 mutation, there have been efforts to clarify which of the many cellular functions of Hsp27 are affected by the mutations. The first paper to describe Hsp27 mutations in 2004 also showed preliminary experiments describing the effects of the most clinically prevalent mutation *in vitro* (Evgrafov *et al*., 2004). A neuronal-like cell line (N2A) was transfected with the Ser135Phe mutation and a biochemical MTT assay was used to

Table 1.5 Disease-causing Hsp27 mutations

Mutations in Hsp27 were first described by Evgrafov *et al.* in 2004. Since then, a wide range of novel mutations have been described in many populations. The mutations examined in this Thesis are highlighted in blue.

Table 1.5 Disease-causing Hsp27 mutations

Diagnosis	Nucleotide Change	Amino Acid Change	Protein Domain Affected	Inheritance	Age of Onset	Origin	Reference
dHMN	C116T	Pro39Leu	Conserved, not in α-crystallin	Autosomal Dominant	54	English	(Houlden *et al*., 2008)
Asymmetrical dHMN	G250C	Gly84Arg	Conserved not in α-crystallin	Autosomal Dominant	48	English	(Houlden *et al*., 2008) (James *et al*., 2008)
dHMN	C295A	Leu99Met	α-crystallin	Autosomal Recessive	37	Pakistan	(Houlden *et al*., 2008)
dHMN CMT 2F	C379T	Arg127Trp	α-crystallin	Autosomal Dominant	33	Belgium, China, Italy	(Solla *et al*., 2010) (Evgrafov *et al*., 2004) (Tang *et al*., 2005)
dHMN CMT 2F	C404T	Ser135Phe	α-crystallin	Autosomal Dominant	21	UK, Russia, Korea	(Evgrafov *et al*., 2004) (Houlden *et al*., 2008) (Chung *et al*., 2008)
CMT 2F	C404G	Ser135Cys	α-crystallin	Autosomal Dominant	35	Italy	(Benedetti *et al*., 2010a)
CMT 2F	C406T	Arg136Trp	α-crystallin	Autosomal Dominant	_	Belgium	(Evgrafov *et al*., 2004)
dHMN	C418T	Arg140Gly	α-crystallin	Autosomal Dominant	34	India	(Houlden *et al*., 2008)
dHMN	A421C	Lys141Gln	α-crystallin	Autosomal Dominant	57	Japan	(Ikeda *et al*., 2009)
dHMN	C452T	Thr151Ile	α-crystallin	Autosomal Dominant	_	Croatia	(Evgrafov *et al*., 2004)
dHMN CMT 2F	C539T	Thr180Ile	not in α-crystallin	Autosomal Dominant	7	Italy	(Luigetti *et al*., 2010)
dHMN	C545T	Pro182Leu	not in α-crystallin	Autosomal Dominant	_	Austria	(Evgrafov *et al*., 2004)
dHMN	C544T	Pro182Ser	not in α-crystallin	Autosomal Dominant	4	Japan	(Kijima *et al*., 2005a)
dHMN CMT 2F	476_477delCT	Ser158X	not in α-crystallin	Autosomal Dominant	_	Italy	(Mandich *et al*., 2010)

assess cell viability. These experiments demonstrated a 50% decrease in cell viability and transfection with the mutation in comparison to untransfected cells at 48 hours, demonstrating that this mutation is indeed pathogenic (Evgrafov *et al*., 2004). Evgrafov *et al* then transfected neurofilament light (NF-L) and wild type or mutant Hsp27 *in vitro* and showed aggregates containing both NF-L and Hsp27 in cells transfected with the Ser135Phe mutant Hsp27, but not with the wild type Hsp27 (Evgrafov *et al*., 2004), suggesting a possible toxic interaction between the mutant Hsp27 and NF-L.

These findings were followed up in a study by Zhai *et al.* (2007) who also co-expressed NF-L proteins with Hsp27, this time working with mutations of both proteins known to cause CMT 2E/1F and CMT 2F, respectively. Mutations in NF-L cause a motor and sensory neuropathy with evidence of central nervous involvement in some patients (Miltenberger-Miltenyi *et al*., 2007; Mersiyanova *et al*., 2000; Jordanova *et al*., 2003; See Table 1.1 and 1.2). CMT 2E/1F, like CMT 2F, demonstrates a clinical heterogeneity in age of onset and disease severity and progression that has not yet been linked to mutation type using a genotype/ phenotype correlation (Miltenberger-Miltenyi *et al*., 2007). Zhai *et al.* (2007) demonstrated an interaction between NF-L and Hsp27 in several ways, firstly by showing that the transfection of wild type Hsp27 into cells transfected with mutated NF-L diminished the aggregation of the NF-L protein and increased motoneuron viability and secondly, by transfecting mutant Hsp27 it was possible to disrupt the filamentous network caused by the transfection of wild type NF-L *in vitro,* giving large aggregates containing both NF-L and mutant Hsp27 (Zhai *et al*., 2007). Thus, while wild type Hsp27 can improve cell pathology induced by mutant NF-L, wild type NF-L cannot rescue mutant Hsp27 induced cell pathology.

Therefore, it appears that there is a functional relationship between Hsp27 and neurofilaments, and that for normal function of the neuronal cytoskeletal, both proteins have to function normally. On the other hand, disruption in the conformation of either neurofilament or Hsp27 leads to the dysfunction and aggregation of the other. Ackerley *et al* (2006), using a mutation located in a different domain of the Hsp27 protein (Pro182Leu), examined the assembly of neurofilaments and the effect of Hsp27 on neurofilament aggregation and specific motor proteins (Ackerley *et al*., 2006). These experiments, which involved transfection of primary mouse cortical neurons, demonstrated the aggregation of both neurofilament medium (NFM) and transfected p150 (a subunit of dynactin, an interegral protein of retrograde axonal transport) in the presence of the mutated Hsp27, but not in the presence of wild type Hsp27. The authors postulated that the mutated protein could not be transported along cellular neurites, as it was only detected in the cell body and proximal neurites, unlike the wild type transfected protein (Ackerley *et al*., 2006).

More recently, the focus of the effects of mutant Hsp27 on peripheral neurons shifted to the putative role in microtubules and axonal integrity. In 2011, d'Ydewalle *et al*., published two transgenic mouse lines expressing human Hsp27 carrying either one of two known patient mutations; Ser135Phe or Pro182Leu (d' Ydewalle *et al*., 2011). This study demonstrated that the expression of either mutation caused differential neuronal phenotypes, with the C-terminus Pro182Leu Hsp27 causing a more severe, motor phenotype and the α-crystallin Ser135Phe Hsp27 mouse displaying a mixed sensory-motor phenotype (d' Ydewalle *et al*., 2011). They also showed that the expression of both mutations *in vivo* led to the de-acetylation of α-tubulin, a component of the microtubule network, and that inhibition of histone de-acetylase 6 (HDAC6), a major de-acetylation enzyme of the tubulin network restored

the amount of α-tubulin acetylation and rescued disease phenotype (d' Ydewalle *et al*., 2011). The study claimed that different sub-types of neuron were more vulnerable to different mutations in Hsp27, suggesting underlying differences of disease phenotype and clinical presentation are linked to mutation position, and that the pathogenic mechanism of axonal degeneration in CMT 2F involves the de-acetylation of α-tubulin, a component of the microtubule network (d' Ydewalle *et al*., 2011).

Although the widely accepted theory for the aberrant functions of Hsp27 mutations is that of a disruption of axonal transport, as supported above, a recent paper by Almeida-Souza *et al.* (2010) suggests that the Ser135Phe mutation, the most prevalent and the most studied Hsp27 mutation, leads to an increase in the chaperoning function of the protein and a shift in the oligomerisation balance of the protein towards increased Hsp27 monomerisation (Almeida-Souza *et al*., 2010). Surprisingly the same study did not find an increase in phosphorylation of Hsp27 in mutant cells. This is intriguing since the oligomerisation state of Hsp27 depends on its level of phosphorylation (See Section 1.8.2).

Although possible aberrant interactions between Hsp27 and intermediate filament or microtubule proteins have been described (Evgrafov *et al*., 2004; Zhai *et al*., 2007; Ackerley *et al*., 2006; d' Ydewalle *et al*., 2011), there is little evidence for an interaction between these proteins under unstressed conditions *in vivo*, although Hsp27 has been shown to functionally interact with actin (Perng *et al*., 1999; Kostenko *et al*., 2009; Williams *et al*., 2005). Thus any association observed between neurofilaments or microtubules and Hsp27 may be a result of a gain of function of the mutant Hsp27 (Toivola *et al*., 2010; d' Ydewalle *et al*., 2011). To summarise, the results from *in vitro* studies examining the cellular effects of mutant

Hsp27 indicates strong histological evidence for the involvement of mutant Hsp27 in cytoskeletal stability and axonal transport. Disruptions in these vital cellular functions may explain the specific clinical phenotype of dHMN.

1.11. Characteristics of individual Hsp27 mutations

Since the first description of CMT-causing Hsp27 mutations (Evgrafov *et al*., 2004), a number of other mutations have been found in the gene (Figure 1.4). It appears that within *HSPB1* there is at least one 'hot spot' where clusters of mutations have been discovered in different populations. This hot spot is located within exon two of the *HSPB1* gene and corresponds to the highly conserved α-crystallin domain of the Hsp27 protein between amino acids 127 and 158, a region which not only contains the highest frequency of mutations, but also the most prevalent mutations in all populations and multiple families (Dierick *et al*., 2005). Outside of this hot spot region of the gene, mutations are less commonly seen in the highly conserved N-terminus and less well conserved C-terminus of the protein.

Since the functional versatility of Hsp27 is linked to different regions of the protein, it is possible that there are fundamental differences in the cellular effects of mutations located at different points within the *HSPB1* gene. To investigate this hypothesis in the experiments described in this Thesis, different mutations were chosen for the study based on the following individual characteristics:

- **Ser135Phe** is a dominant mutation located in the hot-spot of the *HSPB1* gene. The Ser135Phe mutation is a base change of a C to a T at position 404, causing an amino acid change in the α-crystallin domain of the protein of a Serine to a Phenylalanine. Serine is a polar, neutral (balanced charge side chains) amino acid and is one of three that are commonly

Figure 1.4

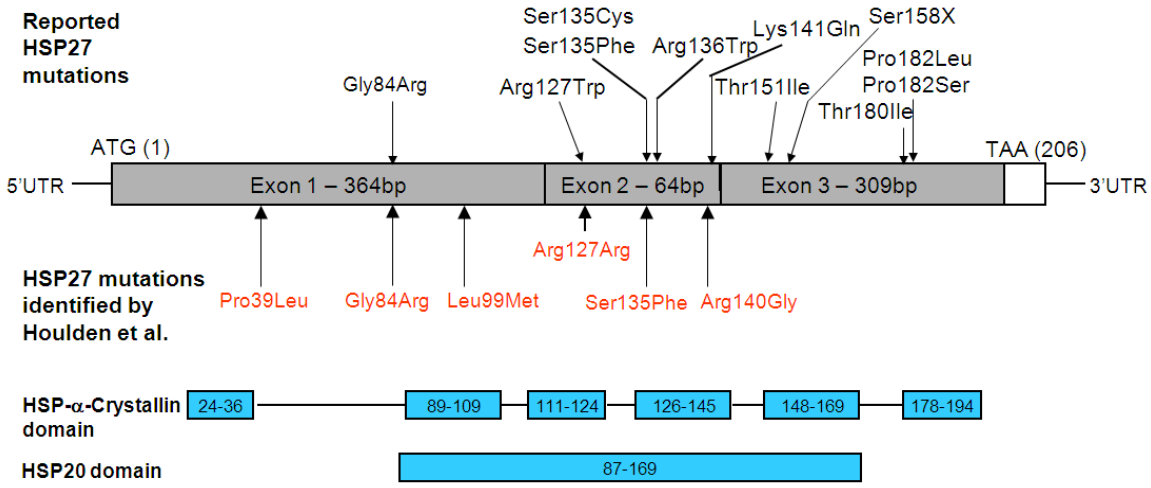

Figure 1.4 Location of known mutations in the Hsp27 (*HSPB1*) gene

The start ATG (codon 1) is indicated in the Figure and all mutations are labeled from this codon up to the stop codon TAA at position 206. Previously reported Hsp27 mutations and the mutations identified by Houlden *et al.* (2008) are indicated in red. The position of these mutations is shown in relation to the α-Crystallin and the Hsp20 domains which are drawn to scale in blue.

phosphorylated. Phenyalanine is a non-polar, neutral amino acid. Ser135Phe is the most prevalent mutation of *HSPB1* causing CMT 2F or dHMN II. Due to the prevalence of the mutation in the population of affected individual patients and the large number of families with this mutation, Ser135Phe is to date the most investigated of the *HSPB1* mutations (Evgrafov *et al*., 2004) and therefore is used in this study as a 'positive' control.

- **Arg140Gly** is a dominant mutation located in the hot-spot of the *HSPB1* gene. The Arg140Gly mutation is a base change of a C to a T at position 418, causing an amino acid change from an Arginine to a Glycine. Arginine is a polar, positively charged amino acid. Glycine is non-polar and neutral. Arg140Gly is a novel mutation found in 3 separate families (Houlden *et al*., 2008), which functionally corresponds to disease-causing mutations in the related sHSP α-crystallin proteins; α-A Crystallin (Arg116Cys mutation causing dominant congenital cataracts)(Li *et al*., 2010) and α-B Crystallin (Arg120Gly mutation causing desmin-related myopathy) (Inagaki *et al*., 2006).
- **Leu99Met** is a recessive mutation located in the α-crystallin domain of the Hsp27 protein. The Leu99Met mutation is a base change of a C to an A at position 295, causing an amino acid change from Leucine to a Methionine. Leucine and Methionine are both non-polar, neutral amino acids. Leu99Met is the only recessive mutation discovered in the *HSPB1* gene, but can only be classed as 'assumed recessive' as there was no genetic testing on maternal DNA (Houlden *et al*., 2008).
- **Pro39Leu** is a dominant mutation located in an area of the gene translating to the N-terminus of the protein. The Pro39Leu mutation is a base change of a C to a T at position 116, causing an amino acid change from Proline to a Leucine. Proline and Leucine are both non-polar, neutral amino acids.

Pro39Leu is a novel mutation in a single family with a later age of onset (Table 1.3) but the same clinical diagnosis.

1.12. Aims

Mutations within Hsp27 give rise to both CMT 2F and dHMN II, presenting clinically with a specific phenotype of axonal degeneration of long motoneurons over an extended period of time. Hsp27 has many roles within the cell, and each of these roles utilise different domains of the protein in different pathways. Hsp27 can also be phosphorylated, dynamically modifying the state of association with itself and other sHSPs and thus the roles of Hsp27 within the cell dependent on the cellular environment and activation of the HSR. Due to the varied roles and protein interactions of Hsp27, it is possible that there are fundamental differences in the cellular manifestation of pathology between different disease-causing mutations and that motoneurons are specifically vulnerable to the mutations because of their high metabolic load, an active balance of ions and an increased dependency on axonal transport and cytoskeletal stability.

The aims of this Thesis are therefore –

1. To optimise two *in vitro* cellular models based on a neuronal-like neuroblastoma cell line and primary motoneurons using different transfection techniques, thereby creating cellular systems that can reliably be used for sensitive readouts of cellular function and morphology. *In vitro* models are important tools to examine proposed cellular mechanisms which may be disrupted by the abnormal functioning of mutated Hsp27.
2. To study the cellular phenotypes of the different mutations within Hsp27 using readouts of cell toxicity, neurite outgrowth, cellular morphological changes and Hsp27 protein interactions, teasing out whether there are

fundamental differences in the manifestation of cellular pathology between disease causing mutations.

3. To examine of the pathomechanisms of specific mutations using refined methods of analysis, examining the effects of Hsp27 mutations on cellular functions. These investigations will focus on functions which are linked to Hsp27 and fundamental to the homeostatic balance of the cell, for example, mitochondrial function.

The aim of the experiments described in this Thesis are therefore to examine the deleterious effects of mutations in heat shock protein 27, in order to improve our understanding of the cellular pathomechanisms of mutant Hsp27-linked CMT.

Chapter 2. Materials and Methods

2.1. Generation of constructs containing mutant Hsp27

HSPB1 mutations were generated using pcDNA3.1/V5-His TOPO plasmids (*Invitrogen, Paisley, UK*, Figure 2.1) containing wild type Hsp27 as a template for site-directed mutagenesis. The Hsp27 mutations investigated in this study were: Pro39Leu; Leu99Met; Ser135Phe and Arg140Gly (See Table 1.3).

2.1.1. Site-directed mutagenesis primer design

Mutagenic oligonucleotide primers were individually designed using the *Ensembl project* (http://www.ensembl.org) & *PrimerX* (http://www.bioinformatics.org/primerx/), an online program which specifically generates primers for site-directed mutagenesis. Selected sequences were then ordered from *Sigma Genosys (Dorset, UK)*. Site-directed mutagenesis primers contained the 12-15 base pair sequences forward and backwards from the desired mutation and were complimentary sequences. Primers were between 25-30 base pairs long, with a melting temperature of ≥ 77°C and a minimum GC content of 40%. Three pairs of primers were designed with the sequences shown in Table 2.1.

Table 2.1

Mutation	Sequence (5'-3')	Sequence length (base pairs)	GC content (%)	Melting temperature (°C)
C116T Pro39Leu	CTG CCC CGG CTG CTG GAG GAG TGG TCG	27	74	85.3
C295A Leu99Met	CTG GCG CGT GTC CAT GGA TGT CAA CCA C	28	61	82.2
C418G Arg140Gly	CGG TGC TTC ACG GGG AAA TAC ACG C	25	60	77.4

Table 2.1 Site-directed mutagenesis primers.

Primers were designed to be optimal for site-directed mutagenesis. Details include sequence length, GC content and melting temperature.

Figure 2.1

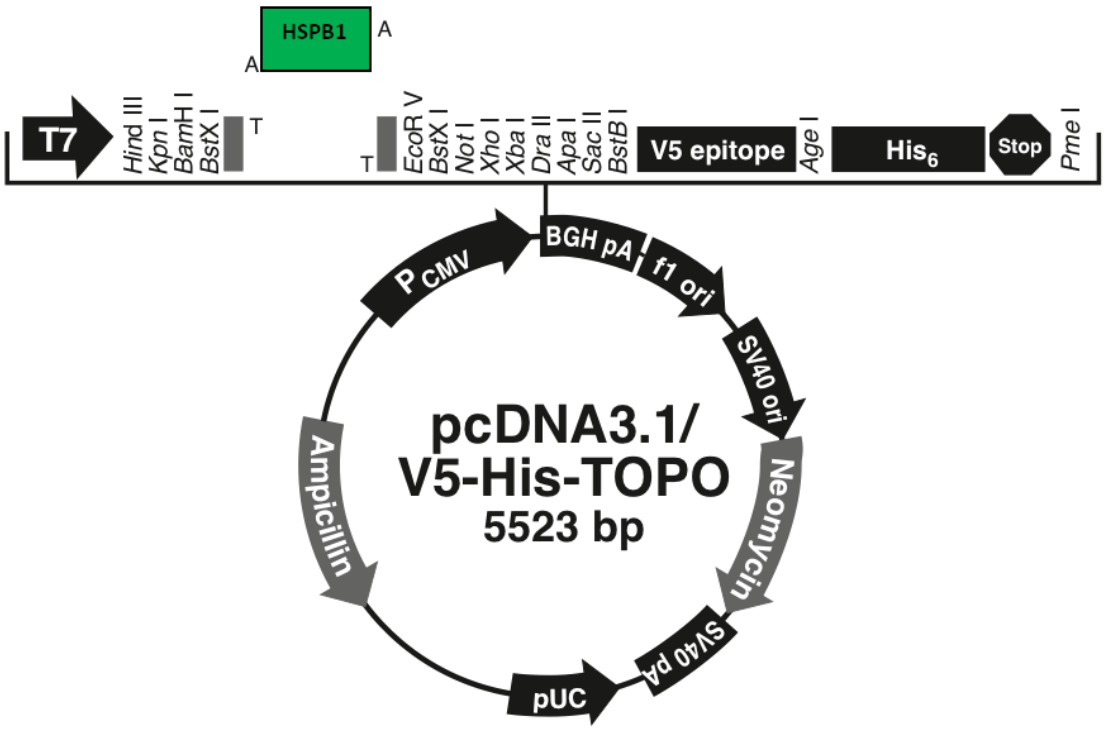

Figure 2.1 pcDNA3.1/V5-His-TOPO Vector Map

Showing the pcDNA3.1/V5 plasmid and open reading frame with restriction sites and recognition tags. Schematic adapted from *Invitrogen*, http://products.invitrogen.com/ivgn/product/K480001

2.1.2. *In vitro* site-directed mutagenesis and transformation

Primers were diluted to a stock solution of 100µM, and then further diluted to give a final working primer content of 125ng in the PCR mix. The mutagenesis reaction (Site-directed mutagenesis kit, Stratagene, La Jolla, CA, USA) was carried out using the reaction mixture detailed below in Section 2.1.2.1, and a reaction with 16 annealing cycles was initiated (see Section 2.1.2.1). To control for the presence of PCR products, samples were run out on a 2% agarose electrophoresis gel (*Sigma Genosys, Dorset, UK*) in TBE buffer (*Invitrogen, Paisley, UK*).

The PCR product was then incubated with 1µl Dpn1 for 4 hours at 37°C. For the transformation of E. coli cells using the mutagenesis PCR product, One Shot® TOP10 Chemically competent E. coli (Invitrogen, Paisley, UK) were gently thawed on ice and 50µl aliquoted into pre-chilled 14ml BD Falcon polypropylene round-bottomed tubes (BD Biosciences, Oxford, UK). Dpn1-treated DNA (3µl) was added to the cells and carefully swirled to mix; the reactions were then incubated on ice for 30 minutes. Cells were heat-pulsed in a water bath for 30-45 seconds at 42°C and incubated on ice for a further 2-5 minutes. The cells were gently transferred to Eppendorf tubes containing 500µl of room-temperature S.O.C medium (Invitrogen, Paisley, UK) and incubated at 37°C for 1 hour in a table-top shaker at 1400rpm. The reaction was then spun down for 1 minute at 13200rpm and the pellet was resuspended in 50µl of S.O.C medium and plated onto LB agar plates which were prepared the day before transformation using LB Agar Amp IPTG/X-Gal (Fermentas, Life Sciences, York, UK). The transformation plates were incubated at 37°C for >16 hours.

2.1.2.1. Mutagenesis reaction and cycling parameters

The reaction mixture used for the mutagenesis reaction and the cycling parameters are summarised below;

Reaction mixture

40µl dH_2O (final volume 50µl)

5µl 10x reaction buffer

1µl (125ng) primer Forward

1µl (125ng) primer Reverse

1µl dNTP mix

1µl 50ng Plasmid template

1µl *PfuUltra* HF DNA polymerase

Cycling parameters for site-directed mutagenesis

Segment	**Cycles**	**Temperature (°C)**	**Time**
1	1	95	30 seconds
2	2 – 18	95 55 68	30 seconds 1 minute 1 minute/kb of plasmid length
3	19	4	Hold

2.1.3. Hsp27 PCR and sequencing primer design

PCR primers used in both the amplification of a specific length of the genomic DNA sequence and further sequencing were designed using *Ensembl* and *PrimerX*. Selected sequences were then ordered from *Sigma Genosys*. Primers were between 15-25 base pairs long, with a melting temperature of ≥55°C and GC

content of between 40-70%. Two forward and two reverse primers were designed to give different fragments of the *HSPB1* gene. The sequences used are shown in Table 2.2.

2.1.4. Hsp27 PCR

Individual colonies from transformed One Shot® TOP10 cells on the transformation plates were sampled and subcultured by collecting a small amount of the colony with a sterilized 1-10µl pipette tip, streaking a separate LB agar plate, and inoculating 5µl aliquots of dH_2O using the same pipette tip.

A PCR reaction was used to amplify the targeted sequences of Hsp27 to confirm the presence of full length Hsp27. PCRs were carried out in thin-walled PCR tubes using the reaction mixture and protocol shown below (see Section 2.1.4.1). DNA-negative and positive controls were used in all reactions.

Bands were separated and analysed by gel electrophoresis. Agarose powder (1g) was added to 50mls 10% TBE buffer and heated in a microwave on medium heat until dissolved to create a 2% gel. Ethidium bromide (5µl, *Sigma Genosys, Dorset, UK*) was added to the solution for band visualisation and the slightly cooled solution was poured into a gel mould.

PCR product (5µl) was mixed with 5µl of Blue Juice loading dye (added to visualise the PCR product) and all 10µl was added to the wells. A 1Kb ladder was also added at the start of the gel. The PCR products were run at 75V for 25 minutes and visualised under ultraviolet light and a picture was taken.

Table 2.2

Primer	Sequence	Sequence length (base pairs)	GC content (%)	Melting temperature (°C)
Hsp27 Forward (long)	ATA GCC GCC TCT TCG ACC AG	20	60	67.6
Hsp27 Forward (short)	TGT CCC TGG ATG TCA ACC	18	56	62.1
Hsp27 Reverse (long)	ACT TGG CGG CAG TCT CAT C	19	58	65.5
Hsp27 Reverse (short)	ACA GGG AGG AGG AAA CTT G	19	53	60.7

Table 2.2 PCR primer pairs designed for Hsp27

Primers were designed to be optimal for PCR. Details include sequence length, GC content and melting temperature.

2.1.4.1. Hsp27 PCR reaction and cycling parameters

The reaction mixture and cycling parameters for Hsp27 PCR are summarised below;

Reaction mixture

15.65µl dH_2O (final volume 25µl)

2.5µl 10x reaction buffer

2.5µl Q Solution (*Qiagen, Crawley, UK*)

0.75µl $MgCl_2$

0.25µl (125ng) primer Forward (long)

0.25µl (125ng) primer Reverse (short)

0.5µl dNTP mix

2.0µl DNA

0.1µl Taq polymerase (*Roche, Welwyn, UK*)

Cycling parameters for Hsp27 PCR

Segment	**Cycles**	**Temperature (°C)**	**Time**
1	1	95	3 minutes
2	2 – 35	95 55 72	30 seconds 1 minute 45 seconds
3	36	72	2 minutes

2.1.5. DNA sequencing

The PCR product from the Hsp27 PCR from selected single colony templates (approximately 20µl) was purified using a vacuum filter, leaving the filtered DNA sequence which was reconstituted in 20µl dH_2O by rocking gently for 20 minutes.

The purified DNA was then added to the 2 sequencing reactions detailed below (see Section 2.1.5.1) using BigDye terminator v3.1 sequencing chemistry (Applied Biosystems, Foster City, CA, USA) and cycled using the cycling parameters outlined below.

The sequencing reaction was then cleaned using Millipore plates and the purified product was sequenced on an ABI3730 genetic analyser (Applied Biosystems) and analysed using Sequencher software (Genecodes).

2.1.5.1. DNA sequencing reaction and cycling parameters

The reaction mixture and cycling parameters for DNA sequencing are summarised below;

Reaction mixture

4.45µl dH_2O (final volume 10µl)

1.8µl Sequencing buffer

0.75µl Big Dye

1.0µl (3.2ng) primer Forward (long)/ Reverse (short)

2.0µl Purified DNA

Cycling parameters for DNA sequencing

Segment	Cycles	Temperature (°C)	Time
1	1	96	1 minute
2	2-26	96 50 60	10 seconds 5 seconds 4 minutes
3	27	4	Hold

2.1.6. Plasmid sequencing primer design

The whole pcDNA3.1/V5 plasmid and *HSPB1* gene were sequenced. For this, sequencing primers were designed using *Ensembl* and *PrimerX*. Selected sequences were then ordered from *Invitrogen*. Primers were between 20-30 base pairs long, with a melting temperature of ≥55°C and GC content of between 40-70%. Two forward and two reverse primers were designed to amplify components of the open reading frame of the plasmid. Sequences used are shown in Table 2.3.

In this study we also aimed to confirm that the plasmid containing the desired construct was still intact with all tags and restriction sites present. Plasmid sequencing was sent to Geneservice (UCL, UK) with custom primers (3.5 pmol/µl).

2.1.7. Maxi Preps for the production of large volumes of wild type and mutated plasmids

Once all plasmid constructs were generated and sequenced, large quantities were then produced for further experiments. A single colony was picked from the transformation plate and used to inoculate a starter culture of 2mls autoclaved LB broth (Sigma, Dorset, UK) containing 3µl/ml ampicillin. This was incubated for approximately 4 hours at 37°C, shaking at 300rpm. The starter culture (200µl) was diluted into 200mls of autoclaved LB Broth (with 3µl/ml ampicillin) in a flask with a volume at least 4 times the volume of the culture. This was grown up for 12-17 hours at 37°C, shaking at 300rpm.

DNA was purified using the Endofree Plasmid Maxi Kit (*Qiagen, Crawley, UK*), following the manufacturer's instructions. The bacterial cells were harvested by centrifugation at 6000g, at 4°C for 15 minutes. The bacterial pellet was then

resuspended in 10mls of buffer P1 until completely mixed and 10mls of buffer P2 was added and mixed thoroughly by vigorously inverting 4-6 times before incubating at room temperature. After 5 minutes, 10mls of pre-chilled buffer P3 was added to the lysate and immediately mixed by inverting 4-6 times. The lysate was then poured into a pre-prepared QIAfilter maxi cartridge and incubated for 10 minutes. To filter through the column, a plunger was slowly inserted into the tube and carefully pushed down, giving approximately 25mls of lysate in a 50ml Falcon tube. Buffer ER (2.5mls) was added to the filtered lysate and mixed by inverting the tube 10 times before incubating on ice for 30 minutes. During this time, a QIAGEN-tip 500 gravity-flow column was equilibrated by applying 10mls of buffer QBT. After 30 minutes, the filtered lysate was added to the column and allowed to flow due to gravity. The column was then washed with two applications of 30mls of buffer QC. The collection tube was then exchanged to endotoxin-free plasticware (Nalgene, *Thermo Fisher Scientific, Denmark*) and the DNA was eluted with 15mls buffer QN. To precipitate DNA from the buffer, 0.7x the volume of room temperature isopropanol (10.5mls) was added to the elute and immediately mixed and centrifuged at 15,000g for 30 minutes at 4°C. The supernatant was then carefully removed and the pellet of DNA was washed with 5mls of 70% ethanol to make the DNA easier to dissolve. This was then centrifuged at 15,000g for 10 minutes. The supernatant was removed and the pellet was left to air dry for 5-10 minutes. Finally, the pellet was re-dissolved in 50µl of TE buffer and DNA yield was determined via nanodrop.

Table 2.3

Primer	Sequence	Sequence length (base pairs)	GC content (%)	Melting temperature (°C)
Hsp27 end of gene F	AAA TCC GAT GAG ACT GCC	18	50	65
pcDNA3.1 TATA F	GGT GGG AGG TCT ATA TAA	18	44	62
Hsp27 at 759 R	TAC CAG TCG CGG AAG GGG TC	20	65	74
V5 Reverse	GAG AGG GTT AGG GAT AGG	18	55	67
V5 Forward	GTA AGC CTA TCC CTA ACC	18	50	65

Table 2.3 Sequencing primers designed for Hsp27

Primers were designed to be optimal for sequencing. Details include sequence length, GC content and melting temperature.

2.2. Culture of cell lines

Two cell lines were initially used in these experiments. Neuro-2A cells (N2A) derived from a neuroblastoma in an Albino strain A mouse, obtained from the *European Collection of Cell Cultures* (*ECACC*; Catalogue number 89121404), were maintained and grown in DMEM Glutamax medium (*Gibco, Paisley, UK*), containing 10% heat-inactivated Fetal Calf Serum (FCS), 10 IU/ml penicillin, 100 µg/ml streptomycin and 2mM L-glutamine. Cells were maintained at 37°C in a saturated humidity atmosphere of 95% air and 5% CO_2. N2A cells were passaged every 2-3 days depending on cell confluency (~80%).

SH-SY5Y cell lines (*ECACC*; Catalogue number 94030304) derived from female, human neuroblastoma cells were used for the majority of experiments described in this Thesis. Cells were grown in Dulbecco's modified Eagle's medium (DMEM-F12, *Gibco, Paisley, UK*) containing 15% FCS, 2mM L-glutamine, 10 IU/ml penicillin, 100 µg/ml streptomycin (P/S) and 1% final volume non-essential amino acids. Cells were maintained at 37°C in a saturated humidity atmosphere of 95% air and 5% CO_2 in an incubator. The SH-SY5Y cells were passaged every 3-5 days depending on cell confluency (~90%). To split the cells, the media was aspirated and replaced with 5mls PBS to wash the cells. Pre-warmed (37°C) trypsin (0.25%)-EDTA in HBSS (-Ca^{2+}/Mg^{2+}) (*Invitrogen)* was then added and the flask was placed in the incubator for ~40 seconds. When the flask was removed from the incubator, the cells were viewed under a microscope to assess the level of cell dissociation. If cells were still attached to the flask, mechanical force was applied to detach them. When all cells were free-floating, 10mls of fresh culture medium was added to halt the activity of the trypsin and the mixture was transferred to a 15ml falcon tube and centrifuged for 5 minutes (sans brakes) at 1000g at 37°C. The supernatant was then carefully aspirated and the pellet re-suspended and carefully triturated in 1ml of cell medium.

Cells were then plated at a 1:8 ratio in T75 flasks, or at a cell density of 1000, 2000 or 5000 cells/cm^2 on 13mm uncoated glass cover slips in 24-well plates, or at a cell density of 1000, 2000 or 5000 cells/cm^2 in 96-well plates. Cells were not used past passage number 25 to reduce variability caused by lack of neuronal differentiation which increases with each passage. To check level of neuronal differentiation, cells were stained with β-tubulin III (neuronal tubulin, Table 2.4) and DAPI (*Sigma Genosys, Dorset, UK,* nuclear stain) every 5 passages and the number of β-tubulin III negative nuclei determined. When cell lines were received from *ECACC* they were passaged and frozen in liquid nitrogen in freezing medium (10% DMSO and 20% extra FCS).

2.2.1. Transfection and differentiation

Cells were transfected 24 hours after plating using Lipofectamine 2000 (*Invitrogen, Paisley, UK*) as per manufacturer's instructions. For example, in 24 well plates, cell media was replaced with 400µl OPTI-MEM I (*Gibco, Paisley, UK*) per well and left in the incubator for 30 minutes. In solution A, DNA was added (40ng - 160ng) to 50µl of OPTI-MEM I per well, while in solution B, 2.0µl (0.67µl and 1.33µl were also tested) of Lipofectamine 2000 was mixed into 50µl of OPTI-MEM I per well. Solutions A and B were left for 5 minutes before being mixed together (to make 100µl per well) and incubated for 20 minutes at room temperature. 100µl of the mix was then added to each well and the cells were incubated for 6 hours before the transfection medium was replaced with culture medium containing 10µM all-trans retinoic acid (*Sigma Genosys, Dorset, UK*). Cells were differentiated for no more than 72 hours due to the transient nature of Lipofectamine 2000 transfection.

2.2.2. Induction of cell stress

In some experiments, cells were exposed to various forms of cellular stress. Chemical cell stressors known to induce specific forms of stress relevant to Hsp27 function were used in this part of the study.

2.2.2.1. Hydrogen peroxide

Hydrogen Peroxide (H_2O_2, *Sigma Genosys, Dorset, UK*) was used as a model of oxidative stress as well as a positive control of cytotoxicity. When added to cells it causes unsustainable production of Reactive Oxygen Species (ROS), leading to excessive and irreparable cell damage and cell death (Iordanov and Magun, 1999). H_2O_2 was added at a final concentration of 100μM in SH-SY5Y medium for 24 hours before fixation and analysis of experiments.

2.2.2.2. Cytochalasin D

Cytochalasin D disrupts actin microfilaments, therefore destabilising the cellular architecture and effecting cellular functions directly dependent on its integrity. Therefore, Cytochalasin D disrupts axonal transport, neurite outgrowth and other normal functions of the cellular actin network (Goddette and Frieden, 1986). Under normal conditions, Hsp27 has been shown to actively bind to actin within the cell (Mounier and Arrigo, 2002), so Cytochalasin D was used to measure the effects of a cell stressor which has an action on a protein directly linked to the Hsp27 pathway. Cytochalasin D (*Sigma Genosys, Dorset, UK*) was added at final concentrations of 0.1μM, 0.2μM, 1μM, 5μM, 10μM, 20μM, 50μM, 100μM and 150μM in SH-SY5Y medium for 24 hours before fixation and analysis.

2.2.2.3. Colchicine

Colchicine is a microtubule-disrupting agent widely used in anticancer therapy research due to its effects on the stability of microtubules (Cuthbert and Shay, 1983). It irreversibly binds to tubulin and disrupts the cells natural dynamic instability (Falconer *et al*., 1994). Hsp27 has been shown to functionally interact directly with actin *in vitro* (Mounier and Arrigo, 2002), but has a less well defined interaction with tubulin (Williams *et al*., 2005) so Colchicine was used as an Hsp27 independent cell stressor. Colchicine (*Sigma Genosys, Dorset, UK*) was added at final concentrations of 0.1μM, 0.2μM, 1μM, 5μM, 10μM, 20μM, 50μM, 100μM and 150μM in SH-SY5Y medium for 24 hours before fixation and analysis.

2.2.2.4. Heat shock

Heat shock was performed on cells after 7DIV at 43˚C for 30 minutes. Cells were then incubated at 37°C in a saturated humidity atmosphere of 95% air and 5% CO_2 for 4 hours before fixation.

2.2.3. Cell fixation

At 4 days after plating (4DIV) and 3 days following transfection, cells were analysed live under the microscope to gauge confluence and health status. The culture medium was replaced by 4% paraformaldehyde for 15 minutes and then washed three times with PBS. The cover slips were then stored at 4°C until analysis or less than 1 month. If coverslips were to be stored for more than 1 month, the PBS was supplemented with 0.1% Sodium azide to inhibit bacterial and fungal growth. For some experiments, cells were fixed 7DIV.

2.2.4. Transfection efficiency

To determine the transfection efficiency, cover slips were immunostained for V5 (1:500, *Invitrogen, Paisley, UK*, Table 2.4) and co-stained with the nuclear marker DAPI. Details of the staining protocol are given in Section 2.5. Images of the stained cultures were captured at 40x magnification. For each experiment, 5 representative images per coverslip were captured measuring 328 x 246μm using fluorescent microscopy (*Leica HC*), using a Leica DFC 420C colour camera and the *Leica Application Suite Version 2.8.1* (*LAS*). The pictures were then individually analysed using *Adobe Photoshop* (*Adobe*). The number of DAPI stained cells was counted to give a total number of cells per visual field. The number of cells strongly and weakly immunoreactive for V5 was established using Photoshop's auto-contrast function to standardise intensity between cultures, allowing comparison of strong and weak V5 immunoreactivity. In this way, the total number of transfected cells and the number of cells that had been transfected with single or multiple copies of the DNA could be determined. The total number of cells per coverslip was divided by the total number of transfected cells per coverslip and the average was plotted graphically.

2.3. Biochemical assays

In order to determine the effects of Hsp27 mutations on the response to cellular stress, we examined cell viability using a biochemical assay.

2.3.1. The lactate dehydrogenase (LDH) assay

Lactate Dehydrogenase (LDH) is a cytoplasmic enzyme which is released into the medium upon cell lysis. Released LDH oxidizes lactate to pyruvate, which then reacts with the tetrazolium salt INT (2-(4-iodophenyl)-3-(4-nitrophenyl)-5-phenyl tetrazolium) to form water-soluble formazan dye which can be detected spectrophotometrically. The principle of the LDH assay is based on the fact that as

cells die, LDH is released and this can be measured from the supernatant and therefore can be used as an assay of cytotoxicity. Because LDH is released into the culture medium upon cell lysis, a protein assay can also be carried out on the adherent cell layer, allowing the results to be standardised.

Cells were plated at a cell density of 2000 cells/cm^2 96-well plates in 100µl supplemented DMEM-F12 for 24 hours. After 1DIV, cells were transfected with wild type or mutant Hsp27 constructs. All drugs and toxic agents were added to the cells at 4DIV. At 5DIV, 2% Triton X-100 was added to some control wells. These controls produced the maximum release of LDH from all cells in culture which was then measured. These controls were used to ensure maximum saturation levels. Cells were then centrifuged at 250g for 5 minutes. The supernatant was removed and transferred to a 96-well plate for LDH analysis. The pellet containing cells was kept for protein analysis. The 2 separate LDH reagents (*Roche, Welwyn, UK*) used for the assay, Diaphorase (a catalyst) and INT (the dye solution) were mixed as per manufacturer's instructions to create 100µl per well. After addition of reagents to the cell supernatant, the 96-well plate was incubated at room temperature in the dark (as reagents are photosensitive) for 40 minutes. All experiments were incubated for the same length of time for consistency. Absorbance was measured at 490nm on a spectrophotometer. Absorbance values from LDH assays were individually normalized against protein values obtained from a protein assay on the pellet.

2.3.2. Protein assay

To standardise the LDH assay and normalise for cell density variation, a protein assay was carried out on the cell pellet from the 96-well plates. 100µl homogenising buffer (2% SDS, 2mM EDTA, 2mM EGTA dissolved in 500ml 5mM Tris (5mM TRIS HCL, 5mM Trizma base in dH_2O) pH6.8) was added to each well and cell pellet was

triturated three times. BSA standards (Bovine Serum Albumin, *Sigma Genosys, Dorset, UK*) were diluted to make a protein concentration gradient (2mg/ml – blank) and 10µl of BSA standards and samples were added to a clean 96-well plate. The Bio-Rad DC (detergent compatible) Protein Assay contained 3 reagents, A, B and S (*Bio-Rad, Hercules, CA***)** that were mixed as per manufacturer's instructions to give 225µl per sample well (200µl reagent B and 25µl reagent A and S). Plates were incubated at room temperature for 15 minutes and absorbance was measured at 750nm on a spectrophotometer.

2.3.3. Data and statistical analysis

Absorbance values obtained from the LDH release assay from each individual well was normalised to concentration of protein per well to standardise individual wells to each other (Abs/mg protein) giving the absorbance of LDH relative to protein content per well. All calculations were carried out using Excel (*Microsoft Office).* Normalised LDH values were calculated for each condition (6 wells per condition) using the following formula.

$$= \left(\frac{Abs_{\lambda 450}}{C_{Prot\ (mg/ml)}} \right) * 10$$

In each experiment, and for each experimental condition, an average and a standard error of the 6 wells of each condition was calculated. For each plate and for each condition, values were further normalised against the mean LDH results of 6 wells transfected with wild type Hsp27, so the effects of the Hsp27 mutations was expressed as a percentage change compared to cultures transfected with the wild type protein.

$$= (Av.\ Value / Av.\ wt\ Hsp27\ Control) * 100$$

By standardising against Hsp27wt transfection, cell death due to protein overexpression and transfection toxicity was accounted for and differences in plate variation were negated. This ratio could then be compared between experiments.

Data was statistically analysed using the Kruskal-Wallis One Way Analysis of Variance on Ranks (*SigmaStat*). In addition, following advice from a statistician, multilevel mixed model analysis with estimates of fixed effects and multiple comparisons (*SPSS*) was also performed.

2.4. Cell death assessed using fluorescence-activated cell sorting (FACS)

To further assess cell survival, FACS was used as an alternative method to assess the extent of cell death in transfected cultures. To differentiate between live and dead cells, a fluoro-labelled Annexin-V antibody was applied. FACS is a sub-type of flow cytometry. It provides a method for sorting a heterogeneous mixture of cells based on the specific light scattering and fluorescent characteristics of each cell.

Cells were first plated at a cell density of 10,000 cells/cm^2 onto 24-well plates and supplemented with SH-SY5Y media for 24 hours. After 1DIV, cells were transfected using Lipofectamine 2000 as per manufacturer's instructions and differentiated as described above. At 5DIV, all media was removed and the cells were carefully suspended in Dulbecco's PBS (*Sigma Genosys, Dorset, UK*). All the following steps were carried out on ice. Cells were washed twice to remove media by centrifugation at 4˚C at 1000rpm for 5 minutes before the supernatant was aspirated and replaced with PBS. The cells were triturated and the process was repeated. Cells were then resuspended at 1-2 x 10^6 cells/ml in 1x Annexin-V Binding Buffer (10 mM HEPES/NaOH, pH 7.4, 140 mM NaCl, 2.5 mM $CaCl_2$) (*Invitrogen, Paisley, UK*). The cells were aliquotted into 100µl before 5µl of Annexin-V FITC and 10µl of Propidium

Iodide (PI) Buffer were added to each tube. They were incubated at room temperature for 15 minutes in the dark before 400µl of 1x Annexin-V Binding Buffer was added to each tube. The cells were analysed by flow cytometry within 1 hour of staining.

2.5. Immunocytochemistry

Transfected cells were examined for the presence and expression pattern of a number of protein markers using immunocytochemistry. The primary and secondary antibodies used in this study are shown in Table 2.4. To identify transfected cells when using either SH-SY5Y cells or primary motoneurons, all cultures were stained with a V5 unconjugated antibody (*Sigma Genosys, Dorset, UK*) (Table 2.4) which recognised the V5 epitope which was contained in the pcDNA3.1/V5 plasmid and attached to virally transfected Hsp27 in transfected primary motoneurons.

The cells were permeabilised in PBS-0.1% Triton X-100 for 15 minutes before being washed three times with PBS. To block non-specific binding sites, the cells were incubated in 3% normal serum (dependent on 2˚ antibody, see Table 2.4) and 5% milk protein in PBS for 1 hour at room temperature. A primary antibody (Table 2.4) in blocking serum was then added to the cells and incubated overnight at 4˚C. The cover slips were then washed three times in PBS. The cells were then incubated for 2 hours at room temperature with an appropriate secondary antibody conjugated to a fluorophore (see Table 2.4 for concentration). If no more protein markers were to be stained for, DAPI (1:1000 in PBS) was applied for 15 minutes to identify the nuclei of cells. Cover slips were mounted onto uncharged glass slides (*VWR*) using non-set mounting medium (*Citifluor*), covered and stored at 4°C for up to 1 month before analysis. If a coverslip was to be co-stained with other markers of protein

Table 2.4 Antibodies used in this Thesis

Primary and secondary antibodies used to determine the presence and expression pattern of protein markers *in vitro* using immunocytochemistry. Details include species they were raised in, concentration used and source.

Table 2.4

Antibody	Dilution	Species	Manufacturer and Cat. Number
Primary Antibodies			
V5	1:500	mouse	Sigma #V8012-50UG
Hsp27	1:1000	goat	Santa-Cruz #sc-1048
β-tubulin III	1:1000	rabbit	Covance #PRB-435P
Phalloidin-488	1:250	toxin	Invitrogen #A12379
Neurofilament 200 – heavy chain	1:100	rabbit	Sigma #N4142
Tau	1:2000	mouse	Dako #A0024
SC35	1:1000	mouse	Sigma #S4045
TDP-43 C-terminus	1:500	rabbit	ProteinTech #10782-2-AP
Ubiquitin	1:500	rabbit	GeneTex #GTX78236
SMN, clone 2B1	1:200	mouse	Millipore #05-1532
MAP2	1:1000	rabbit	
Secondary Conjugates			
AlexaFluor-568 anti-mouse	1:1000	goat	Invitrogen #A-11004
AlexaFluor-488 anti-rabbit	1:1000	goat	Invitrogen #A-11008
AlexaFluor-568 anti-rabbit	1:1000	donkey	Invitrogen #A-11011
AlexaFluor-568 anti-goat	1:1000	donkey	Invitrogen #A-11057
DAPI	1:2000		Sigma #D8417

expression (double-stained), the above protocol was repeated with appropriate primary and secondary antibodies (Table 2.4) before staining with DAPI.

Immunostained cells were analysed using two different image capture systems (Figure 2.2). In most cases, cells were analysed by fluorescent microscopy (*Leica HC*), and images were captured on a Leica DFC 420C colour camera using the *Leica Application Suite Version 2.8.1* (*LAS*). In some cases confocal microscopy was used to visualise cellular inclusions and create 3D images (Z-stacking). Images were captured on a Confocal Laser Scanning Microscope (Zeiss LSM 510 Meta) using manufacturer's software (*Carl Zeiss Ltd, Hertfordshire,* UK**).** Images were then analysed in *Adobe Photoshop* (*Adobe*) and *Metamorph* (*Molecular Devices, UK).*

2.6. Analysis of cell morphology and neurite outgrowth

In order to characterise morphological changes in the wild type and mutant Hsp27 transfected cells, cell cultures were transfected with either wild type or mutant Hsp27. After 5DIV and 7DIV to give varying time courses of cellular differentiation, all media was removed from the cells and they were fixed in 4% paraformaldyhyde. Cover slips were stained for V5, β-tubulin III (a neuronal marker to visualise the cell) and DAPI. Neurite outgrowth measurements were performed using a previously described method (Ransome and Turnley, 2008), with some modifications. Four coverslips per condition were analysed per experiment. Images were captured at 20x magnification measuring 655 x 491μm. Approximately 20 images were captured per coverslip using fluorescent microscopy (*Leica HC*), on a Leica DFC 420C colour camera using *LAS*. From the images captured, 1 in every 4 was randomly chosen and analysed using *Metamorph* (*Molecular Devices, Berkshire, UK*) software. At least 100 cells per condition were analysed. A cell process was considered as a neurite if its length was at least 1.5 times the cell body diameter. The total number of

Figure 2.2

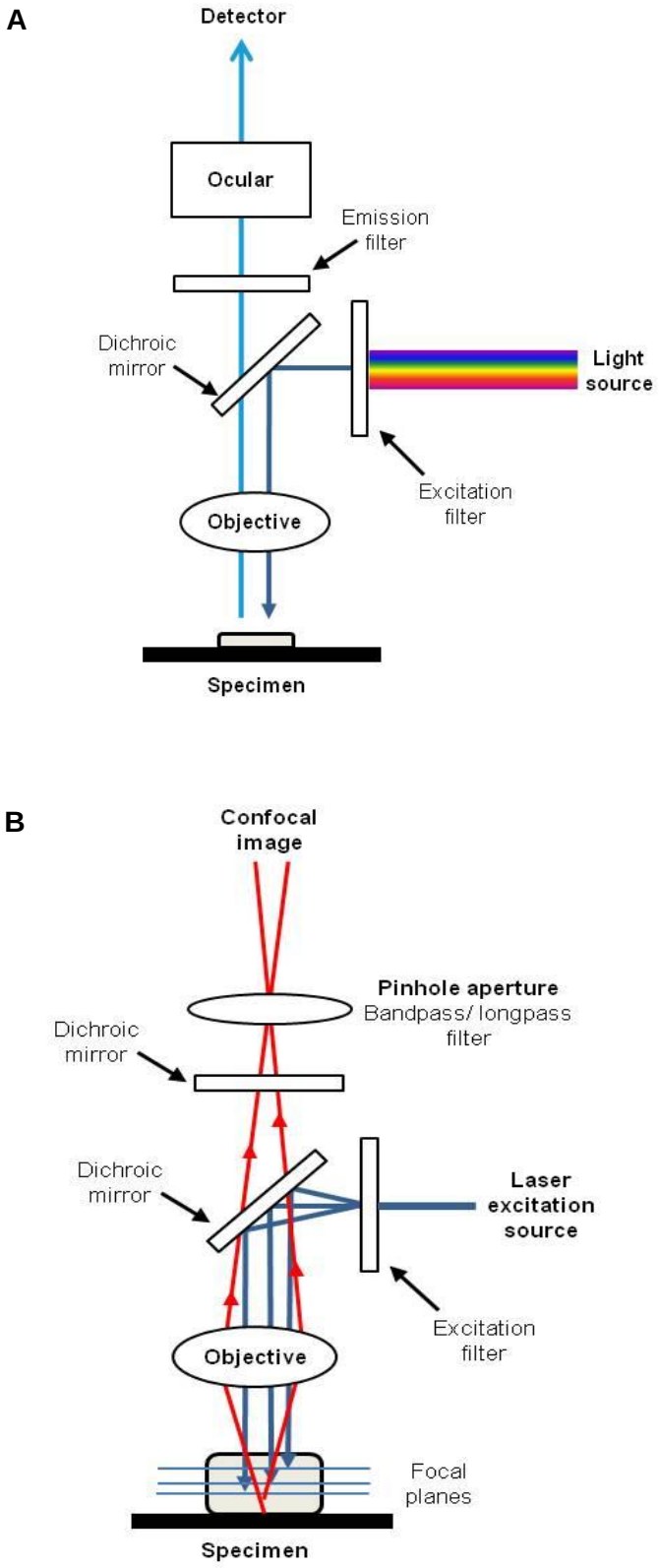

Figure 2.2 Diagrammatic representations of the wide field fluorescent microscope and confocal laser scanning microscope.

A. wide field fluorescent microscope, **B**. confocal laser scanning microscope

neurites was counted for each cell, and the length of each individual neurite was measured. For each cell, the following parameters were established;

- Total neurite number per cell (μm)
- Average neurite length per cell (μm)
- Length of the longest neurite (μm)

Further morphological assessment included;

- Assessment of neuritic branching as a measure of differentiation. An example of neurite branches is shown in Figure 3.14A.
- Presence of neuritic stumps. Figure 3.15A shows a cell with neuritic stumps.
- Presence of lamellipodia. Figure 3.16A shows a cell with lamellipodia.
- Investigation of vacuolisation (See Figure 3.17A for examples of vacuoles).

Data was logged and all analysis was undertaken in *Excel* (*Microsoft Office 2007*). Statistical analysis was carried out using *SigmaStat.*

2.7. Primary mixed ventral horn neuron cultures

Mixed motoneuron cultures were prepared using a protocol adapted from that described by Camu and Henderson (Camu and Henderson, 1994). Primary mouse motoneurons were isolated from wild type mouse embryos at gestational age E13. Pregnant C57BL/6 x SJL females were killed by cervical dislocation, in accordance with the code of practice for the humane killing of animals under schedule 1 of the Animals (Scientific Procedures) Act 1986.

Embryos were removed from the uterine horn and transferred to a Petri dish containing Hank's Balanced Saline Solution (HBSS) (*Sigma-Aldrich Genosys, Dorset, UK)* supplemented with 2% P/S. Spinal cords were separated from the

surrounding tissue using fine curved forceps. The meninges were carefully removed and the dorsal horn cut away from the ventral portion of the spinal cord and discarded. The ventral horns of individual embryos were pooled in fresh HBSS + 2% P/S on ice and transferred to a class II microbiological flow hood; all further steps were performed under sterile conditions.

The spinal cords were incubated in a 0.025% trypsin solution (type XII-S) (*Sigma Genosys, Dorset, UK)* in HBSS for 10 minutes and cells were agitated after 5 minutes to ensure full trypsination. They were then transferred to a fresh solution containing 800µl L-15 medium *(GIBCO/Invitrogen, Paisley, UK*), 100µl 4% bovine serum albumin (BSA) (*Sigma-Aldrich Genosys, Dorset, UK)* and 100µl Dnase (1mg/ml) (*Sigma-Aldrich Genosys, Dorset, UK)*. The spinal cords were agitated until they had disaggregated and were then slowly triturated 6 times using a P1000 tip and left to settle. After 2 minutes the solution was transferred to a fresh 15ml centrifuge tube (care was taken to avoid transferring any un-dissociated fragments). This process was repeated twice, increasing the L-15 medium to 900µl and decreasing the Dnase (1mg/ml) to 30µl while increasing levels of trituration. The three supernatants were pooled together before being spun through a 1ml 4% BSA cushion for 5 minutes at 370g.

Once the supernatant had been removed, the pellet was resuspended in complete neurobasal medium (CNB) containing neurobasal medium *(GIBCO/Invitrogen, Paisley, UK*), B27 supplement (1unit/ml) *(GIBCO/Invitrogen, Paisley, UK*), 2% horse serum (HS) (*PAA, Somerset, UK*), 0.5 mM L-glutamine *(GIBCO/Invitrogen, Paisley, UK*), 0.05% 2-mercaptoethanol *(GIBCO/Invitrogen, Paisley, UK*), ciliary neurotrophic factor (CNTF) (500pg/ml) *(Alomone labs, Bucks, UK)*, glial cell-line derived neurotrophic factor (GDNF) (100pg/ml) *(Alomone labs, Bucks, UK)*, brain derived

neurotrophic factor (BDNF) (100 pg/ ml) *(Alomone labs, Bucks, UK)* and 1% P/S. Cell density was calculated using a haemocytometer and the cells were then ready for plating.

Glass coverslips (13mm) were put into 24 well plates, treated with poly-ornithine (1.5mg/ml in sterile, distilled H_20) (*Sigma-Aldrich Genosys, Dorset, UK)* and stored in an incubator at 37°C in a saturated humidity atmosphere of 95% air and 5% CO_2 the night before culturing. Before isolation of the motoneurons, the poly-ornithine was taken off of the plate and replaced with laminin (1mg/ml in L-15 medium) (*Sigma-Aldrich Genosys, Dorset, UK)*; the plate was then returned to the incubator for the duration of the isolation protocol.

Once the laminin solution had been removed, 500µl of CNB was added to each well and the mixed ventral horn cells were seeded on to the treated coverslips at a density of 50,000 cells/cm^2. The plate was returned to the incubator and the cultures maintained for 7 days before being fixed by replacing culture medium with 4% paraformaldehyde for 15 minutes and then washing three times with PBS for staining. During this culture period, the cells were virally transduced 48 hours after plating, see Section 2.7.2 for methods.

2.7.1. Determination of purity of ventral horn motoneuron cultures

To determine the percentage of motoneurons in an average culture, ventral horn preparations from 3 different days were examined. For each experiment, 3 coverslips were immunostained for MAP-2 (Table 2.4) and co-stained with the nuclear marker DAPI. Details of the staining protocol are given in Section 2.5. Images of the stained cultures were captured at 10x magnification. For each experiment, 5 representative images per coverslip were captured measuring 328 x

246µm using fluorescent microscopy (*Leica HC*), using a Leica DFC 420C colour camera and the *Leica Application Suite Version 2.8.1* (*LAS*). The pictures were then individually analysed using *Metamorph* (*Molecular Devices, UK)*. The number of DAPI stained cells was counted to give a total number of cells per visual field. The number of cells immunoreactive for MAP-2 was then established using Metamorphs cell count function. The percentage of MAP-2 positive cells per coverslip was calculated and the average was plotted graphically.

2.7.2. Generation of third generation lentiviral vectors for the delivery of wildtype and mutant Hsp27

Primary ventral horn motoneuron cultures were transfected 48 hours after plating using third generation lentiviral vectors containing wildtype and mutant Hsp27. All viral vectors were created by Dr Bernadett Kalmar and a basic description of the viral components is given here.

2.7.2.1. Viral backbone

For the generation of the lentivirus a third generation lentiviral backbone (pCDH1-MCS1-EF1-copGFP, *Systems Biosciences, US*) was used. The removal of replication elements made this HIV-1 virus safe to work with. The expression lentivirus contained the genetic elements responsible for packaging, transduction and stable integration of the viral expression construct into genomic DNA and expression of the target gene sequence. The expression system chosen had dual promoters: a CMV promoter to ensure high expression level of the target gene and an EF1 housekeeping promoter to drive the expression of a reporter gene, GFP (see vector map in Figure 2.3A).

Figure 2.3

A

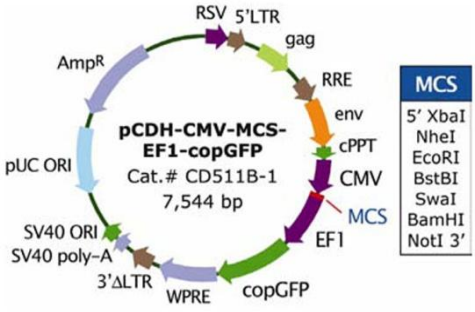

B

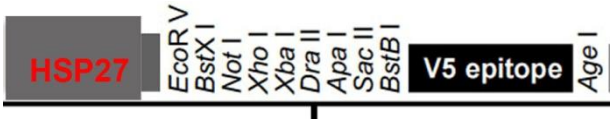

C

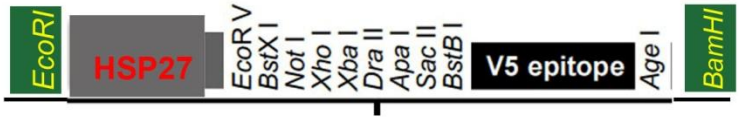

Figure 2.3 Diagrammatic representations of lentiviral vector map and gene inserts.

A. pCDH1-MCS1-EF1-copGFP lentiviral vector map, **B**. DNA selected from pcDNA3.1 plasmids for the generation of lentiviruses and **C.** Gene insert generated using PCR from the original pcDNA3.1b plasmid.

2.7.2.2. Gene inserts and restriction site choice

Gene inserts for the generation of lentiviral vectors were PcDNA3.1/V5 plasmid constructs containing either wildtype Hsp27 or mutant Hsp27 genes (Ser135Phe, Arg140Gly and Pro39Leu mutations were used). Thus, in total 4 vectors were generated: wildtype Hsp27 and 3 mutants. From the bacterial plamids the sequence containing the Hsp27 gene, several restriction sites and the V5 tag was selected (vector map of the selection is shown in Figure 2.3B)

First the restriction sites for cloning were selected from the viral backbone: on the 5' end EcoRI; on the 3' end BamHI was selected. In order to be able to insert the Hsp27 genes into the viral backbone, these restriction sites were added to the Hsp27 gene (Figure 2.3C).

2.7.2.3. Titration of viral particles

The relative titre (strength) of the viral stock is measured by flow cytometry using the host cell line used increase viral stock. This titre, however is always specific to that given cell type and may not be useful for other cell types, particularly not for the use of primary cells. Here, it was used to produce comparable titre data between batches of viruses and to titre values measured by other laboratories. The key terms used for the titration are:

Transducing Units (TU)/ml: gives an indication of the concentration of virus.

Multiplicity of Infection (MOI): the ratio of TUs to the number of cells being infected. For example, when $5x10^4$ cells are to be infected at an MOI of 10, then $5x10^5$ TUs should be added to the cells. The titre in TU/ml was calculated according to the formula:

$$\frac{1x10^5 \text{ seeded cells} \times \% \text{ GFP positive cells} \times 1000}{\mu l \text{ of vector added to the well}}$$

Using the calculation above, the following titres were calculated for use in HEK cells:

	Titre (TU/ml)
Empty vector	$2.9x10^7$
WT Hsp27	$1.07x10^6$
Ser135Phe Hsp27	$8.5x10^5$
Pro39Leu Hsp27	$1.56x10^6$
Arg140Gly Hsp27	$1.6x10^6$

2.7.2.4. Viral transduction and multiplicity of infection

Primary ventral horn motoneuron cultures were prepared as described in Section 2.7 and transfected 48 hours after plating using serial dilutions of known concentrations of virus to ascertain the correct MOI. In the literature, the MOI of primary motoneurons ranges from 10 to 20 (Tang *et al*., 2001)(Kirby *et al*., 2011). Cells were fixed and immunostained for MAP-2, a marker of motorneurons (Details of the staining protocol are given in Section 2.5). Images taken using the method described in Section 2.7.1 were used to calculate when 10% of motoneurons were virally transfected. At this concentration there is a low level of infection to give lower protein over expression and less protein level variability.

2.8. Western blot

2.8.1. Sample preparation

Primary motoneuron cultures were grown *in vitro* on 6-well plates at a concentration of $2.5x10^4$ cells per cm^2. To prepare samples for western blots the culture media was firstly removed and the cells washed in 5ml of PBS on ice. Next the cells were homogenized on ice for 5 minutes using 200µl homogenising buffer consisting of 50mM Tris, 150mM Sodium Chloride, 0.1% SDS and 1% Triton X100 (Sigma-Aldrich, Dorset, UK). The buffer also contained a protease inhibitor cocktail (1:100, Sigma-Aldrich, Dorset, UK) to prevent protein digestion. Homogenised cells were removed from the 6-well plates using a cell scraper and pipetted into 1ml Eppendorf tubes. The homogenised samples when then left on ice for 30 minutes to ensure the complete breakdown of all cell membranes in the sample. The samples were then centrifuged at 14,000 rpm at 4°C for 25 minutes and the supernatant transferred to fresh Eppendorf tubes, discarding the pellet. These tubes were labelled appropriately and stored at -80°C or used immediately for western blots.

2.8.2. Polyacrylamide gel preparation

Electrophoresis polyacrylamide gels were prepared using the *Biorad* gel casting system to create gels of 1mm thickness. The resolving gel was prepared at a 10% concentration (2.5ml Protogel resolving buffer, 4.135ml dH_2O, 3.3ml 30% acrylamide, 100µl 10% ammonium persulphate and 10µl tetramethylethylenediamine (TEMED)) and pipetted into pre-prepared glass chambers. A thin layer of water saturated butanol (1:1) was then added to prevent evaporation of the gel buffer and the gel was left to set for approximately 1 hour. When the gel was set, the butanol was removed and the stacking gel was prepared (4.137ml Protogel stacking buffer, 833µl 30% acrylamide, 25µl 10% ammonium

persulphate and 5µl TEMED) and added on top of the set resolving gel. Combs were then added to create 10 sample wells and the gel was left to set for a further 30 minutes at room temperature.

2.8.3. Gel electrophoresis and nitrocellulose membrane transfer

Each protein sample (30µg) was prepared using PBS to equalize all volumes between samples. Laemmli buffer stock solution (0.5 M Tris, 25 ml glycerol, 20 ml 10% SDS and 20 ml 0.05% bromophenol-blue in 22.5 ml dH_2O) was prepared by adding 50 µl β-mercaptoethanol to 950 µl laemmli buffer (1:20 dilution). Laemmli buffer was then added to the protein samples at 1:4 dilution and the diluted samples were incubated at 95^oC for 5 minutes to denature the proteins. Protein samples were next loaded into separate wells of a 10% polyacrylamide gel. Precision Plus Protein Western C standards (10 µl, Bio-Rad Laboratories, CA, USA) was loaded into one well to provide a protein ladder for reference of molecular weights. Loaded gels were clamped into an electrode block and submerged in running buffer consisting of 15.15g Tris base, 72g glycine and 5g SDS dissolved in a litre of water. Electrodes were attached to the block and electrophoresis run at 160 volts for 60 minutes.

Next the polyacrylamide gel was removed from the apparatus and placed on top of a nitrocellulose membrane soaked in an ice cold transfer buffer consisting of 100 ml stock transfer buffer (29.3 g glycine, 58.1 g Tris base and 3.75 g SDS in 1 litre dH_2O), 200 ml methanol and 700 ml dH_2O. Filter paper and sponges were placed on either side of the gel and membrane to ensure moisture was retained at all times. The gel and membrane were clamped into an electrode block such that the membrane was between the gel and the positive electrode. This allows the transfer of negatively charged protein from the gel onto the membrane. The block was

immersed in ice cold transfer buffer and run at 90 volts force for 70 minutes. Once complete the nitrocellulose membrane was taken out and stained with Ponceau solution (Sigma-Aldrich, Dorset, UK) for protein bands which confirms the transfer of proteins from the gel to the membrane.

2.8.4. Immunofluorescent-staining and analysis of western blots

All room temperature incubations in the immunoblotting step were done on a plate rocker to ensure full coverage of the nitrocellulose membranes. Membranes were washed 3x10 minutes in PBS-Tween (0.1%) to remove the Ponceau solution before being blocked in 10ml of blocking solution consisting of 0.1% Tween and 3% milk fat protein in PBS for 1 hour at room temperature. The membranes were again washed 3x10 minutes with PBS-Tween to remove blocking solution and 10ml of primary antibody solution (HSF1; 1:500, α-tubulin; 1:1000 in fresh blocking solution) was added. The membranes were incubated at 4^{o}C overnight.

Following this incubation, the membranes were washed 3x10 minutes in PBS-Tween. Secondary antibody solutions were prepared using rabbit anti-mouse IRDye 800CW or goat anti-rabbit IRDye 700DX conjugated IgG (1:5000, *LI-COR Biosciences, UK*) diluted in PBS-Tween. The membranes were subsequently incubated with the secondary antibody solution for 2 hours at room temperature. Three final washes in PBS-Tween were performed to remove the secondary antibody.

For visualisation of the protein bands, membranes were scanned on an Odyssey Infrared Imaging System (*LI-COR Biosciences, UK*) and quantification of developed images was performed using Odyssey program quantification software.

2.9. Live-cell imaging of mitochondrial membrane potential (Δψm)

In order to functionally examine the health and integrity of mitochondrial function, Tetramethylrhodamine methyl ester (TMRM) was utilised to measure Δψm. TMRM is a cell-permanent potentiometric indicator which is non-toxic to live cells. TMRM has a single delocalised positive charge and so becomes sequestered in mitochondria as a result of the electrochemical potential gradient that exists between the cytoplasm and mitochondria. Thus, the cationic nature of TMRM will cause higher fluorescence intensity at a more negative Δψm, and a loss of fluorescence intensity as Δψm becomes more positive (as the mitochondrial membrane depolarises)(Gandhi *et al*., 2009).

Primary ventral horn motoneuron cultures were plated at 25,000 cells/cm^2 in 2mls CNB on commercially available imaging dishes (*MatTek, Ashland, US*), virally transduced after 48 hours and used for imaging after 7DIV. Cells were first washed twice with 1ml of recording media (RM) warmed to 37˚C and consisting of 10mM HEPES (*Fisher Scientific, New Jersey, US*), 156mM NaCl, 10mM D-Glucose, 3mM KCl, 2mM $MgSO_4$, 2mM $CaCl_2$ and 1.25mM KH_2PO_4 (all *VWR/BDH, Poole, UK*) in dH_2O, pH 7.35. After washing, cells were incubated for 30 minutes in RM with 30nM TMRM, 1μM Calcein blue AM and 0.005% Pluronic F-127 acid (all *Invitrogen, Paisley, UK*). Calcein, a cell-permanent dye used as a short-term labeller of cells, was used to visualise motoneurons in a mixed cell culture. Pluronic acid, acting as a surfactant, was added to aid the dispersion of Calcein, a water insoluble molecule. After the 30 minute loading period, cells were washed with RM containing only 30nM TMRM and cells were then incubated in fresh RM/TMRM for the remainder of the experiment.

All recordings and images aquired were performed on a Confocal Laser Scanning Microscope (Zeiss LSM 510 Meta) described in Figure 2.2 using manufacturer's heated staging and software (*Carl Zeiss Ltd, Hertfordshire,* UK). TMRM was excited at 543nm and the emitted fluorescence was imaged using a 545nm dichroic filter and a 560nm longpass emission filter. Before the first experiment the microscope settings for laser intensity (laser power), amplifier onset and detector gain were adjusted to create reference settings which were not adjusted during analysis. The only parameter which could be changed once the experiments had begun was laser power as the linear relationship between the laser power and fluorescent intensity allowed correction for changes to the laser power. This meant that all measurements taken could be compared. To get optimum resolution, the pinhole was set to 1 airy unit (Between 0.8 and 1µm) and laser power was reduced to the lowest level possible, between 0.05% and 2% while still maintaining a dynamic range (the resolution of light intensity) of TMRM intensity which was judged by a cell staining profile containing intensity levels of between 1000 and 4000. Laser power reduction was important due to induction of photobleaching and the release of reactive oxygen species which in turn would induce a depolarisation of $\Delta\psi m$**.** The amplifier onset (black level setting) and detector gain (PMT sensitivity) were then set (and not changed) by using the range indicator to eliminate any areas of saturation while maintaining dynamic range. Motoneurons were identified based on morphology including size, number of neurites (generally at least 3 main projections from the cell body) and intensity of Calcein staining which tended to be higher in motoneurons. Firstly an image at 63x magnification of the neurons was taken to visualise the GFP marker in virally transfected cells. This was used to distinguish between transfected and nontransfected cells within the same imaging dish. Finally, a Z-stack was taken of the cells which were set to include the whole cell body volume. Images were taken at a scan speed of 7, with a size of 512 x 512 pixels and digitised to 12 bits which provided 4096 grey levels to improve resolution. Images of

TMRM and Calcein were taken successively on two separate channels to avoid cross talk and to distinguish and measure only the TMRM within the volume of the cell, not in the glial layer below. An average of 15 motoneurons was imaged over a 30 minute period after which the cells were discarded. In this system, TMRM signal is stable for at least one hour post-loading (Figure 5.7).

2.9.1. Live-cell imaging of Δψm and drug application

To functionally examine the health and integrity of the individual components maintaining the Δψm and therefore mitochondrial function, drugs with known modes of action upon different mitochondrial components were added at specific times. Cells were plated and washed as described above in Section 2.8 although they were not loaded with Calcein or Pluronic F-127 acid.

All recordings and images were gained using the same microscope and settings as described above in section 2.8. Only one field per imaging dish could be used due to the single application of drugs while following a single time series and so fields had to include both transfected and non-transfected motoneurons as comparative controls. Images were taken every 5 seconds on a time series and drugs were added in a specific order directly to the RM/TMRM in the imaging dish at prescribed time points (described in Section 2.8.1.1). Firstly, Oligomycin (2µg/ml, *Sigma Genosys, Dorset, UK*), an ATPase inhibitor was added after a 30 second baseline reading. After a further 120 seconds, Rotenone (5µM, *Sigma Genosys, Dorset, UK*) was added directly to the imaging dish to inhibit Complex I of the mitochondrial electron transport chain. Finally, FCCP (1µM, *Sigma Genosys, Dorset, UK*) was added 30 seconds after the addition of Rotenone. FCCP uncouples oxidation from phosphorylation so ATP synthesis cannot occur and is used to completely

depolarise the Δψm. The recording was finished after a further 20 seconds and the cells discarded.

2.9.1.1. Protocol for addition of drugs and expected responses

The drug protocol and expected responses in TMRM fluorescence intensity are summarised below;

30 seconds Oligomycin (2µg/ml)

If ATPase has been reversed by cell to maintain Δψm will see a steady decline in TMRM fluorescence intensity.

If Δψm is not being actively maintained there will be no change in TMRM fluorescence intensity.

150 seconds Rotenone (5µM)

Immediate decrease in TMRM fluorescence intensity.

If cell is more reliant on Complex I than Complex II then there will be a bigger decline.

180 seconds FCCP (1µM)

Immediate dissipation of TMRM signal as Δψm depolarises.

2.9.2. Data and statistical analysis

In both Δψm and drug Δψm analysis experiments, at least 3 imaging dishes from at least 5 pooled wild type embryos were used per experimental parameter per culture, and experiments were carried out on at least 3 cultures prepared on separate occasions. Images were analysed using *Volocity* (*PerkinElmer, US*) image analysis software. Levels of TMRM 3D pixel (voxel) intensity were measured in individual cells. Cell bodies (objects) were identified by calcein voxel intensity levels set at the

start of experimentation and the volume of intensity measured was turned into a region of interest (ROI). The intensity levels of TMRM staining were then calculated only within that ROI. TMRM intensity levels were set with a lower level of 311 to distinguish individual clumps of mitochondria and a fine filter was added to remove background noise. The average intensity of the TMRM was then calculated:

$$\frac{\text{mean intensity (Ch3-T1) x volume } (\mu m^3)}{\text{total volume } (\mu m^3)}$$

By standardising the intensity reading, individual voxel intensity was represented. Mitochondria clumps within the cell and smaller groups or individual mitochondria having a lower TMRM intensity, therefore standardisation gives a representative intensity of $\Delta\psi m$.

The standardised intensities of individual cells were grouped into transfected or non-transfected based on whether cells with or without GFP expression and averaged within an imaging dish to give a ratio comparison of transfected and nontransfected cells within the same dish. The standard error of the mean (SEM) was calculated for each average and paired t-tests were performed using *SigmaStat*.

Chapter 3. The effects of Hsp27 mutations on cell survival and cellular morphology *in vitro*.

In this Chapter, the effects of disease-causing mutations in Hsp27 were investigated *in vitro*. In addition, the possibility that these pathogenic mutations, found in different regions of the gene, have differential effects on cellular pathology was also examined. In order to compare the effects of Hsp27 mutations, I firstly established and optimised an *in vitro* cellular model using a neuronal-like neuroblastoma cell line transfected with the aid of plasmids. The effects of wild type and mutant Hsp27 on readouts of cell toxicity, neurite outgrowth and cellular morphological changes were examined.

The results of these experiments were used to screen for the most deleterious and interesting mutations that would then be taken forward for a more detailed analysis of their effects on cellular functions in the experiments described in Chapters 5 and 6.

3.1. Generation of plasmid constructs containing Hsp27

Plasmid constructs containing 4 different Hsp27 mutations as well as a wild type Hsp27 construct were generated (see Chapter 2, Section 2.1).

For the generation of plasmid constructs containing Hsp27 mutations, a pcDNA3.1/V5 plasmid expressing wild type Hsp27 was used as a template. Using a site-directed mutagenesis kit (*Strategene*), two mutations, Arg140Gly and Leu99Met were generated following a standard protocol that was highly successful.

Mutagenesis was repeated several times in an effort to mutate and transform mutation Pro39Leu. Although the *Stratagen* kit gave a high success rate using the standard protocol with two of the Hsp27 mutations, the Pro39Leu mutation proved difficult to transform, and so the protocol was modified in several ways to produce a colony. Changes to the mutagenesis PCR reaction included the addition of 10% Q Solution (5M Betaine) and DMSO (Dimethyl sulfoxide) to reduce the formation of secondary structures and facilitate strand separation, changing the *Taq* used to get a higher purity of DNA, increasing the time given for DNA annealing from 1 minute/kb of plasmid length to 2 minutes, and changing the annealing temperatures from 68˚C to 72˚C.

An Hsp27 PCR was used to confirm the presence of the gene product after the first stage of mutagenesis, and the reaction was optimised to give the strongest signal for analysis. When optimising the PCR reaction, different primers were tested to attain the best signal by amplifying different lengths of the gene (Table 2.3, Chapter 2 and Figure 3.1). The PCR was also optimised by the addition of Q Solution. The individual colonies that grew from the products of site-directed mutagenesis were then genotyped to confirm the presence of the Hsp27 gene (Figure 3.2).

Figure 3.1

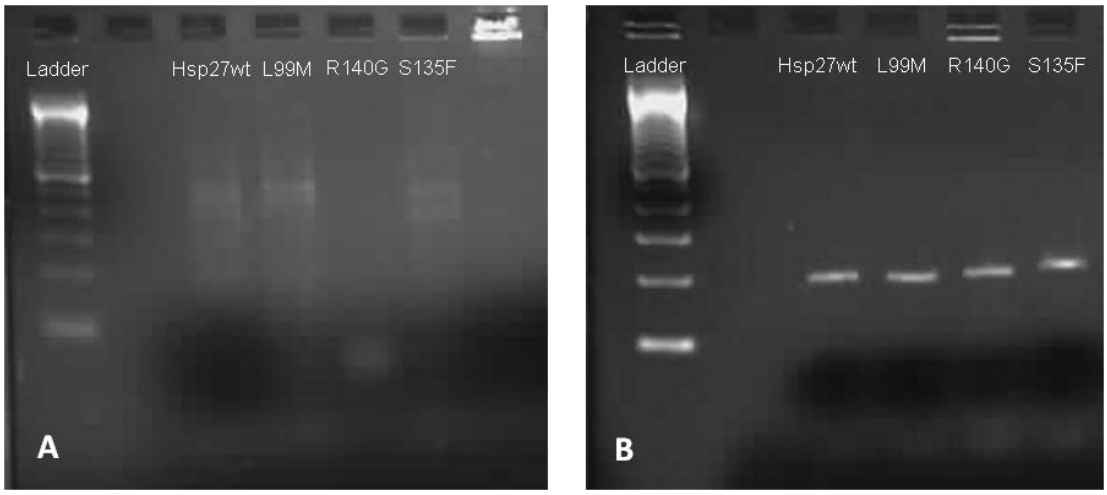

Figure 3.1 Hsp27 PCR of wild type and mutant Hsp27 showing optimisation of PCR reaction

A) PCR before optimisation using a general PCR protocol. **B)** PCR protocol with 10% Q solution added to the reaction and the annealing stage of the PCR program was lengthened from 30 seconds to 1 minute at 55°C.

Figure 3.2

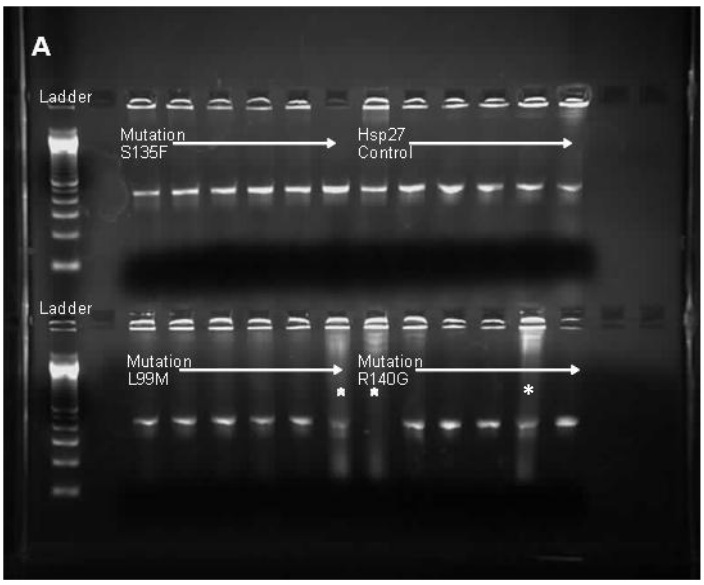

Figure 3.2 Hsp27 PCR showing genotyping of individual colonies to confirm gene presence

Six colonies were sampled from each transformed agar plate. The DNA band is seen at 450Kb. * donates streaking of well due to excess of DNA in the sample.

3.2. Analysis of constructs

Following completion of site-directed mutagenesis, transformation of bacteria and growing of bacterial colonies expressing the plasmid constructs, single bacterial colonies were selected and plasmid DNA was sequenced. The results are shown in Figure 3.3. This allowed me to:

1. Confirm that the correct sequence of the DNA plasmid was retained and intact after the mutagenesis process.
2. Confirm the correct positioning of the mutations (Figure 3.3).
3. Confirm that there were no other point mutations or sequence changes within *Hsp27*.

Sequenced colonies showed the presence of the mutations and confirmed that there were no other base changes within the gene of interest (Figure 3.3).

Primers were then designed to sequence the open reading frame of the pcDNA3.1/V5 plasmid to determine whether it was intact without base changes, insertions or deletions. Plasmids were sent to UCL GeneService where they were confirmed as being intact.

Figure 3.3 Sequencing of *HSPB1*

Representative chromatograms displaying sequencing results and base changes of plasmid DNA from transformed colonies, all contain a control colony for comparison. **A)** Arrow denotes the base change from a C in the control to a T in Colonies 1, 2 and 3 leading to an amino acid change of a Serine to a Phenylalanine in Ser135Phe. **B)** Arrow denotes the base change from a C in the control to a T in Colonies 1 and 2 leading to an amino acid change of a Proline to a Leucine in Pro39Leu. **C)** Arrow denotes the base change from a C in the control to an A in Colonies 1, 2 and 3 leading to an amino acid change of a Leucine to a Methionine in Leu99Met and **D)** Arrows denote the base change from a G in the control to a C in Colonies 1, 2 and 3 leading to an amino acid change of an Arginine to a Glycine in Arg140Gly.

Figure 3.3

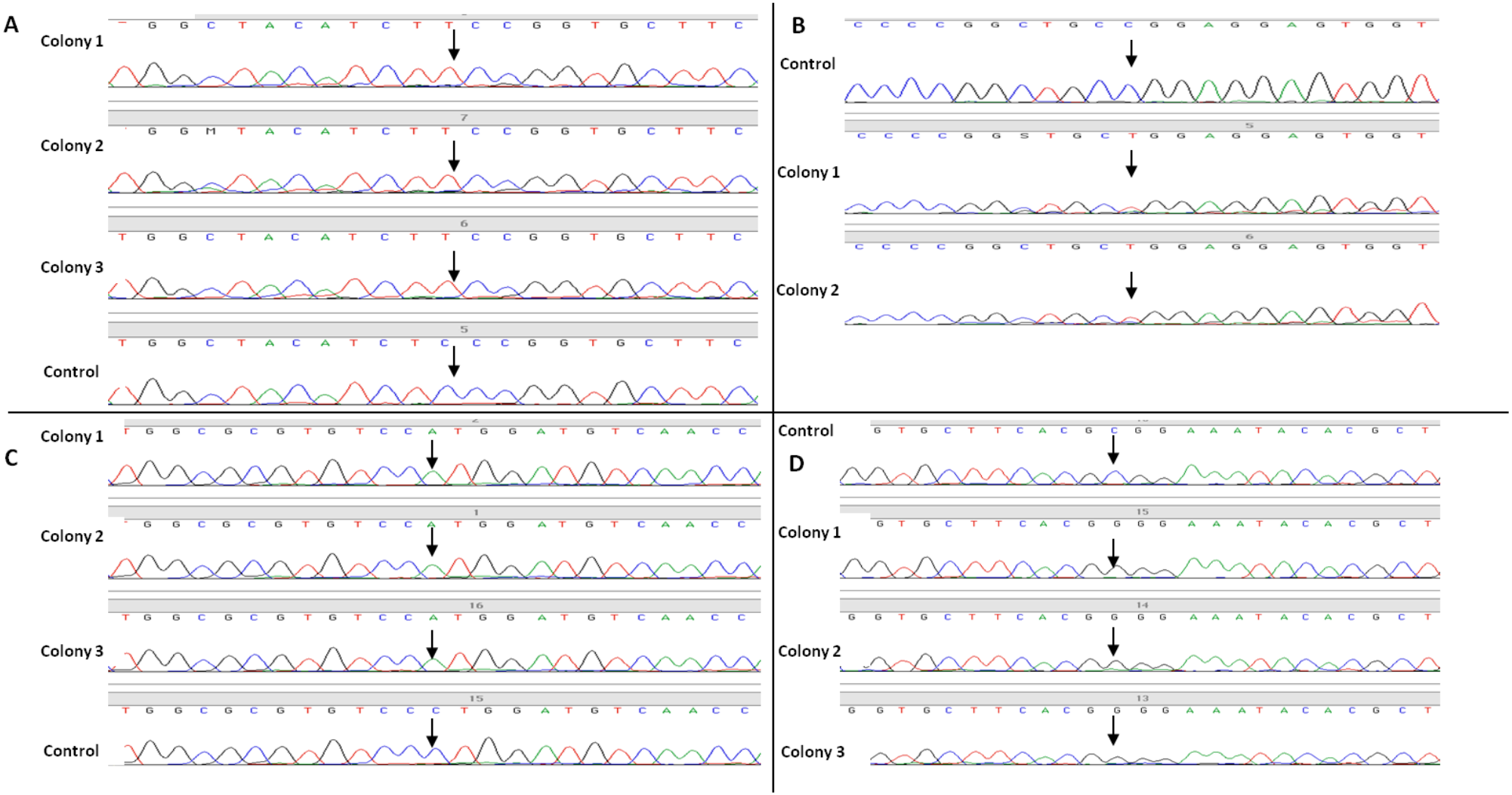
A
Colony 1
Colony 2
Colony 3
Control
B
Control
Colony 1
Colony 2
C
Colony 1
Colony 2
Colony 3
Control
D
Control
Colony 1
Colony 2
Colony 3

3.3. Optimisation of a cell culture model to study the effects of Hsp27 mutations

In order to examine the effects of the different Hsp27 mutations, a suitable cell culture model was first established. This involved identification of the most appropriate cell line, as well as optimisation of cell density and transfection conditions.

3.3.1. Selection of optimal cell line and morphological assessments

There are several neuronal-like immortalised cell lines that are commonly used in neurodegenerative research. In this study, two different, well characterised cell models were initially examined in order to establish which was more suitable to model the effects of mutant Hsp27. Thus Neuro-2A cells derived from mouse neuroblastoma cells, established from the spontaneous tumour of a strain A albino mouse (Biedler *et al*., 1973)(Helson and Biedler, 1973)(de Laat *et al*., 1977) and SH-SY5Y cells, third generation clones derived from SK-N-SH, were examined (See Figure 3.4A and B). Work to characterise N2A cells was carried out by Miho Tsuda, an MSc student in the lab under my supervision. An advantage of Neuro-2A cells was that they do not endogenously express Hsp27 as the endogenous rodent homologue is Hsp25.

In order to determine which cell line would be better suited for the experiments described in this Chapter, two main features were taken into account:

i. Rate of differentiation; important for morphological studies
ii. Transfection efficiency; important for biochemical assays

Figure 3.4

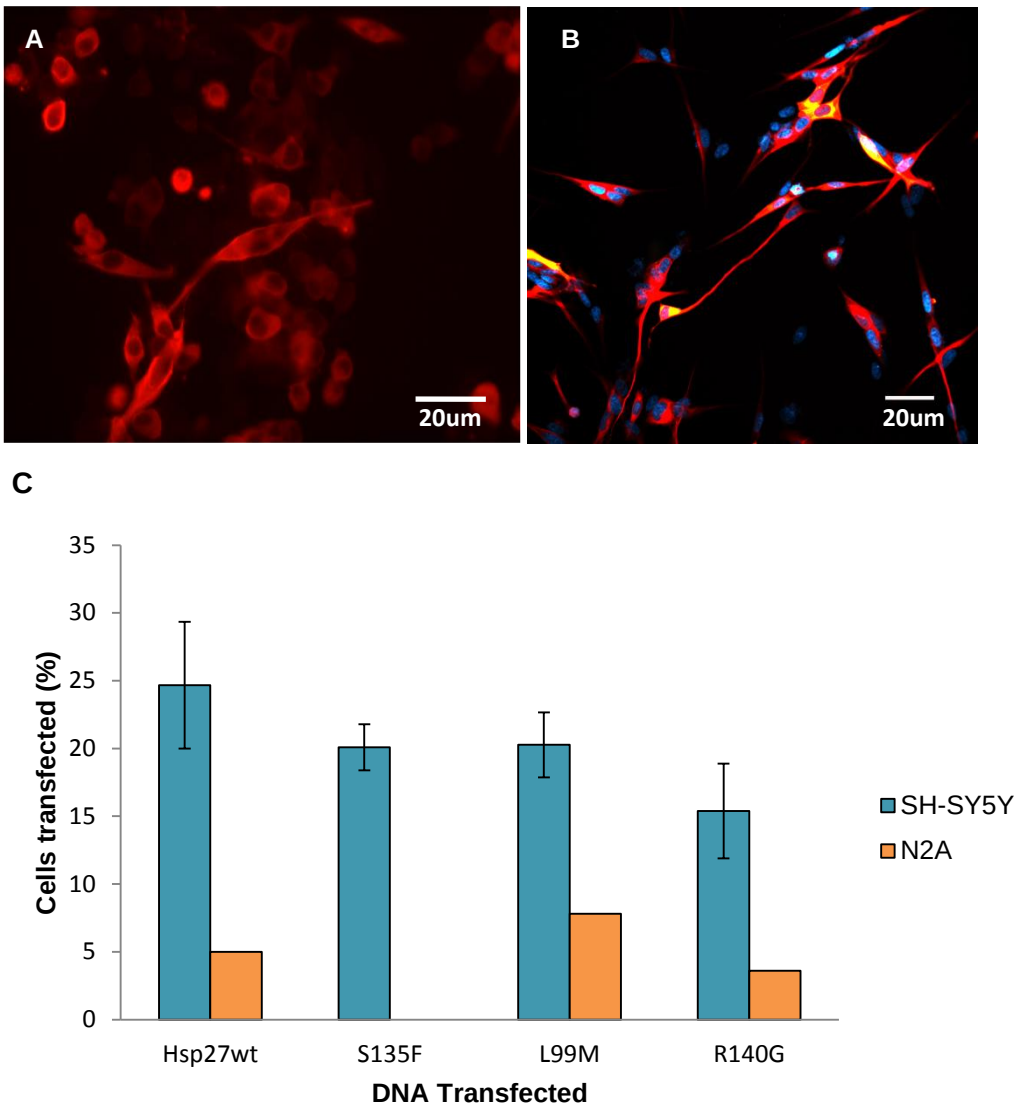

Figure 3.4 Selection of optimal cell line

A) Examples of Neuro-2A cells at 4 DIV immuno-stained with β-tubulin III antibody with low levels of cellular differentiation and **B)** SH-SY5Y cells at 7 DIV with differentiated neurites stained for β-tubulin III (red) and V5 (green) to visualise transfection, and counterstained with DAPI (blue). **C)** The bar chart shows the average percentage of SH-SY5Y and N2A cells in culture which were transfected at 7 DIV. Error Bars = SEM

Neuro-2A cells were easy to manage with a rapid growth rate, but transfection of this cell line was extremely transient with transfection rates declining from 25% transfection at 4DIV to 3 and 8% at 7 DIV (Figure 3.4C). Neuro-2A cells were also slow to differentiate. In comparison, SH-SY5Y cells showed a higher transfection efficiency of approximately 45% at 4DIV and between 15 and 25% at 7 DIV (Figure 3.4C). Although SH-SY5Y cells multiplied at a slower rate overall than Neuro-2A cells, they were quicker to differentiate, which is important when investigating neuronal morphology in transiently transfected cells. SH-SY5Y cells also had a lower tendency to form clumps in the cultured cells. Therefore, all experiments described below were carried out using the SH-SY5Y cell line.

3.3.2. Cell culture optimisation

In order to optimise cell culture conditions, a number of culture parameters were tested including variations in cell plating density, concentrations of transfection reagents and identification of the time after transfection and differentiation that was optimal for analysis.

3.3.2.1. Cell culture density

Neuronal cells in culture must be plated at the optimal density to ensure they are close enough together to encourage differentiation and neurite outgrowth, and at a sufficient density to ensure high transfection rates, maximum cell survival and clear paths of neuritic growth for accurate measurement of neurite length and branching (Figure 3.5). In these experiments the optimum cell plating density varied according to the specific experiment the cells were to be used for. For example, when examining neurite outgrowth in a 24-well plate and undertaking biochemical assays in a 96-well plate, cells were plated at a density of 2000 cells/cm^2. For all

Figure 3.5

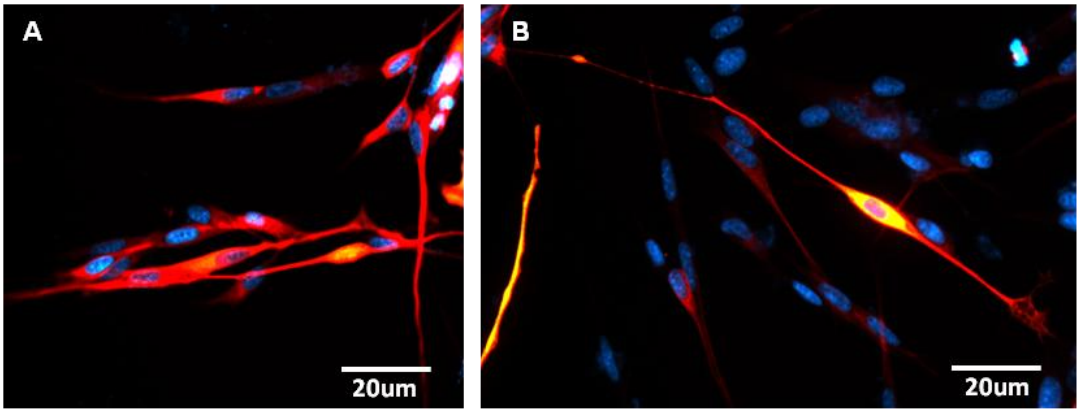

Figure 3.5 Cell Culture Densities

SH-SY5Y cells in culture immune-stained for β-tubulin III (red), V5 (green) and stained with the nuclear marker DAPI (blue) are shown, plated at 2 different densities **A)** shows differentiated cells plated at too high a density to permit accurate measurement of neurite growth. **B)** shows a neuron that has been plated at an ideal density to undertake measurements of neurite outgrowth as the ends of the neurites can be clearly identified and have an obvious point of origin.

experiments, the optimum cell confluence for differentiation and transfection was found to be ~30%.

3.3.2.2. Optimal transfection conditions

Cells were transfected using Lipofectamine 2000 and a pcDNA3.1/V5 plasmid containing a V5 epitope tag (for subsequent labelling of transfected cells) and either wild type or mutant Hsp27. In most cases, cells were immune-stained with an anti-V5 antibody against the epitope present on the transfected pcDNA3.1/V5 plasmid. The V5 tag was essential as SH-SY5Y cells are derived from human origin and so contain endogenous Hsp27 and the V5 tag was therefore used as a marker for transfected Hsp27. All optimisation experiments were carried out using both the wild type Hsp27 plasmid and Hsp27 Ser135Phe mutant plasmid as a positive control as this mutation has been previously shown to have deleterious effects in cells (Evgrafov *et al*., 2004). Cells expressing either the wild type or mutant construct appeared healthy and showed no apparent abnormalities when compared to untransfected cells. The *Invitrogen* protocol supplied with the Lipofectamine 2000 suggests an optimum working dilution of 0.4% (2µl per 500µl). However, in these experiments, there was a low cell confluency, therefore, the transfection conditions needed to be further optimised using a Lipofectamine 2000 concentration of 0.27% (1.33µl per 500µl) and 0.13% (0.67µl per 500µl). The results are summarised in Figure 3.6. Although a higher level of cell survival was observed at the lower concentrations (Figure 3.6A) a significantly lower number of cells were transfected at the lower concentrations (Figure 3.6B).

Another problem encountered with this method of cell transfection which involves cationic delivery of DNA, is that it is not possible to control how many copies of DNA enter each cell, resulting in a variable rate of transfection between experiments.

Figure 3.6 Effects of varying Lipofectamine 2000 and DNA concentrations on survival of SH-SY5Y cells

A) The bar chart shows the effect of different concentrations of Lipofectamine on cell survival. **B)** The bar chart summarises the percentage of SH-SY5Y cells in culture that were transfected using different concentrations of Lipofectamine 2000 and varying DNA concentrations. Cells were treated with differing levels of Lipofectamine 2000 and wild type Hsp27 DNA. Error bars = SEM

Figure 3.6

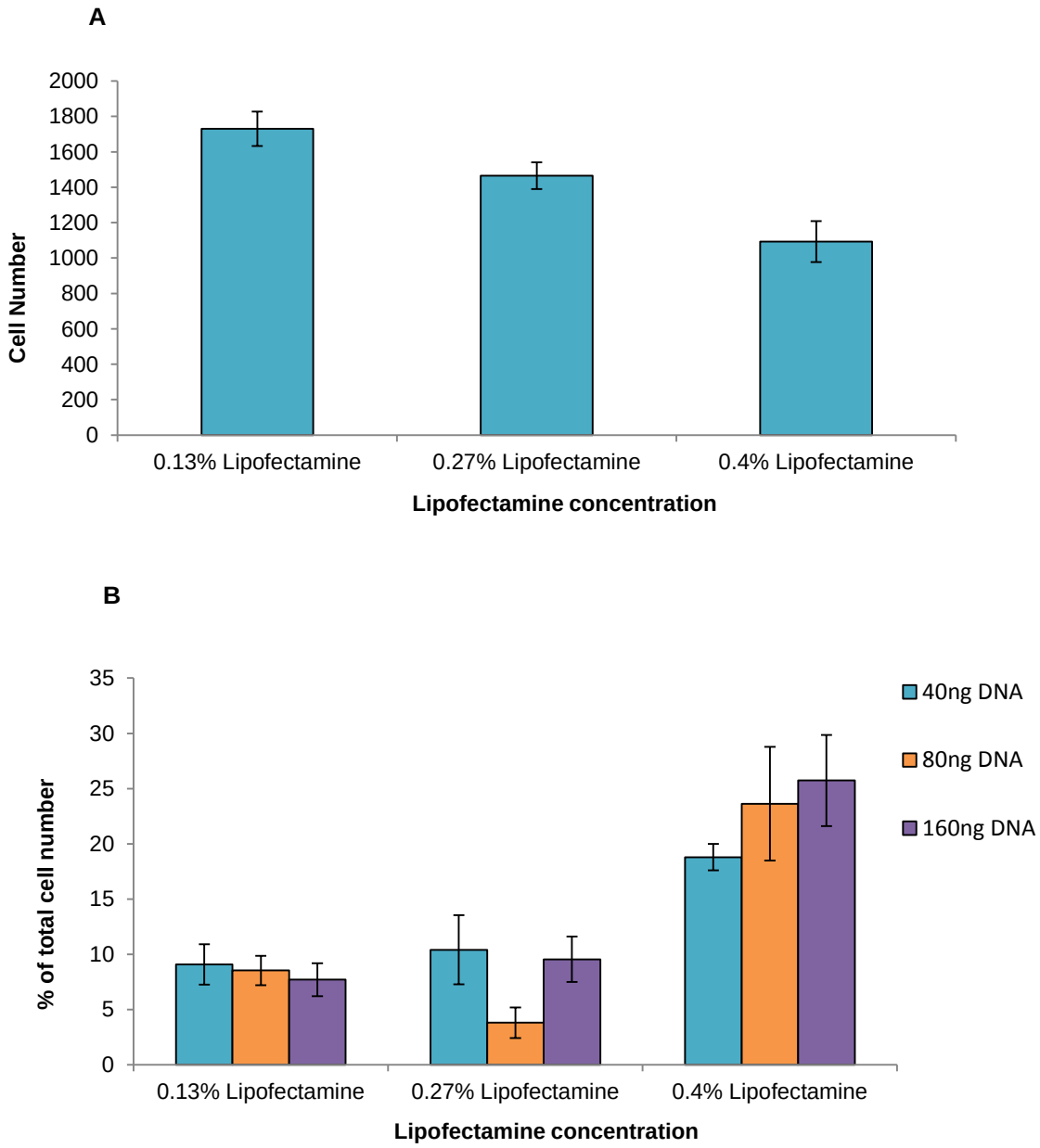
A
2000
1800
1600
1400
1200
1000
800
600
400
200
0
Cell Number
0.13% Lipofectamine
0.27% Lipofectamine
0.4% Lipofectamine
Lipofectamine concentration
B
35
30
25
20
15
10
5
0
% of total cell number
40ng DNA
80ng DNA
160ng DNA
0.13% Lipofectamine
0.27% Lipofectamine
0.4% Lipofectamine
Lipofectamine concentration

Single or multiple copies present in individual cells can be detected using immunofluorescence for a V5 marker on the plasmid but cannot be detected in any other way. The aim of optimising the concentration of transfected DNA was to increase the transfection rate and decrease the number of cells that had been transfected with multiple copies of the DNA. The results of these experiments showed that 40ng of DNA per well resulted in a low level of transfection (18% transfection using optimised Lipofectamine 2000) and therefore this concentration of DNA was not used any further (Figure 3.6B). Although 160ng of DNA gave the highest rate of transfection (27%, Figure 3.6B), it also resulted in increased numbers of cells that contained multiple copies of DNA. 80ng of DNA per well was found to be the optimum concentration resulting in a high percentage of transfected cells (20-30%) (Figure 3.6B) with low numbers of multiple DNA transfection (~3%). These transfection parameters were therefore used for all following experiments using all mutations to analyse the effects on the SH-SY5Y cell line survival, development and morphology.

3.4. The effect of mutant Hsp27 on cell survival

After optimisation of culture conditions and transfection of the SH-SY5Y cell line, the cell model was used to assess cell survival in cells expressing the different Hsp27 mutations, in the presence and absence of pharmacological cell stressors.

3.4.1. The effect of mutant Hsp27 on neuronal cell survival under basal conditions

Following transfection of SH-SY5Y cells with either wild type Hsp27 or each of the Hsp27 mutations, the effect on cell survival was assessed by means of an LDH assay. LDH is a cytoplasmic enzyme that is released into the medium following cell lysis and this supernatent is analysed. A protein assay is then undertaken using the

cellular layer in order to normalise the results to protein content, giving an accurate measure of cytotoxicity. In order to minimise plate variability, each experiment was repeated six times. For each experiment, each experimental condition was repeated 6 times on at least 6 different occasions and the results for cells transfected by each Hsp27 mutation were normalised to the value obtained from cells transfected with the wild type Hsp27 plasmid in order to control for Lipofectamine 2000 toxicity and the over-expression of a foreign protein. Thus, any differences recorded in LDH levels between wild type and mutant Hsp27 constructs were likely to be the result of the mutant proteins.

As shown in Figure 3.7, under basal conditions, all Hsp27 mutations significantly increased cytotoxicity compared to the wild type plasmid. In untransfected cells and those transfected with wild type Hsp27, no significant cell death was detected, with that observed in untransfected cells being -1.6% ± 2.4% of wild type transfected cells (taken as a 0% baseline to control for cell culture conditions, Lipofectamine transfection, addition of a plasmid and over expression of a foreign protein). However in cells transfected with any of the Hsp27 mutations, there was a significant increase in cytotoxicity for all mutations. Thus, relative to wild type transfected cells, cytotoxicity was found to be 20.8% ± 6.0%, 14.8% ± 3.3%, 16.6% ± 6.4% and 20.1% ± 10.6% (± SEM) in cells transfected with Ser135Phe, Pro39Leu, Leu99Met and Arg140Gly, respectively. Thus, all mutations showed a statistically significant increase in toxicity as determined by the non-parametric Krustal-Wallis ANOVA ($P=<0.001$) and by multilevel mixed model analysis with estimates of fixed effects and multiple comparisons ($P<0.05$). However, there was no significant difference in the level of toxicity between any of the individual Hsp27 mutations.

Figure 3.7

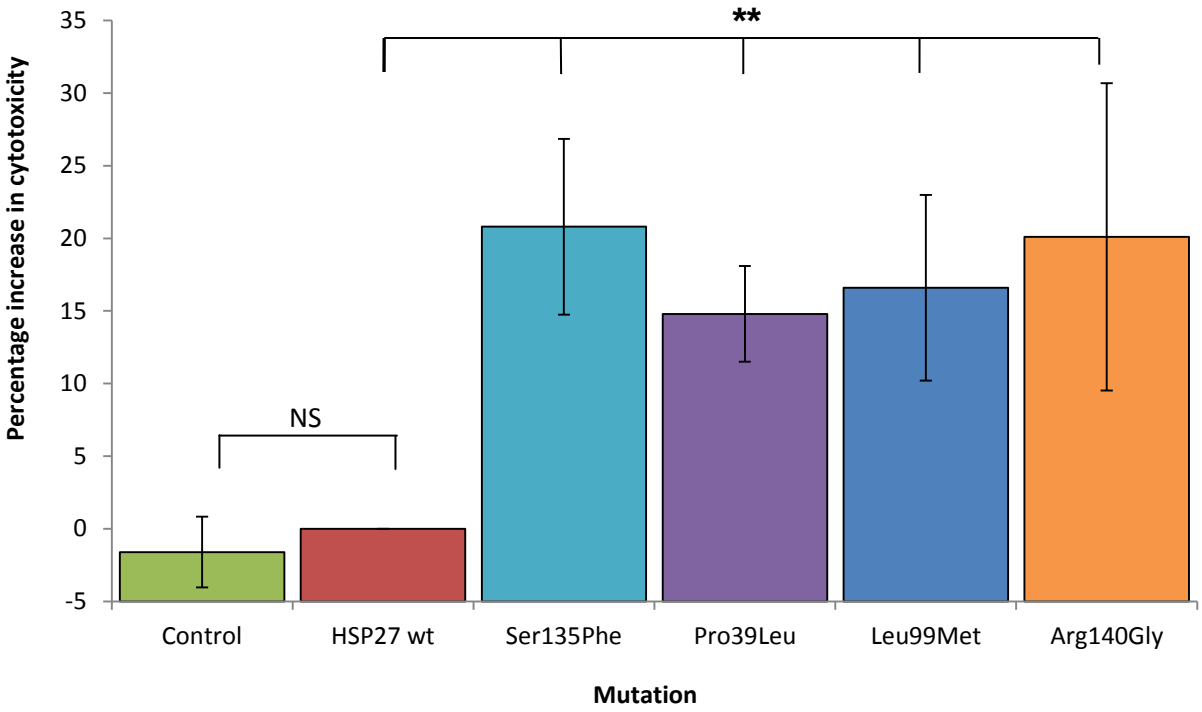

Figure 3.7 Toxicity of Hsp27 mutations in unstressed conditions

The bar chart shows the percentage increase in cytotoxicity relative to cells transfected with wild type Hsp27. Error bars = SEM; **p=0.05, multilevel mixed model analysis with estimates of fixed effects and multiple comparisons; NS = non-significant.

3.4.2. The effect of Hsp27 mutations on cell survival under conditions of cellular stress

Since transfection with any of the Hsp27 mutations resulted in a significant increase in cell death under basal, unstressed conditions, to determine if the different mutations exerted differential cytotoxic effects under conditions of cellular stress, the toxicity of the individual Hsp27 mutations was next tested by means of an LDH assay in the presence of different pharmacological cell stressors. Each drug or agent was chosen to exert specifically defined cellular stress. The morphological effects of each agent on untransfected SH-SY5Y cells is shown in Figure 3.8 and the effects on the survival of cells transfected with mutant Hsp27 are summarised in Figure 3.9.

3.4.2.1. Hydrogen peroxide

Hydrogen peroxide (H_2O_2) was used as a positive control that is known to induce cytotoxicity. When added to the cells it causes production of Reactive Oxygen Species (ROS), leading to excessive and irreparable cell damage (Figure 3.8C) and cell death (Figure 3.9A) (Iordanov and Magun, 1999). Under experimental conditions, H_2O_2 (100µM) was added to wild type and mutant Hsp27 transfected cells for 24 hours. The effects of H_2O_2 on the morphology of SH-SY5Y cells are significant in comparison to untreated cells, showing a complete loss of neurites, pyknotic nuclei, cellular detachment from the glass coverslip and clumping (Figure 3.8C). H_2O_2 caused a statistically significant increase (121.5% ± 14.1%, $p<0.001$, ± = SEM) in cell death in H_2O_2 treated wild type Hsp27 cultures compared to untreated wild type Hsp27 cells (Figure 3.9A). Cells expressing mutant Hsp27 were not more sensitive to H_2O_2 and cells expressing any of the Hsp27 mutations induced similar levels of cell death to cells transfected with wild type Hsp27, i.e. 174.8% ± 33.4%, 131.2% ± 38.1%, 105.8% ± 27.1% and 120.9% ± 26.0% (± = SEM) cytotoxicity in

Figure 3.8

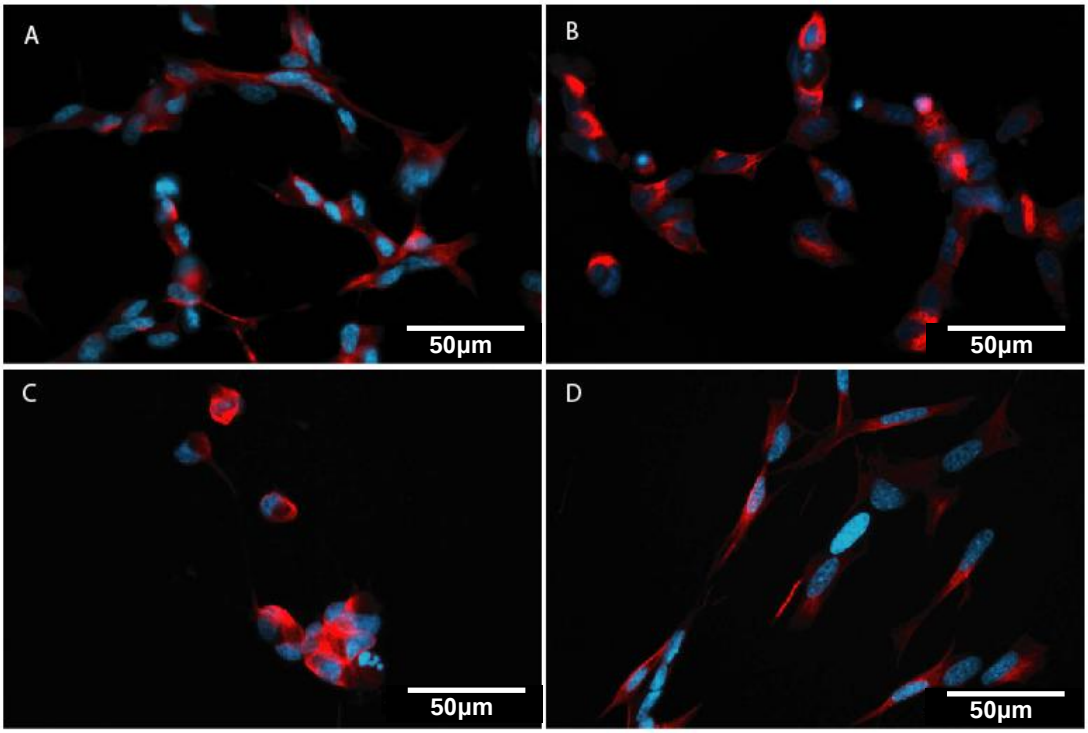

Figure 3.8 Morphological effects of cell stress on SH-SY5Y morphology

SH-SY5Y cells stained for β-tubulin III (red) and counterstained with DAPI (blue) to visualise the differential morphological effects of pharmacological cell stressors; **A)** Cytochalasin D (10µM) shows a loss of neurites, some pyknotic nuclei and clumping of cells, **B)** Colchicine (10µM) shows greater effects on the cells with complete lack of neurites, aggregation of β-tubulin III, pyknotic nuclei and cell clumping**, C)** H_2O_2 (100µM) is used as a positive control to show massive detrimental effects upon surviving cells with all cells clumping together and showing pyknotic nuclei. **D)** Shows untreated SH-SY5Y cells with neurite growth, not cellular clumping and healthy nuclei.

Figure 3.9 Toxicity of Hsp27 mutations under conditions of cell stress

The bar charts show the effects of the treatment with cell stressors **A)** H_2O_2 (100μM), **B)** Cytochalasin D (10μM), **C)** Colchicine (10μM) on cell survival in SH-SY5Y cells transfected with either wild type or each of the various Hsp27 mutations, as determined by an LDH assay. The extent of cytotoxicity in each condition is expressed as a percentage of that detected in untreated Hsp27 wild type cells. Error bars = SEM; *p=0.001, multilevel mixed model analysis with estimates of fixed effects and multiple comparisons.

Figure 3.9

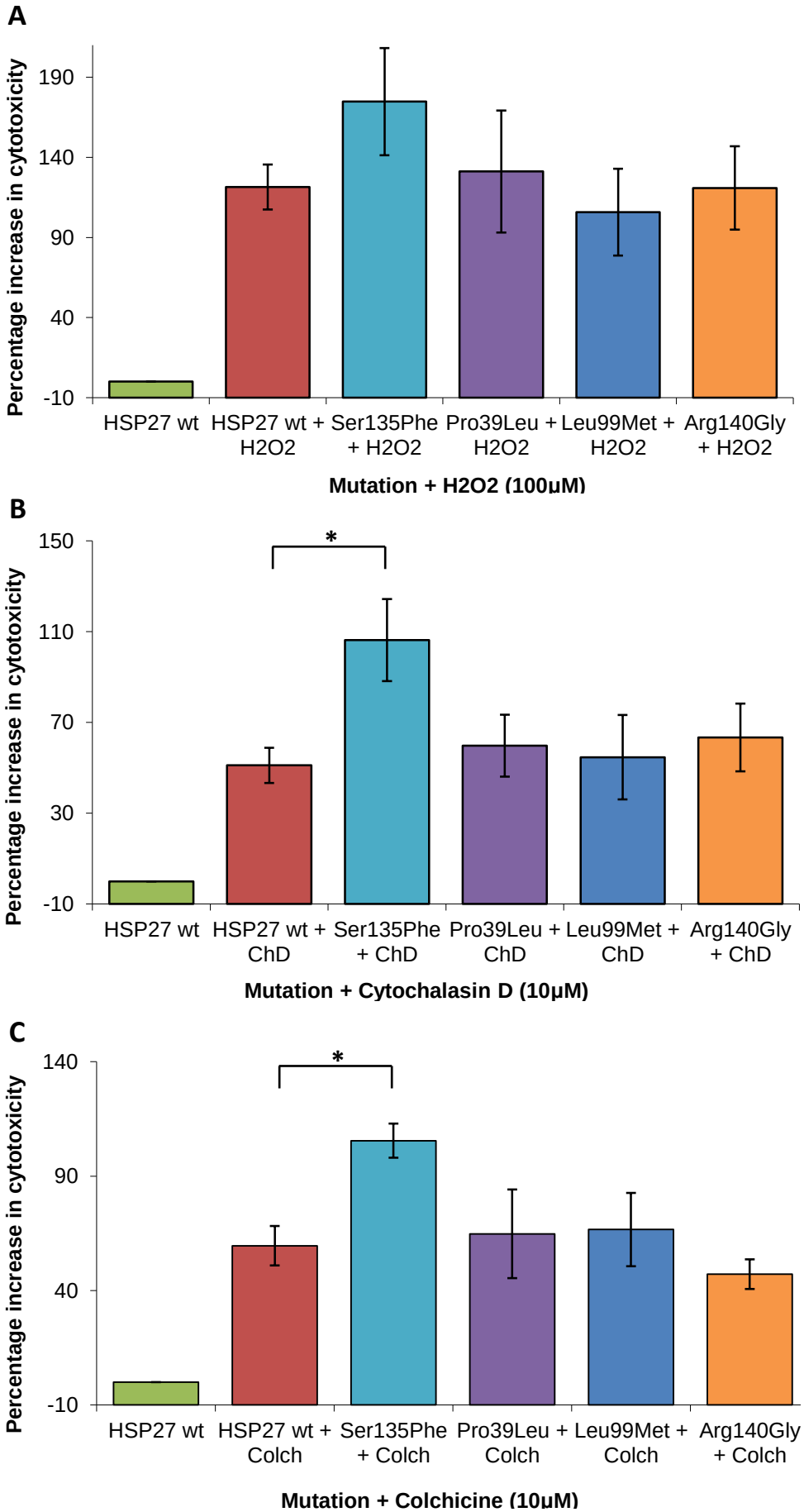
A
Percentage increase in cytotoxicity
190
140
90
40
-10
HSP27 wt
HSP27 wt + H2O2
Ser135Phe + H2O2
Pro39Leu + H2O2
Leu99Met + H2O2
Arg140Gly + H2O2
Mutation + H2O2 (100μM)
B
Percentage increase in cytotoxicity
150
110
70
30
-10
*
HSP27 wt
HSP27 wt + ChD
Ser135Phe + ChD
Pro39Leu + ChD
Leu99Met + ChD
Arg140Gly + ChD
Mutation + Cytochalasin D (10μM)
C
Percentage increase in cytotoxicity
140
90
40
-10
*
HSP27 wt
HSP27 wt + Colch
Ser135Phe + Colch
Pro39Leu + Colch
Leu99Met + Colch
Arg140Gly + Colch
Mutation + Colchicine (10μM)

cells transfected with Ser135Phe, Pro39Leu, Leu99Met and Arg140Gly, respectively. Due to the excessive damage caused by the addition of H_2O_2 over 24 hours, any cytotoxicity caused by mutated Hsp27 may have been too subtle to have any additive effect on cell survival.

3.4.2.2. Cytochalasin D

Cytochalasin D was used as a cell stressor agent since it is known to disrupt actin microfilaments, therefore disrupting axonal transport, neurite outgrowth and other normal functions of the cellular actin network (Goddette and Frieden, 1986). Under normal conditions, Hsp27 has been shown to actively bind to actin within the cell, so Cytochalasin D was used as a drug that has an action on a protein directly linked to the Hsp27 pathway. The morphological effects of Cytochalasin D (10μM) on SH-SY5Y cells is shown in Figure 3.8A, and the effects on cell survival on cells transfected with mutant Hsp27 are summarised in Figure 3.9B. The effects of Cytochalasin D on cellular morphology are significant in comparison to untreated cells; including loss of neurites, some pyknotic nuclei and clumping, but are less marked than those observed with H_2O_2 which also causes significantly more cell death than Cytochalasin D (Figure 3.8C, Figure 3.9A and B). Addition of Cytochalasin D to wild type Hsp27 transfected cells resulted in a significant increase (51.1% ± 7.8%, $p<0.001$, ± = SEM) in cytotoxicity compared to untreated wild type cultures. When Cytochalasin D was added to cells transfected with Ser135Phe Hsp27, cell death increased in comparison to cells transfected with wild type Hsp27 to 106.3% ± 18.1% (Figure 3.9B, $p<0.001$, ± = SEM). All other mutations showed an increase in cytotoxicity in response to Cytochalasin D, however, there was no difference between wild type Hsp27 and the Pro39Leu, Leu99Met and Arg140Gly mutations when Cytochalasin D was added and cytotoxicity was found to be 59.8% ± 13.7%, 54.7% ± 18.6% and 63.4% ± 14.9% (± = SEM) respectively (Figure 3.9B).

3.4.2.3. Colchicine

Colchicine disrupts axonal transport, stabilising microtubule formation by binding to tubulin (Falconer *et al*., 1994). The morphological effects of Colchicine (10μM) on SH-SY5Y cells is shown in Figure 3.8B, and the effects on cell survival on cells transfected with mutant Hsp27 are summarised in Figure 3.9C. The effects of Colchicine on cellular morphology are significant in comparison to untreated cells; including loss of all neurites, pyknotic nuclei and clumping. Colchicine causes a more severe cellular phenotype than Cytochalasin D at the same concentration, but its effects are less marked than those of H_2O_2 which also causes significantly more cell death than Colchicine (Figure 3.8B, Figure 3.9A and C). Addition of Colchicine to wild type Hsp27 transfected cells gave a statistically significant (59.6% ± 8.6%, $p<0.001$, ± = SEM) increase in cytotoxicity above untreated wild type cultures. When added to cells transfected with Ser135Phe Hsp27, this increased to 105.5% ± 7.4%, ($p<0.001$, ± = SEM) (Figure 3.9C). All other mutations showed an increase in cytotoxicity caused by the addition of Colchicine, however, there was no difference between wild type Hsp27 and the Pro39Leu, Leu99Met and Arg140Gly mutations when Colchicine was added, 64.8% ± 19.4%, 66.7% ± 16.0% and 47.2% ± 6.5% (± = SEM) respectively (Figure 3.9C).

3.4.3. Fluorescent activated cell sorting analysis of cell survival

Although the LDH assay revealed that all the Hsp27 mutations were toxic to SH-SY5Y cells, the assay was not sensitive enough to detect any differences between the various Hsp27 mutations or to dissect out mutation-specific changes in transfected cells. Therefore a sensitive Fluorescent Activated Cell Sorting (FACS) sorting method to analyse fluorescently labelled dead or dying cells was examined next.

The cells were labelled with Propidium Iodide (PI) and immunostained for Annexin V, both markers of dead cells. PI intercalates with DNA to identify dead cell material and Annexin V binds to epitopes on the cell surface which are exposed as the extracellular membrane breaks down during cell apoptosis, so that fluorescence intensity increases as the apoptotic process advances. Cells are grouped according to fluorescence to differentiate between healthy cells, damaged cells, apoptotic cells, and dead cell material as shown in Figure 3.10. H_2O_2 was used to treat cells for 24 hours previous to FACS as a positive control for mutational cell damage and cell death (Figure 3.10E). Quantification of scatter plots showed that H_2O_2 treatment resulted in 63.8% cell death, with 8.2% live cells and 10.2% apoptotic cells (Figure 3.10F) Experiments with non-transfected cells showed high proportions of cell damage and death. The first experiment carried out showed that there were 16.2% live cells, 41.3% dead cells and 32.6% apoptotic cells (Figure 3.10A,B), while the second experiment gave 32.1%, 24.3% and 38.1% live, dead and apoptotic cells, respectively (Figure 3.10C,D).

Therefore, although FACS analysis is a sensitive method of cell sorting, in this experiment the results were not reliable or reproducible. High levels of cell damage and apoptosis in transfected and non-transfected cultures meant that any effects of the Hsp27 mutations could not be detected. The cause of the excessive cellular disruption could have been due to many steps within the experimental protocol, many of which were unavoidable and so this method was not used further.

Figure 3.10 FACS analysis of cell survival in SH-SY5Y cells

Representative FACS scatter plots showing SH-SY5Y cells in culture with corresponding pie charts showing the percentage of cell populations. The x-axis of the scatter plot shows increasing signal strength of the Annexin V staining on individual cells and the y-axis shows signal strength of PI. All graphs have been adjusted to distinguish four different cell population groups. Quartile (Q) 1 shows high PI fluorescence and low Annexin V fluorescence, suggesting stained cell debris, Q2 shows cells with high fluorescence of both Annexin V and PI so all the cells in this section are dead. Q3 captures cells with low fluorescence of both Annexin V and PI so all the cells in this section are alive and relatively healthy, and Q4 cells are highly stained with Annexin V but are not fluorescent for PI, suggesting these cells are damaged and are in the process of apoptosis. **A-D)** Non-transfected cells in two different experiments. **E-F)** Non-transfected cells treated with H_2O_2 for 24 hours previous to experiment. **G-H)** Cells transfected with wild type Hsp27.

Figure 3.10

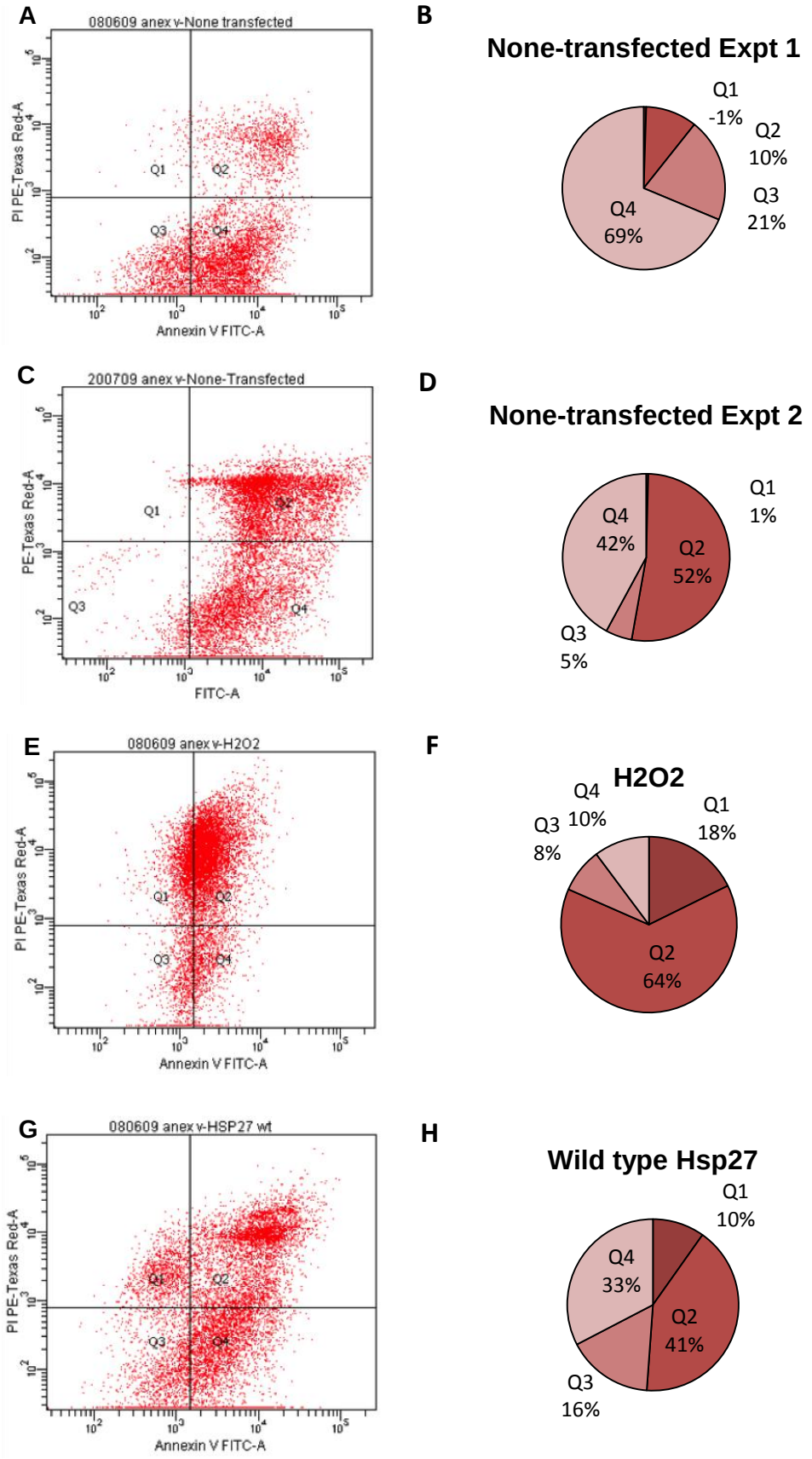

Q1 – Stained cell debris Q2 – Dead cells

Q3 – 'Healthy' cells Q4 – Apoptosing cells

3.5. The effects of Hsp27 mutations on cell morphology

3.5.1. Changes in cell morphology

Following confirmation of the cytotoxicity of all Hsp27 mutations, the effect of each mutation on cell growth and morphology was examined next. SH-SY5Y cells were immunostained for V5, the epitope present in transfected cells and β-tubulin III, the neuronal form of β-tubulin. In the first instance, neurite morphology was analysed by measuring the length of neurites and assessing the complexity of neuritic branching. Neurites which were a minimum of 1.5 times longer than the cell soma diameter were analysed (see Figure 3.11 for illustration) and the appearance of the following features determined:

i. Total neurite length (μm)
ii. Length of the longest neurite (μm)
iii. Cell complexity, determined by the extent of axonal branching, an indicator of cell differentiation and complexity

3.5.1.1. The effect of Hsp27 mutations on total neurite length

SH-SY5Y cells usually exhibit primary branching of one or more neurites from the cell body (Figure 3.11) and with further development the presence of secondary and tertiary branching. Total neurite length was measured as a representation of neuritic and developmental changes and the effect of Hsp27 mutations on these characteristics. The results are summarised in Figure 3.12.

In these experiments, the mean (± SEM) total neurite length was found to be 144.6μm ± 3.0μm (± SEM) in untransfected cells, 119.6μm ± 4.2μm in cells

Figure 3.11

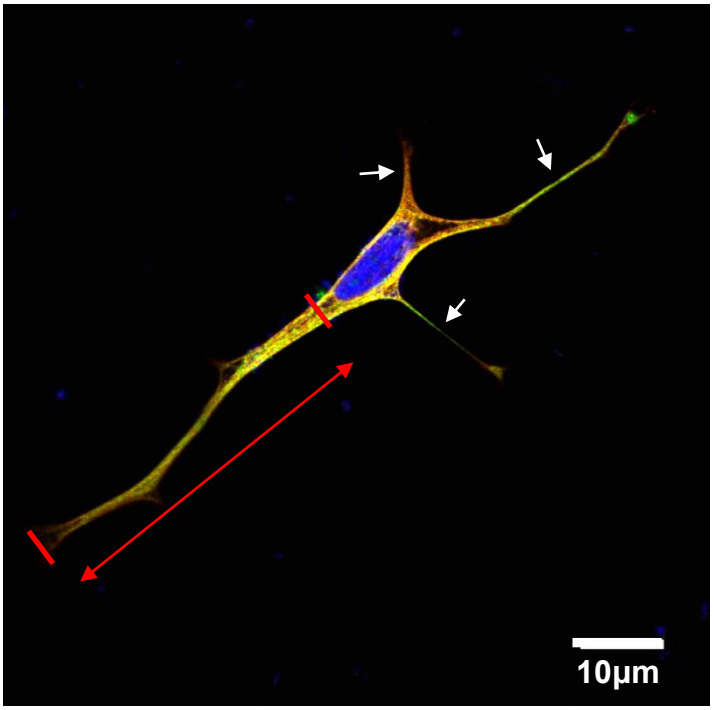

Figure 3.11 Analysis of neuritic branching in SH-SY5Y cells

SH-SY5Y cells were stained with V5 (red), β-tubulin III (green) and counterstained with DAPI (blue). This cell shows an example of neurite length calculation. Primarily, the length of the longest neurite was judged to be from the soma to the end of the neurite as indicated by the red arrow and red lines. Cells were only counted if the longest neurite was over 1½ times the length of the cell body. The white arrows identify all other neurite growth which is then considered to give the total neurite growth from the cell body.

Figure 3.12 The effect of Hsp27 mutations on total neurite length

A) The bar chart shows the mean total neurite length in untransfected cells and those transfected with wild type or the various Hsp27 mutations. In all cases, each experiment was repeated 3 times. Error bars = SEM; * $p<0.0001$; ** $p=0.03$; ***$p=0.04$, one-way ANOVA. **B)** A frequency distribution graph of the mean total neurite length was created for each experimental condition.

Figure 3.12

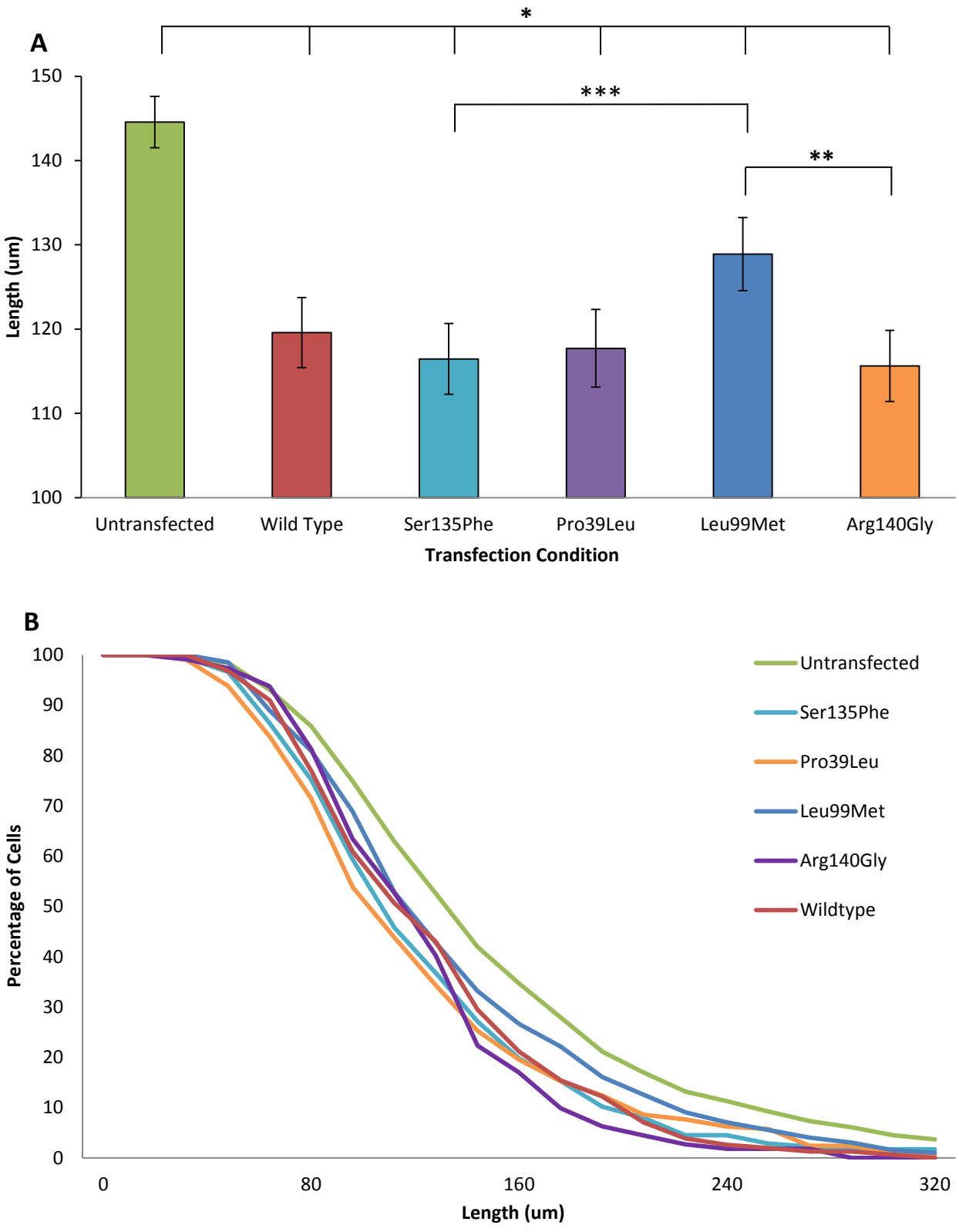
A
*
***
**
150
140
130
120
110
100
Length (um)
Untransfected
Wild Type
Ser135Phe
Pro39Leu
Leu99Met
Arg140Gly
Transfection Condition
B
100
90
80
70
60
50
40
30
20
10
0
Percentage of Cells
0
80
160
240
320
Length (um)
Untransfected
Ser135Phe
Pro39Leu
Leu99Met
Arg140Gly
Wildtype

transfected with wild type Hsp27 and 116.5µm ± 9.0µm, 117.7µm ± 4.6µm, 128.9µm ± 4.3µm and 115.6µm ± 4.2µm (± = SEM) in cells transfected with Ser135Phe, Pro39Leu, Leu99Met and Arg140Gly respectively (Figure 3.12A). When comparing untransfected cells with those transfected with either wild type or mutant Hsp27, a statistically significant decrease in total neurite length was observed (Figure 3.12A, $p<0.0001$). These results are also illustrated as a frequency graph, which indicates a shift to the left (i.e. a reduced total neurite length) in all transfected cells compared to untransfected cells (Figure 3.12B). Furthermore, when comparing the specific effects of individual Hsp27 mutations, a statistically significant difference in total neurite length was observed in cells transfected with the Leu99Met mutation when compared to other mutations Ser135Phe and Arg140Gly (Figure 3.12A, $p=0.04$ and $p=0.04$, respectively).

3.5.1.2. The effect of Hsp27 mutations on the length of the longest neurite

Although SH-SY5Y cells can exhibit polarisation, they tend to display one long 'axon-like' structure (See Figure 3.11). This enables us to more accurately measure any effects of the Hsp27 mutations on the development of the cells in a more specific fashion, separating development from cellular dysregulation (See Figure 3.13).

As shown in Figure 3.13A, the mean length of the longest neurite was 91.0µm ± 1.6µm in untransfected cells, 77.9µm ± 3.1µm in cells transfected with wild type Hsp27 and 72.0µm ± 2.6µm, 76.2µm ± 3.0µm, 79.9µm ± 2.7µm, and 68.8µm ± 2.4µm (± = SEM) in cells transfected with Ser135Phe, Pro39Leu, Leu99Met and Arg140Gly respectively (Figure 3.13A). When comparing untransfected cells with cells transfected with either wild type or mutant Hsp27, a statistically significant

Figure 3.13 The effect of Hsp27 mutations on neurite length

A) The bar chart shows the mean length of the longest neurite in untransfected cells and those transfected with wild type or various Hsp27 mutations. The results are the mean of three experiments. Error bars = SEM; * $p<0.0001$; ** $p<0.006$, one-way ANOVA. **B)** A frequency distribution graph was created of the mean longest neurite length for each experimental condition.

Figure 3.13

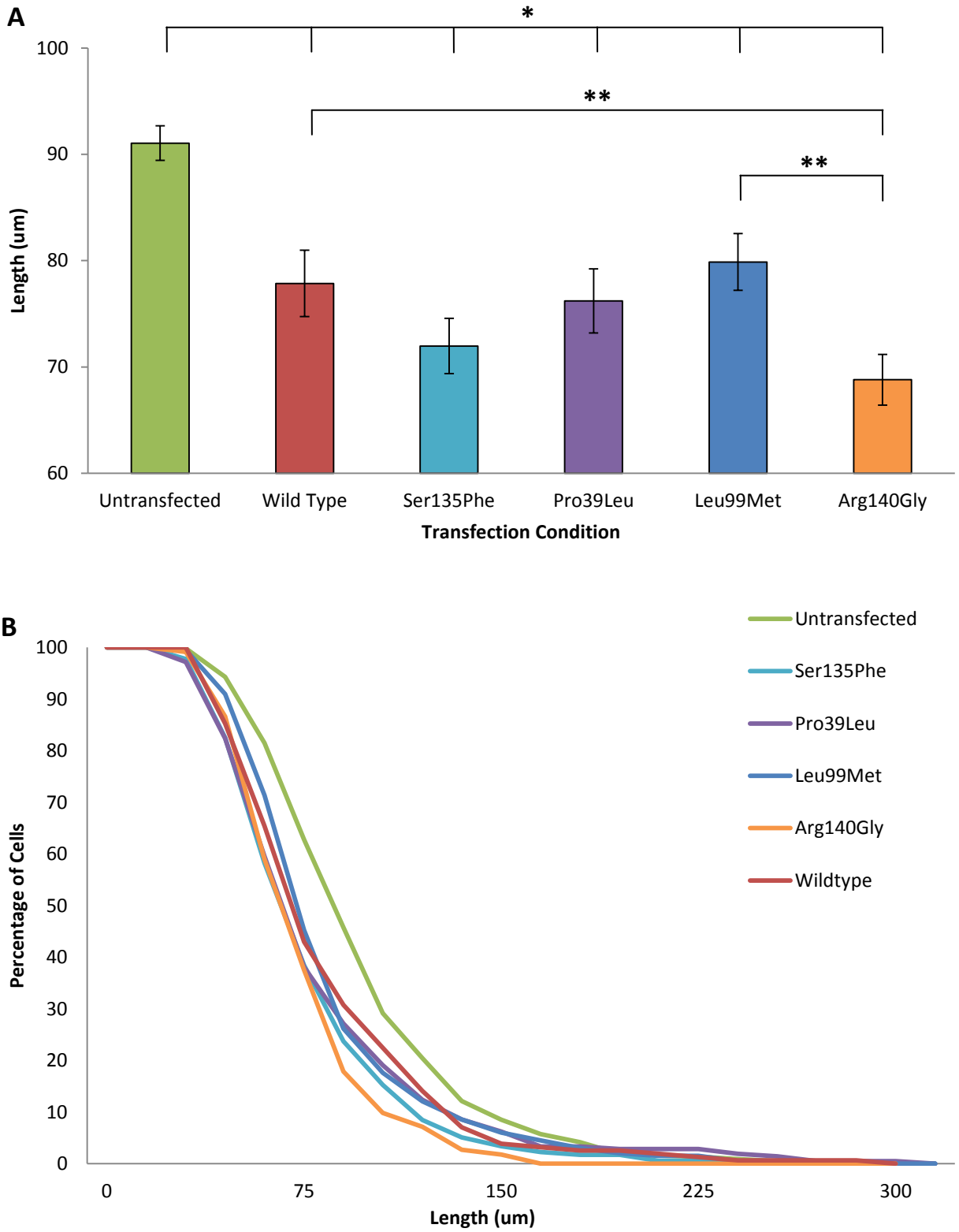
A
*
**
**
100
90
80
70
60
Length (um)
Untransfected
Wild Type
Ser135Phe
Pro39Leu
Leu99Met
Arg140Gly
Transfection Condition
B
Untransfected
Ser135Phe
Pro39Leu
Leu99Met
Arg140Gly
Wildtype
Percentage of Cells
100
90
80
70
60
50
40
30
20
10
0
0
75
150
225
300
Length (um)

decrease in total neurite length was seen in all transfected cells (Figure 3.13A, $p<0.0001$). This finding is also illustrated as a frequency graph, which shows a shift to the left, i.e. shorter neurites in transfected cells (Figure 3.13B). Furthermore, when cells transfected with the various Hsp27 mutations were compared, a statistically significant difference in total neurite length was also observed in cells transfected with the Arg140Gly mutation when compared to Leu99Met and wild type Hsp27 transfected cells (Figure 3.13A, $p=0.06$).

3.5.1.3. The effect of Hsp27 mutations on cellular complexity and differentiation

Following the analysis of cell development and growth, the neuritic branching and complexity of differentiation was determined next to examine more subtle effects of both the Lipofectamine 2000 transfection process and the Hsp27 mutations on the development of the neuritic network.

The number of primary neurites extending from the cell body was determined. The results showed that irrespective of transfection or expression of Hsp27 mutations, there was no change in the average number of neurites, so that each cell had an average of 1.9 ± 0.02 (± = SEM) neurites per cell (Figure 3.14A,C).

Cell differentiation was assessed by analysing branching from neurites and cell bodies (Figure 3.14B,D). Neurites were categorised as exhibiting secondary and tertiary branching, with the presence of tertiary branches taken as an indication of cellular maturation and complex differentiation. Cells were defined as exhibiting secondary differentiation if the cell had at least one neurite branching from a primary neurite (Figure 3.14B). Cells in the tertiary stage of differentiation were defined as

Figure 3.14 The effect of Hsp27 mutations on cellular development and neuritic complexity in neuronal cells

Cells stained with V5 (red), β-tubulin III (green) and counterstained with DAPI (blue) showing examples of cellular development and complexity. **A)** shows a partially differentiated SH-SY5Y cell with bidirectional branching of primary neurites from the cell body (white arrow). **B)** shows a differentiated SH-SY5Y cell with neurites extending from the cell body (white arrow), secondary neurite branching (red arrow) and tertiary branching (blue arrow). **C)** The bar chart shows the average number of primary neurites extending from the cell body when transfected with different Hsp27 mutations. **D)** The bar chart shows the level of secondary (dark bars) and tertiary (light bars) differentiation in cells transfected with different Hsp27 mutations. Error bars = SEM.

Figure 3.14

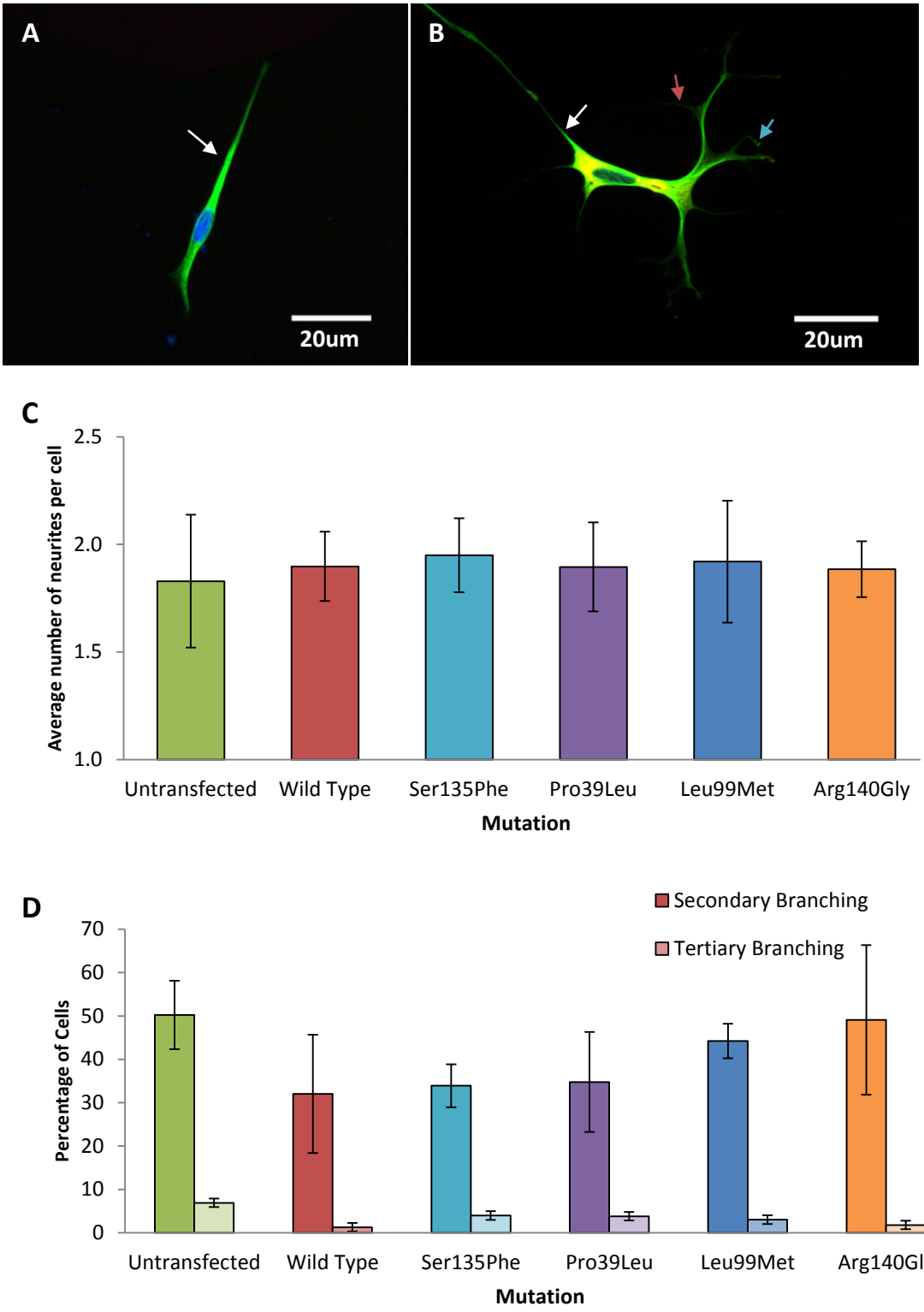
A
20um
B
20um
C
Average number of neurites per cell
2.5
2.0
1.5
1.0
Untransfected
Wild Type
Ser135Phe
Pro39Leu
Leu99Met
Arg140Gly
Mutation
D
Secondary Branching
Tertiary Branching
Percentage of Cells
70
60
50
40
30
20
10
0
Untransfected
Wild Type
Ser135Phe
Pro39Leu
Leu99Met
Arg140Gly
Mutation

showing neuritic branching that was removed from the cell body by two separate branch points (Figure 3.14B).

In untransfected cells, 50.3% ± 7.9% of cells were found to exhibit secondary neuritic branching. In cells transfected with wild type Hsp27, the number of cells with secondary neuritic branching was reduced to 32.1% ± 13.6% (non-significant). Transfection with mutant Hsp27 also reduced secondary branching to a similar extent as wild type Hsp27, so that 33.9% ± 5.0%, 34.8% ± 11.5%, 44.2% ± 4.0%, and 49.1% ± 17.3% (± = SEM) of cells transfected with Ser135Phe, Pro39Leu, Leu99Met and Arg140Gly respectively showed secondary branching (Figure 3.14D). No transfection or mutational condition showed a differential effect on secondary branching of neurites over and above that observed in wild type transfected cells.

The extent of tertiary neuritic branching was found to be 6.9% ± 0.01% in untransfected cells. In cells transfected with wild type Hsp27, the number of cells with tertiary neuritic branching was reduced to 1.28% ± 0.65% (non-significant). Transfection with mutant Hsp27 also reduced tertiary branching to a similar extent as wild type Hsp27, so that 3.95% ± 0.76%, 3.81% ± 0.30%, 3.02% ± 0.86%, and 1.79% ± 0.16% (± = SEM) in cells transfected with Ser135Phe, Pro39Leu, Leu99Met and Arg140Gly respectively (Figure 3.14D). Untransfected cells did show a significantly higher level of tertiary branching in comparison to transfected cells irrespective of mutation (Figure 3.14D, $p<0.05$). No transfection or mutational condition showed a differential effect on secondary branching of neurites (Figure 3.14D).

3.5.2. Hsp27 mutations induce pathological changes in neuronal cells

The effect of Hsp27 mutations on morphological features considered to be indicative of pathology in the regulation of cellular pathways was also examined. Cells were assessed for the presence of:

i. Neuritic stumps (See Figure 3.15A)
ii. Lamellipodia (See Figure 3.16A)
iii. Vacuoles (See Figure 3.17A)

3.5.2.1. The effect of Hsp27 mutations on the occurrence of neuritic 'stumps'

The term 'neuritic stump' is used in this study to define the presence of protrusions and neuritic projections, morphological changes at the end of the neurites, which may not be abnormal or pathological, but are of unknown function. They can be slightly varied in appearance (Figure 3.15A) and therefore this category represents a wide range of neuritic projections. The number of cells displaying stump-like features was established for each culture condition, based on the visual characteristics of cells.

Neuritic stumps were observed in 15.4% ± 4.4% of all untransfected cells, in cells transfected with wild type Hsp27, there was a small non-significant increase in the occurrence of such stumps, so that 28.2% ± 9.7% of cells exhibited neuritic stumps (Figure 3.15B). However, in cells transfected with mutant Hsp27 there was a clear increase in the number of cells with neuritic stumps. Thus, neuritic stumps were found in 44.1% ± 12.9%, 46.2% ±4.8%, 50.8% ± 10.7% and 60.7% ± 12.0% (± = SEM) of cells transfected with Ser135Phe, Pro39Leu, Leu99Met and Arg140Gly respectively (Figure 3.15B). Thus, in all mutant Hsp27 expressing cultures, the occurrence of neuritic stumps increased, however, this only reached statistical

Figure 3.15

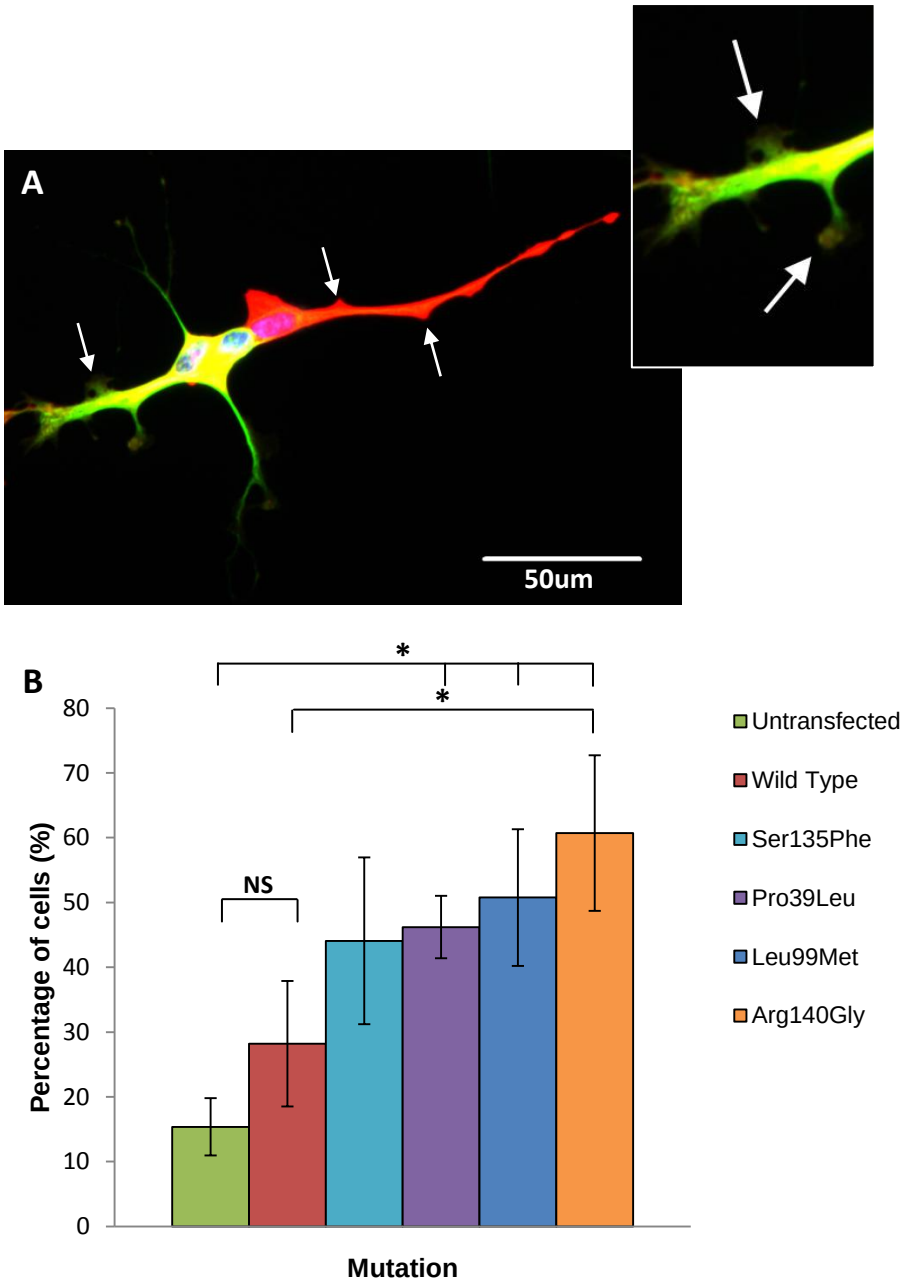

Figure 3.15 The effect of Hsp27 mutations on the occurrence of neuritic stumps in neuronal cells

A) Cells immuno-stained for V5 (red), β-tubulin III (green) and counterstained with DAPI (blue) are shown, illustrating the presence of neuritic stumps (white arrows, insert = magnification of neuritic stumps. **B)** The bar chart shows the percentage of cells with neuritic stumps in untransfected cells and those transfected with wild type and mutant Hsp27. Error bars = SEM; NS = non-significant; *p<0.05; **p=0.05, one-way ANOVA.

significance in Arg140Gly mutant cells (when compared to wild type Hsp27, $p<0.05$).

3.5.2.2. The effect of Hsp27 mutations on the occurrence of lamellipodia

Lamellipodia are cytoskeletal actin projections on the leading edge of the neurite (Figure 3.16A). Although they are a normal cellular process observed in differentiating or developing cells, an increase in the number of cells with lamellipodia is indicative of dysregulation of cell differentiation and motility (Mattila and Lappalainen, 2008).

Lamellipodia were found in 16.4% ± 3.3% (± = SEM) of all untransfected cells. In cells transfected with wild type Hsp27, the incidence of lamellipodia increased to 27.6% ± 5.4% (Figure 3.16B). All Hsp27 mutations caused a significant increase in the number of cells with lamellipodia compared to wild type Hsp27 expressing cells. Specifically, 3 mutations caused a statistically significant increase in lamellipodia to 55.9% ± 5.8%, 55.2% ± 7.0%, 48.7% ± 0.9% and 33.0% ± 6.4% (± = SEM) in cells transfected with Ser135Phe, Pro39Leu, Leu99Met ($p<0.03$) and Arg140Gly respectively (Figure 3.16B).

3.5.2.3. The effect of Hsp27 mutations on the occurrence of cellular vacuoles

The presence of vacuoles in cells *in vivo* is a well recognised sign of cellular pathology. While the presence of vacuoles on cells *in vitro* is also a deleterious sign, the high turnover and artificial conditions of cell culture increase the presence of vacuoles in untransfected cells (Figure 3.17A).

Figure 3.16

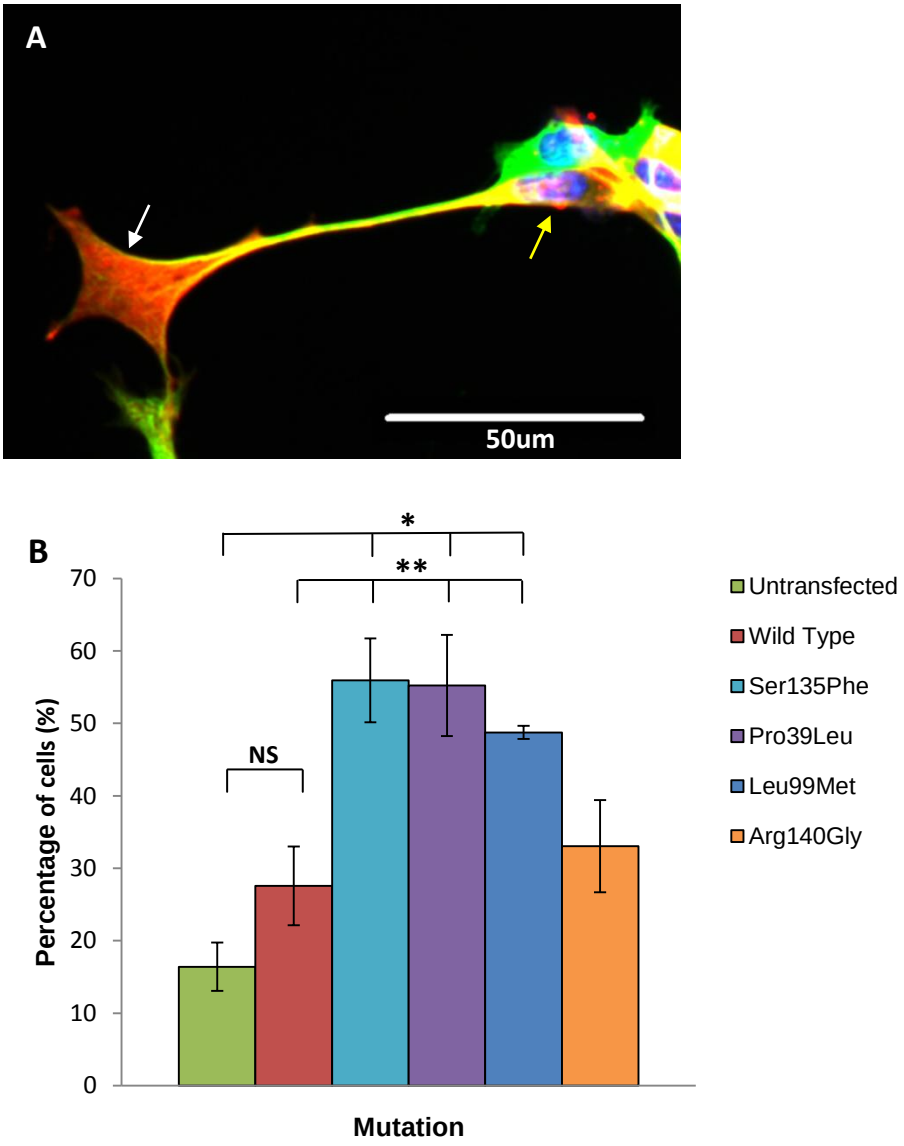

Figure 3.16 The effect of Hsp27 mutations on the occurrence of lamellipodia in neuronal cells

A) Cells immuno-stained for V5 (red), β-tubulin III (green) and counterstained with DAPI (blue) are shown, illustrating the presence of lamellipodia (white arrow) and a cell body (yellow arrow). **B)** The bar chart shows the percentage of untransfected cells and cells transfected with wild type or mutant Hsp27. Error bars = SEM; NS = none significant; *p<0.01; **p<0.03, one-way ANOVA.

Figure 3.17

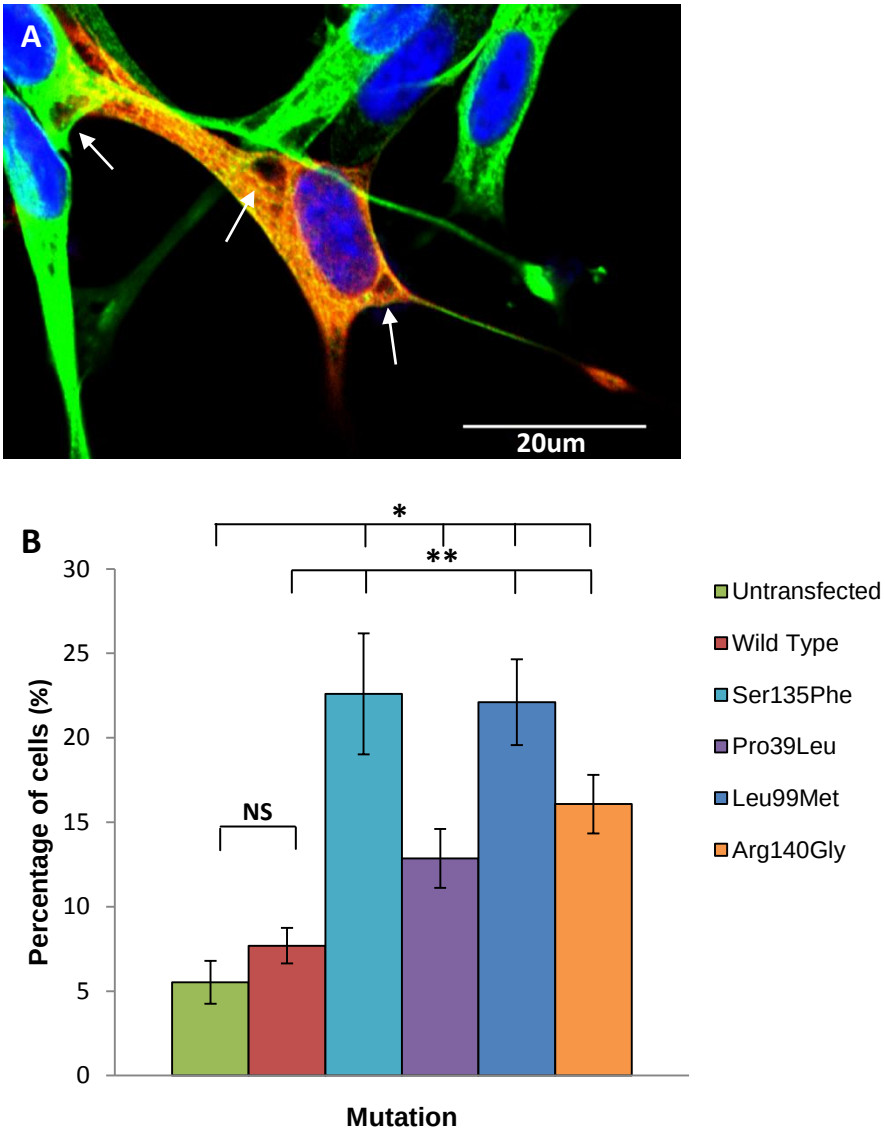

Figure 3.17 The effect of Hsp27 mutations on the occurrence of vacuoles in neuronal cells

A) Cells immuno-stained for V5 (red), β-tubulin III (green) and counterstained with DAPI (blue) illustrating the presence of vacuoles (white arrows) in transfected and untransfected cells. **B)** The bar chart shows the occurrence of vacuoles in untransfected cells and cells transfected with wild type or mutant Hsp27. Error bars = SEM; NS = non-significant; *p<0.04; **p<0.05, one-way ANOVA.

As shown in Figure 3.17B, analysis of untransfected SH-SY5Y cells in this study established a relatively modest incidence of vacuoles with only 5.5% ± 1.3% (± = SEM) of cells presenting any vacuoles. Transfection with wild type Hsp27 had little effect on this level of vacuole occurrence, and only 7.7% ± 1.1% of wild type Hsp27 cells had vacuoles. However, transfection with mutant Hsp27 resulted in a clear increase in vacuole occurrence compared to cells expressing wild type Hsp27. In particular, 3 mutations caused a statistically significant increase in vacuole occurrence, and 22.6% ± 3.6%, 22.1% ± 2.5%, 16.1% ± 1.7% and 12.3% ± 1.8% (± = SEM) vacuoles were found in cells transfected with Ser135Phe, Leu99Met, Arg140Gly ($p<0.05$) and Pro39Leu respectively (Figure 3.17B). Furthermore, the vacuoles within the transfected cells appeared larger than in untransfected SH-SY5Y cells.

3.6. Chapter 3 Summary

In these experiments, primarily designed to screen for differential effects of Hsp27 mutations, I demonstrated that all the Hsp27 mutations examined significantly increased cell death of otherwise unstressed cells, confirming the toxicity of the patient mutations. In conditions of cellular stress, one specific mutation, Ser135Phe, showed a significant increase in cellular vulnerability due to cytoskeletal disruption and increased cytotoxicity.

Furthermore, a detailed immunocytochemical analysis showed that the Ser135Phe mutation, which increased cellular vulnerability due to cytoskeletal disruption and had a negative impact on neurite growth, although this did not reach significance. However, the Arg140Gly mutation significantly inhibited neurite outgrowth, but did not alter cellular differentiation. Since Hsp27 is known to play a role in neurite outgrowth (Williams *et al*., 2005), several studies investigating the effects of Hsp27 mutations have focused on the disruption of neurite growth and axonal transport. For example, Irobi *et al.* (2010) demonstrated a significant >50% reduction in neurite length in primary motoneurons transfected with CMT 2L disease-causing mutations in Hsp22 (Irobi *et al*., 2010). The mutations, Lys141Asn and Lys141Glu in a small heat shock protein known to associate with Hsp27 (Irobi *et al*., 2004; Sun *et al*., 2004) cause CMT 2L, an axonal form of CMT with a phenotype that is clinically indistinguishable from CMT 2F (Evgrafov *et al*., 2004; Irobi *et al*., 2004). Lys141Asn and Lys141Glu are equivalent to the Arg140Gly mutation in Hsp27 with respect to both gene position and protein region (Irobi *et al*., 2010), suggesting that not only is this region of the small heat shock protein important for neurite outgrowth in motoneurons, but that mutations in this area of the protein may be particularly detrimental to the structure and function of the axon such as the cytoskeleton and axonal transport. In the experiments described in Chapter 3, the negative effect of

the Arg140Gly mutation and to a lesser extent, the Ser135Phe Hsp27 mutation on neurite outgrowth may be the result of differential interactions between the Hsp27 mutant proteins and different cytoskeletal components during the development of cell neurites.

However, while only Hsp27 mutations, Ser135Phe and Arg140Gly, located in the hot spot α-crystallin domain of the protein affected the development of the cell, all mutations caused alterations in the normal morphology of the cell and possible dysregulation of cytoskeletal features. Previous studies have shown that mutations in Hsp27 can cause perturbations of cytoskeletal components, possibly causing dysregulation and disorganisation of the cytoskeleton. For example, in the study by Irobi *et al.* 2010, significant numbers of primary cells transfected with mutant Hsp22 displayed spheroids, or beaded neurites, a clear indication of cytoskeletal dysregulation and degeneration (Irobi *et al*., 2010). Here, it was observed that cells transfected with wild type Hsp27 showed no significant increase in morphological perturbations, while all mutations had a significant impact on the morphology of the cell and possible dysregulation of the cytoskeleton as determined by a number of cellular features.

When taken together, the results presented in Chapter 3 suggest a role in cytoskeletal disruption for two mutations located in the α-crystallin domain of the protein. The experiments described in this Chapter were designed to screen for differential effects of Hsp27 mutations. So far, even though the Pro39Leu mutation (located in the N-terminus of the protein) and the recessive Leu99Met mutation (located in the α-crystallin domain of the protein, but out of the genetic hot spot) have both been shown to be significantly cytotoxic to cells, the other basic outcome measures tested here have not revealed any other differential effects.

Chapter 4. The effect of Hsp27 mutations on the interaction of Hsp27 with cellular proteins and structures

The experiments described in Chapter 3 summarise the optimisation of an SH-SY5Y *in vitro* cellular model of mutations in Hsp27. Using this model, I undertook a screen for differential effects of mutant Hsp27 using outcome measures based on the known functional roles of Hsp27 within the cell. The effects of wild type and mutant Hsp27 on readouts of cell toxicity, neurite outgrowth and cellular morphological changes were examined. The results suggest that mutations Ser135Phe and Arg140Gly, located in the hot spot α-crystallin domain of Hsp27, may selectively disrupt aspects of the cytoskeleton, although the mode of action is, as yet, unknown.

Although the Pro39Leu Hsp27 mutation (located in the N-terminus of the protein) and the recessive Leu99Met Hsp27 mutation (located in the α-crystallin domain of the protein, but outside the genetic hot spot) were both found to be significantly cytotoxic, other outcome measures tested did not show any specific effects of the mutations. Therefore, in this Chapter, the protein interactions of mutant Hsp27 with different proteins, including key proteins of the cytoskeleton, were examined using immunocytochemistry to identify any further, potential differences between the different Hsp27 mutations and to identify some of the pathways that may be altered by these mutations.

4.1. Co-localisation of the V5 epitope and transfected Hsp27

SH-SY5Y cells were transfected using a pcDNA3.1/V5 plasmid containing a V5 epitope as a marker of the transient expression of the exogenous, transfected Hsp27 protein (Materials and Methods, Chapter 2, Figure 2.2). The V5 epitope is essential as a protein marker as SH-SY5Y cells are derived from human origin and therefore contain endogenous Hsp27.

To distinguish transfected and endogenous Hsp27, cells were co-stained with V5 (Figure 4.1A) and Hsp27 (Figure 4.1B) demonstrating co-localisation of the two proteins and validating V5 as a reliable marker for transfected Hsp27. Cells showed cytoplasmic co-localisation of V5 and Hsp27 in all forms of transfected Hsp27 (Figure 4.1C).

Hsp27 has a relatively small molecular weight of 27KDa and its functions are dependent on its phosphorylation state and protein conformation. Therefore, it is important to establish that the V5 tag had no functional impact on the actions of Hsp27 when attached to the transfected protein. Evidence for this is presented in this Chapter (Section 4.7).

4.2. The phenotypic effects of pharmacological cell stressors on cellular morphology

To assess the effects of mutations in Hsp27 on the normal functions of the protein in cells under conditions of specific stress, SH-SY5Y cells were stressed using pharmacological agents that act on different proteins of the cytoskeleton with which Hsp27 interacts and functions. Cytochalasin D and Colchicine were added at low concentrations (0.2µM) to detect morphological changes in the neurite, as higher

Figure 4.1

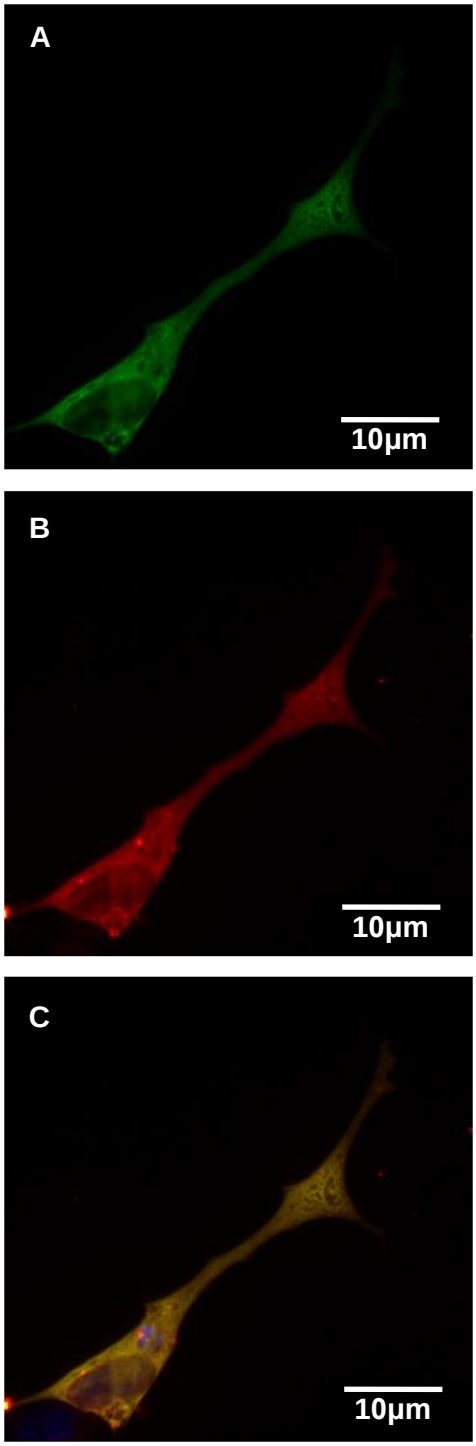

Figure 4.1 Co-localisation of V5 epitope and transfected wild type Hsp27

Cells immuno-stained for V5 (red) and Hsp27 (green), showing an example of co-localisation and demonstrating that the V5 epitope is suitable to be used as a marker to distinguish transfected Hsp27 and endogenous Hsp27. **A)** V5 **B)** Hsp27 **C)** Overlay of V5 and Hsp27.

concentrations (10µM) caused extensive damage to the morphology of the cell making it difficult to determine the full extent of the mutational effects (Figure 3.8). Although both stressors affect the cytoskeleton, they have different modes of action that are clearly demonstrated by the differential effects on the cellular morphology at lower concentrations. As described below, cells were examined under different conditions of cell stress at 4DIV using Phalloidin, a marker for F-actin, β-tubulin III - a neuron-specific microtubule protein, and neurofilament-200 heavy chain, which is a member of the neurofilament network.

In vitro cell culture is a physiologically unnatural environment. Therefore, the baseline 'unstressed' conditions of *in vitro* cells will be physiologically different to those *in vivo.* In unstressed cells transfected with wild type Hsp27 there was little sign of disruption to the cellular morphology in comparison to untransfected cells, and in both conditions, cells also developed long neurites. In contrast, some cells which had been transfected with mutant Hsp27 showed actin stress fibres, even under unstressed conditions, which were not observed in untransfected or wild type Hsp27 transfected cells (Figure 4.2C-E).

In cells treated with Cytochalasin D (0.2µM), an agent which binds to F-actin and thereby stabilises the cytoskeletal network and halts neurite outgrowth, the cellular morphology changed and neurite outgrowth appeared stunted. The ends of the neurites showing either disrupted bulbed ends or a sudden halt at the end of the neurite, with the majority of cells displaying actin stress fibres.

To examine the effects of microtubule disruption on the cell, the effects of Colchicine (0.2µM) was also examined. Colchicine disrupts cellular structure by irreversibly binding to tubulin and stabilising the microtubule network. The addition of Colchicine

to the cells caused a dramatic change in phenotype. Thus the length and diameter of the neurites decreased, the cells lost polarity and became more rounded with irregular neurites, a dysregulated cytoskeleton and an increase in actin stress fibres.

4.3. Effects of Hsp27 mutations on the co-localisation of Hsp27 with cytoskeletal proteins

The effects of the various Hsp27 mutations on the normal pattern of co-localisation with various cytoskeletal proteins including F-actin, β-tubulin and neurofilament-200 heavy chain was examined in stressed and unstressed conditions, in untransfected cells, and cells transfected with either wild type Hsp27 or each of the Hsp27 mutations. Cells were examined by immunostaining for V5 and each of the cytoskeletal markers for:

i. The extent of co-localisation between Hsp27 and cytoskeletal proteins
ii. The localisation of cytoskeletal protein and Hsp27 immunoreactivity within the cell, to establish whether this was altered by any of the Hsp27 mutations.

4.4. Hsp27 mutations alter the co-localisation of Hsp27 with F-actin

As previously shown in Chapter 3 (Figures 3.12 and 13), certain mutations in Hsp27 decrease neurite outgrowth; a process driven by the actin-based growth cone at the end of the neurite (Geraldo and Gordon-Weeks, 2009). As discussed in the Introduction, Section 1.8.8., Hsp27 functionally interacts with F-actin while in a phosphorylated, monomeric form (Lavoie *et al*., 1993b; Mounier and Arrigo, 2002b). Monomeric Hsp27 binds to F-actin to stabilise the cytoskeleton and this action is more prominent in cells under stress conditions (Lavoie *et al*., 1993a). To investigate whether changes in the interaction between Hsp27 and F-actin may be caused by mutations in Hsp27, the cells were immunostained with V5 to visualise the

transfected protein and Phalloidin which binds to F-actin with high selectivity. The cells were examined under both non-stressed and stressed conditions.

4.4.1. Co-localisation of endogenous, wild type and mutant transfected Hsp27 with F-actin in unstressed conditions

The effects of Hsp27 mutations on cellular morphology in unstressed conditions were examined first. As well as mutant Hsp27, the interaction of wild type and endogenous Hsp27 with F-actin was examined. Under basal conditions at 4DIV, endogenous Hsp27 did not co-localise with the actin cytoskeleton (Figure 4.2A). Similarly, wild type Hsp27, Pro39Leu Hsp27 and Leu99Met Hsp27 did not interact with the actin cytoskeleton (Figures 4.2B, E and F) shown by the lack of co-localisation of transfected Hsp27 tagged with V5 and the Phalloidin-stained actin cytoskeleton.

In contrast, in cells transfected with either the Ser135Phe or Arg140Gly Hsp27 mutations, a clear increase in the co-localisation of V5 with Phalloidin-stained F-actin was observed (Figure 4.2C and D). The Ser135Phe Hsp27 mutation showed co-localisation with actin stress fibres, indicated by yellow staining in Figure 4.2C. Cells transfected with Arg140Gly Hsp27 also had increased co-localisation with actin stress fibres. Although these mutations demonstrated an increase in stress fibres, these structures were also increased in cells transfected with the Pro39Leu Hsp27 mutation, where no co-localisation between transfected Hsp27 and actin stress fibres was observed, suggesting a mutant-specific effect (Figure 4.2E). The transfection of wild type or mutant Hsp27 did not change the localisation of the F-actin immunoreactivity within the cell.

Figure 4.2 Co-localisation of endogenous, wild type transfected and mutant transfected Hsp27 with F-actin in unstressed conditions.

A) Untransfected cells were stained for Hsp27 (red), phalloidin (green) labelling F-actin and counterstained with the nuclear marker DAPI (blue) to show normal cellular distribution of endogenous Hsp27 and in unstressed cellular conditions. Yellow arrows specify a lack of co-localisation between endogenous Hsp27 and F-actin.

B-F) Cells transfected with wild type and mutant Hsp27 were also stained for V5, phalloidin and DAPI as above, to show cellular distribution of transfected mutant and wild type Hsp27 in *in vitro,* unstressed cellular conditions. White arrows specify co-localisation between wild type and mutant Hsp27 and F-actin, co-localisation indicated by yellow staining, while yellow arrows indicate a lack of co-localisation. **B)** Wild type transfected Hsp27, **C)** Ser135Phe Hsp27, **D)** Arg140Gly Hsp27, **E)** Pro39Leu Hsp27 and **F)** Leu99Met Hsp27.

Figure 4.2

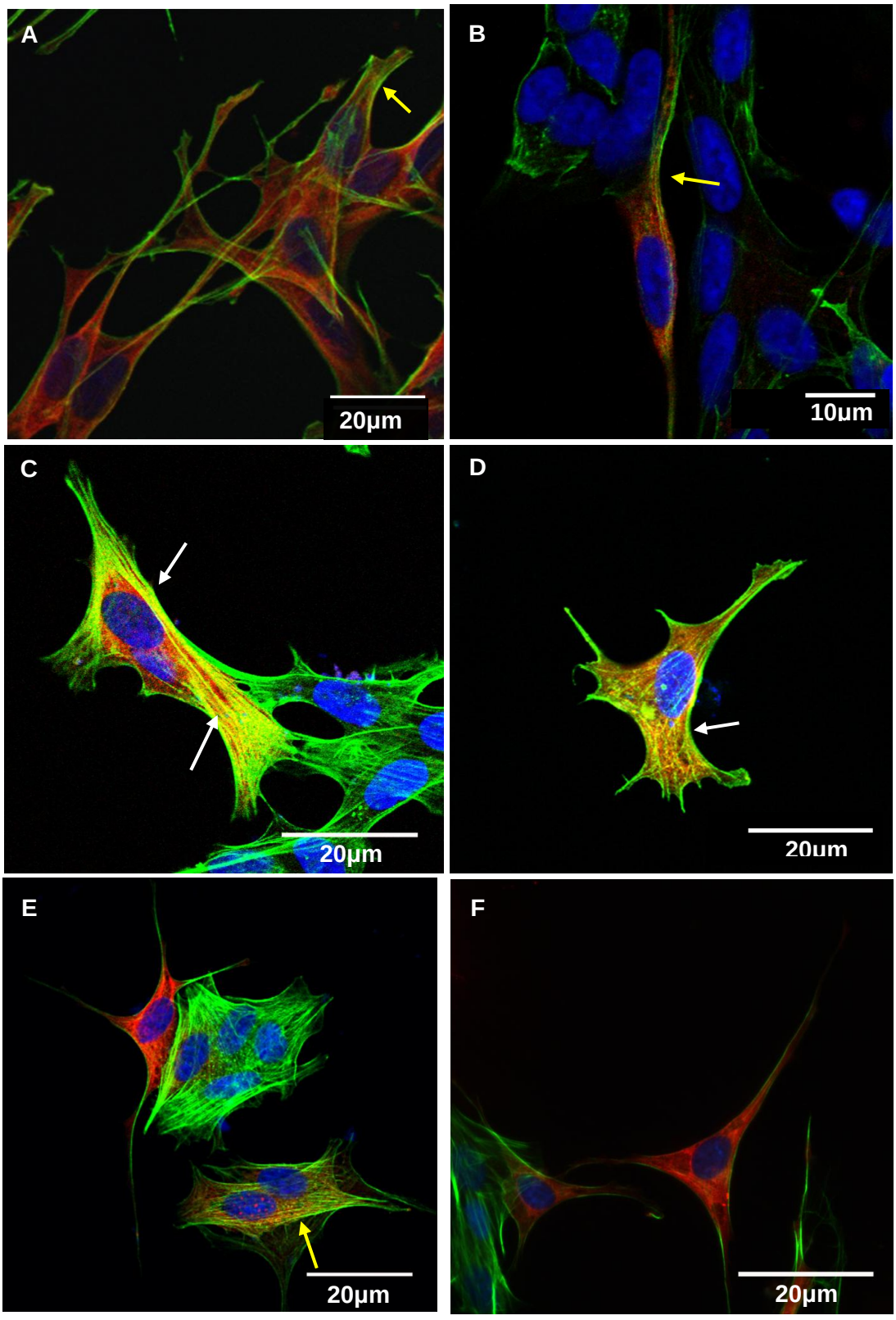

4.4.2. Co-localisation patterns of endogenous, wild type and mutant transfected Hsp27 with F-actin in Cytochalasin D treated cells

As discussed in Chapter 3, Section 3.4.2., Cytochalasin D acts on the actin cytoskeleton by stabilising F-actin. Following treatment of cells with Cytochalasin D (0.2uM), there was a small increase in the extent of co-localisation between endogenous Hsp27 and F-actin, proximal to the cell soma as well as signs of co-localisation between the Hsp27 and the actin stress fibres which formed (Figure 4.3A). This is in contrast to the staining pattern observed in unstressed cells (Figure 4.2A), described above. The same pattern of staining was observed in cells transfected with wild type Hsp27, where Hsp27 co-localised with actin stress fibres and with F-actin in the cell soma (Figure 4.3B).

Whilst the treatment of the cells with a cell stressor increased the co-localisation of both endogenous and wild type transfected Hsp27 with the actin cytoskeleton, this was not the case with either the Pro39Leu or Leu99Met Hsp27 mutations, which showed a lack of co-localisation with the actin cytoskeleton (Figure 4.3E and F).

In unstressed conditions, in cells transfected with both the Ser135Phe and Arg140Gly Hsp27 mutations there was a clear co-localisation of the mutant Hsp27 with the actin cytoskeleton, especially with actin stress fibres. When Cytochalasin D was added to the cells, both mutations showed a lack of co-localisation with actin stress fibres (Figure 4.3C and D), demonstrating an opposite reaction to endogenous and wild type transfected Hsp27 which showed actin co-localisation in Cytochalasin D stress conditions. While the Ser135Phe Hsp27 mutation showed increased cell soma localisation (Figure 4.3C), the Arg140Gly Hsp27 mutation showed an increased expression at the leading edges of the cell, co-localising with F-actin in the growth cone, lamellipodia-like structures formed at the end of the

Figure 4.3 Co-localisation of endogenous, wild type and mutant transfected Hsp27 with F-actin in Cytochalasin D treated cells.

A) Untransfected cells were stained for Hsp27 (red), phalloidin (green) labelling F-actin and counterstained with the nuclear marker DAPI (blue) to show the normal cellular distribution of endogenous Hsp27 and actin in cells treated with Cytochalasin D. White arrows specify co-localisation between endogenous Hsp27 and F-actin, co-localisation is indicated by yellow staining.

B-F) Cells transfected with wild type and mutant Hsp27 were also stained for V5, phalloidin and DAPI, to show cellular distribution of transfected mutant and wild type Hsp27 in cells treated with Cytochalasin D *in vitro*. White arrows specify co-localisation between wild type and mutant Hsp27 and F-actin co-localisation is indicated by yellow staining and yellow arrows indicate the absence of co-localisation. **B)** Wild type transfected Hsp27, **C)** Ser135Phe Hsp27, **D)** Arg140Gly Hsp27, **E)** Pro39Leu Hsp27 and **F)** Leu99Met Hsp27.

Figure 4.3

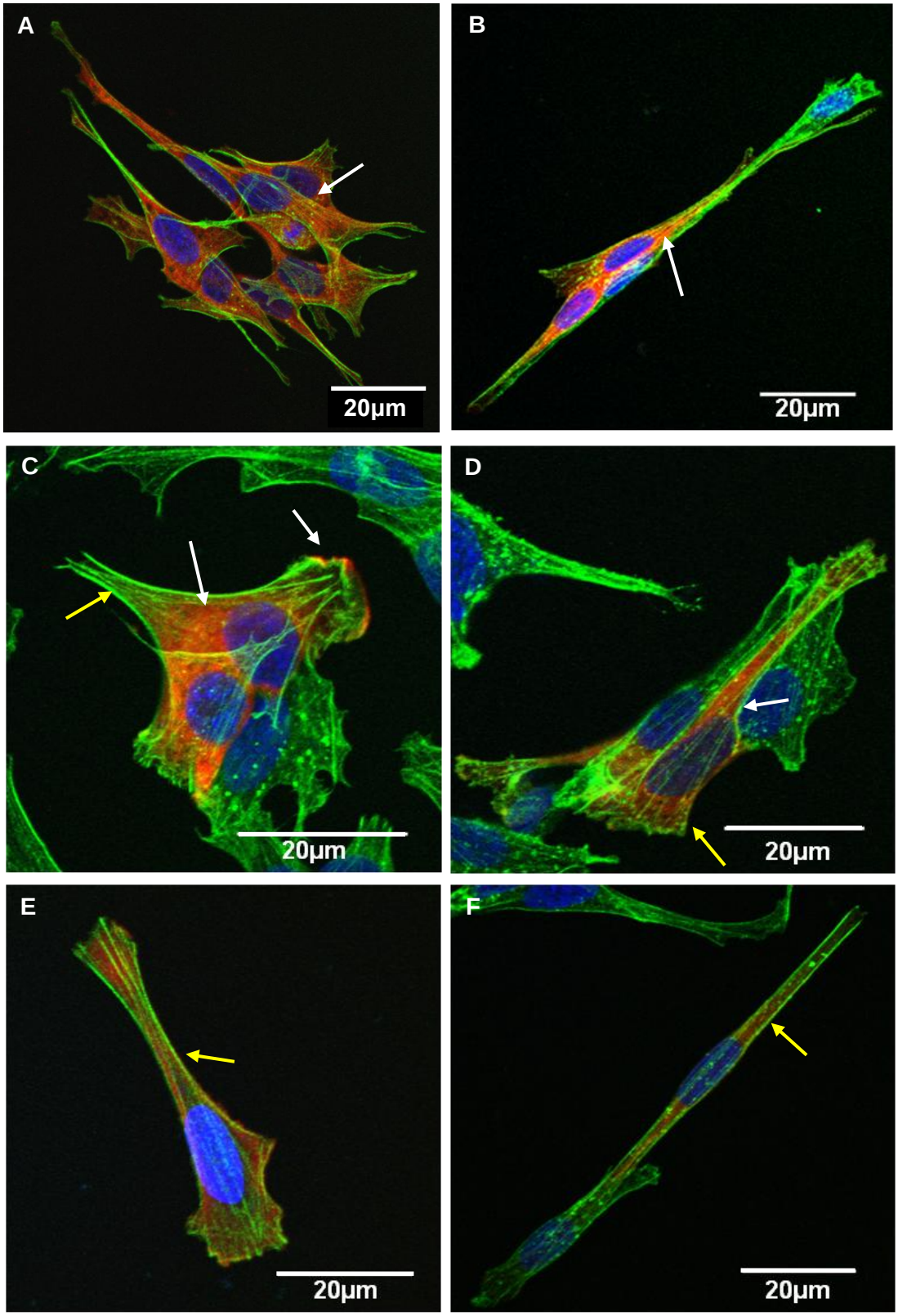

neurites (Figure 4.3D). Although the addition of Cytochalasin D altered the location and expression pattern of the F-actin, the transfection of mutant Hsp27 did not alter the localisation of the F-actin immunoreactivity.

4.4.3. Co-localisation patterns of endogenous, wild type and mutant transfected Hsp27 with F-actin in Colchicine treated cells

Colchicine, an agent which acts by irreversibly binding to the microtubule network, was used in this study as it acts on a protein which has been shown to co-localise with Hsp27, but has not yet been functionally linked to the small heat shock protein (Williams *et al*., 2005). Colchicine also causes a more severe phenotype than Cytochalasin D at the same concentration indicating higher levels of cellular stress. Neither endogenous Hsp27 nor transfected wild type Hsp27 was found to co-localise with Phalloidin-stained F-actin (Figure 4.4A and B).

When Colchicine-stressed cells were transfected with Ser135Phe or Arg140Gly Hsp27 co-localisation between the mutant Hsp27, actin stress fibres and the actin cytoskeleton was observed in some, but not all, transfected cells (Figure 4.4C and D). However, not all cells transfected with the mutants showed a co-localisation with F-actin. The Leu99Met Hsp27 did not co-localise with Phalloidin-stained F-actin (Figure 4.4F) and the Pro39Leu Hsp27 mutant showed some co-localisation with actin stress fibres (Figure 4.4E). Although the addition of Colchicine altered the location and expression pattern of the F-actin, the transfection of mutant Hsp27 did not alter the localisation of the F-actin immunoreactivity.

Figure 4.4 Co-localisation of endogenous, wild type and mutant transfected Hsp27 with F-actin in Colchicine treated cells.

A) Untransfected cells were stained for Hsp27 (red), phalloidin (green) labelling F-actin and counterstained with the nuclear marker, DAPI (blue), to show normal cellular distribution of endogenous Hsp27 and actin in cells treated with Colchicine. Yellow arrows indicate the absence of co-localisation.

B-F) Cells transfected with wild type and mutant Hsp27 were also stained for V5, phalloidin and DAPI, to show cellular distribution of transfected mutant and wild type Hsp27 in cells treated with Colchicine *in vitro*. White arrows specify co-localisation between wild type and mutant Hsp27 and actin, co-localisation is indicated by orange and yellow staining, while the yellow arrows indicate a lack of co-localisation. **B)** Wild type transfected Hsp27, **C)** Ser135Phe Hsp27, **D)** Arg140Gly Hsp27, **E)** Pro39Leu Hsp27 and **F)** Leu99Met Hsp27.

Figure 4.4

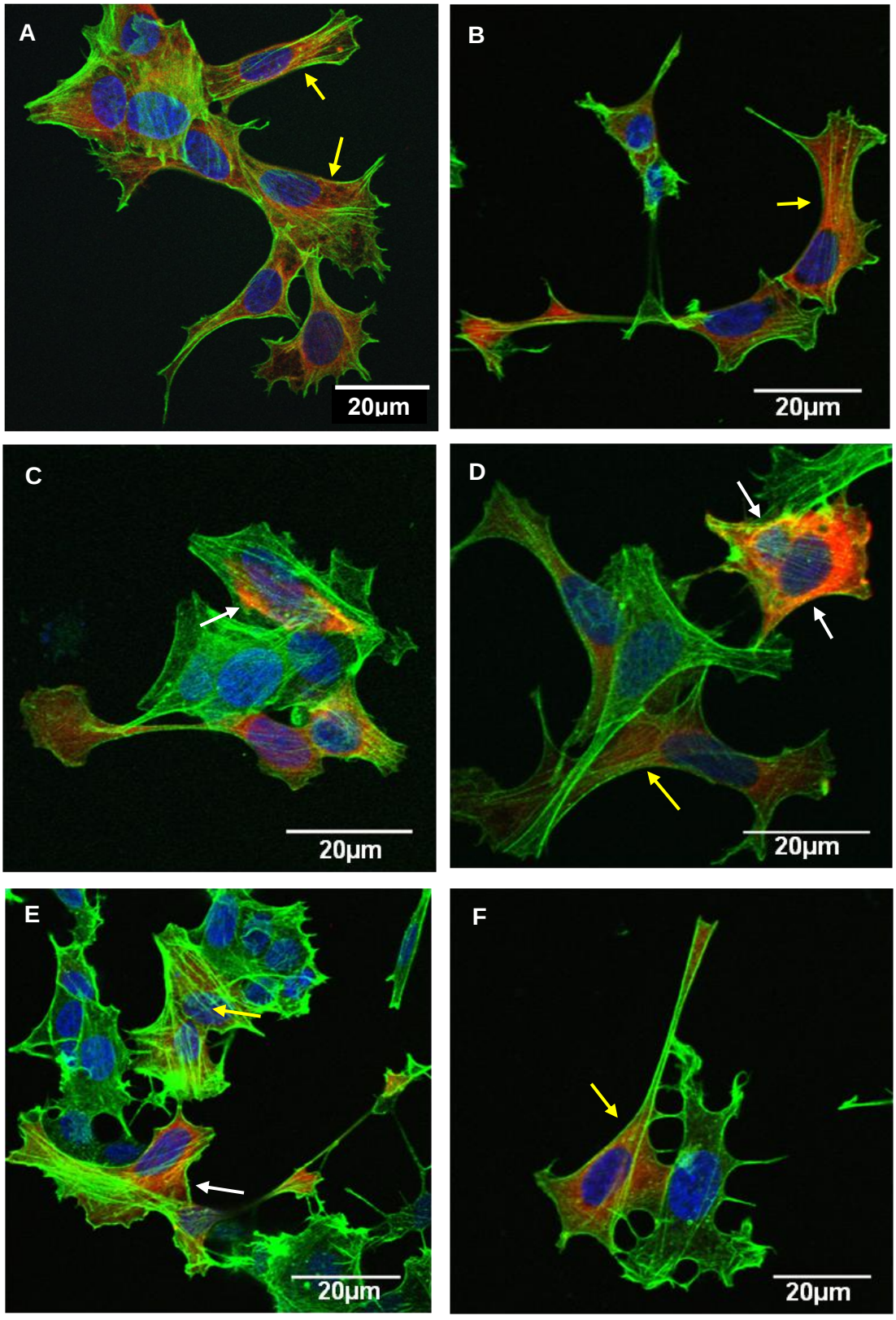

4.5. Co-localisation of Hsp27 with β-tubulin III is not altered by the expression of mutant Hsp27

Hsp27 has not been previously shown to functionally interact with the microtubule network, but *in vitro*, Hsp27 co-localises with tubulin (Williams *et al*., 2005). The microtubule network is integral to axonal transport and the dynamic structure of the cell axon (Geraldo and Gordon-Weeks, 2009) which has been shown to be affected by mutations in Hsp27 (Chapter 3, Figures 3.12 and 13). Therefore, the co-localisation of β-tubulin III (a component of the microtubule network) and Hsp27 was examined under basal as well as different conditions of cellular stress.

4.5.1. Co-localisation patterns of endogenous, wild type and mutant transfected Hsp27 with β-tubulin III in unstressed cells

Under baseline, unstressed conditions, the co-localisation of both endogenous and transfected wild type and mutant Hsp27 was assessed. The results showed clear co-localisation between β-tubulin III and endogenous Hsp27 in all cells (Figure 4.5A). This staining pattern was recapitulated by all transfected Hsp27 with no difference between the wild type or mutant transfected proteins or no difference in localisation of the β-tubulin III immunoreactivity (Figure 4.5B-F).

4.5.2. Co-localisation patterns of endogenous, wild type and mutant transfected Hsp27 with β-tubulin III in Cytochalasin D and Colchicine treated cells

While cells showed co-localisation of β-tubulin III with all forms of Hsp27 in unstressed cells, this co-localisation was reduced when cells were stressed using Cytochalasin D Although the cellular localisation of Hsp27 or β-tubulin III did not appear to change, the appearance of co-localisation was reduced (Figure 4.6).

Figure 4.5 Co-localisation of endogenous, wild type and mutant transfected Hsp27 with β-tubulin III in unstressed conditions.

A) Untransfected cells were stained for Hsp27 (red), β-tubulin III (green) and counterstained with nuclear marker, DAPI (blue), to show the normal cellular distribution of endogenous Hsp27 in unstressed cellular conditions. White arrows specify co-localisation between wild type and mutant Hsp27 and β-tubulin III, co-localisation indicated by orange and yellow staining, while yellow arrows indicate the absence of co-localisation.

B-F) Cells transfected with wild type and mutant Hsp27 were also stained for V5, β-tubulin III and DAPI, to show cellular distribution of transfected mutant and wild type Hsp27 in *in vitro,* unstressed cellular conditions. White arrows specify co-localisation between wild type and mutant Hsp27 and β-tubulin III, co-localisation indicated by yellow staining while yellow arrows indicate the absence of co-localisation. **B)** Wild type transfected Hsp27, **C)** Ser135Phe Hsp27, **D)** Arg140Gly Hsp27, **E)** Pro39Leu Hsp27 and **F)** Leu99Met Hsp27.

Figure 4.5

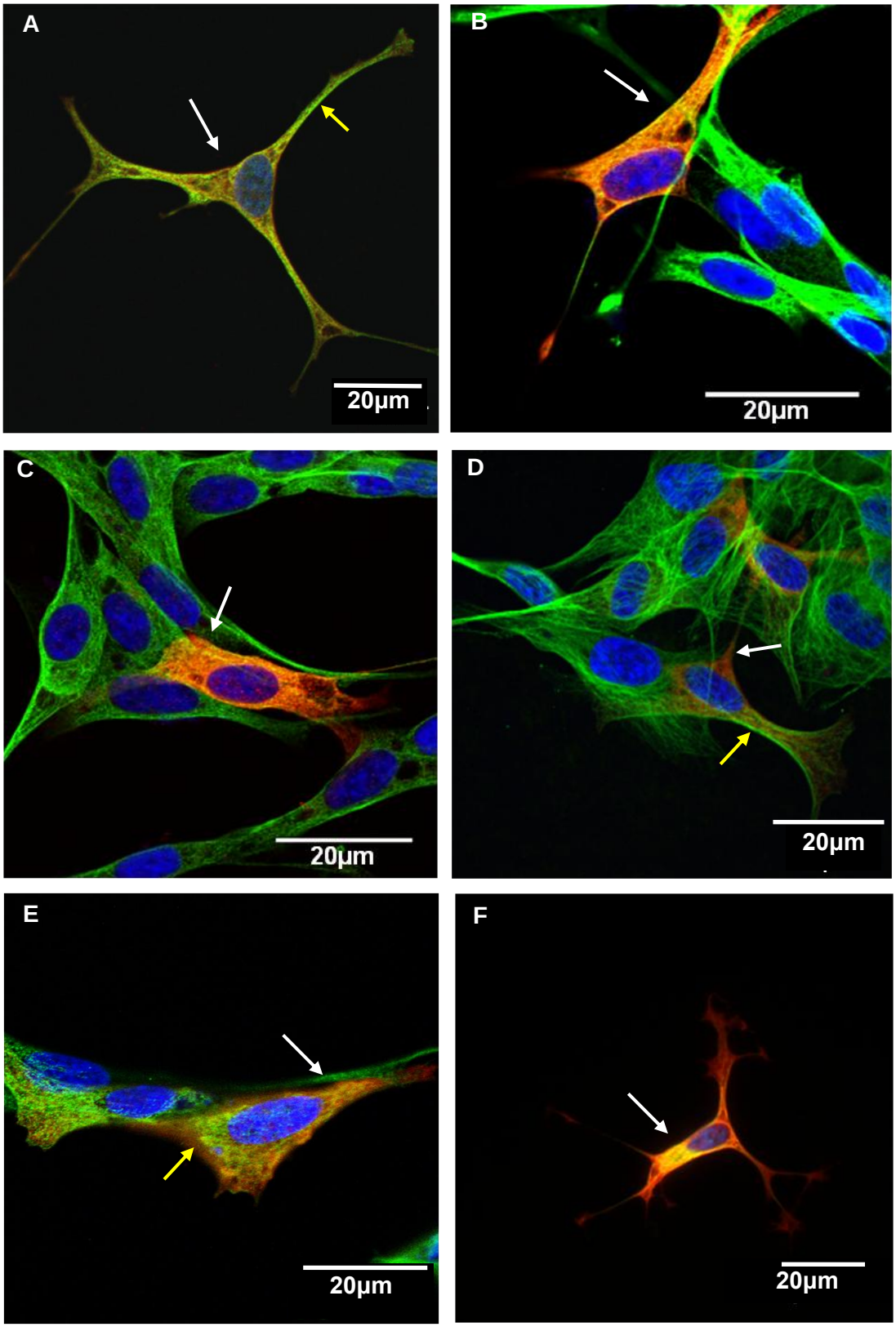

Figure 4.6 Co-localisation of endogenous, wild type and mutant transfected Hsp27 with β-tubulin III in Cytochalasin D treated cells.

A) Untransfected cells were stained for Hsp27 (red), β-tubulin III (green) and counterstained with the nuclear marker DAPI (blue), to show normal cellular distribution of endogenous Hsp27 in cells treated with Cytochalasin D. White arrows specify co-localisation between wild type and mutant Hsp27 and β-tubulin III, co-localisation is indicated by orange and yellow staining while yellow arrows indicate the absence of co-localisation.

B-F) Cells transfected with wild type and mutant Hsp27 were also stained for V5, β-tubulin III and DAPI to show cellular distribution of transfected mutant and wild type Hsp27 in cells treated with Cytochalasin D *in vitro*. White arrows specify co-localisation between wild type and mutant Hsp27 and β-tubulin III, co-localisation is indicated by orange and yellow staining, while yellow arrows indicate a lack of co-localisation. **B)** Wild type transfected Hsp27, **C)** Ser135Phe Hsp27, **D)** Arg140Gly Hsp27, **E)** Pro39Leu Hsp27 and **F)** Leu99Met Hsp27.

Figure 4.6

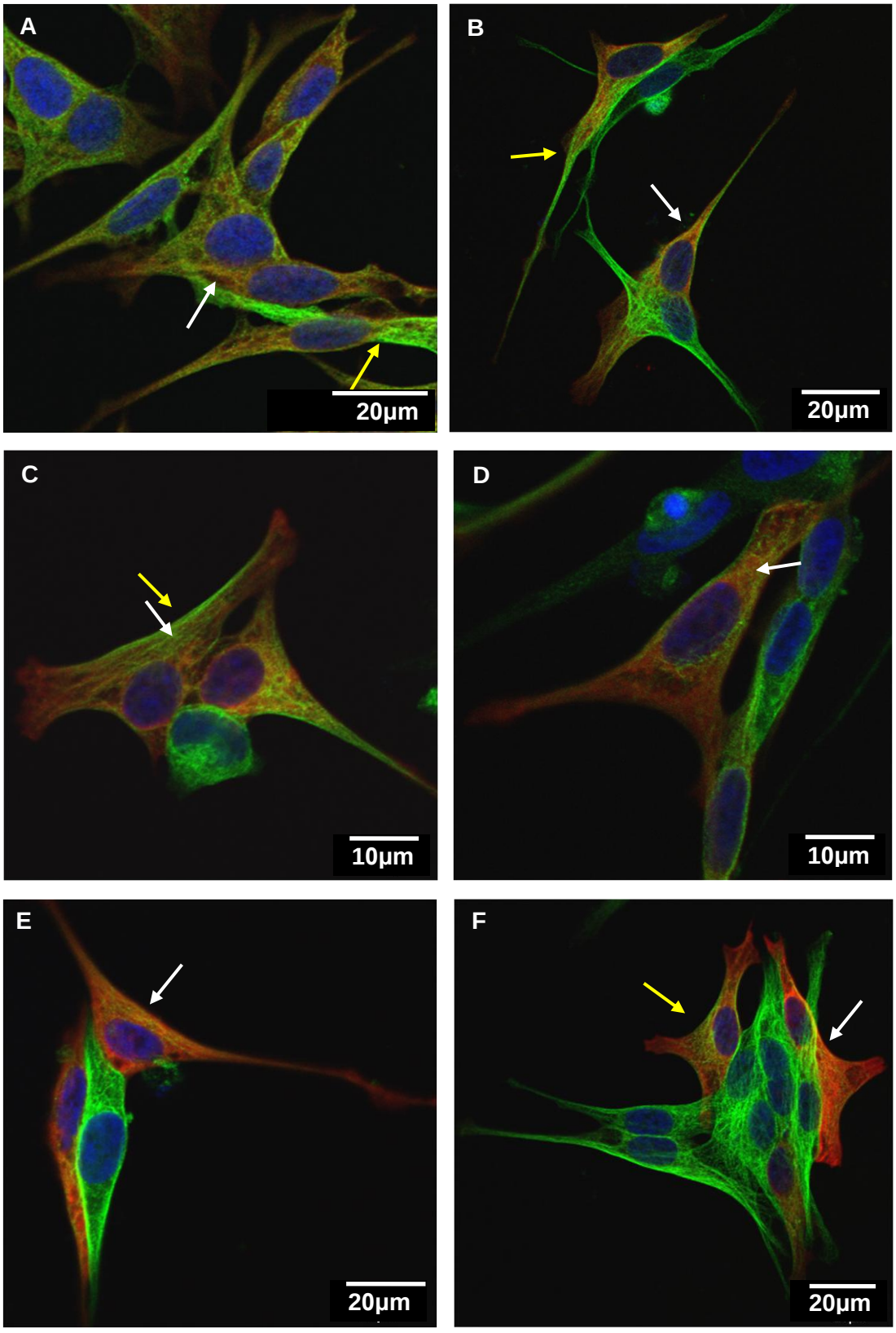

The addition of Colchicine, a cell stressor acting on the microtubule network, disrupted the cellular organisation and localisation of β-tubulin III across the cell and caused the co-localisation of all forms of Hsp27 with β-tubulin III in the cell soma (Figure 4.7). This finding suggests that both the endogenous and transfected wild type and mutant Hsp27 may play more of a chaperoning role than a stabilising role under these conditions. Little co-localisation was observed between the two proteins in those neurites that remained on the cells.

In all cells stained with β-tubulin III, in both unstressed and stressed conditions, there were no differences in the extent of co-localisation between endogenous Hsp27, wild type Hsp27 or any of the Hsp27 mutants. However, addition of different cell stressors revealed a change in the location of the co-localised β-tubulin III and Hsp27 from the neurites to the cell body, specifically to around the nucleus.

4.6. The effect of Hsp27 mutations on the interaction of Hsp27 with Neurofilament-200

The neurofilament network is particularly important in maintaining the integrity and calibre of the axon (Yum *et al*., 2009). Mutations in neurofilament light chain cause both demyelinating and axonal CMT (Abe *et al*., 2009), as discussed in the General Introduction, Section 1.2. In CMT, the aggregation or loss of neurofilament proteins is also a pathological feature of axonal degeneration (Benedetti *et al*., 2010). Therefore, the expression of neurofilament-200 heavy chain (NF-200) was used to examine the effect of Hsp27 mutations on the neurofilamentous network in unstressed and stressed conditions.

Figure 4.7 Co-localisation of endogenous, wild type and mutant transfected Hsp27 with β-tubulin III in Colchicine treated cells.

A) Untransfected cells were stained for Hsp27 (red), β-tubulin III (green) and counterstained with the nuclear marker DAPI (blue), to show normal cellular distribution of endogenous Hsp27 in cells treated with Colchicine. White arrows specify co-localisation between wild type and mutant Hsp27 and β-tubulin III, co-localisation is indicated by orange and yellow staining, while yellow arrows indicate the absence of co-localisation.

B-F) Cells transfected with wild type and mutant Hsp27 were stained for V5, β-tubulin III and DAPI, to show cellular distribution of transfected mutant and wild type Hsp27 in cells treated with Colchicine *in vitro*. White arrows specify co-localisation between wild type and mutant Hsp27 and β-tubulin III, co-localisation is indicated by orange and yellow staining, while yellow arrows indicate the absence of co-localisation. **B)** Wild type transfected Hsp27, **C)** Ser135Phe Hsp27, **D)** Arg140Gly Hsp27, **E)** Pro39Leu Hsp27 and **F)** Leu99Met Hsp27.

Figure 4.7

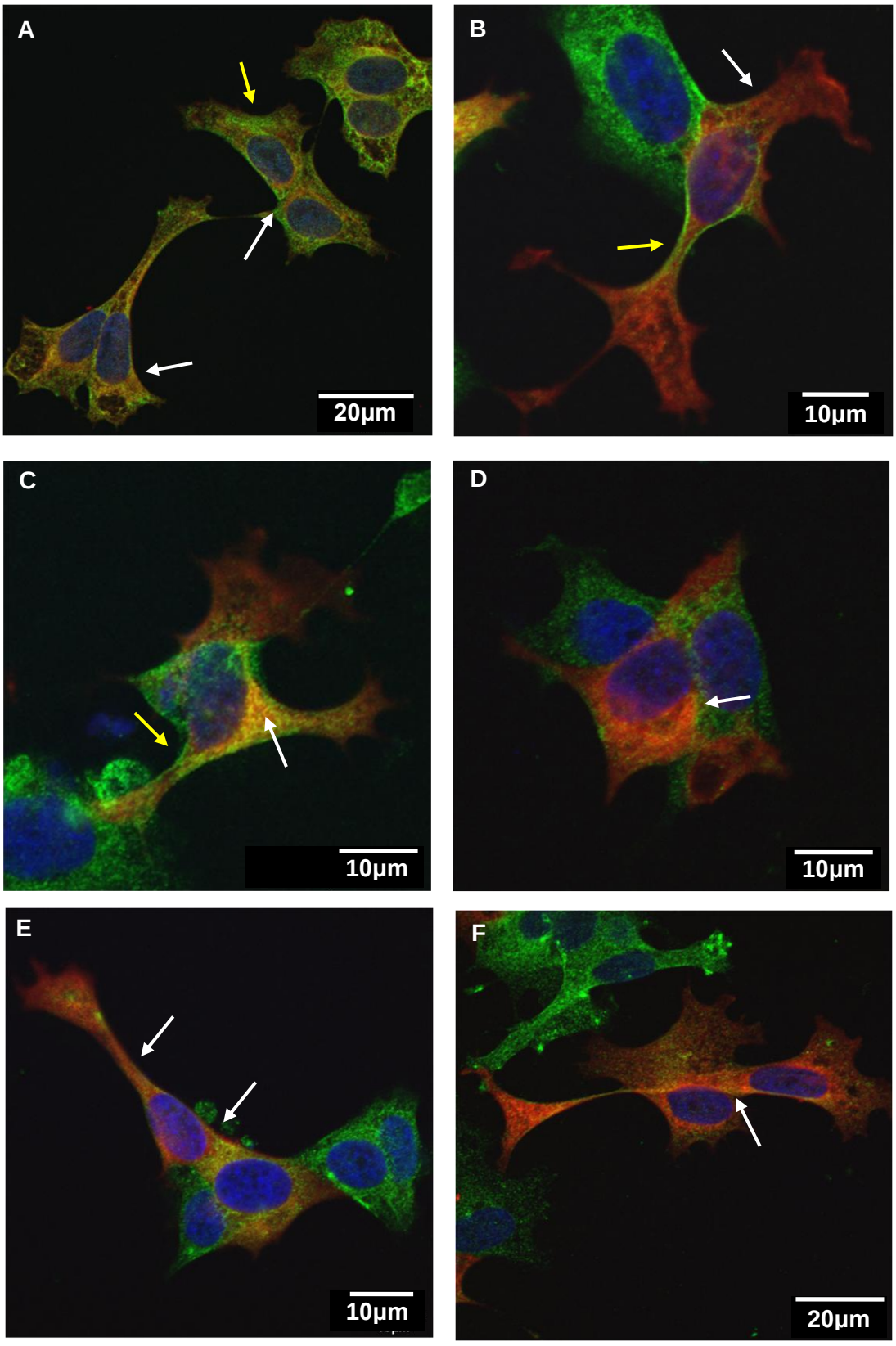

4.6.1. Co-localisation patterns of endogenous, wild type and mutant transfected Hsp27 with NF-200 in unstressed conditions

In unstressed conditions, endogenous Hsp27 displayed partial co-localisation with the NF-200 protein (Figure 4.8A). When cells were transfected with wild type Hsp27, a similar staining pattern to the endogenous protein with some co-localisation of wild type Hsp27 with NF-200 was seen (Figure 4.8B).

Transfection with the Ser135Phe mutant of Hsp27 also resulted in a similar phenotype to wild type Hsp27, with some co-localisation detected (Figure 4.8C). In contrast, transfection with Arg140Gly Hsp27, Pro39Leu Hsp27 and Leu99Met Hsp27 in unstressed conditions, resulted in less co-localisation with NF-200 (Figure 4.8D-F) with a clear separation of NF-200 and V5 throughout the cells.

4.6.2. Co-localisation of endogenous, wild type and mutant transfected Hsp27 with NF-200 in Cytochalasin D treated cells

Treatment with Cytochalasin D had a clear effect on the neurofilament network in all cells examined (Figure 4.9). Regardless of Hsp27 expression, NF-200 aggregated in the cell soma and formed neurofilament bundles in neurites - a pathological hallmark of axonal degeneration in CMT (Fabrizi *et al*., 2004; Benedetti *et al*., 2010).

Under unstressed conditions, endogenous Hsp27 displayed co-localisation with NF-200 (Figure 4.9A) which was also seen in cells transfected with wild type Hsp27 (Figure 4.9B). The staining pattern of endogenous and transfected wild type Hsp27 did not change in cells treated with the F-actin stressor. However when Cytochalasin

Figure 4.8 Co-localisation of endogenous, wild type and mutant transfected Hsp27 with NF-200 in unstressed conditions.

A) Untransfected cells were stained for Hsp27 (red), NF-200 (green) and counterstained with the nuclear marker DAPI (blue), to show normal cellular distribution of endogenous Hsp27 in unstressed cellular conditions. White arrows specify co-localisation between wild type and mutant Hsp27 and NF-200, co-localisation is indicated by orange and yellow staining, while yellow arrows indicate the absence of co-localisation.

B-F) Cells transfected with wild type and mutant Hsp27 were also stained for V5, NF-200 and DAPI, to show cellular distribution of transfected mutant and wild type Hsp27 in *in vitro,* unstressed cellular conditions. White arrows specify co-localisation between wild type and mutant Hsp27 and NF-200, co-localisation is indicated by yellow staining, while yellow arrows indicate the absence of co-localisation. **B)** Wild type transfected Hsp27, **C)** Ser135Phe Hsp27, **D)** Arg140Gly Hsp27, **E)** Pro39Leu Hsp27 and **F)** Leu99Met Hsp27.

Figure 4.8

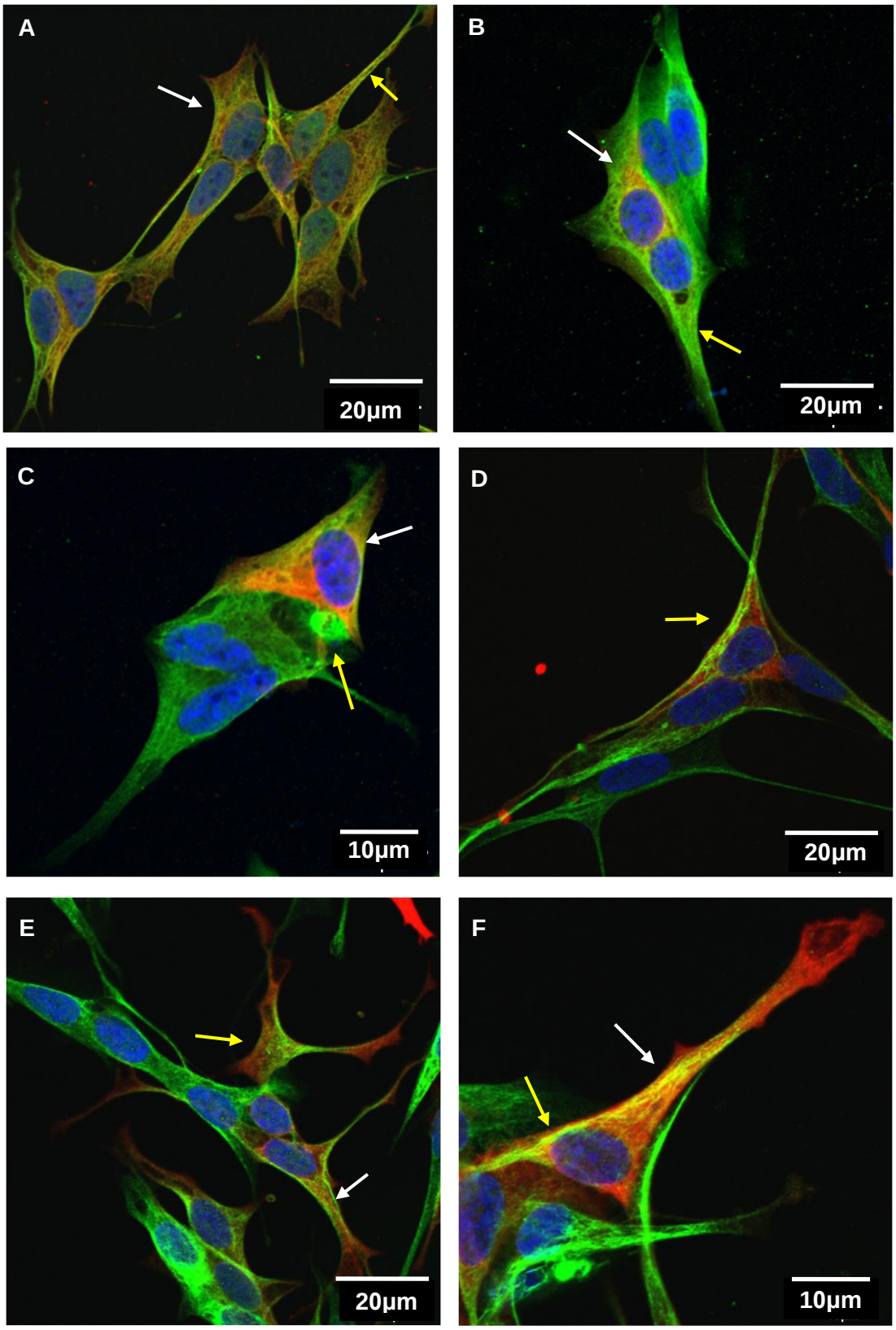

Figure 4.9 Co-localisation of endogenous, wild type and mutant transfected Hsp27 with NF-200 in Cytochalasin D treated cells.

A) Untransfected cells were stained for Hsp27 (red), NF-200 (green) and counterstained with the nuclear marker DAPI (blue), to show normal cellular distribution of endogenous Hsp27 in cells treated with Cytochalasin D. White arrows specify co-localisation between wild type and mutant Hsp27 and NF-200, co-localisation is indicated by orange and yellow staining, while yellow arrows indicate the absence of co-localisation.

B-F) Cells transfected with wild type and mutant Hsp27 were also stained for V5, NF-200 and DAPI, to show cellular distribution of transfected mutant and wild type Hsp27 in cells treated with Cytochalasin D *in vitro*. White arrows specify co-localisation between wild type and mutant Hsp27 and NF-200, co-localisation is indicated by orange and yellow staining, while yellow arrows indicate a lack of co-localisation. **B)** Wild type transfected Hsp27, **C)** Ser135Phe Hsp27, **D)** Arg140Gly Hsp27, **E)** Pro39Leu Hsp27 and **F)** Leu99Met Hsp27.

Figure 4.9

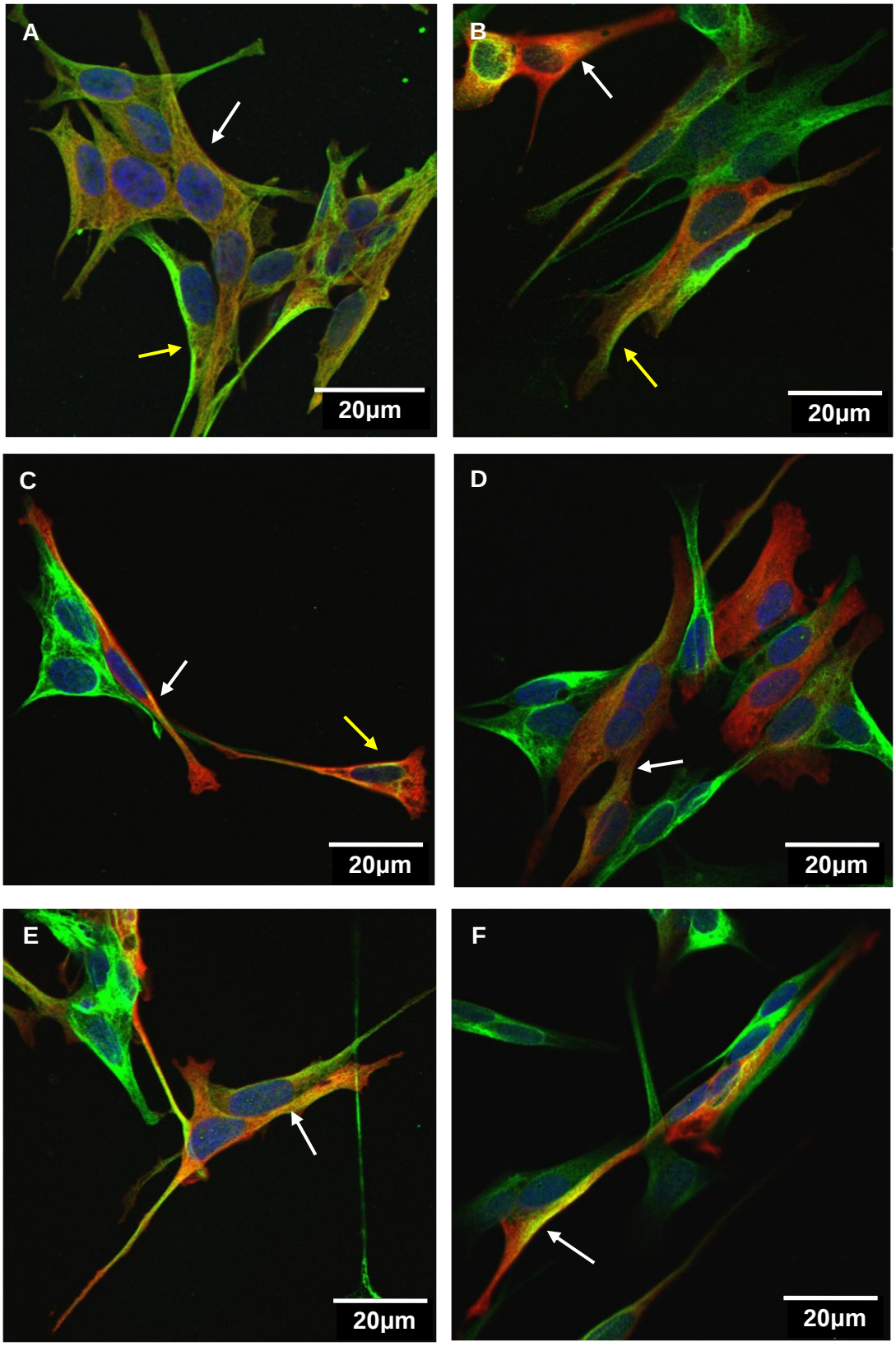

D was added to cells which had been transfected with the various Hsp27 mutations, all cells displayed co-localisation between the mutant protein and NF-200 (Figure 4.9C-F). In unstressed conditions, only the Ser135Phe and Leu99Met Hsp27 mutations had shown any co-localisation with NF-200 (Figure 4.8C and F).

4.6.3. Co-localisation of endogenous, wild type and mutant transfected Hsp27 with NF-200 in Colchicine treated cells

The addition of Colchicine to SH-SY5Y cells caused significant aggregation of NF-200, predominantly in the cell soma around the nuclei (Figure 4.10). This was not reduced or increased by the over expression of either wild type or mutant Hsp27.

Untransfected cells displayed some co-localisation between endogenous Hsp27 and NF-200, but not within the aggregates of NF-200 in the cell cytoplasm (Figure 4.10A). Transfected wild type Hsp27 showed reduced co-localisation in comparison to unstressed and Cytochalasin D treated cells (Figure 4.10B).

Cells transfected with Hsp27 mutations largely also showed a lack of co-localisation with NF-200 (Figure 4.10C-F) although in cells transfected with Hsp27 Ser135Phe, Hsp27 Arg140Gly and Hsp27 Pro39Leu, there was a co-localisation of the transfected proteins with the aggregated NF-200 in the cell soma (Figure 4.10C, D and E).

4.7. Ser135Phe Hsp27 causes aggregation of tau in some transfected cells

In a small number of cells transfected with Ser135Phe Hsp27, aggregates positive for both the transfected protein and tau, a microtubule associated protein, were

Figure 4.10 Co-localisation of endogenous, wild type and mutant transfected Hsp27 with NF-200 in Colchicine treated cells.

A) Untransfected cells were stained for Hsp27 (red), NF-200 (green) and counterstained with the nuclear marker DAPI (blue), to show normal cellular distribution of endogenous Hsp27 in cells treated with Colchicine. White arrows specify co-localisation between wild type and mutant Hsp27 and NF-200, co-localisation is indicated by orange and yellow staining.

B-F) Cells transfected with wild type and mutant Hsp27 were also stained for V5, NF-200 and counterstained with DAPI, to show cellular distribution of transfected mutant and wild type Hsp27 in cells treated with Colchicine *in vitro*. White arrows specify co-localisation between wild type and mutant Hsp27 and NF-200, co-localisation is indicated by orange and yellow staining, while yellow arrows indicate an absence of co-localisation. **B)** Wild type transfected Hsp27, **C)** Ser135Phe Hsp27, **D)** Arg140Gly Hsp27, **E)** Pro39Leu Hsp27 and **F)** Leu99Met Hsp27.

Figure 4.10

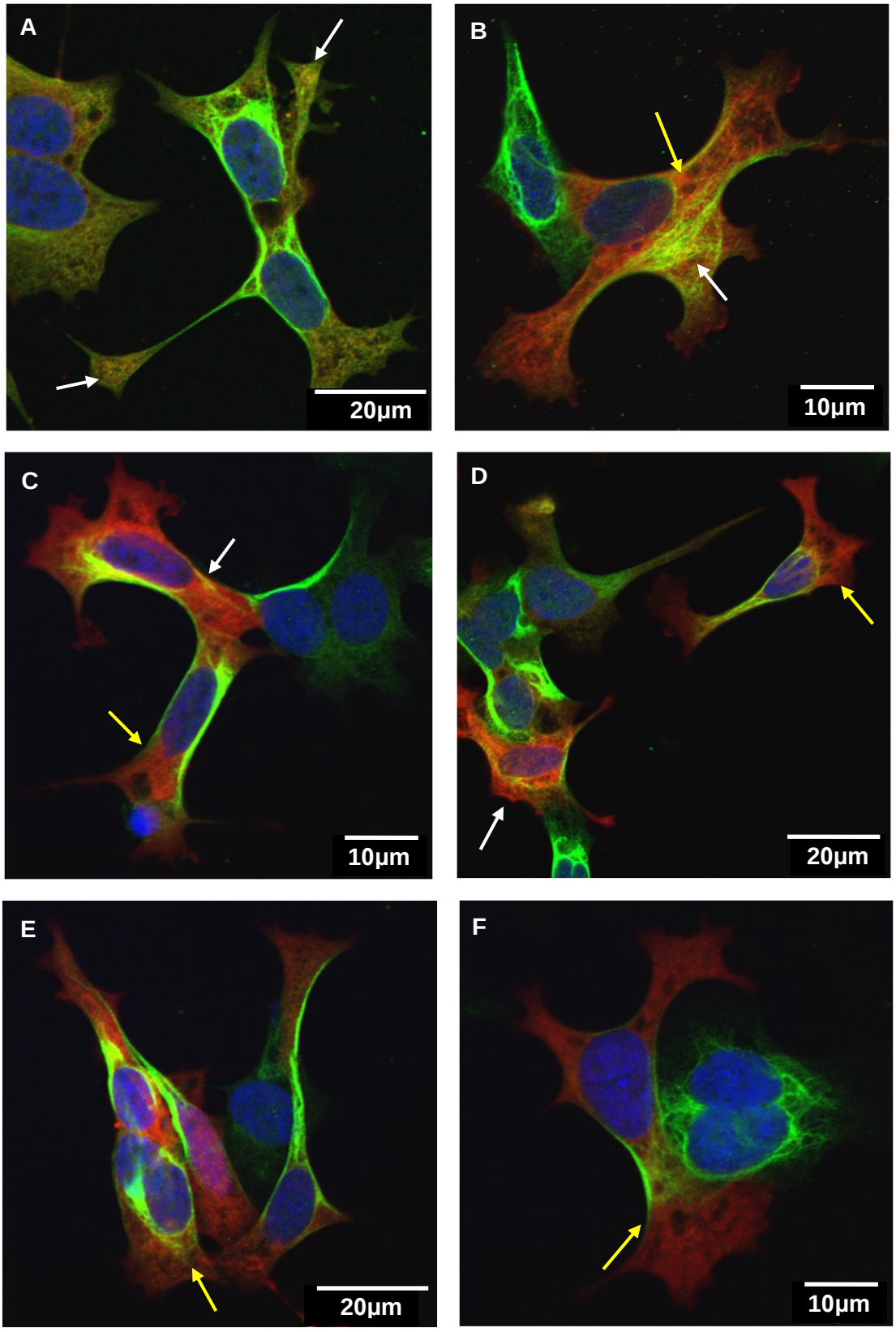

Figure 4.11

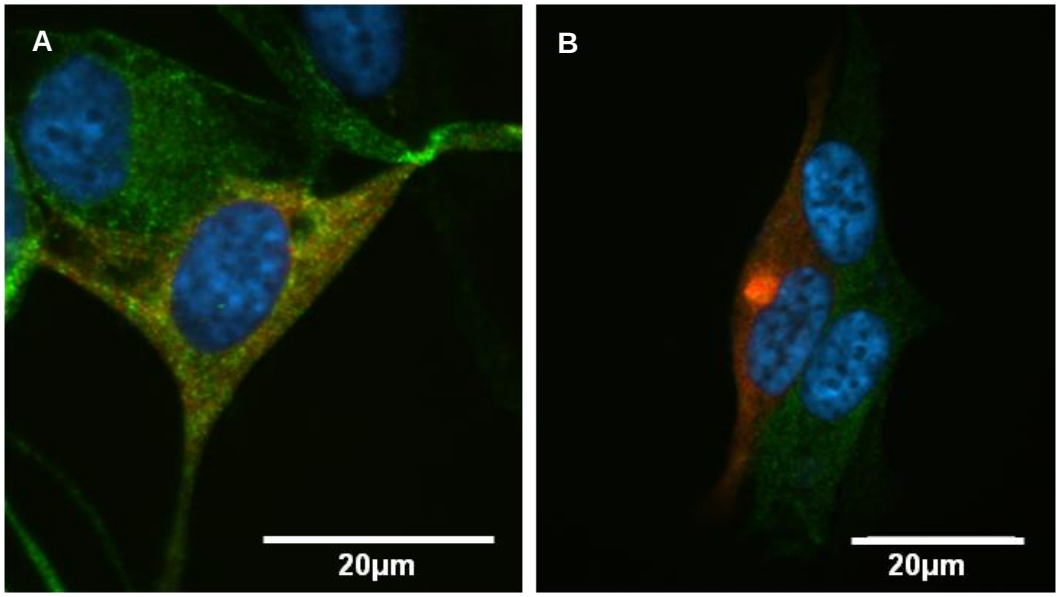

Figure 4.11 The Ser135Phe Hsp27 mutation causes aggregation of tau in some transfected cells

Cells stained with V5 (red) and tau (green) showing an example of **A)** Cell transfected with wild type Hsp27 with little co-localisation between transfected Hsp27 and tau. **B)** A cell transfected with Ser135Phe mutant Hsp27 showing a large inclusion impinging on the nucleus positive for both tau and transfected Ser135Phe Hsp27.

observed, some of which were large enough to impinge on the nucleus (Figure 4.11B). These aggregates were never detected in cells expressing wild type Hsp27 (Figure 4.11A) or any other mutation of Hsp27, suggesting a mutation-specific cytoskeletal disruption.

4.8. Pro39Leu Hsp27 aggregates into nuclear inclusions

When cells were transfected with the Pro39Leu mutant Hsp27, 38.9% ± 6.59% (± = SEM) of cells contained nuclear inclusions which were positive for V5 and Hsp27, suggesting that the transfected mutant Hsp27 was aggregating with itself or other proteins within the nucleus (Figure 4.12). Such nuclear inclusions were not observed in untransfected cells and cells transfected with either wild type Hsp27 or any other mutant Hsp27.

4.9. Morphological characterisation of cells transfected with Pro39Leu Hsp27

Since nuclear inclusions were found in such a high proportion of cells transfected with Pro39Leu Hsp27, the morphological data for Pro39Leu Hsp27 transfected cells analysed in Chapter 2 and presented in Figures 2.16 – 2.19, was reanalysed according to whether the cells contained nuclear inclusions or not (Figure 4.13). The methods for the morphological analysis of these cells are described in the Materials and Methods in Chapter 2.

The presence of inclusions had no effect on morphological features which were considered to be indicative of changes in the regulation of cellular pathways. Thus, there was no change in the number of lamellipodia, neuritic ‘stumps’ or vacuoles in

Figure 4.12 Pro39Leu Hsp27 forms nuclear inclusions

Cells transfected with the Pro39Leu Hsp27 mutation have nuclear inclusions that contain Hsp27 (red) and the V5 epitope (green), a marker for transfected, mutant Hsp27. **A)** Two SH-SY5Y cells stained for Hsp27 **B)** V5-positive cell containing Pro39Leu Hsp27 **C)** Overlay of Hsp27 and V5 showing exogenous and/or transfected Hsp27 in the cytoplasm of the cell and in nuclear inclusions.

Figure 4.12

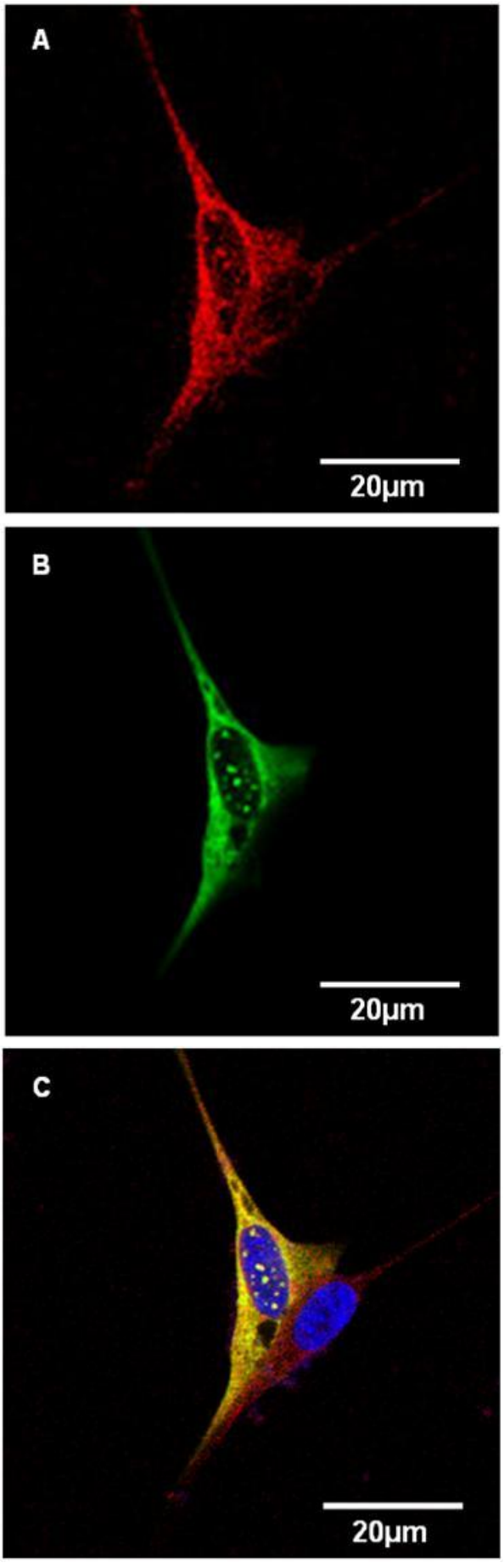

Figure 4.13

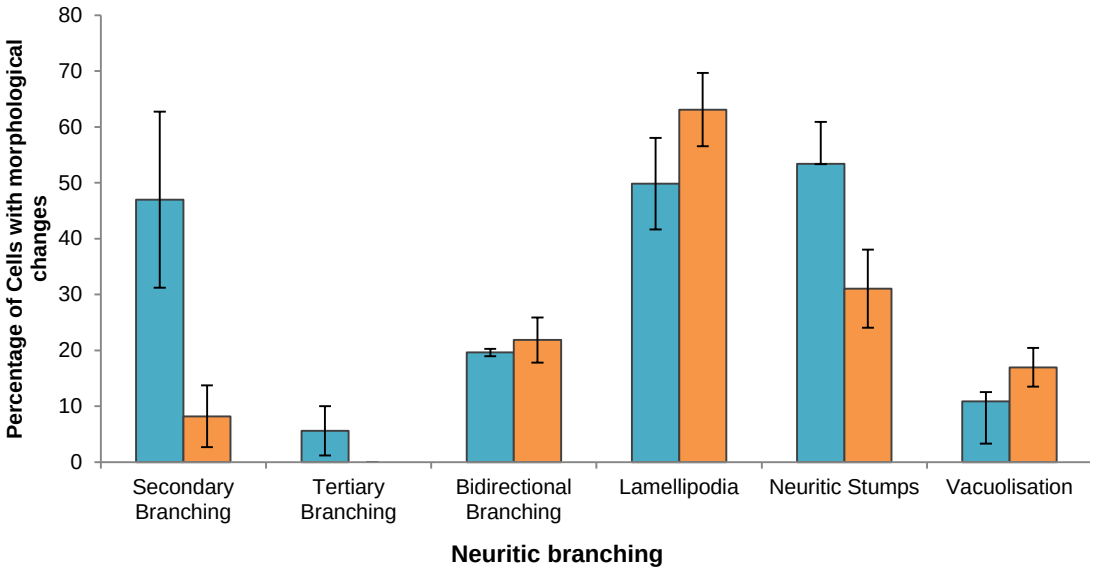

Figure 4.13 Comparison of morphological characteristics of cells transfected with Pro39Leu Hsp27 with and without nuclear inclusions.

The bar chart summarises the characterisation of the morphological features of cells transfected with mutant Pro39Leu Hsp27 and which either contain nuclear inclusions (orange bars) or do not (blue bars). Error bars = SEM.

comparison to Pro39Leu Hsp27 transfected cells which did not contain nuclear inclusions (Figure 4.13). The presence of nuclear inclusions was also not associated with changes in bidirectional branching, and therefore had no effect on the number of neurites sprouting from the cell soma. However, nuclear inclusions did correlate with decreased secondary and tertiary branching from primary neurites in comparison to Pro39Leu Hsp27 transfected cells with no nuclear inclusions, suggesting that the presence of nuclear inclusions in Pro39Leu cells was associated with a decrease in cellular differentiation (Figure 4.13).

4.10. Which proteins co-localise with Pro39Leu Hsp27 nuclear inclusions?

Whether the Pro39Leu Hsp27-positive nuclear inclusions contained key cellular proteins was examined next by immunostaining for ubiquitin, SMN1 and TDP-43.

4.10.1. Pro39Leu Hsp27 positive nuclear inclusions are not ubiquitinated

To attempt to characterise the nuclear inclusions observed in cells transfected with Pro39Leu Hsp27, the cells were stained with ubiquitin and co-stained with V5. Figure 4.14 shows that Pro39Leu Hsp27 nuclear inclusions were not positive for ubiquitin, indicating that they were not targeted for degradation by the proteosome.

4.10.2. Pro39Leu Hsp27 positive nuclear inclusions do not contain survival of motor neuron 1 protein

In Spinal muscular atrophy, survival of motor neuron 1 (SMN1) protein is deleted or truncated causing a severe, predominantly lower motor neurodegenerative disease (Lefebvre *et al*., 1995). SMN1 is thought to be a housekeeping gene and is ubiquitously expressed. The roles of SMN1 include processing of pre-mRNA and maintenance of the growth cone (Morse *et al*., 2011). When in the nucleus, SMN1

Figure 4.14

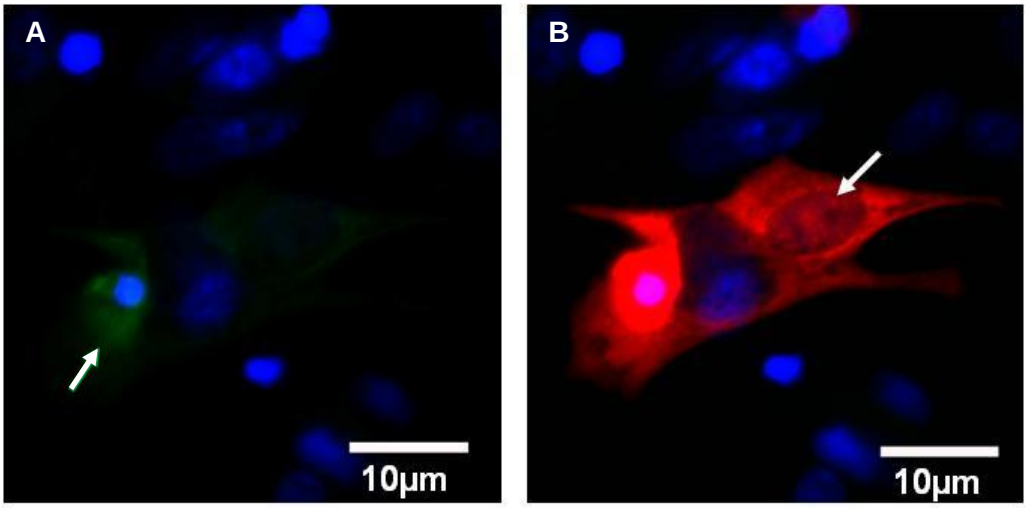

Figure 4.14 Pro39Leu Hsp27-positive nuclear inclusions are not ubiquitinated.

A) Cells were transfected with Pro39Leu and stained for ubiquitin (green, white arrow) and counterstained for DAPI (a nuclear marker). **B)** Cells were also co-stained with V5 (red) showing cells transfected with Pro39Leu Hsp27 forming nuclear inclusions (white arrows). In cells positive for nuclear inclusions, there was no co-localisation with the transfected Pro39Leu Hsp27 inclusions and ubiquitin.

resides in Cajal bodies (Morse *et al*., 2011). This made SMN1 an attractive target to ascertain whether it co-localised with Pro39Leu mutant Hsp27. When cells were immunostained for V5 and SMN1 no co-localisation was seen, and the presence of mutant Hsp27 positive nuclear inclusions did not affect the cellular localisation of SMN1 (Figure 4.15).

4.10.3. Pro39Leu Hsp27 positive nuclear inclusions co-localise with TDP-43

Mutations in TDP-43, an mRNA splicing protein, have been shown to cause familial amyotrophic lateral sclerosis (ALS) and frontotemporal lobar dementia (FTD) (Sreedharan *et al*., 2008)(Chiò *et al*., 2010). TDP-43 positive, ubiquitinated inclusions have also been found in several neurodegenerative diseases including ALS, FTD and inclusion body myositis (IBM) (Neumann *et al*., 2006; Salajegheh *et al*., 2009). TDP-43 is normally located in the nucleus, but upon cell stress and in pathological conditions, the C-terminus of the protein translocates to the cytoplasm where its functions remain elusive (Dormann *et al*., 2009).

In cells positive for Pro39Leu Hsp27 inclusions, TDP-43 co-localised with a proportion, but not all inclusions (Figure 4.16). The appearance of inclusions in transfected cells did not precipitate the translocation of TDP-43 to the cytoplasm (Figure 4.16).

When cells were transfected with wild type or mutant Hsp27, TDP-43 did not translocate to the cytoplasm (Figure 4.16). This was also the case when cells were stressed using Cytochalasin D and Colchicine (Data not shown).

Figure 4.15

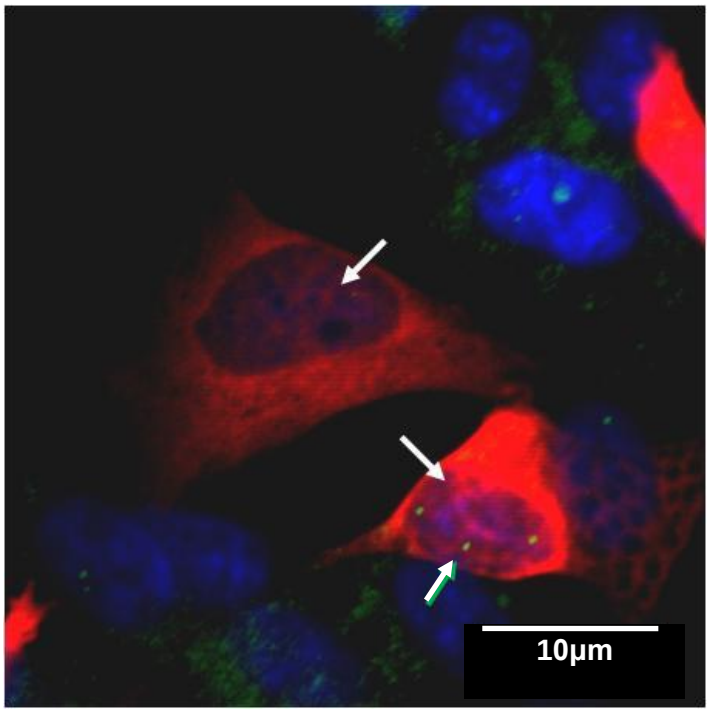

Figure 4.15 Pro39Leu Hsp27-positive nuclear inclusions do not contain survival of motor neuron protein 1.

Cells stained with V5 (red), SMN1 (green) and counter stained for DAPI (a nuclear marker) showing an example of cells transfected with Pro39Leu Hsp27 and forming nuclear inclusions (white arrows). In cells positive for SMN1 (white arrow), there was no co-localisation with the transfected Pro39Leu Hsp27 inclusions and SMN1 protein.

Figure 4.16

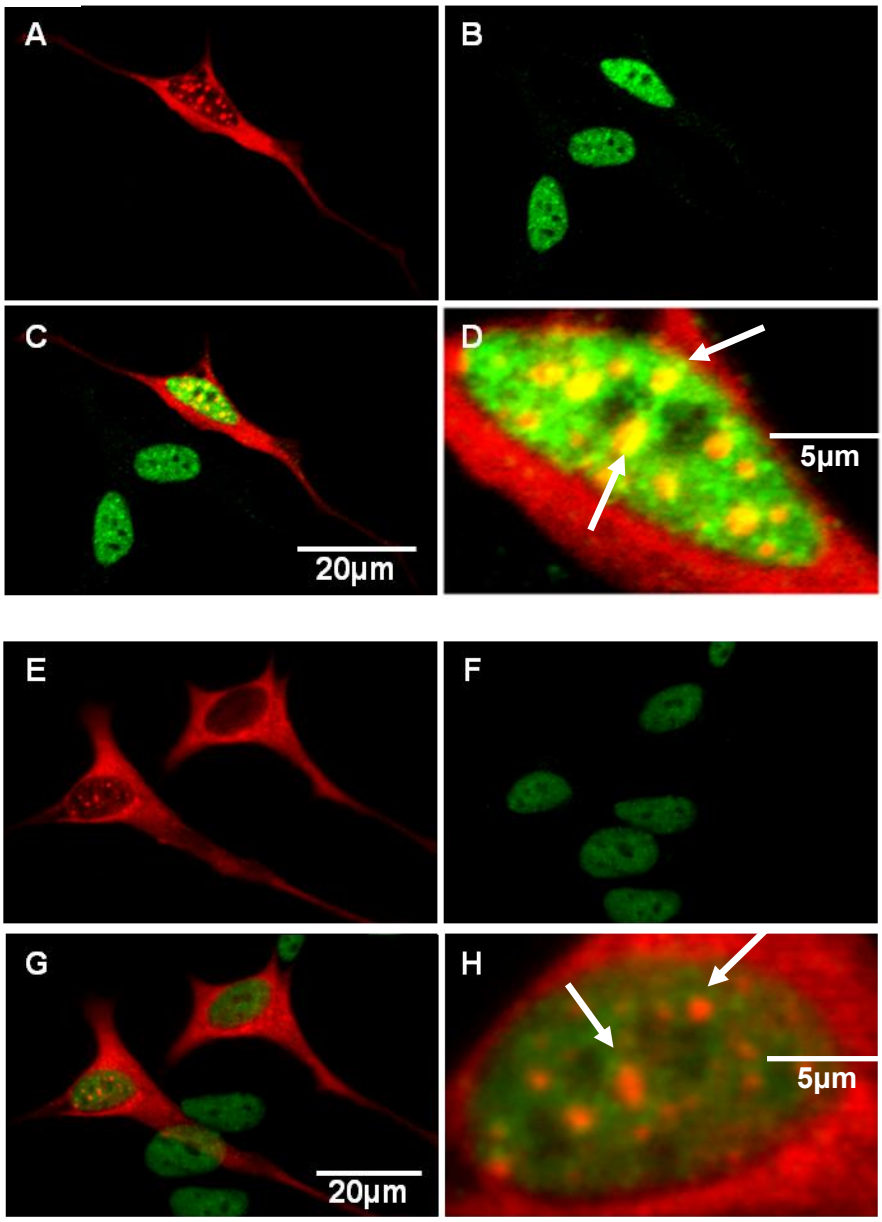

Figure 4.16 Pro39Leu Hsp27 positive nuclear inclusions sometimes contain TDP-43

Nuclear inclusions (marked by white arrows) in cells transfected with the Pro39Leu Hsp27 mutation stained for V5 and TDP-43. **A-D)** Show a Pro39Leu Hsp27 positive cell with TDP-43 co-localised with mutant Hsp27 positive nuclear inclusions. **E-H)** Show a Pro39Leu Hsp27 positive cell with TDP-43 in the nucleus but not co-localised with mutant Hsp27 positive nuclear inclusions. **A,E)** V5 (red), **B,F)** TDP-43 (green) **C,G)** Overlay of V5 and TDP-43 **D,H)** Magnification of nucleus of overlay picture.

4.10.4. Pro39Leu Hsp27 nuclear inclusions are SC35-positive nuclear speckles

Under conditions of cellular stress, Hsp27 translocates into the nucleus. Its function in this action is currently unknown although it thought to modulate transcriptional activity (Friedman *et al*., 2009). Small heat shock proteins, including Hsp27 have been shown to co-localise with nuclear speckles that are positive for SC35, a regulator of pre-mRNA splicing associated with tau splicing (Björk *et al*., 2009; Vos *et al*., 2009; Qian *et al*., 2011). Analysis of the Pro39Leu Hsp27 inclusions revealed that on all occasions, these 'nuclear inclusions' were immunoreactive for SC35 and were therefore likely to be SC35-positive nuclear splicing speckles (Figure 4.17).

Figure 4.17

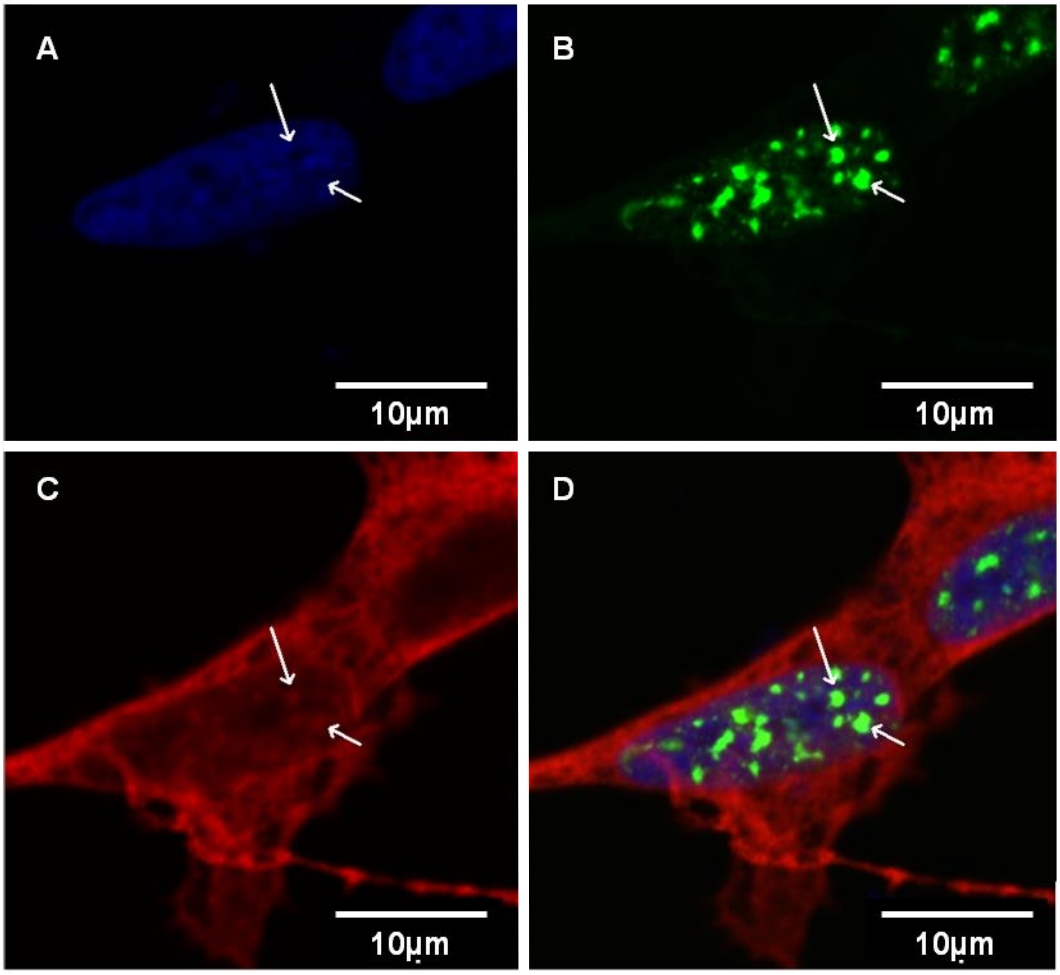

Figure 4.17 Pro39Leu Hsp27 nuclear inclusions are positive for SC35

Nuclear inclusions (marked by white arrows) in cells transfected with the Pro39Leu Hsp27 mutation stained for SC35 and V5. **A)** Counterstained with DAPI (blue) to show cell nucleus **B)** SC35-positive nuclear speckles (green) in the cell nucleus **C)** V5-positive cells (red) containing Pro39Leu Hsp27 staining cytoplasm and nuclear bodies **D)** Overlay of SC35 and V5 showing co-localisation of mutant Hsp27 with SC35-positive nuclear bodies.

4.11. Chapter 4 Summary

The data presented in Chapter 3 established that all Hsp27 mutations examined were cytotoxic and that some showed differential affects on the cytoskeleton which could possibly have been due to the mutation position on the gene of interest. In this Chapter, I further examined the possible differences between the mutations by examining the expression patterns of several proteins by immunocytochemistry in cells under non-stressed and stressed conditions.

Hsp27 has been shown to play an important role in the development, repair and stability of the cytoskeleton in the presence and absence of cellular stress (Benndorf *et al*., 1994; Mounier and Arrigo, 2002; Williams *et al*., 2006). In the experiments described in this Chapter, analysis of actin microfilaments, microtubules and neurofilaments revealed further differences in the interaction of the Hsp27 mutations with key proteins of the cytoskeleton. Both the Ser135Phe and Arg140Gly mutations were distinguished by an apparent increase in co-localisation with F-actin in comparison to endogenous and wild type transfected Hsp27as well as the Pro39Leu and Leu99Met Hsp27 mutations. These findings were more marked in unstressed conditions but were still observed in cells stressed with cytoskeletal agents (Figures 4.2-4.4).

Perhaps surprisingly in the light of the current literature on Hsp27 mutations, there was a lack of co-localisation between Hsp27 mutations and NF-200 in unstressed conditions, in contrast to the expression pattern of endogenous Hsp27 (Figure 4.8). In cells stressed with Cytochalasin D, all forms of Hsp27 co-localised with NF-200, but not with NF-200 bundles which also formed (Figure 4.9). In contrast, in cells stressed with Colchicine, there was a distinct lack of co-localisation of NF-200 and mutant Hsp27 with large aggregates of NF-200 which formed (Figure 4.10). In this

study, neither the Ser135Phe Hsp27 mutation, nor any other mutation examined had any effect on the cellular location or pathology of NF-200 caused by treatment with cytoskeletal stressors, and mutant Hsp27 showed very little co-localisation with NF-200 aggregates or bundles.

In comparison, in Colchicine-treated cells, all mutant Hsp27s co-localised with β-tubulin III, a neuronal-specific member of the microtubule network, not only in the cytoplasm but also in cytoplasmic aggregates (Figure 4.7). It is worth noting that the Ser135Phe Hsp27 mutation also resulted in the formation of tau (a microtubule-associated protein) aggregates in some cells (Figure 4.11). In other conditions examined, all forms of Hsp27 co-localised with β-tubulin III (Figure 4.5 and 4.6).

While the addition of mutations in an over-expressed foreign protein caused some similar morphological changes as well as differential interactions with the cytoskeleton, one mutation also caused a distinctive differential effect in the cells. The Pro39Leu Hsp27 mutation (amino acid change in the N-terminus of the protein) caused the formation of nuclear inclusions in 39% of transfected cells. These inclusions were determined to be SC35-positive nuclear speckles. Nuclear speckles are non-pathological nuclear bodies involved in mRNA splicing.

Indeed, all mutations, apart from one, showed differential effects in SH-SY5Y cells, albeit on different parameters. The recessive Leu99Met Hsp27 mutation (located in the α-crystallin domain, but out of the hot spot region) was shown in Chapter 3 to be toxic to cells under basal conditions, but has not displayed any differential effects using any other outcome measure assessed.

The cell model used in the experiments described in Chapters 3 and 4, has revealed robust phenotypic differences between nearly all the Hsp27 mutations with all the outcome measures examined. However, there are several limitations to this model which limit its applicability. Due to these limitations, it is not appropriate for use in experiments which aim to examine more functional aspects of cellular function, which are critically dependent on cellular identity. Therefore, primary motoneurons are a more appropriate cell model in which to examine the functional effects of Hsp27 mutations *in vitro*.

In Chapter 6, the effects of the Hsp27 mutations on functional outcome measures are examined in primary motoneuron cultures transfected with 3rd generation viruses containing wild type Hsp27, Pro39Leu Hsp27, Ser135Phe Hsp27 and Arg140Gly Hsp27. Due to the addition of supplementary control conditions and the recessive nature of the mutation, the Leu99Met was not taken forward in further experiments for functional testing.

Chapter 5. The functional effects of Hsp27 mutations in primary motoneurons *in vitro*.

The results presented in Chapters 3 and 4 show that mutations in Hsp27 have differential effects on the phenotype of transfected neuronal-like cells. All of the mutations examined showed significant levels of cytotoxicity. In addition, the Ser135Phe and Arg140Gly mutations, located in the α-crystallin domain of the Hsp27 protein, significantly increased cellular vulnerability to pharmacological cytoskeletal stressors and inhibited neurite outgrowth. These mutations also abnormally co-localised with F-actin in comparison to not only endogenous and wild type transfected Hsp27, but also to the Pro39Leu and Leu99Met Hsp27 mutations. Conversely, Pro39Leu, a mutation located in the N-terminus of Hsp27, accumulated in SC35-positive nuclear splicing speckles.

The differential effects described above were observed in a generic model in which a mutant protein is over expressed in a neuronal cell line. However, mutations in Hsp27 cause CMT 2F, a disease which preferentially targets motoneurons, which are highly specialised neurons that transmit signals along axons which are some of the longest in the body. Motoneurons are metabolically highly active and must generate enough energy to maintain membrane potential along the entire length of the axon and throughout its dendritic tree. Motoneurons are therefore highly dependent upon an efficient cytoskeletal network in order to transport key proteins, electrical signals as well as organelles including mitochondria to their site of action. Thus, any disturbance in the cytoskeletal network will immediately affect motoneuron functions. The results presented in Chapters 3 and 4, together with

previous published data, shows that mutant Hsp27 can interfere with a number of cytoskeletal proteins, resulting in dysfunction of not only the transport machinery, but with the function of individual cargoes, such as mitochondria. Mitochondria not only provide ATP for the cell, but also regulate apoptosis, produce reactive oxygen species (ROS) and buffer intracellular calcium. Mitochondria are very susceptible to changes in the cellular environment and changes in mitochondrial activity are one of the first signs of motoneuron stress. Thus, assessment of the mitochondrial membrane potential is a sensitive readout of motoneuron vulnerability. In this Chapter, the effect of Hsp27 mutations on the mitochondrial membrane potential in primary motoneurons was examined as a readout of the functional effects of these mutations in motoneurons.

While motoneurons are highly specialised to transmit signals between the CNS and muscles, they are heavily reliant on surrounding cells for support, such as transmitter recycling, some elements of energy metabolism and even cellular protection against toxic insults. Indeed, surrounding astroglia have been shown to supply neurons with intermediate products of energy metabolism as well as cytoprotective heat shock proteins (Robinson *et al*., 2005; Benarroch, 2010).

In order to understand the effects of Hsp27 mutations on physiological changes in cellular functions, primary embryonic motoneuron cultures were transfected with 3rd generation viruses containing either wild type Hsp27, or one of three Hsp27 mutations; Pro39Leu, Ser135Phe and Arg140Gly and the effects on morphological and functional characteristics of motoneurons was examined.

5.1. Characterisation and transfection of primary motoneuron cultures

In order to examine the effects of Hsp27 mutations on cellular functions in motoneurons, primary embryonic mixed ventral horn cultures were optimised for viral transfection of mutant and wild type Hsp27. All viruses used in this Chapter were generated by Dr Bernadett Kalmar. In the first instance, the culture model was optimised in order to produce a consistent ratio of cell types and motoneuron purity in the culture, and optimisation of viral transfection to ensure comparable culture conditions across experiments.

5.1.1. Motoneuron purity in primary mixed ventral horn cultures

The primary motoneuron cultures used in these experiments consist of mixed ventral horn cells obtained from mouse embryonic spinal cord (Figure 5.1) using an established protocol adapted from that described by Camu and Henderson (Camu and Henderson, 1994; Kalmar and Greensmith, 2009b). Due to the number of different cell types in the mixed culture preparation, motoneuron purity was established by immunostaining for motoneuron specific protein markers as well as their characteristic morphology, as illustrated in Figure 5.1B. Neurons can be identified by immunoreactivity to neuronal specific markers including microtubule-associated protein 2 (MAP2) (Figure 5.1A), β-tubulin III (Figure 5.1B) and peripherin (Figure 5.5). Motoneurons were then differentiated from other neurons in culture (primarily interneurons) by size and shape. Therefore in this study, a cell was determined as a motoneuron if it stained for specific neuronal markers, eg MAP2, and showed the following morphological characteristics: a soma diameter of >15μm and possessing of 3 or more neuritic processes. In the motoneuron cultures described in this Chapter the average motoneuron content was consistently found to be 43.2% (± 6.4%, SEM; Figure 5.1A).

Figure 5.1

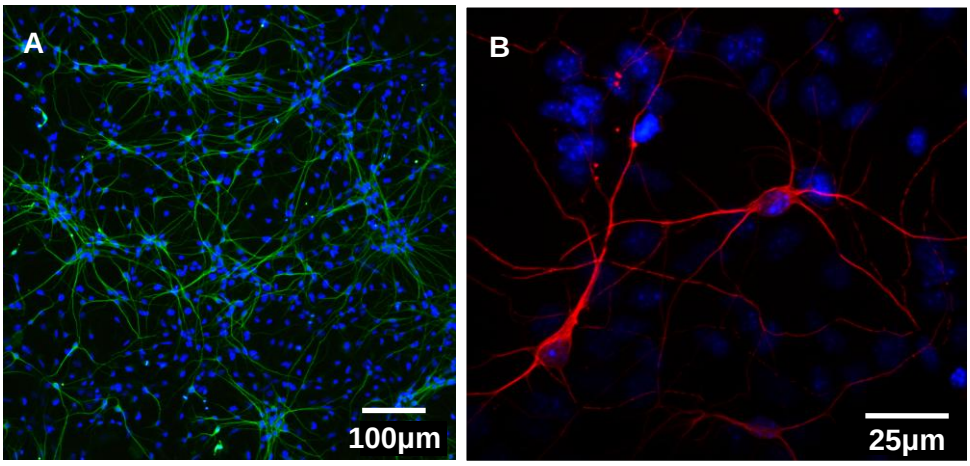

Figure 5.1 Primary embryonic motoneuron cultures.

A) Representative image of a mixed ventral horn culture with neurons stained for neuronal-specific MAP2 (green). **B)** Primary motoneurons in culture immunostained for neuronal-specific β-tubulin III (red) and counterstained with DAPI (blue) with large cell somas of <15µm diameter and 3 or more neuritic processes.

5.1.2. Optimal viral transfection rate and multiplicity of infection (MOI)

Primary motoneurons are particularly vulnerable to *in vitro* environmental stress including over-expression of foreign proteins. It was therefore important in these experiments to control for protein over-expression, not only to functionally assess the effect of Hsp27 mutations, but to avoid multiple expression of the protein that can lead to effects on the cell unrelated to the mutations investigated and to maintain the motoneurons as functionally viable. Therefore, the viral titre was optimised by series dilutions so that 10-20% of motoneurons would express the transgene and therefore probably contain few copies of the transgene. An example of a transfected motoneuron is illustrated in Figure 5.2, using a wild type Hsp27 viral vector (See Materials and Methods, Chapter 2, Section 2.7.2.). The average viral titre produced $1.07x10^{6}$TU/ml (tested in HEK cells). In order to achieve 10% transfection, an MOI of 10 was applied. Virally transducing primary motoneurons at time points of 12, 24 or 48 hours post-plating made no difference to transfection efficiency at 7 days *in vitro* (DIV).

5.1.3. GFP and Hsp27 are both expressed in transfected neurons

The expression system chosen for the 3rd generation virus had dual promoters: an EF1 housekeeping promoter to drive the expression of a green fluorescent protein (GFP) reporter gene, and a CMV promoter to ensure high expression level of the target gene (See vector map in Materials and Methods, Chapter 2, Figure 2.3A for illustration). The V5 epitope used here to identify transfected Hsp27 is a 14 amino acid sequence with a predicted molecular weight of 1kDa, while GFP is a protein tag with 238 amino acids and a weight of 26.9kDa. Addition of a V5 epitope on to Hsp27 does not affect the cellular location or function of the protein (Chapter 4, Section 4.1) making V5 a model tag for the exogenous Hsp27 protein. However, GFP is

Figure 5.2

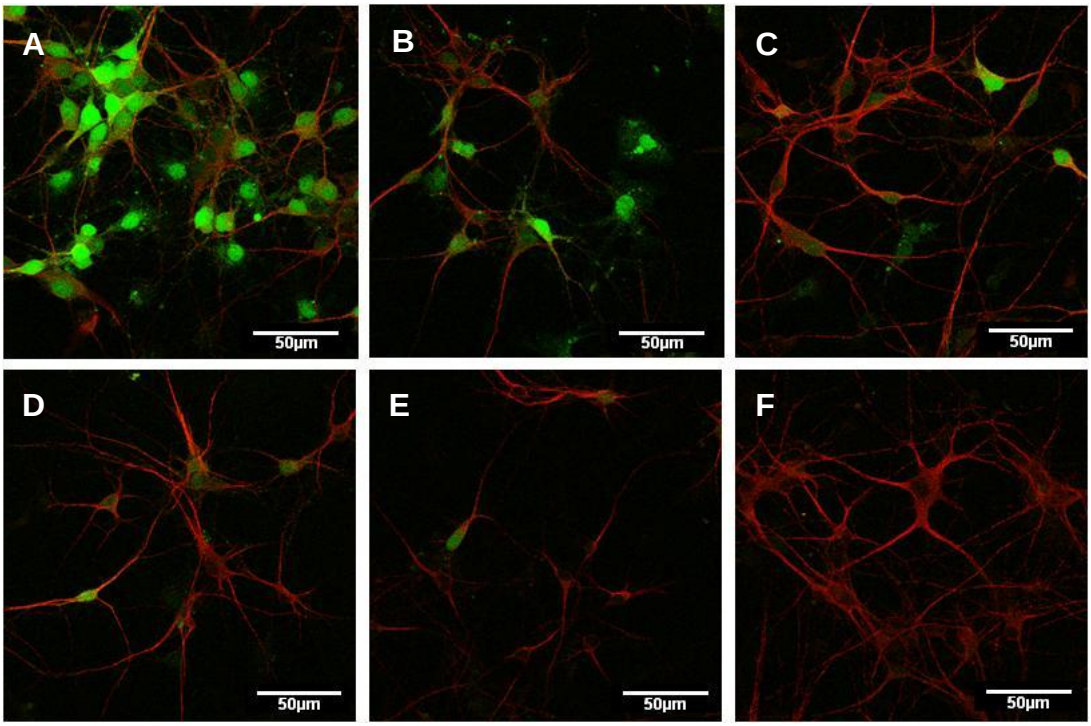

Figure 5.2 Optimisation of viral titres in primary motoneuron cultures.

Representative images of a mixed ventral horn culture virally transfected with different concentrations of a GFP expressing virus containing wild type Hsp27 (green). Motoneurons are stained for neuronal-specific MAP2 (red). **A)** 1:100 dilution, **B)** 1:200 dilution, **C)** 1:500 dilution, **D)** 1:1000 dilution, **E)** 1:1500 dilution and **F)** 1:2000 dilution.

approximately the same weight as the target protein; therefore the addition of GFP to Hsp27 may have had a significant impact on the function of the protein. Therefore, the GFP and V5-tagged Hsp27 protein were expressed via different promoters. As shown in Figure 5.3, both proteins were expressed in the same cells but in different compartments, with the GFP located in the nucleus and cytoplasm, and the V5-tagged Hsp27 only present in the cytoplasm.

5.2. Pro39Leu mutant Hsp27 does not accumulate in SC35-positive nuclear speckles in primary motoneurons

Using SH-SY5Y cells as a model of protein over-expression in experiments described in Chapters 3 and 4, nuclear inclusions were observed in cells transfected with the Pro39Leu Hsp27 mutations, located in the N-terminus of Hsp27 (Figure 4.12). Further investigation showed that the mutant Hsp27 was present in SC35-positive nuclear splicing speckles which are found in the nuclei of all cells (Figure 4.17). However, when primary motoneurons were transfected with the Pro39Leu Hsp27 mutation, immunostaining for SC35 and V5 revealed no aggregates of Pro39Leu mutated Hsp27 present.

5.3. Mutant Hsp27 may impair the heat shock response of primary motoneurons in culture

An important cellular function of Hsp27 is to act as a protein holdase and co-chaperone of Hsp70 and is an important component of the heat shock response (HSR). To investigate the effect of Hsp27 mutations on the HSR, the expression levels of Hsp70 were examined by immunofluorescence under both non-stressed and stressed conditions in untransfected and transfected primary motoneuron cultures. Cellular stress was induced by exposing the motoneurons to heat shock

Figure 5.3

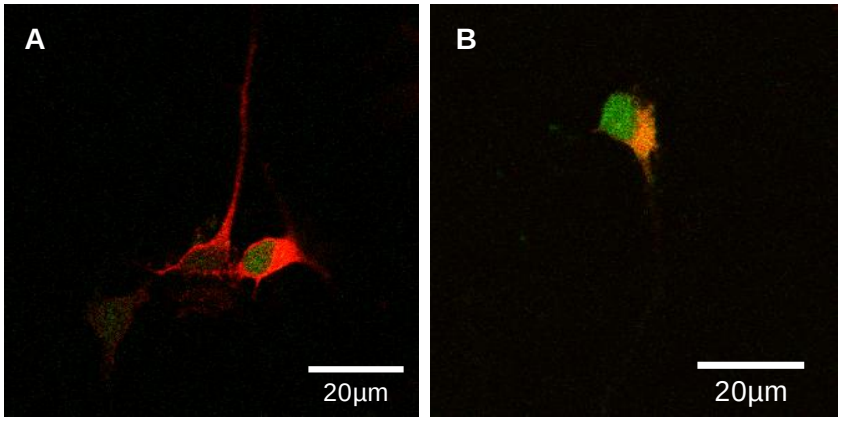

Figure 5.3 Motoneurons in culture express GFP and V5-tagged Hsp27 separately.

Representative images of motoneurons from mixed ventral horn cultures virally transfected with a GFP (green) expressing virus containing V5-tagged wild type Hsp27 (red). **A)** GFP is located in the cell nucleus while V5-tagged wild type Hsp27 can be found in the cytoplasm. **B)** GFP is located both in the cell nucleus and cytoplasm while Hsp27 can only be observed in the cytoplasm.

at 42˚C for 30 minutes. The cultures were then fixed 6 hours later and immunostained for Hsp70 and the neuronal marker β-tubulin III.

Examples of the pattern of immunofluorescence observed in stressed motoneuron cultures transfected with wild type Hsp27 or Arg140Gly Hsp27 are shown in Figure 5.4A-D. The intensity of Hsp70 immunofluorescence in untransfected motoneurons and those transfected with empty vector, wild type or each of the three Hsp27 mutations in non-stressed and stressed conditions was determined and the results are summarised in Figure 5.4E. The bar chart shows that in non-stressed conditions, there was no difference in the expression of Hsp70 in any of the cultures. This finding suggests that neither viral transfection nor expression of mutant Hsp27 altered the expression of Hsp70 in primary motoneurons, indicating that the HSR was not activated under these conditions. As expected, when untransfected, empty vector and wild type transfected primary motoneurons were exposed to heat shock, they showed a large increase in Hsp70 (Figure 5.4E). In contrast, in motoneurons transfected with each of the Hsp27 mutations, the increase in Hsp70 expression was clearly reduced (Figure 5.4E); suggesting a diminished HSR in motoneurons containing mutant Hsp27 compared to untransfected, empty vector and wild type transfected primary motoneurons.

5.4. The effect of Hsp27 mutations on mitochondrial membrane potential (Δψm) in primary motoneurons

Due to the large size and high-energy functions of motoneurons, these cells are critically dependent on fully functioning mitochondria (Shaw and Eggett, 2000). However, mitochondria are very sensitive to changes in the cellular environment and changes in ATP production are one of the first signs of motoneuron dysfunction in a transgenic mouse model of ALS expressing mutant SOD1

Figure 5.4 Expression of mutant Hsp27 reduced the stress response of primary motoneurons in vitro

Primary motoneurons were transfected with a virus containing V5-tagged wild type or mutant Hsp27. Some cultures were stressed by heat shock at 42˚C for 30 minutes and fixed 6 hours after stress stimulation. The cultures were then immunostained for Hsp70 (red) and the neuronal marker β-tubulin III (aqua). **A.** A primary motoneuron transfected with wild type Hsp27 and **B.** the same cell immunostained for Hsp70. **C.** A primary motoneuron transfected with Arg140Gly Hsp27 and **D.** immunostained for Hsp70. The intensity of Hsp70 immunofluorescence was measured. **E.** The bar chart shows the intensity of Hsp70 immunofluorescence in each culture condition under non-stressed and stressed conditions. Error bars = SEM.

Figure 5.4

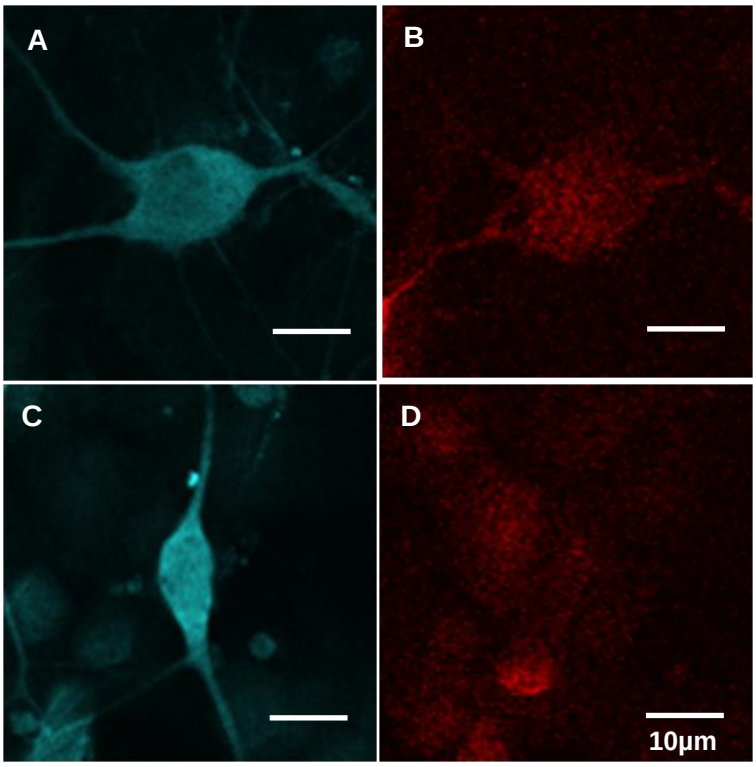
A
B
C
D
10µm

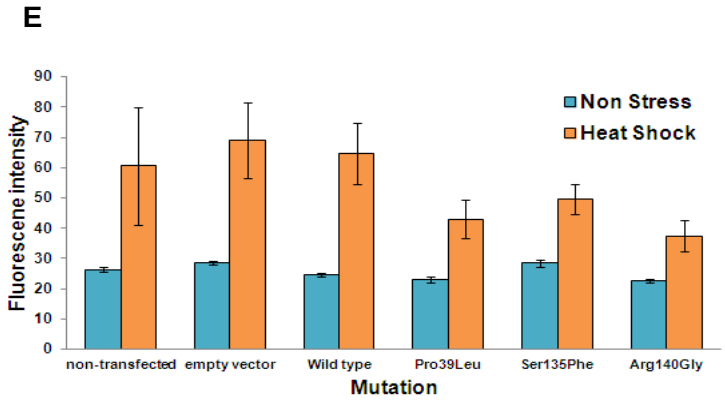
E
Fluorescene intensity
90
80
70
60
50
40
30
20
10
0
Non Stress
Heat Shock
non-transfected
empty vector
Wild type
Pro39Leu
Ser135Phe
Arg140Gly
Mutation

(Bilsland *et al*., 2008). Measurement of the mitochondrial membrane potential (Δψm) is a sensitive, functional readout of cellular health. Therefore, the affect of Hsp27 mutations on Δψm in primary motoneurons was examined next.

5.4.1. TMRM as a measure of Δψm

Tetramethylrhodamine methyl ester (TMRM) was used to measure Δψm. TMRM is a cell-permanent potentiometric indicator that is non-toxic to live cells (Figure 5.5). The cationic nature of TMRM causes higher fluorescence intensity at a more negative Δψm, and a loss of fluorescence intensity as Δψm becomes more positive, as the mitochondrial membrane depolarises (Gandhi *et al*., 2009).

Firstly, the specificity and stability of TMRM was confirmed by recording a time series of images from the time TMRM is added and the fluorescence intensity of cell bodies was measured. TMRM is a highly lipid soluble, potentiometric indicator that has a single, delocalised positive charge, and therefore becomes sequestered and fluoresces in mitochondria as a result of the electrochemical gradient between the cytoplasm and mitochondria. As the TMRM is sequestered into the mitochondria the fluorescence intensity increases and stable fluorescence intensity was recorded from 1,700 seconds, or 28 minutes (Figure 5.6). To confirm TMRM localisation to the mitochondrial membrane, 1μM FCCP, a mitochondrial uncoupler of oxidation from phosphorylation meaning ATP synthesis cannot occur and causes complete depolarisation of the Δψm was added, and an immediate reduction in TMRM fluorescence was observed. Under complete depolarisation, TMRM loses fluorescence and disperses from the mitochondrial membrane, causing the observed immediate reduction in TMRM fluorescence demonstrating that the TMRM was indeed specifically fluorescing in the mitochondrial membrane (Figure 5.6).

Figure 5.5

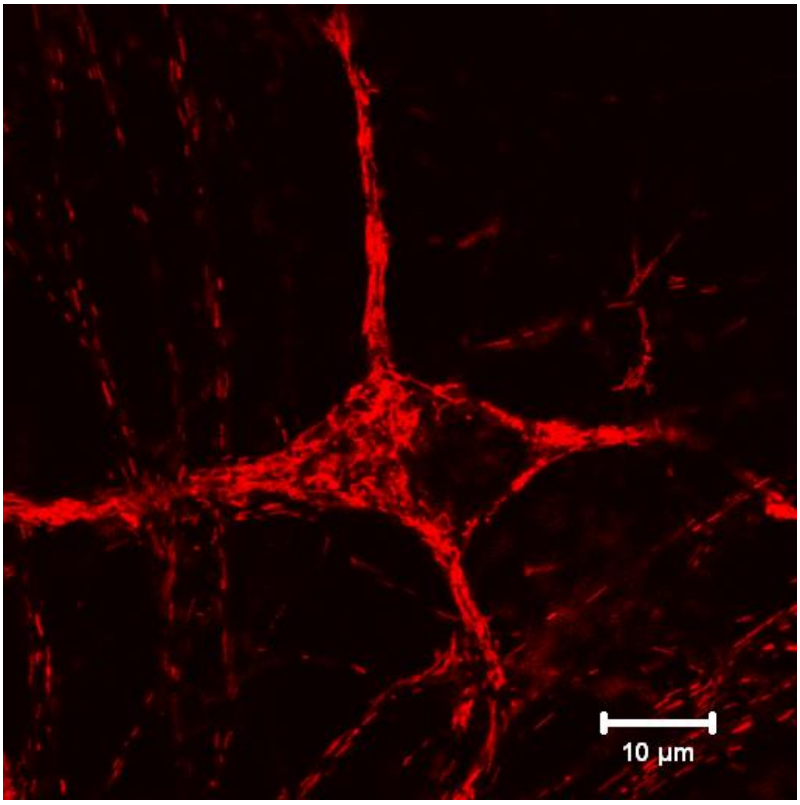

Figure 5.5 Confocal image of a TMRM-loaded motoneuron.

TMRM is a cationic fluorophore which accumulates in the mitochondria due to the electrochemical gradient between the mitochondria and cytoplasm measured by intensity.

Figure 5.6

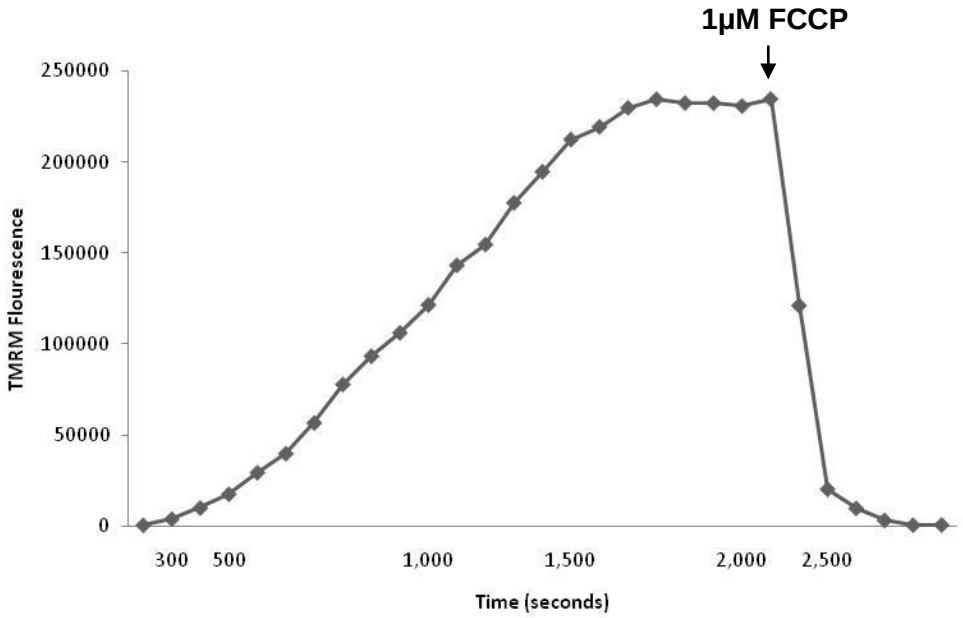

Figure 5.6 TMRM as a reliable probe for mitochondrial membrane potential

An example traces showing increasing TMRM fluorescent intensity over time. Addition of 1µM FCCP (a mitochondrial uncoupler) gives an immediate reduction in TMRM signal as the mitochondrial membrane depolarises.

5.4.2. Mutations in Hsp27 do not disrupt the Δψm in primary motoneurons

To assess the impact of Hsp27 mutations on the Δψm, TMRM fluorescence intensity was measured in both transfected primary motoneurons, visualised by GFP fluorescence, and non-transfected primary motoneurons, identified by a lack of GFP expression, from the same culture dish. These measurements were then compared to give a ratio of the fluorescence change between transfected and non-transfected motoneurons. To control for the addition of a virus and foreign protein, cells transfected with empty vector or virus containing wild type Hsp27 were analysed using the same parameters.

As shown in Figure 5.7, transfection with an empty viral vector or viral particles expressing wild type Hsp27 had no measurable effect on the Δψm, with no change or difference in TMRM intensity compared to non-transfected primary motoneurons in the same culture dish (Figure 5.7). Transfection with the Pro39Leu, Ser135Phe or Arg140Gly Hsp27 mutations also had no significant effect on the Δψm in comparison to non-transfected co-cultured primary motoneurons, although motoneurons transfected with the Ser135Phe or Arg140Gly Hsp27 mutations showed a non-significant trend of hyperpolarisation of the Δψm (Figure 5.7).

5.4.3. Motoneurons containing Hsp27 mutations do not actively maintain Δψm

Although hyperpolarisation of the mitochondrial membrane does not directly suggest a deficit in the membrane potential, it may indicate a reversal of the ATPase. This may be the result of active maintenance of the Δψm via reversal of the ATP-pump, using ATP to remove protons, or positive charge, from the membrane inner space. To examine the Δψm more thoroughly for specific stresses, three mitochondrial inhibitors acting on different complexes of the mitochondrial machinery were applied

Figure 5.7

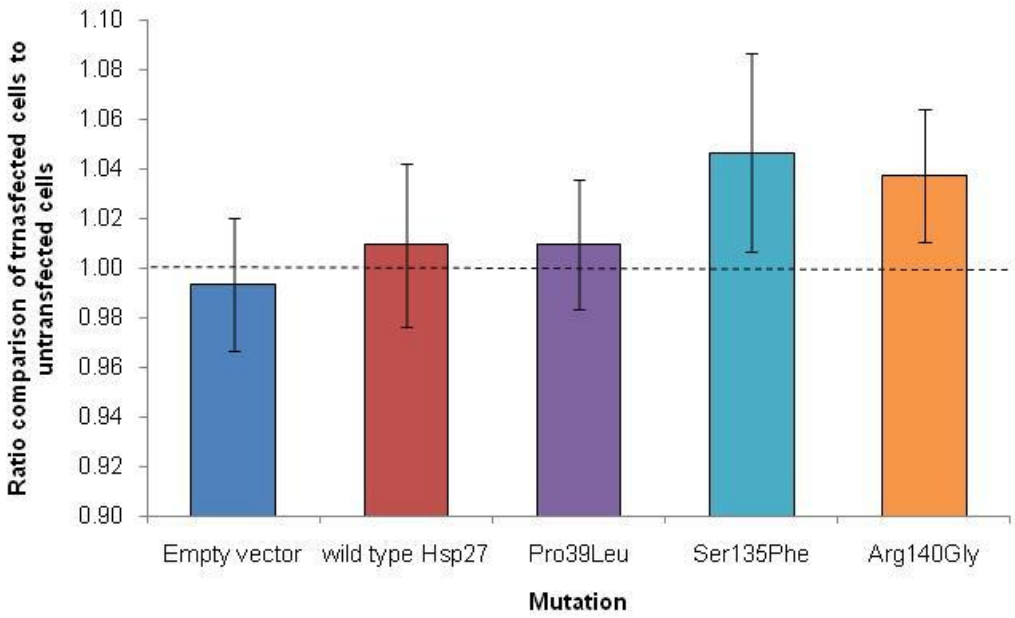

Figure 5.7 Hsp27 mutations do not alter mitochondrial membrane potential in primary motoneurons

A bar chart showing mitochondrial membrane potential of primary motoneurons transfected with either empty vector, wild type Hsp27 or various mutants of Hsp27 relative to untransfected cells which have a value of 1. Error bars = SEM, n=10.

over a time series to elucidate the mechanism by which Hsp27 mutants may increase the Δψm. As shown in Figure 5.7, primary motoneurons transfected with the Ser135Phe and Arg140Gly mutations, showed a small, albeit non-significant hyperpolarisation in comparison to non-transfected primary motoneurons under normal *in vitro* conditions (Figure 5.7). Therefore these mutations were taken forward for further examination. Representative traces over time of TMRM fluorescence intensity from one primary motoneuron per condition are shown in Figure 5.8 to illustrate the change in TMRM fluorescence intensity in response to different mitochondrial inhibitors.

Oligomycin (2μg/ml), an ATPase inhibitor was added first. If the ATPase had reversed to maintain Δψm, TMRM fluorescence intensity would have steadily decreased with the addition of Oligomycin, as the membrane would no longer have been actively maintaining a negative Δψm. The addition of Oligomycin to the cell-imaging dish prompted an initial decrease in TMRM fluorescence intensity which did not increase with time in all cells measured, including motoneurons transfected with Ser135Phe or Arg140Gly Hsp27 and non-transfected motoneurons from the same imaging dishes (Figure 5.8).

Rotenone, an inhibitor of Complex I of the electron transport chain, was then added to the cells to investigate mitochondrial reliance on the different complexes within the electron transport chain. Upon addition of Rotenone there was a steep, immediate decline in TMRM fluorescence intensity indicating a heavy reliance on Complex I. This is not an unusual response in cells such as motoneurons that have a fast metabolism and high-energy demands. The addition of Rotenone (5μM) gave an immediate decrease in TMRM fluorescence intensity in all cells irrespective of transfection condition. This observation demonstrates that all the primary

Figure 5.8

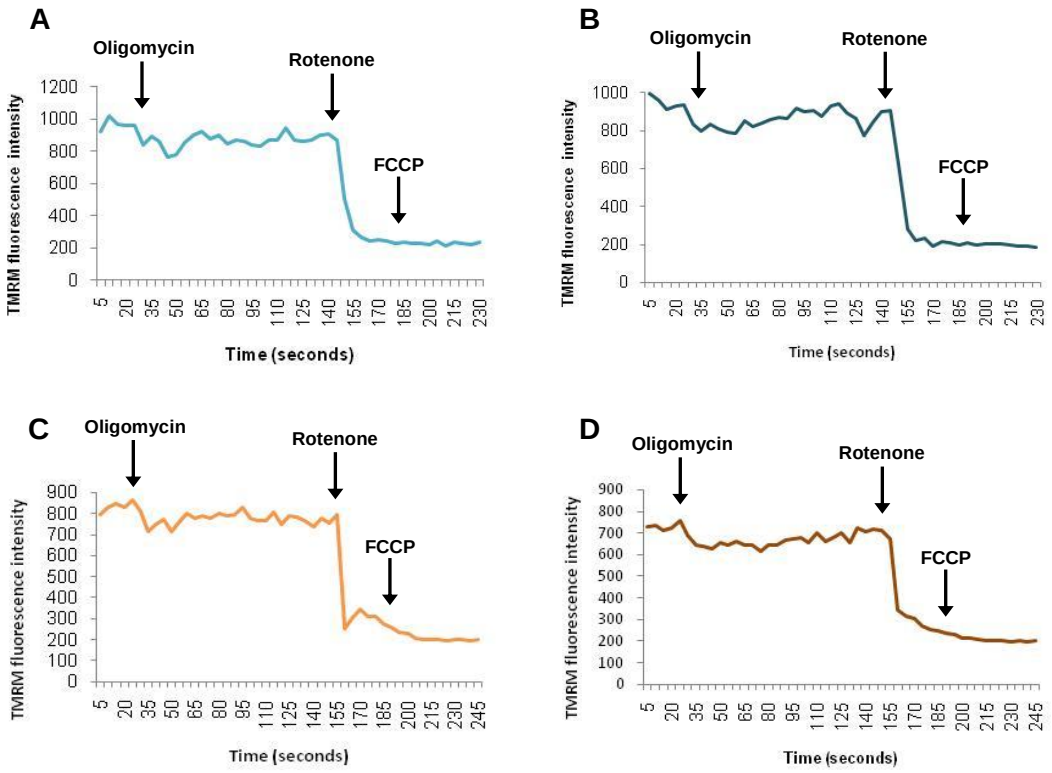

Figure 5.8 Hsp27 mutations do not alter mitochondrial membrane potential in the presence of different mitochondrial inhibitors

Representative traces over time depicting the addition of different mitochondrial inhibitors; Oligomycin, Rotenone and FCCP to cells under different transfection conditions. The traces show that Hsp27 mutations do not alter the ATPase pump in the presence of Oligomycin, and that all motoneurons have a heavy reliance on Complex I. Fluorescence intensity of TMRM over time in **A)** a cell transfected with Ser135Phe Hsp27 and, **B)** an untransfected, co-cultured cell. **C)** A cell transfected with Arg140Gly Hsp27, and **D)** a co-cultured untransfected cell.

motoneurons investigated were more reliant on Complex I than Complex II of the electron-transfer chain causing a large decline in the Δψm (Figure 5.8). In all cells, the Δψm depolarisation in response to the addition of Rotenone was so great that the effect of the further addition of FCCP, a mitochondrial uncoupler, which causes maximal depolarisation of the Δψm, was undetectable. With the addition of all three drugs, the presence of Hsp27 mutations had no differential effect on the Δψm compared to untransfected motoneurons.

5.5. Chapter 5 Summary

The experiments described in this chapter were designed to examine whether Hsp27 mutations resulted in functional deficits in primary motoneurons in culture.

The plasmid-transfected SH-SY5Y cell model used in Chapters 3 and 4 to examine the differential effects of Hsp27 mutations, involved the over expression of a mutated, foreign protein to examine the pathology arising from the cellular pathways that are affected by the different Hsp27 mutations. The cellular model developed in this Chapter was designed to measure the functional consequences of low expression of the mutant Hsp27 in motoneurons, rather than the differences in mutant pathology highlighted by over expression of the protein in a genetically homogeneous cell line. Clear differences in the effects of expression of the Hsp27 mutations in the two cellular models were detected. For example, the nuclear inclusions observed in Pro39Leu Hsp27 plasmid-transfected SH-SY5Y cells were not detected in virally-transfected primary motoneurons.

To ascertain which basic cellular functions may be being affected by Hsp27 mutations to cause a peripheral axonal neuropathy, experiments were undertaken to examine some of the key functions that are fundamentally important for motoneurons, and in which Hsp27 is thought to play a role. Hsp27 has a number of cytoprotective functions including protein handling and folding, inhibition of apoptosis, protection against oxidative stress and promotion of axonal growth, all of which make Hsp27 essential for motoneuron growth and survival (Kalmar *et al*., 2002).

As a co-chaperone of Hsp70, one of the most important roles Hsp27 has within the cell is that of a protein holdase, making Hsp27 an important component of the HSR.

Hsp27 has also been implicated in the modulation of the HSR by sumolaytion of HSF1, a protein that regulates the activation of the HSR (Brunet Simioni *et al*., 2009). Hsp27 blocks the transactivation capacity of HSF1, thereby inhibiting chaperone and co-chaperone activation and modulating the HSR (Brunet Simioni *et al*., 2009). A recent paper by Almeida-Souza *et al.* (2010) suggests that the Ser135Phe mutation leads to an increase in the chaperoning function of Hsp27 (Almeida-Souza *et al*., 2010). However, this finding was not examined contextually as Hsp27 works as a small component of a complex cascade of heat shock proteins, and it was not known if the addition of the Ser135Phe Hsp27 mutation affected the HSR as a whole. By using virally transfected primary motoneurons, the experiments described in this Chapter examined the effect of mutations of Hsp27 on the expression levels of Hsp70, as an important member of the HSR, under both stressed and unstressed conditions. Firstly, I found that in unstressed conditions, the addition of mutant Hsp27 did not stress the cells above normal levels of primary motoneurons in culture to activate or increase the HSR. However, when stressed, motoneurons transfected with mutant Hsp27 did not display as high an increase in Hsp70 as untransfected, empty vector and wild type transfected primary motoneurons, suggesting a decreased activation of the HSR. This is unexpected and suggests that mutations in Hsp27 may alter the ability of motoneurons to respond to stress. However, the results shown here are not a full investigation of the HSR in cells expressing mutant Hsp27, and caution is required when interpreting quantification of immunofluorescence. The need for further experiments is discussed more fully in Chapter 6.

While the correct functioning of the HSR is vital to the cells response to times of stress, the healthy function of mitochondria is vital to all functions and the overall homeostasis of motoneurons particularly in light of their large size and high-energy

demands (Shaw and Eggett, 2000). However, as has been previously shown, mitochondria are very sensitive to changes in the cellular environment; for example, changes in ATP production are one of the first signs of motoneuron stress in animal models of mutant SOD1 ALS (Bilsland *et al*., 2008). To maintain ATP production and a functional mitochondrial membrane potential (Δψm), mitochondrial transport, autophagy and structure must be tightly regulated. Hsp27 has been implicated in the maintenance of all three of these pathways via indirect actions. For example, Hsp27 may affect Δψm by regulating mitochondrial structure and mitophagy, acting as a downstream mediator of high-mobility group box-1 (HMGB1), an essential regulator of mitochondrial autophagy, via manipulation of trafficking along actin fibres during mitophagy (Tang *et al*., 2011). As shown in Chapter 4, Section 4.4, mutations in Hsp27 cause abnormal interactions of actin and Hsp27 under normal, and stress conditions, and this may have implications for motoneuron mitophagy during trafficking. In addition, transgenic mice carrying human Hsp27 containing either the Ser135Phe or Pro182Leu mutation show disrupted mitochondrial transport along microtubules, although there has been no further examination of the effect this may have on the Δψm (d' Ydewalle *et al*., 2011). Thus, measurement of the Δψm can be a sensitive, functional readout of cellular health. Thus, examination of Δψm in mutant Hsp27 motoneurons will give an indication of the affect of Hsp27 mutations on cell homeostasis and vulnerability. As shown in Section 5.4.2., in motoneurons transfected with mutations of Hsp27, no deficits in the Δψm were detected, suggesting that the mutations in Hsp27 examined do not affect cellular pathways in which mitochondria interact.

When taken together, the results presented in Chapter 5 suggest that there are no mitochondrial deficits in motoneurons expressing mutant Hsp27, however, mutant Hsp27 may decrease the cells ability to activate the HSR under stress conditions,

altering the ability of motoneurons to respond to stress and increasing vulnerability to cellular insults.

Chapter 6. Discussion

CMT 2F and dHMN are axonal hereditary neuropathies that present with predominantly motor deficits with a variable age of onset and which result in significant disability. Although the disease is predominantly of a motor presentation, there is a spectrum of moderate to mild sensory involvement, with dHMN showing no sensory involvement (Ismailov *et al*., 2001; Houlden *et al*., 2008). There are currently approximately 50 known loci and over 40 genes with mutations associated with different forms of CMT (Pareyson and Marchesi, 2009). From this diverse genetic background, many of the genes affected in CMT code for proteins that are essential to neurons and glial cells. While it is understandable that mutations in neuron-specific proteins may result in a neuronal phenotype, it is not clear why these mutations may affect specific subpopulations of neurons, e.g. motor rather than sensory. Furthermore, many CMT-causing mutations are in ubiquitously expressed proteins, and so the reasons for their deleterious effects in neurons alone are less clear. However, when considered in terms of their biological role, for example in myelin maintenance, fast metabolism, high protein turnover and axonal transport, it becomes clear that these proteins play key roles in pathways that are particularly important for neurons.

Hsp27 is one such protein. Mutations in the gene coding for this small heat shock protein have been shown to cause CMT 2F and dHMN in unrelated families from different populations (Kijima *et al*., 2005; Tang *et al*., 2005; Evgrafov *et al*., 2004; Chung *et al*., 2008; Houlden *et al*., 2008; James *et al*., 2008; Ikeda *et al*., 2009; Benedetti *et al*., 2010**;** Luigetti *et al*., 2010; Mandich *et al*., 2010; Solla *et al*., 2010). However, Hsp27 is a ubiquitous protein with a number of housekeeping and

cytoprotective functions, which include protein handling and folding, inhibition of apoptosis, protection against oxidative stress and promotion of axonal growth, making Hsp27 essential for neuronal survival (Kalmar *et al*., 2002; (Franklin *et al*., 2005a). CMT caused by mutations in Hsp27 is relatively rare, and represents only 4% of all cases of CMT2 and 8% of all dHMN cases, in comparison to the most common causes of hereditary neuropathy, for example PMP22 mutations that are responsible for ~70% of all CMT1 (Capponi *et al*., 2011). However, mutant Hsp27 induced CMT is an interesting subtype of peripheral neuropathy, as it represents a large group of patients with a motor-dominant phenotype, a very specific presentation caused by mutations in a protein that has many important cellular functions, including anti-apoptotic, anti-oxidative roles.

Published findings of *in vitro* and *in vivo* studies in which the cellular effects of mutant Hsp27 have been examined, show histological and functional evidence for the involvement of mutant Hsp27 in cytoskeletal stability and axonal transport (Benedetti *et al*., 2010; d' Ydewalle *et al*., 2011). Studies have shown that Hsp27 mutations cause disruption and aggregation of cytoskeletal and axonal transport proteins, including light and medium chain neurofilament, microtubules and the p150 subunit of the dynactin motor complex (Ackerley *et al*., 2006; d' Ydewalle *et al*., 2011; Evgrafov *et al*., 2004; Zhai *et al*., 2007). However, while much of the evidence for the aberrant functions of Hsp27 mutations suggests disruption of axonal transport, Almeida-Souza *et al.* (2010) propose that Hsp27 mutations may lead to increased chaperoning function of the protein and a shift in the oligomerisation balance of the protein towards increased Hsp27 monomerisation, a state more commonly seen under stress conditions (Almeida-Souza *et al*., 2010).

The aim of the experiments described this Thesis was to examine the deleterious effects of mutations in heat shock protein 27, which cause Charcot-Marie-Tooth disease and distal Hereditary Motor Neuropathy. The pathogenicity, differential cellular effects and some of the functional consequences of each mutation were investigated in two *in vitro* models. The results showed that all the mutations examined are cytotoxic. Further investigation revealed that the nature and appearance of some features of cellular pathology differ depending on the position of the mutation within the gene, as summarised in Figure 6.1. Preliminary results presented in Chapter 5 also suggest that some Hsp27 mutations may have functional consequences for the HSR.

6.1 Hsp27 mutations are cytotoxic and cause CMT 2F

The first investigation to examine the effects of mutant Hsp27 was undertaken in SH-SY5Y cells, a neuroblastoma cell line in which the Hsp27 mutations were transiently over-expressed and their effects on cell survival examined. Mutations examined were significantly cytotoxic, causing an average increase in cell death of 20%. These results confirm that Hsp27 mutations have significant pathological effects, even in this simple cellular model system. This finding expands on previous work described by Evgrafov *et al*. who demonstrated the cytotoxicity of the Ser135Phe Hsp27 mutation (Evgrafov *et al*., 2004).

6.2. The position of the Hsp27 mutation in the gene has differential effects on Hsp27 protein function

The Hsp27 protein has three separate functional domains; a poorly conserved N-terminus, a highly conserved α-crystallin domain near the middle of the protein and a highly flexible, variable C-terminus (Kostenko and Moens, 2009). Mutations found in patients with CMT 2F are spread across the gene in areas corresponding to all

Figure 6.1.

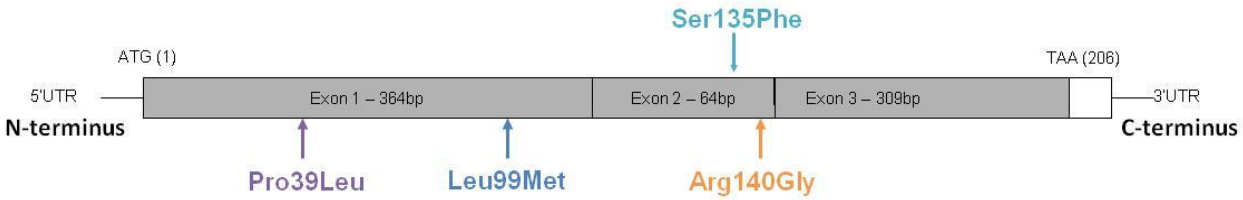

	Pro39Leu	Leu99Met	Ser135Phe	Arg140Gly
Cytotoxicity	↑	↑	↑	↑
Vulnerability to cellular stress			↑	
Neurite outgrowth				↓
Co-localises with cytoskeletal proteins			↑	↑
Nuclear inclusions	✓			

Figure 6.1 Differential effects of Hsp27 mutations in a cell model

A schematic representation of the Hsp27 gene with the positions of the mutations described in this Thesis marked. The table below demonstrates the differential effects of Hsp27 mutations on parameters tested in this thesis. Arrows indicate an increase or decrease in effect. The tick indicates the presence of potentially pathological mutant Hsp27 positive nuclear inclusions.

three domains, however there is a cluster, or 'hot-spot' area located in the middle of the α-crystallin domain (see Figure 1.4). These different domains have been shown to be differentially involved in Hsp27 functions. However, the phenotypic variations of age of onset and sensory involvement in CMT 2F are not dependent on the mutation position or amino acid change (Solla *et al*., 2010).

d'Ydewalle *et al.,* have very recently developed two lines of transgenic mice that express mutant human Hsp27 in their neurons. The first mouse strain expresses the Ser135Phe mutation, located in the α-crystallin domain, whereas the other strain expresses the Pro182Leu mutation, located in the C-terminus of Hsp27 (d' Ydewalle *et al*., 2011). These two transgenic mice display markedly different phenotypes, with the C-terminus Pro182Leu Hsp27 causing a more severe, pure motor phenotype while the transgenic mouse expressing the Ser135Phe mutation located in the α-crystallin domain of Hsp27 has a mixed sensory-motor phenotype (d' Ydewalle *et al*., 2011). The authors' claim that different sub-types of neurons were more vulnerable to different mutations in Hsp27, suggesting underlying differences of disease phenotype and clinical presentation are linked to mutation position (d' Ydewalle *et al*., 2011).

The results presented in this Thesis, showing differential morphological vulnerabilities in cells expressing mutations at different regions of the Hsp27 gene, generally support the findings by d' Ydewalle *et al.* Thus, my results in an *in vitro* model of CMT showed that although all the mutations examined are toxic, the different Hsp27 mutations do not have a uniform effect on cell morphology. For example, mutations in the N-terminus of the protein give a more subtle cellular change, with the mis-localisation of the mutated protein to the nucleus. In contrast,

mutations in the α-crystallin domain in the C-terminus of the protein have a more dramatic effect on cellular vulnerability, neurite outgrowth and cytoskeletal stability.

Hsp27 is a vitally important component of the stress response of the cell, the heat shock response (HSR), which is activated to protect the cell from environmental challenges. Independent from its heat shock protein function, Hsp27 has also been shown to inhibit members of the apoptosis signalling pathway (Arrigo, 2007). Small HSPs, such as Hsp27 have also been shown to interact with the actin cytoskeletal network and play a role in the regulation of actin polymerization (Goddette and Frieden, 1986; Falconer *et al*., 1994; Williams *et al*., 2005). Therefore, the effect of expression of Hsp27 mutations on the cellular response to cytoskeletal stressors was examined. These stressors have proven effects on either the actin cytoskeleton or the microtubular network, and were chosen due to the specifically defined cellular stress each agent exerted on proteins and structures with which Hsp27 had been shown to functionally interact. Under these stress conditions, the addition of one mutation, Ser135Phe Hsp27, caused a further significant rise in cytotoxicity over and above that caused by the pharmacological agents in cells that express the wild type Hsp27. This suggests that the Ser135Phe mutation makes cells more vulnerable to cellular insults than any of the other mutations that cause CMT 2F.

Previous studies using Hsp27 mutations have suggested that the mutations affect the cytoskeleton of the cell, for example neurofilaments, which have been shown to aggregate in the presence of Hsp27 mutations (Ackerley *et al*., 2006; Zhai *et al*., 2007). The increased vulnerability of cells expressing Ser135Phe Hsp27 to cytoskeletal cell stressors demonstrated a differential pattern of response by an immortal cell line to an individual mutation. However, the biochemical assay used in these experiments was not sensitive enough to give an idea of how or why the

Ser135Phe Hsp27 mutation increases cellular vulnerability to cytoskeletal cell stressors. The cytoskeleton is fundamentally important to the integrity and structure of the cell, as well as being the driving force of cellular differentiation and growth. Therefore a more detailed immunocytochemical analysis of the effects of Hsp27 mutations on length and structural changes of neurite outgrowth was undertaken. In previous studies, the results from *in vitro* experiments examining the cellular effects of mutant Hsp27 indicated involvement of the mutant protein in cytoskeletal stability, with the addition of the Ser135Phe Hsp27 mutation, located in the α-crystallin domain and the Pro182Leu mutation located in the C-terminus of the protein causing the aggregation of neurofilament proteins (Evgrafov *et al*., 2004; Ackerley *et al*., 2006; Zhai *et al*., 2007). By examining the effects of Hsp27 mutations on neurite outgrowth and development I aimed to establish whether the Hsp27 mutations affected the morphological appearance of neurons. Neurite outgrowth and morphology of neuronal processes were investigated as cytoskeletal abnormalities would most likely affect these parameters in cultured neurons. Aggregation of neurofilament seen in previous studies could also indicate neuronal degeneration rather than being a direct consequence of the mutation of Hsp27 as neurofilament aggregation is a pathological hallmark of many forms of CMT (Tradewell *et al*., 2009; Benedetti *et al*., 2010).

Of the four Hsp27 mutations examined, Arg140Gly and Ser135Phe had pronounced inhibitory effects on neurite outgrowth, with the Arg140Gly showing a significant effect. Both of these mutations are located in the α-crystallin domain of the Hsp27 protein, with the Arg140Gly being an amino acid change in Hsp27 equivalent to mutations in the related small heat shock protein, Hsp22, which have been shown to cause CMT 2L (Irobi *et al*., 2004). The patient mutations that cause CMT 2L, Lys141Asn and Lys141Glu, reduce neurite outgrowth by 50%, suggesting that this

specific region of Hsp22 and Hsp27 is important for neurite outgrowth in motoneurons, and that mutations in this area of the protein may be particularly detrimental to the structures and functions of the axon (Irobi *et al*., 2004). However, in my experiments I found a much smaller reduction in neurite length, which may be due to Arg140Gly and Ser135Phe mutations affecting neurite length to a lesser extent than Lys141Asn and Lys141Glu mutations in the Hsp22 gene. The process of neurite outgrowth is highly complex, and while measuring neurite length demonstrates that individual mutations can affect the process, it does not give any indication as to how the mutation may be disrupting the normal functions and interactions of Hsp27.

Neurite outgrowth is driven by the cytoskeleton and associated proteins, and so to start to elucidate the effects of the Hsp27 mutations on the individual components of vital cellular processes such as neurite outgrowth and axonal transport, the interactions of mutant Hsp27 with different proteins of the cytoskeleton were compared to that of endogenous Hsp27 under unstressed and stressed conditions. The hypothesis underlying the choice of pharmacological cell stressors that acted on different aspects of the cytoskeleton was that mutations affect particular functions of the Hsp27 protein. Since it has been shown that wild type Hsp27 can ameliorate cellular pathology induced by mutant neurofilament, there appears to be intrinsic relationship between the cytoskeleton and Hsp27 that goes beyond the known interaction of Hsp27 with actin filaments (Zhai *et al*., 2007). It is therefore likely that there is an interaction between Hsp27 and intermediate filaments regulating axonal diameter, transport and structure. Therefore, we hypothesised that mutant Hsp27 causes pathological alterations in the interaction with cytoskeletal elements, such as actin, tubulin and intermediate filaments. One of the functions of Hsp27 in the cell is as a stabiliser of the actin cytoskeleton, which becomes more important under

conditions of stress. Hsp27 is also a modifying molecule of neurite outgrowth. The evidence presented in previous studies looking at the cellular consequences of Hsp27 mutations demonstrate that the Ser135Phe mutation in particular, causes the aggregation of proteins of the neurofilament network in unstressed conditions, demonstrating that this mutation in particular is detrimental to the cytoskeleton (Lavoie *et al*., 1993; Mounier and Arrigo, 2002; Ackerley *et al*., 2006; Read and Gorman, 2009; Evgrafov *et al*., 2004; Zhai *et al*., 2007). Perhaps surprisingly, the results described in this Thesis demonstrated an absence of co-localisation between any Hsp27 mutation and neurofilament heavy (NF-200), a large component of the neurofilament network. In addition, although cytoskeletal-stressing agents caused aggregation of NF-200 into neurofilament bundles, this was regardless of the presence of mutant Hsp27, and neither endogenous nor mutant Hsp27 co-localised with these pathological bundles. However, the expression of some of the Hsp27 mutations did have an effect on the co-localisation patterns of Hsp27 with other components of the cytoskeleton.

In all conditions examined, all mutant forms of Hsp27 co-localised with β-tubulin III, a neuronal-specific member of the microtubule network, including in cytoplasmic aggregates formed by Colchicine treatment. It is worth noting that the Ser135Phe Hsp27 mutation also resulted in the formation of tau (a microtubule-associated protein) aggregates in some cells. Hsp27 has been shown to co-localise, but not functionally interact with tubulin (Williams *et al*., 2005), which is an integral member of the microtubule network, and the findings presented here suggest that the importance of the interaction between these two proteins may have been underestimated in cellular functions where both proteins have a role, for example growth cone formation (Geraldo and Gordon-Weeks, 2009).

The possible importance of the interaction of Hsp27 with tubulin was also suggested by the results of d'Ydewalle *et al.* (2011), which showed a possible interaction between Hsp27 and microtubules in motor and sensory neurons in two lines of transgenic mice that neuronally expressed human *HSPB1* with either one of two disease-causing mutations; Ser135Phe or Pro182Leu (d' Ydewalle *et al*., 2011). These authors suggested that the pathogenic mechanism of axonal degeneration in CMT 2F is via the de-acetylation of α-tubulin, a component of the microtubule network, which could then be reversed by inhibiting a class II histone deacetylase, HDAC6 in the mice expressing the Ser135Phe Hsp27 mutation. Hsp27 has previously been shown to co-localise, but never functionally interact with any form of tubulin (Hino *et al*., 2000; Williams *et al*., 2005). Therefore, it is likely that the deacetylation of α-tubulin described is via secondary mechanisms involving Hsp27. This possibility is supported by a recent study by Gilbert *et al*. (2012), which suggests that HDAC6 is a client protein of Hsp27 and that knock-down of Hsp27 causes an increase in HDAC6 degradation (Gibert *et al*., 2012). Although my results showed co-localisation between mutant Hsp27 and β-tubulin III, I found no difference from the patterns of expression of endogenous Hsp27. However, this was not analysed by d'Ydewalle *et al* (2011).

Both the Ser135Phe and Arg140Gly mutations demonstrated an apparent increase in co-localisation with F-actin in comparison to endogenous and wild type transfected Hsp27, and the Pro39Leu and Leu99Met Hsp27 mutations. Hsp27 is thought to bind to actin via the α-crystallin domain and interacts with actin as a phosphorylated monomer, a state that is more prevalent under cell stress (Mounier and Arrigo, 2002). However, the findings presented in this Thesis showed that co-localisation between mutant Hsp27 and actin was more marked in unstressed conditions, while still being observed in cells stressed with cytoskeletal agents. In

stressed conditions, Hsp27 functionally interacts with F-actin by acting as an actin-capping protein, stabilising the actin filaments. In unstressed conditions, Hsp27 has an ill-defined function in neurite outgrowth via interactions with actin (Lavoie *et al*., 1993; Mounier and Arrigo, 2002; Williams *et al*., 2005; Williams *et al*., 2006). Although the actions of Hsp27 on the actin cytoskeleton are well known and are important for the normal functioning of the cell, the results presented here show for the first time, that Hsp27 mutations might alter this important functional interaction. Thus, mutant Hsp27 may have an increased ability to bind to F-actin, possibly causing a reduction in actin dynamics and slowing of actin polymerization, on which neurite outgrowth is dependent on. This would have a significant impact on particularly large cells, such as motoneurons, that rely on a stable and functional cytoskeleton.

To further investigate the change in interaction between Hsp27 and actin caused by these two mutations, the next step would be to carry out a protein complex immunoprecipitation, to pull down Hsp27 to calculate its level of actin binding and assess any differences between the two mutations in stressed and unstressed conditions.

While the addition of mutations in an over-expressed foreign protein caused some similar morphological changes in neurities such as a non-specific increase in lamellipodia and neuritic stumps as well as differential interactions with the cytoskeleton, one mutation also caused a distinctive differential effect in the cells. The Pro39Leu Hsp27 mutation (amino acid change in the N-terminus of the protein) caused the formation of nuclear inclusions in 39% of SH-SY5Y cells transfected with this mutation. These inclusions were found to be SC35-positive nuclear speckles. Normally, nuclear speckles are non-pathological nuclear bodies involved in mRNA

splicing, possibly of highly active genes, for example, most recently, SC35-positive speckles have been associated with tau mRNA (Hall *et al*., 2006; Qian *et al*., 2011). In previous studies, Hsp27 and other sHSPs have been associated with SC35 speckles, and although their function in these nuclear bodies remains unknown, it is speculated to be a chaperoning role of the holding of mRNAs targeted for degradation, not for refolding as Hsp70 is not present in SC35-positive nuclear speckles (van den IJssel *et al*., 2003; Bryantsev *et al*., 2007; Vos *et al*., 2009). However, although the presence of Pro39Leu Hsp27 positive nuclear speckles was easily detectable in SH-SY5Y cells over expressing the mutated protein, these speckles were not observed in primary motoneurons transfected with a virus, resulting in a low expression of mutant Hsp27. The reason for the accumulation of Pro39Leu Hsp27 in SC35 speckles in a cell model of protein over expression is unclear. It is possible that the differential effect of this mutation may be the consequence of the over-expression of a mutated foreign protein in a cell line to produce an unnatural aggregate. However, the finding of speckle aggregates in cells with varying levels of protein over expression, and their absence in any other cells, including cells transfected with other mutations, suggests that this is a manifestation of a specific effect of the N-terminus mutation. The next step to understand the role of Hsp27 in SC35-positive nuclear speckles could be to use laser dissection to isolate cells containing Pro39Leu Hsp27 aggregates to use real-time quantitative PCR to identify any changes in Hsp27 or other common proteins that may be associated with the speckles. This may help to identify which pathways and processes maybe affected downstream by the aggregation of Hsp27 in the nucleus.

Using an *in vitro* cell model of protein over expression, I have demonstrated significant differences in the effects of Hsp27 mutations that are caused by the position of the mutation in the protein affecting the properties of the protein. Indeed,

as shown in Figure 6.1, all mutations apart from one showed differential effects in SH-SY5Y cells, albeit on different parameters. The recessive Leu99Met Hsp27 mutation (located in the α-crystallin domain, but out of the hot spot region) was shown in Chapter 3 to be toxic to cells under basal conditions, but did not display any differential effects using any other outcome measure assessed. This may be due to the endogenous Hsp27 in SH-SY5Y cells, which may negate the recessive nature of the gene. However, it is more likely that the outcome measures tested here to screen for differential effects may not be sensitive enough to distinguish the cellular effects of this mutation. There is also a possibility that the Leu99Met mutation, which has only been found in one family, may not be recessive, as the maternal DNA was never screened. It may not be a recessive mutation if the mother did not carry the same mutation, or may have carried a different mutation in a different gene.

6.3. The functional effects of Hsp27 mutations

While the results presented in this Thesis demonstrate that mutations of Hsp27 have different cellular effects that are associated with the position of the mutation in the gene, the diseases caused by these mutations demonstrate strikingly similar disease phenotypes. Thus, dHMN caused by mutant Hsp27 affects very specific subpopulations of neurons, mainly motoneurons, causing a predominantly motor phenotype in patients. This is interesting, as not only is Hsp27 expression ubiquitous, but Hsp27 is involved in within the cell, including cell survival, protein chaperoning, redox maintenance (Kalmar *et al*., 2002; Franklin *et al*., 2005). More recently, it has been suggested that Hsp27 may play a role in mitochondrial autophagy (Tang, *et al*. 2011). These processes are critical for all cell types. Although the results obtained in the SH-SY5Y cell line showed robust differences between the effects of the Hsp27 mutations, this model is not very suitable to

examine functional differences, as the readouts of the model are not sensitive enough. Therefore, lentiviral particles were used to deliver and stably express Hsp27 mutations in primary motoneurons. Primary embryonic mixed ventral horn cultures are more representative of motoneurons and contain a number of glial cells, as there is heterogeneity in cell type in a mixed cell culture. Therefore, this primary cell model is a more accurate model system for a neuromuscular disease affecting motoneuron axons.

Motoneurons are particularly vulnerable to changes in their cellular environment as even a small shift in protein, ionic and energy homeostasis can cause a significant dysfunction. Motoneurons rely on surrounding cells for synthesis and recycling of transmitters, rapid energy production and this reliance on other cells makes motoneurons vulnerable to pathological events affecting either themselves or supporting cells that surround them.

Work by d'Ydewalle *et al.,* (2011) suggests that mutations in the α-crystallin domain of Hsp27 may disrupt axonal transport of mitochondria. However, although the paper shows abnormal acetylation of microtubules, it is currently unknown if the disruption of mitochondrial transport is due to changes in the transport system or disruptions within the mitochondria themselves. For example, the failure of the cell to transport mitochondria normally could be due to misshaped mitochondria being present in the cell. Hsp27 has been proposed to play a role in the process of mitophagy, acting as a downstream mediator of high-mobility group box-1 (HMGB1), an essential regulator of mitochondrial autophagy by regulating actin-mitochondria interactions (Tang *et al.,* 2011). Mutations in Hsp27 may affect mitophagy. Therefore, to analyse whether mitochondrial function was affected by mutant Hsp27, the mitochondrial membrane potential (Δψm) was measured by *in vitro* live imaging

of cell body mitochondria in primary motoneurons. Expression of mutant Hsp27 did not disrupt the Δψm in the cell body of primary motoneurons. However, CMT 2F is a peripheral axonal disorder in nerves that can be over a metre in length, meaning that there could be a significant difference between mitochondrial viability in the cell body and in the periphery. Therefore, analysis of Δψm of mitochondria along the axons of primary motoneurons in comparison to the Δψm of cell body mitochondria, and an assessment of the shape of mitochondria throughout the axon and cell body, in cells containing mutant and wild type Hsp27 may determine whether Hsp27 mutations alter mitofunction. In addition, a study of mitophagy in wild type and mutant Hsp27 motoneurons would clarify the role of Hsp27 in this critical cellular process.

Mitochondria not only provide ATP for the cell, but they also regulate apoptosis, produce reactive oxygen species (ROS) and buffer intracellular calcium. Hsp27 aides in the regulation of ROS by the maintenance of reduced glutathione, therefore, currently in the Greensmith laboratory; Dr Bernadett Kalmar is continuing mitochondrial functional investigations by examining the effects of Hsp27 mutations on intracellular levels of ROS.

While mitochondria are essential to cell homeostasis and disturbances in mitochondrial membrane potential can be an early indication of neuronal dysfunction, the heat shock response (HSR) is fundamental to the maintenance and restoration of protein homeostasis following cellular stress. As Hsp27 has significant roles in the HSR and its modulation, it was important to examine whether the addition of Hsp27 mutations altered aspects of the HSR. One of the most important roles Hsp27 has within the cell is that of a protein holdase, stabilising misfolded proteins and preventing protein aggregation until Hsp70 actively refolds the protein

or until the misfolded protein is sent for degradation at the proteosome. A recent paper by Almeida-Souza *et al.* (2010) suggests that the Ser135Phe mutation leads to an increase in the chaperoning function of Hsp27, possibly affecting the role of the protein as a holdase, rather than a co-chaperone, increasing the stabilisation of microtubules by stronger binding of mutant Hsp27 to tubulin (Almeida-Souza *et al*., 2010; Almeida-Souza *et al*., 2011). However, this finding was not examined contextually as Hsp27 works as a small component of a complex cascade of heat shock proteins, and the authors' did not examine whether the addition of the Ser135Phe Hsp27 mutation affected the HSR as a whole.

To examine the effects of Hsp27 mutations on the HSR, the expression of Hsp70, an integral member of the HSR was measured by quantitative immunofluoresence in primary motoneurons expressing mutant and wild type Hsp27, in non-stressed cells following heat shock. Firstly, I found that in unstressed conditions, the addition of mutant Hsp27 did not alter the expression of Hsp70, suggesting that the HSR was not activated above normal levels in primary motoneurons in culture. However, when the cells were stressed, motoneurons transfected with mutant Hsp27 did not display as high an increase in Hsp70 expression as untransfected, empty vector and wild type transfected primary motoneurons, suggesting a decreased activation of the HSR.

Virally transfected primary motoneurons may be considered to be in a state of mild stress when in cell culture, irrespective of expression of the wild type or mutant Hsp27. It is therefore surprising that there appeared to be a reduced HSR in mutant Hsp27 expressing motoneurons; since it has previously been shown that exposure to a prior stress augments the HSR caused by a second cell stressor (Slepian *et al*., 1996). Therefore, these results suggest that mutations in Hsp27 may alter the ability

of motoneurons to respond to stress. However, the results shown here are not a full investigation of the HSR in cells expressing mutant Hsp27, and caution is also required when interpreting quantification of immunofluorescence. To examine this result further the first thing to do would be to reaffirm the Hsp70 findings with western blots of Hsp70, 90 and HSF1. The next question may be to examine the activation of the HSR and to try to determine at what point mutant Hsp27 may be depressing the response. This could be done by co-IP of HSF1 to determine any changes in levels of inactive/active HSF1 in complex, or by cytoplasmic and nuclear fractionation of cells to assess changes in HSF1 translocation, a key step in the activation of the HSR. The effects of Hsp27 mutants on the HSR is important in motoneurons which have been shown to have a higher threshold for the activation of the HSR, therefore if the presence of these mutations has a dampening effect on the cell's response to stress, motoneurons would be particularly vulnerable to these changes (Batulan *et al*., 2003).

Axonal transport is a fundamentally important process to all cells and motoneurons in particular, are heavily reliant on the correct functioning of axonal transport, as there are significant distances between sites of organelle and protein biosynthesis, function, recycling and degradation. As such, axonal transport of mitochondria, lysosomes and the p75 receptor in primary motoneurons transfected with wild type and three different mutations of Hsp27; Pro39Leu, Ser135Phe and Arg140Gly is now being examined in the Greensmith laboratory. The recent paper by d'Ydewalle *et al.,* (2011) examining transgenic mice neuronally expressing either Ser135Phe or Pro182Leu human *HSPB1* found a reduction in moving mitochondria in dorsal root ganglion (DRG) cells from symptomatic Ser135Phe mice. However, pre-symptomatic Ser135Phe and symptomatic Pro182Leu Hsp27 DRG cells showed no differences in the total number of moving mitochondria in comparison to cells

expressing wild type Hsp27 (d' Ydewalle *et al*., 2011), suggesting that the reduction in moving mitochondria may be a symptom rather than a cause of underlying pathology. d'Ydewalle *et al.,* (2011) also show, as discussed above, that neurites of peripheral nerves in all symptomatic mice contained a reduction in the abundance of acetylated α-tubulin, a major component of microtubules, the rails upon which long-distance axonal transport occurs (d' Ydewalle *et al*., 2011). As discussed above, Almeida-Souza *et al*., (2011) also suggested that mutations in Hsp27 may increase the protein role as a holdase, increasing the stabilisation of microtubules by stronger binding of mutant Hsp27 to tubulin, therefore affecting the dynamic instability of the microtubule 'rails' of axonal transport. In my earlier studies looking at cell toxicity and cellular vulnerability to certain cell stressors, I demonstrated that one Hsp27 mutation, Ser135Phe, caused an increase in vulnerability of SH-SY5Y cells to cytoskeletal stressors Cytochalasin D, acting to stabilise actin filaments and Colchicine, which works by stabilising microtubules. This increased cell vulnerability to these stressors could be due to mutant Hsp27 having already negatively stabilised microtubules, thereby making the SH-SY5Y cells less able to cope with the stabilising mechanisms of the cytoskeletal stressors and more susceptible to cytotoxicity.

6.4. Limitations of *in vitro* models

Using two different cellular models to examine the effect of mutations in Hsp27, I have demonstrated fundamental differences of mutations relating to their position in the *HSBP1* gene, and have started to elucidate the functional effects of these mutations that may explain why motoneurons in particular are susceptible to mutations in a ubiquitous protein. However, *in vitro* modelling has limitations that need to be taken into account when applying the findings to a wider hypothesis.

The cell model used in the experiments described in Chapters 3 and 4 has revealed robust differences between nearly all the Hsp27 mutations with all outcome measures examined. However, there are several limitations to this model that limit its applicability and capability to measure sensitive functional changes that may be caused by Hsp27 mutations. The model involves the use of a human neuroblastoma cell line, SH-SY5Y, which does not fully represent a neuronal population and in particular is not representative of motoneurons. Cell lines are limited as a model for cells as they are genetically altered to produce immortal cell lines, thereby changing the expression patterns of some proteins over the lifetime of the cell, they are more robust and they certainly show reduced vulnerability to cells stress. Some cell lines, including SH-SY5Y cells, also have a high mutation rate meaning that over time and with every passage, cells can lose neuronal characteristics and alter the findings of experiments. Therefore, in these studies, cells were only used for 10 passage rounds to minimise genetic changeability.

As well as the inherent problems with using cell lines as *in vitro* model systems, there is also the method of transfection to take into account. In this model, cells were transiently transfected, meaning that all experiments had to be carried out within 72 hours of transfection to ensure optimum transfection. However SH-SY5Y cells take 7 days to reach full differentiation. SH-SY5Y cells were transfected with plasmids using Lipofectamine 2000, a cationic transfection agent that disrupts the cellular membrane and causes cellular stress. Lipofectamine 2000 transfection of cells results in the unregulated over expression of the transfected plasmid containing a foreign protein. While the transfection of wild type Hsp27 was used throughout these experiments as a control for the toxic effects of the Lipofectamine 2000 transfection process, it only partially controlled for the over expression of the mutant proteins as it cannot account for the cellular stresses caused by over

expression of a foreign protein and it's affects on the potential actions of the mutations. Due to the limitations of this model, it was deemed not appropriate for use in experiments that aimed to examine more functional aspects of cellular functions, which are critically dependent on cellular integrity.

The second *in vitro* cell model used in these experiments involved infection of primary embryonic mixed ventral horn cultures using 3rd generation viruses containing either wild type Hsp27, or one of three Hsp27 mutations; Pro39Leu, Ser135Phe and Arg140Gly. This is a more appropriate cell model in which to examine the functional effects of Hsp27 mutations *in vitro* for several reasons. Primary embryonic motoneurons within mixed ventral horn cultures are more representative of mouse motoneurons. These cultures consist of approximately 45% primary motoneurons, and also contain a number of glial cells, interneurons and fibroblasts. Due to the sensitivity of primary motoneurons in culture, viral transfection results in the least disruption to cell viability and important processes such as axonal transport. The level of viral transduction also has to be relatively low (~10%) to try to ensure minimum effects of viral over-expression.

However, using mixed primary motoneuron cultures does have drawbacks For example, it is a mixed culture, which, although it gives a closer representation of the cellular support networks of *in vivo*, the mixed cell population makes some experimental techniques difficult to interpret, as cell specificity is difficult to determine. A significant drawback of this cellular model is that it is an *in vitro* cell model of embryonic motoneurons which have a different genetic expression profile than mature motoneurons. This is particularly important in the study of CMT, a slowly degenerative disease with an age of onset typically in the second decade of life and a normal lifespan. Another drawback of using primary motoneurons is their

high sensitivity to the surrounding environment, including the number of supporting cells in culture (too few gives to little support for motoneuron growth, too many decreases the available nutrition and overgrows the culture), movement, transfection, pH, and temperature. This means that certain techniques, for example biochemical cytotoxicity, cannot be carried out, as the experimental techniques are too harsh for the motoneurons to survive.

6.5. Concluding remarks

In this Thesis, I have characterised the effects of mutations located in different positions along the different domains of the *HSBP1* gene. I have shown that mutations in the N-terminus of Hsp27 may cause a disruption to the nuclear functions of Hsp27, where the role of Hsp27 is likely to be that of a holdase for mis-folded proteins targeted for protein degradation. However, to fully elucidate the role of Hsp27 in the nucleus and the importance of the N-terminus of the protein in that role, the composition of SC35-positive speckles and Pro39Leu Hsp27 aggregates should be investigated further. Therefore, the Pro39Leu Hsp27 mutation could be a helpful tool in revealing the role of Hsp27 and other small heat shock proteins in the nucleus.

My results have shown that mutations in the α-crystallin domain of the protein have a multitude of effects: increasing cellular vulnerability to cytoskeletal stressors, decreasing neurite outgrowth and increasing co-localisation of mutant Hsp27 with cytoskeletal proteins. I have also shown that mutations in the α-crystallin domain of Hsp27 may have an effect on the HSR in unstressed conditions. This is particularly important for motoneurons, which already have an impaired response to cellular stress. While mutations in Hsp27 have been shown to have effects on the nucleus and cytoskeleton of neurons, they have not as yet, been shown to have any effect

on the function of mitochondria in the cell body. However, d'Ydewalle *et al*., (2011) showed a disruption of mitochondrial transport along DRG axons, which may have an effect on the functioning of mitochondria in the distal axon terminals of the cell.

Since the first identification of mutations in Hsp27 that cause CMT 2F and dHMN II much work has been undertaken to elucidate why mutations in such an important and ubiquitous protein cause such a specific disease phenotype. These studies have nearly all led to the similar conclusion that mutations in Hsp27 disrupt axonal transport, most likely by having an, as yet, unidentified effect on cytoskeletal proteins. The work described in this Thesis supports this theory. However, the functional mechanism by which cytoskeletal dysfunction specifically affects only a sub-type of neuron remains unclear.

Hsp27 has many cellular functions, and I have demonstrated that the position of the mutation along the gene affects Hsp27 pathology. However, these differences do not necessarily correlate to disease phenotype, for example, age of disease onset and severity of sensory deficit do not correlate to the position of the Hsp27 mutation as might be expected.

In future *in vitro* experiments, it would be interesting to compare the effects of Hsp27 mutations in both primary motor and sensory neurons to try and elucidate what properties of motoneurons make them so specifically vulnerable. It will also be interesting to compare the effects of mutations on different cargoes of the transport system along the axon to try to ascertain more clearly the underlying point of dysfunction, whether it is the rails that all cargoes transverse, or whether the effects of the mutations are more detrimental to certain carriers. These findings will not only be important in the elucidation of a disease mechanism for CMT 2F and dHMN II,

but to the field of peripheral neuropathy research as a whole, where many disease mechanisms are poorly understood, and to the understanding of Hsp27 itself, who's properties and functions are not yet fully identified.

References

Abe A, Numakura C, Saito K, Koide H, Oka N, Honma A, Kishikawa Y, Hayasaka K (2009) Neurofilament light chain polypeptide gene mutations in Charcot-Marie-Tooth disease: nonsense mutation probably causes a recessive phenotype. J Hum Genet 54:94-97.

Abisambra JF, Blair LJ, Hill SE, Jones JR, Kraft C, Rogers J, Koren J 3rd, Jinwal UK, Lawson L, Johnson AG, Wilcock D, O'Leary JC, Jansen-West K, Muschol M, Golde TE, Weeber EJ, Banko J, Dickey CA (2010) Phosphorylation dynamics regulate Hsp27-mediated rescue of neuronal plasticity deficits in tau transgenic mice. J Neurosci 30:15374-15382.

Abravaya K, Myers MP, Murphy SP, Morimoto RI (1992) The human heat shock protein hsp70 interacts with HSF, the transcription factor that regulates heat shock gene expression. Genes Dev 6:1153-1164.

Ackerley S, James PA, Kalli A, French S, Davies KE, Talbot K (2006) A mutation in the small heat-shock protein HSPB1 leading to distal hereditary motor neuronopathy disrupts neurofilament assembly and the axonal transport of specific cellular cargoes. Hum Mol Genet 15:347-354.

Akbar MT, Lundberg AMC, Liu K, Vidyadaran S, Wells KE, Dolatshad H, Wynn S, Wells DJ, Latchman DS, de Belleroche J (2003) The Neuroprotective Effects of Heat Shock Protein 27 Overexpression in Transgenic Animals against Kainate-induced Seizures and Hippocampal Cell Death. Journal of Biological Chemistry 278:19956 - 19965.

Almeida-Souza L, Asselbergh B, d' Ydewalle C, Moonens K, Goethals S, de Winter V, Azmi A, Irobi J, Timmermans J-P, Gevaert K, Remaut H, Van Den Bosch L, Timmerman V, Janssens S (2011) Small Heat-Shock Protein HSPB1 Mutants Stabilize Microtubules in Charcot-Marie-Tooth Neuropathy. The Journal of Neuroscience: The Official Journal of the Society for Neuroscience 31:15320-15328.

Almeida-Souza L, Goethals S, de Winter V, Dierick I, Gallardo R, Van Durme J, Irobi J, Gettemans J, Rousseau F, Schymkowitz J, Timmerman V, Janssens S (2010) Increased monomerization of mutant HSPB1 leads to protein hyperactivity in Charcot-Marie-Tooth neuropathy. J Biol Chem 285:12778-12786.

Amato AA, Barohn RJ (1996) Hereditary neuropathy with liability to pressure palsies: assocation with central nervous system demyelination. Muscle Nerve 19:770-773.

Antonellis A, Ellsworth RE, Sambuughin N, Puls I, Abel A, Lee-Lin S-Q, Jordanova A, Kremensky I, Christodoulou K, Middleton LT, Sivakumar K, Ionasescu V, Funalot B, Vance JM, Goldfarb LG, Fischbeck KH, Green ED (2003) Glycyl tRNA synthetase mutations in Charcot-Marie-Tooth disease type 2D and distal spinal muscular atrophy type V. Am J Hum Genet 72:1293-1299.

Arrigo A-P (2007) The cellular 'networking' of mammalian Hsp27 and its functions in the control of protein folding, redox state and apoptosis. Adv Exp Med Biol 594:14-26.

Arrigo A-P, Virot S, Chaufour S, Firdaus W, Kretz-Remy C, Diaz-Latoud C (2005) Hsp27 consolidates intracellular redox homeostasis by upholding glutathione in its reduced form and by decreasing iron intracellular levels. Antioxid Redox Signal 7:414-422.

Arya R, Mallik M, Lakhotia SC (2007) Heat shock genes - integrating cell survival and death. J Biosci 32:595-610.

Banchs I, Casasnovas C, Montero J, Volpini V, Martínez-Matos JA (2010) Charcot-Marie-Tooth disease with intermediate conduction velocities caused by a novel mutation in the MPZ gene. Muscle Nerve 42:184-188.

Barisic N, Claeys KG, Sirotković-Skerlev M, Löfgren A, Nelis E, De Jonghe P, Timmerman V (2008) Charcot-Marie-Tooth disease: a clinico-genetic confrontation. Ann Hum Genet 72:416-441.

Batulan Z, Shinder GA, Minotti S, He BP, Doroudchi MM, Nalbantoglu J, Strong MJ, Durham HD (2003) High threshold for induction of the stress response in motor neurons is associated with failure to activate HSF1. J Neurosci 23:5789-5798.

Bear MF, Connors BW, Paradiso MA (2007) Neuroscience: exploring the brain. Lippincott Williams & Wilkins.

Beardwell A (1967) The spatial organization of motor units and the origin of different types of potential. Ann Phys Med 9:139-157.

Bejaoui K, Wu C, Scheffler MD, Haan G, Ashby P, Wu L, de Jong P, Brown RH Jr (2001) SPTLC1 is mutated in hereditary sensory neuropathy, type 1. Nat Genet 27:261-262.

Bellyei S, Szigeti A, Pozsgai E, Boronkai A, Gomori E, Hocsak E, Farkas R, Sumegi B, Gallyas F Jr (2007) Preventing apoptotic cell death by a novel small heat shock protein. Eur J Cell Biol 86:161-171.

Benarroch EE (2010) Glycogen metabolism: metabolic coupling between astrocytes and neurons. Neurology 74:919-923.

Benedetti S *et al*. (2010a) Analyzing histopathological features of rare charcot-marie-tooth neuropathies to unravel their pathogenesis. Arch Neurol 67:1498-1505.

Benedetti S *et al*. (2010b) Analyzing histopathological features of rare charcot-marie-tooth neuropathies to unravel their pathogenesis. Arch Neurol 67:1498-1505.

Benn SC, Perrelet D, Kato AC, Scholz J, Decosterd I, Mannion RJ, Bakowska JC, Woolf CJ (2002) Hsp27 upregulation and phosphorylation is required for injured sensory and motor neuron survival. Neuron 36:45-56.

Bennardini F, Wrzosek A, Chiesi M (1992) Alpha B-crystallin in cardiac tissue. Association with actin and desmin filaments. Circ Res 71:288-294.

Benndorf R, Hayess K, Ryazantsev S, Wieske M, Behlke J, Lutsch G (1994) Phosphorylation and supramolecular organization of murine small heat shock protein HSP25 abolish its actin polymerization-inhibiting activity. J Biol Chem 269:20780-20784.

Benndorf R, Sun X, Gilmont RR, Biederman KJ, Molloy MP, Goodmurphy CW, Cheng H, Andrews PC, Welsh MJ (2001a) HSP22, a new member of the small heat shock protein superfamily, interacts with mimic of phosphorylated HSP27 ((3D)HSP27). J Biol Chem 276:26753-26761.

Benndorf R, Sun X, Gilmont RR, Biederman KJ, Molloy MP, Goodmurphy CW, Cheng H, Andrews PC, Welsh MJ (2001b) HSP22, a new member of the small heat shock protein superfamily, interacts with mimic of phosphorylated HSP27 ((3D)HSP27). J Biol Chem 276:26753-26761.

Berciano J, Combarros O, Figols J, Calleja J, Cabello A, Silos I, Coria F (1986) Hereditary motor and sensory neuropathy type II. Clinicopathological study of a family. Brain 109 (Pt 5):897-914.

Berger P, Niemann A, Suter U (2006) Schwann cells and the pathogenesis of inherited motor and sensory neuropathies (Charcot-Marie-Tooth disease). Glia 54:243-257.

Bergmann F, Keller BU (2004) Impact of mitochondrial inhibition on excitability and cytosolic Ca2+ levels in brainstem motoneurones from mouse. J Physiol (Lond) 555:45-59.

Bernard R, De Sandre-Giovannoli A, Delague V, Lévy N (2006) Molecular genetics of autosomal-recessive axonal Charcot-Marie-Tooth neuropathies. Neuromolecular Med 8:87-106.

Berry V, Francis P, Reddy MA, Collyer D, Vithana E, MacKay I, Dawson G, Carey AH, Moore A, Bhattacharya SS, Quinlan RA (2001) Alpha-B crystallin gene (CRYAB) mutation causes dominant congenital posterior polar cataract in humans. Am J Hum Genet 69:1141-1145.

Biedler JL, Helson L, Spengler BA (1973) Morphology and growth, tumorigenicity, and cytogenetics of human neuroblastoma cells in continuous culture. Cancer Res 33:2643-2652.

Bilsland LG, Nirmalananthan N, Yip J, Greensmith L, Duchen MR (2008) Expression of mutant SOD1 in astrocytes induces functional deficits in motoneuron mitochondria. J Neurochem 107:1271-1283.

Bilsland LG, Sahai E, Kelly G, Golding M, Greensmith L, Schiavo G (2010) Deficits in axonal transport precede ALS symptoms in vivo. Proc Natl Acad Sci USA 107:20523-20528.

Birouk N, Gouider R, Le Guern E, Gugenheim M, Tardieu S, Maisonobe T, Le Forestier N, Agid Y, Brice A, Bouche P (1997) Charcot-Marie-Tooth disease type 1A with 17p11.2 duplication. Clinical and electrophysiological phenotype study and factors influencing disease severity in 119 cases. Brain 120 (Pt 5):813-823.

Björk P, Jin S, Zhao J, Singh OP, Persson J-O, Hellman U, Wieslander L (2009) Specific combinations of SR proteins associate with single pre-messenger RNAs in vivo and contribute different functions. J Cell Biol 184:555-568.

Blumen S, Israeli D, Robin V, Astord S, Barkats M, Vignaud L, Porte F, Achiron A, Carasso R, Gurevich M, Braverman I, Blumen N, Viollet L (2008) DNAJB2, a co-

chaperone involved in the ubiquitin proteasome pathway is mutated in a rare distal hereditary motor neuropathy with autosomal recessive inheritance.

Del Bo R, Locatelli F, Corti S, Scarlato M, Ghezzi S, Prelle A, Fagiolari G, Moggio M, Carpo M, Bresolin N, Comi GP (2006) Coexistence of CMT-2D and distal SMA-V phenotypes in an Italian family with a GARS gene mutation. Neurology 66:752-754.

Bolino A, Muglia M, Conforti FL, LeGuern E, Salih MA, Georgiou DM, Christodoulou K, Hausmanowa-Petrusewicz I, Mandich P, Schenone A, Gambardella A, Bono F, Quattrone A, Devoto M, Monaco AP (2000) Charcot-Marie-Tooth type 4B is caused by mutations in the gene encoding myotubularin-related protein-2. Nat Genet 25:17-19.

Borg K, Ericson-Gripenstedt U (2002) Muscle biopsy abnormalities differ between Charcot-Marie-Tooth type 1 and 2: reflect different pathophysiology? Exerc Sport Sci Rev 30:4-7.

Bouhouche A, Benomar A, Bouslam N, Chkili T, Yahyaoui M (2006) Mutation in the epsilon subunit of the cytosolic chaperonin-containing t-complex peptide-1 (Cct5) gene causes autosomal recessive mutilating sensory neuropathy with spastic paraplegia. J Med Genet 43:441-443.

Bova MP, McHaourab HS, Han Y, Fung BK (2000) Subunit exchange of small heat shock proteins. Analysis of oligomer formation of alphaA-crystallin and Hsp27 by fluorescence resonance energy transfer and site-directed truncations. J Biol Chem 275:1035-1042.

Brophy CM, Lamb S, Graham A (1999) The small heat shock-related protein-20 is an actin-associated protein. J Vasc Surg 29:326-333.

de Brouwer APM, van Bokhoven H, Nabuurs SB, Arts WF, Christodoulou J, Duley J (2010) PRPS1 mutations: four distinct syndromes and potential treatment. Am J Hum Genet 86:506-518.

de Brouwer APM, Williams KL, Duley JA, van Kuilenburg ABP, Nabuurs SB, Egmont-Petersen M, Lugtenberg D, Zoetekouw L, Banning MJG, Roeffen M, Hamel BCJ, Weaving L, Ouvrier RA, Donald JA, Wevers RA, Christodoulou J, van Bokhoven H (2007) Arts syndrome is caused by loss-of-function mutations in PRPS1. Am J Hum Genet 81:507-518.

Brown DD, Christine KS, Showell C, Conlon FL (2007) Small heat shock protein Hsp27 is required for proper heart tube formation. Genesis 45:667-678.

Bruey JM, Ducasse C, Bonniaud P, Ravagnan L, Susin SA, Diaz-Latoud C, Gurbuxani S, Arrigo AP, Kroemer G, Solary E, Garrido C (2000a) Hsp27 negatively regulates cell death by interacting with cytochrome c. Nat Cell Biol 2:645-652.

Bruey JM, Paul C, Fromentin A, Hilpert S, Arrigo AP, Solary E, Garrido C (2000b) Differential regulation of HSP27 oligomerization in tumor cells grown in vitro and in vivo. Oncogene 19:4855-4863.

Brunet Simioni M, De Thonel A, Hammann A, Joly AL, Bossis G, Fourmaux E, Bouchot A, Landry J, Piechaczyk M, Garrido C (2009) Heat shock protein 27 is involved in SUMO-2/3 modification of heat shock factor 1 and thereby modulates the transcription factor activity. Oncogene 28:3332-3344.

Bryantsev AL, Chechenova MB, Shelden EA (2007a) Recruitment of phosphorylated small heat shock protein Hsp27 to nuclear speckles without stress. Exp Cell Res 313:195-209.

Bryantsev AL, Kurchashova SY, Golyshev SA, Polyakov VY, Wunderink HF, Kanon B, Budagova KR, Kabakov AE, Kampinga HH (2007b) Regulation of stress-induced intracellular sorting and chaperone function of Hsp27 (HspB1) in mammalian cells. Biochem J 407:407-417.

Bryantsev AL, Loktionova SA, Ilyinskaya OP, Tararak EM, Kampinga HH, Kabakov AE (2002) Distribution, phosphorylation, and activities of Hsp25 in heat-stressed H9c2 myoblasts: a functional link to cytoprotection. Cell Stress Chaperones 7:146-155.

Bukach OV, Glukhova AE, Seit-Nebi AS, Gusev NB (2009) Heterooligomeric complexes formed by human small heat shock proteins HspB1 (Hsp27) and HspB6 (Hsp20). Biochim Biophys Acta 1794:486-495.

Bähr M, Andres F, Timmerman V, Nelis ME, Van Broeckhoven C, Dichgans J (1999) Central visual, acoustic, and motor pathway involvement in a Charcot-Marie-Tooth family with an Asn205Ser mutation in the connexin 32 gene. J Neurol Neurosurg Psychiatr 66:202-206.

Camu W, Henderson CE (1994) Rapid purification of embryonic rat motoneurons: an in vitro model for studying MND/ALS pathogenesis. J Neurol Sci 124 Suppl:73-74.

Capponi S, Geroldi A, Fossa P, Grandis M, Ciotti P, Gulli R, Schenone A, Mandich P, Bellone E (2011) HSPB1 and HSPB8 in inherited neuropathies: study of an Italian cohort of dHMN and CMT2 patients. J Peripher Nerv Syst 16:287-294.

Carper SW, Rocheleau TA, Storm FK (1990) cDNA sequence of a human heat shock protein HSP27. Nucleic Acids Res 18:6457.

Carriedo SG, Yin HZ, Weiss JH (1996) Motor Neurons Are Selectively Vulnerable to AMPA/Kainate Receptor-Mediated Injury In Vitro. The Journal of Neuroscience 16:4069 -4079.

Cassereau J, Chevrollier A, Gueguen N, Malinge M-C, Letournel F, Nicolas G, Richard L, Ferre M, Verny C, Dubas F, Procaccio V, Amati-Bonneau P, Bonneau D, Reynier P (2009) Mitochondrial complex I deficiency in GDAP1-related autosomal dominant Charcot-Marie-Tooth disease (CMT2K). Neurogenetics 10:145-150.

Chan CS, Gertler TS, Surmeier DJ (2009) Calcium homeostasis, selective vulnerability and Parkinson's disease. Trends Neurosci 32:249-256.

Chance B (1965) Reaction of oxygen with the respiratory chain in cells and tissues. J Gen Physiol 49:Suppl:163-195.

Chance PF, Alderson MK, Leppig KA, Lensch MW, Matsunami N, Smith B, Swanson PD, Odelberg SJ, Disteche CM, Bird TD (1993) DNA deletion associated with hereditary neuropathy with liability to pressure palsies. Cell 72:143-151.

Charcot J-M, Marie P (1886) Sur une forme particulaiere d'atrophie musculaire progressive souvent familiale debutant par les pied et les jambes et atteignant plus tard les mains. Rev Med 6:97-138.

Charette SJ, Lavoie JN, Lambert H, Landry J (2000) Inhibition of Daxx-mediated apoptosis by heat shock protein 27. Mol Cell Biol 20:7602-7612.

Chen H (2005) Emerging functions of mammalian mitochondrial fusion and fission. Human Molecular Genetics 14:R283-R289.

Chen H, Chan DC (2006) Critical dependence of neurons on mitochondrial dynamics. Current Opinion in Cell Biology 18:453-459.

Chen H, Chan DC (2009) Mitochondrial dynamics--fusion, fission, movement, and mitophagy--in neurodegenerative diseases. Hum Mol Genet 18:R169-176.

Chen H, Detmer SA, Ewald AJ, Griffin EE, Fraser SE, Chan DC (2003) Mitofusins Mfn1 and Mfn2 coordinately regulate mitochondrial fusion and are essential for embryonic development. J Cell Biol 160:189-200.

Chevalier-Larsen E, Holzbaur ELF (2006) Axonal transport and neurodegenerative disease. Biochim Biophys Acta 1762:1094-1108.

Chinnery PF (2000) Mitochondrial Disorders Overview. Available at: http://www.ncbi.nlm.nih.gov/books/NBK1224/ [Accessed August 11, 2011].

Chiò A, Calvo A, Moglia C, Restagno G, Ossola I, Brunetti M, Montuschi A, Cistaro A, Ticca A, Traynor BJ, Schymick JC, Mutani R, Marrosu MG, Murru MR, Borghero G (2010) Amyotrophic lateral sclerosis-frontotemporal lobar dementia in 3 families with p.Ala382Thr TARDBP mutations. Arch Neurol 67:1002-1009.

Choo QL, Bray D (1978) Two forms of neuronal actin. J Neurochem 31:217-224.

Chow CY, Zhang Y, Dowling JJ, Jin N, Adamska M, Shiga K, Szigeti K, Shy ME, Li J, Zhang X, Lupski JR, Weisman LS, Meisler MH (2007) Mutation of FIG4 causes neurodegeneration in the pale tremor mouse and patients with CMT4J. Nature 448:68-72.

Christensen JH, Nielsen MN, Hansen J, Füchtbauer A, Füchtbauer E-M, West M, Corydon TJ, Gregersen N, Bross P (2010) Inactivation of the hereditary spastic paraplegia-associated Hspd1 gene encoding the Hsp60 chaperone results in early embryonic lethality in mice. Cell Stress Chaperones 15:851-863.

Chrétien P, Landry J (1988) Enhanced constitutive expression of the 27-kDa heat shock proteins in heat-resistant variants from Chinese hamster cells. J Cell Physiol 137:157-166.

Chung KW, Kim S-B, Cho SY, Hwang SJ, Park SW, Kang SH, Kim J, Yoo JH, Choi B-O (2008) Distal hereditary motor neuropathy in Korean patients with a small heat shock protein 27 mutation. Exp Mol Med 40:304-312.

Cingolani LA, Goda Y (2008) Actin in action: the interplay between the actin cytoskeleton and synaptic efficacy. Nat Rev Neurosci 9:344-356.

Cintron NS, Toft D (2006) Defining the Requirements for Hsp40 and Hsp70 in the Hsp90 Chaperone Pathway. Journal of Biological Chemistry 281:26235 -26244.

Conde C, Cáceres A (2009) Microtubule assembly, organization and dynamics in axons and dendrites. Nat Rev Neurosci 10:319-332.

Conforti FL, Muglia M, Mazzei R, Patitucci A, Valentino P, Magariello A, Sprovieri T, Bono F, Bergmann C, Gabriele AL, Peluso G, Nisticò R, Senderek J, Quattrone A (2004) A new SBF2 mutation in a family with recessive demyelinating Charcot-Marie-Tooth (CMT4B2). Neurology 63:1327-1328.

Cozzolino M, Carri MT (2011) Mitochondrial dysfunction in ALS. Progress in Neurobiology Available at: http://www.sciencedirect.com/science/article/pii/S0301008211000918 [Accessed September 22, 2011].

Cuesta A, Pedrola L, Sevilla T, García-Planells J, Chumillas MJ, Mayordomo F, LeGuern E, Marín I, Vílchez JJ, Palau F (2002) The gene encoding ganglioside-induced differentiation-associated protein 1 is mutated in axonal Charcot-Marie-Tooth type 4A disease. Nat Genet 30:22-25.

Cuthbert JA, Shay JW (1983) Microtubules and lymphocyte responses: effect of colchicine and taxol on mitogen-induced human lymphocyte activation and proliferation. J Cell Physiol 116:127-134.

Van Damme P, Van Den Bosch L, Van Houtte E, Callewaert G, Robberecht W (2002) GluR2-dependent properties of AMPA receptors determine the selective vulnerability of motor neurons to excitotoxicity. J Neurophysiol 88:1279-1287.

Daugaard M, Rohde M, Jäättelä M (2007) The heat shock protein 70 family: Highly homologous proteins with overlapping and distinct functions. FEBS Letters 581:3702-3710.

Dawkins JL, Hulme DJ, Brahmbhatt SB, Auer-Grumbach M, Nicholson GA (2001) Mutations in SPTLC1, encoding serine palmitoyltransferase, long chain base subunit-1, cause hereditary sensory neuropathy type I. Nat Genet 27:309-312.

Dierick I, Irobi J, De Jonghe P, Timmerman V (2005) Small heat shock proteins in inherited peripheral neuropathies. Ann Med 37:413-422.

Dorion S, Lambert H, Landry J (2002) Activation of the p38 signaling pathway by heat shock involves the dissociation of glutathione S-transferase Mu from Ask1. J Biol Chem 277:30792-30797.

Dorion S, Landry J (2002) Activation of the mitogen-activated protein kinase pathways by heat shock. Cell Stress Chaperones 7:200-206.

Dormann D, Capell A, Carlson AM, Shankaran SS, Rodde R, Neumann M, Kremmer E, Matsuwaki T, Yamanouchi K, Nishihara M, Haass C (2009) Proteolytic processing of TAR DNA binding protein-43 by caspases produces C-terminal fragments with disease defining properties independent of progranulin. J Neurochem 110:1082-1094.

Döppler H, Storz P, Li J, Comb MJ, Toker A (2005) A phosphorylation state-specific antibody recognizes Hsp27, a novel substrate of protein kinase D. J Biol Chem 280:15013-15019.

Edwards HV, Cameron RT, Baillie GS (n.d.) The emerging role of HSP20 as a multifunctional protective agent. Cellular Signalling In Press, Corrected Proof Available at: http://www.sciencedirect.com/science/article/pii/S089865681100146X [Accessed June 5, 2011].

Einarsdottir E, Carlsson A, Minde J, Toolanen G, Svensson O, Solders G, Holmgren G, Holmberg D, Holmberg M (2004) A mutation in the nerve growth factor beta gene (NGFB) causes loss of pain perception. Hum Mol Genet 13:799-805.

Ericson U, Ansved T, Borg K (1998) Charcot-Marie-Tooth disease--muscle biopsy findings in relation to neurophysiology. Neuromuscul Disord 8:175-181.

Evgrafov OV *et al*. (2004) Mutant small heat-shock protein 27 causes axonal Charcot-Marie-Tooth disease and distal hereditary motor neuropathy. Nat Genet 36:602-606.

Fabricius C, Berthold C-H, Rydmark M (1993) Axoplasmic organelles at nodes of Ranvier. II. Occurrence and distribution in large myelinated spinal cord axons of the adult cat. J Neurocytol 22:941-954.

Fabrizi GM, Cavallaro T, Angiari C, Bertolasi L, Cabrini I, Ferrarini M, Rizzuto N (2004) Giant axon and neurofilament accumulation in Charcot-Marie-Tooth disease type 2E. Neurology 62:1429-1431.

Fabrizi GM, Cavallaro T, Angiari C, Cabrini I, Taioli F, Malerba G, Bertolasi L, Rizzuto N (2007) Charcot-Marie-Tooth disease type 2E, a disorder of the cytoskeleton. Brain 130:394-403.

Fabrizi GM, Taioli F, Cavallaro T, Ferrari S, Bertolasi L, Casarotto M, Rizzuto N, Deconinck T, Timmerman V, De Jonghe P (2009) Further evidence that mutations in FGD4/frabin cause Charcot-Marie-Tooth disease type 4H. Neurology 72:1160-1164.

Falconer MM, Vaillant A, Reuhl KR, Laferrière N, Brown DL (1994) The molecular basis of microtubule stability in neurons. Neurotoxicology 15:109-122.

Feinstein B, Lindegard B, Nyman E, Wohlfart G (1955) Morphologic studies of motor units in normal human muscles. Acta Anat (Basel) 23:127-142.

Feldmeyer D, Kask K, Brusa R, Kornau HC, Kolhekar R, Rozov A, Burnashev N, Jensen V, Hvalby O, Sprengel R, Seeburg PH (1999) Neurological dysfunctions in mice expressing different levels of the Q/R site-unedited AMPAR subunit GluR-B. Nat Neurosci 2:57-64.

Finsterer J (2004) Mitochondriopathies. Eur J Neurol 11:163-186.

Fontaine J-M, Rest JS, Welsh MJ, Benndorf R (2003) The sperm outer dense fiber protein is the 10th member of the superfamily of mammalian small stress proteins. Cell Stress Chaperones 8:62-69.

Franklin TB, Krueger-Naug AM, Clarke DB, Arrigo A-P, Currie RW (2005a) The role of heat shock proteins Hsp70 and Hsp27 in cellular protection of the central nervous system. Int J Hyperthermia 21:379-392.

Franklin TB, Krueger-Naug AM, Clarke DB, Arrigo A-P, Currie RW (2005b) The role of heat shock proteins Hsp70 and Hsp27 in cellular protection of the central nervous system. Int J Hyperthermia 21:379-392.

Fransson S, Ruusala A, Aspenström P (2006) The atypical Rho GTPases Miro-1 and Miro-2 have essential roles in mitochondrial trafficking. Biochem Biophys Res Commun 344:500-510.

Frederick RL, Shaw JM (2007) Moving mitochondria: establishing distribution of an essential organelle. Traffic 8:1668-1675.

Freeman BC, Yamamoto KR (2002) Disassembly of transcriptional regulatory complexes by molecular chaperones. Science 296:2232-2235.

Friede RL, Samorajski T (1970) Axon caliber related to neurofilaments and microtubules in sciatic nerve fibers of rats and mice. The Anatomical Record 167:379-387.

Friedman MJ, Li S, Li X-J (2009) Activation of gene transcription by heat shock protein 27 may contribute to its neuronal protection. J Biol Chem 284:27944-27951.

Gabreëls-Festen AA, Joosten EM, Gabreëls FJ, Jennekens FG, Janssen-van Kempen TW (1992) Early morphological features in dominantly inherited demyelinating motor and sensory neuropathy (HMSN type I). J Neurol Sci 107:145-154.

Gandhi S, Wood-Kaczmar A, Yao Z, Plun-Favreau H, Deas E, Klupsch K, Downward J, Latchman DS, Tabrizi SJ, Wood NW, Duchen MR, Abramov AY (2009) PINK1-associated Parkinson's disease is caused by neuronal vulnerability to calcium-induced cell death. Mol Cell 33:627-638.

Ganea E (2001) Chaperone-like activity of alpha-crystallin and other small heat shock proteins. Curr Protein Pept Sci 2:205-225.

Garcia CA, Malamut RE, England JD, Parry GS, Liu P, Lupski JR (1995) Clinical variability in two pairs of identical twins with the Charcot-Marie-Tooth disease type 1A duplication. Neurology 45:2090-2093.

Garrido C, Bruey JM, Fromentin A, Hammann A, Arrigo AP, Solary E (1999) HSP27 inhibits cytochrome c-dependent activation of procaspase-9. FASEB J 13:2061-2070.

Gemignani F, Marbini A (2001) Charcot-Marie-Tooth disease (CMT): distinctive phenotypic and genotypic features in CMT type 2. J Neurol Sci 184:1-9.

Geraldo S, Gordon-Weeks PR (2009) Cytoskeletal dynamics in growth-cone steering. J Cell Sci 122:3595-3604.

Glater EE, Megeath LJ, Stowers RS, Schwarz TL (2006) Axonal transport of mitochondria requires milton to recruit kinesin heavy chain and is light chain independent. J Cell Biol 173:545-557.

Goddette DW, Frieden C (1986) Actin polymerization. The mechanism of action of cytochalasin D. J Biol Chem 261:15974-15980.

Gotow T (2000) Neurofilaments in health and disease. Medical Electron Microscopy 33:173-199.

Gotow T, Takeda M, Tanaka T, Hashimoto PH (1992) Macromolecular structure of reassembled neurofilaments as revealed by the quick-freeze deep-etch mica method: difference between NF-M and NF-H subunits in their ability to form cross-bridges. Eur J Cell Biol 58:331-345.

Graveley BR (2000) Sorting out the complexity of SR protein functions. RNA 6:1197-1211.

Graw J (2009) Genetics of crystallins: cataract and beyond. Exp Eye Res 88:173-189.

Grohmann K, Schuelke M, Diers A, Hoffmann K, Lucke B, Adams C, Bertini E, Leonhardt-Horti H, Muntoni F, Ouvrier R, Pfeufer A, Rossi R, Van Maldergem L, Wilmshurst JM, Wienker TF, Sendtner M, Rudnik-Schöneborn S, Zerres K, Hübner C (2001) Mutations in the gene encoding immunoglobulin mu-binding protein 2 cause spinal muscular atrophy with respiratory distress type 1. Nat Genet 29:75-77.

Grundtman C, Kreutmayer SB, Almanzar G, Wick MC, Wick G (2011) Heat shock protein 60 and immune inflammatory responses in atherosclerosis. Arterioscler Thromb Vasc Biol 31:960-968.

Gunawardena S, Goldstein LSB (2004) Cargo-carrying motor vehicles on the neuronal highway: transport pathways and neurodegenerative disease. J Neurobiol 58:258-271.

Hall LL, Smith KP, Byron M, Lawrence JB (2006) THE MOLECULAR ANATOMY OF A SPECKLE. Anat Rec A Discov Mol Cell Evol Biol 288:664-675.

Hanisch F, Müller T, Dietz A, Bitoun M, Kress W, Weis J, Stoltenburg G, Zierz S (2011) Phenotype variability and histopathological findings in centronuclear myopathy due to DNM2 mutations. J Neurol 258:1085-1090.

Harding AE, Thomas PK (1980) The clinical features of hereditary motor and sensory neuropathy types I and II. Brain 103:259-280.

Hattori K, Naguro I, Runchel C, Ichijo H (2009) The roles of ASK family proteins in stress responses and diseases. Cell Commun Signal 7:9.

Hattori N, Yamamoto M, Yoshihara T, Koike H, Nakagawa M, Yoshikawa H, Ohnishi A, Hayasaka K, Onodera O, Baba M, Yasuda H, Saito T, Nakashima K, Kira J, Kaji R, Oka N, Sobue G (2003) Demyelinating and axonal features of Charcot-Marie-Tooth disease with mutations of myelin-related proteins (PMP22, MPZ and Cx32): a clinicopathological study of 205 Japanese patients. Brain 126:134-151.

He M, Guo H, Yang X, Zhou L, Zhang X, Cheng L, Zeng H, Hu FB, Tanguay RM, Wu T (2010) Genetic variations in HSPA8 gene associated with coronary heart disease risk in a Chinese population. PLoS ONE 5:e9684.

Helson L, Biedler JL (1973) Catecholamines in neuroblastoma cells from human bone marrow, tissue culture, and murine C-1300 tumor. Cancer 31:1087-1091.

Henneman E, Somjen G, Carpenter DO (1965) Functional significance of cell size in spinal motoneurons. J Neurophysiol 28:560-580.

Herrmann H, Aebi U (2004) Intermediate Filaments : Molecular Structure, Assembly Mechanism, and Integration Into Functionally Distinct Intracellular Scaffolds. Annual Review of Biochemistry 73:749-789.

Hickey E, Brandon SE, Potter R, Stein G, Stein J, Weber LA (1986) Sequence and organization of genes encoding the human 27 kDa heat shock protein. Nucleic Acids Res 14:4127-4145.

Hino M, Kurogi K, Okubo MA, Murata-Hori M, Hosoya H (2000) Small heat shock protein 27 (HSP27) associates with tubulin/microtubules in HeLa cells. Biochem Biophys Res Commun 271:164-169.

Hirokawa N (1998) Kinesin and Dynein Superfamily Proteins and the Mechanism of Organelle Transport. Science 279:519 -526.

Hirokawa N, Glicksman MA, Willard MB (1984) Organization of mammalian neurofilament polypeptides within the neuronal cytoskeleton. J Cell Biol 98:1523-1536.

Hirokawa N, Noda Y (2008) Intracellular transport and kinesin superfamily proteins, KIFs: structure, function, and dynamics. Physiol Rev 88:1089-1118.

Hirokawa N, Noda Y, Tanaka Y, Niwa S (2009) Kinesin superfamily motor proteins and intracellular transport. Nat Rev Mol Cell Biol 10:682-696.

Hoffman PN, Griffin JW, Price DL (1984) Control of axonal caliber by neurofilament transport. J Cell Biol 99:705-714.

Hoffman PN, Lasek RJ (1975) The slow component of axonal transport. Identification of major structural polypeptides of the axon and their generality among mammalian neurons. J Cell Biol 66:351-366.

Hollenbeck PJ, Saxton WM (2005) The axonal transport of mitochondria. J Cell Sci 118:5411-5419.

Holleran EA, Karki S, Holzbaur EL (1998) The role of the dynactin complex in intracellular motility. Int Rev Cytol 182:69-109.

Hollmann M, Hartley M, Heinemann S (1991) Ca2+ permeability of KA-AMPA--gated glutamate receptor channels depends on subunit composition. Science 252:851 -853.

Horwitz J (2003) Alpha-crystallin. Experimental Eye Research 76:145-153.

Houlden H, Laura M, Wavrant-De Vrièze F, Blake J, Wood N, Reilly MM (2008) Mutations in the HSP27 (HSPB1) gene cause dominant, recessive, and sporadic distal HMN/CMT type 2. Neurology 71:1660-1668.

Huang L, Min J-N, Masters S, Mivechi NF, Moskophidis D (2007) Insights into function and regulation of small heat shock protein 25 (HSPB1) in a mouse model with targeted gene disruption. Genesis 45:487-501.

Huang L, Mivechi NF, Moskophidis D (2001) Insights into regulation and function of the major stress-induced hsp70 molecular chaperone in vivo: analysis of mice with targeted gene disruption of the hsp70.1 or hsp70.3 gene. Mol Cell Biol 21:8575-8591.

Hunt CR, Dix DJ, Sharma GG, Pandita RK, Gupta A, Funk M, Pandita TK (2004) Genomic instability and enhanced radiosensitivity in Hsp70.1- and Hsp70.3-deficient mice. Mol Cell Biol 24:899-911.

Huot J, Lambert H, Lavoie JN, Guimond A, Houle F, Landry J (1995) Characterization of 45-kDa/54-kDa HSP27 kinase, a stress-sensitive kinase which

may activate the phosphorylation-dependent protective function of mammalian 27-kDa heat-shock protein HSP27. Eur J Biochem 227:416-427.

Hurd DD, Saxton WM (1996) Kinesin Mutations Cause Motor Neuron Disease Phenotypes by Disrupting Fast Axonal Transport in Drosophila. Genetics 144:1075 - 1085.

van den IJssel P, Wheelock R, Prescott A, Russell P, Quinlan RA (2003) Nuclear speckle localisation of the small heat shock protein alpha B-crystallin and its inhibition by the R120G cardiomyopathy-linked mutation. Exp Cell Res 287:249-261.

Ikeda Y, Abe A, Ishida C, Takahashi K, Hayasaka K, Yamada M (2009) A clinical phenotype of distal hereditary motor neuronopathy type II with a novel HSPB1 mutation. J Neurol Sci 277:9-12.

Inagaki N, Hayashi T, Arimura T, Koga Y, Takahashi M, Shibata H, Teraoka K, Chikamori T, Yamashina A, Kimura A (2006) Alpha B-crystallin mutation in dilated cardiomyopathy. Biochem Biophys Res Commun 342:379-386.

Indo Y, Tsuruta M, Hayashida Y, Karim MA, Ohta K, Kawano T, Mitsubuchi H, Tonoki H, Awaya Y, Matsuda I (1996) Mutations in the TRKA/NGF receptor gene in patients with congenital insensitivity to pain with anhidrosis. Nat Genet 13:485-488.

Ionasescu V, Searby C, Ionasescu R (1994) Point mutations of the connexin32 (GJB1) gene in X-linked dominant Charcot-Marie-Tooth neuropathy. Hum Mol Genet 3:355-358.

Iordanov MS, Magun BE (1999) Different mechanisms of c-Jun NH(2)-terminal kinase-1 (JNK1) activation by ultraviolet-B radiation and by oxidative stressors. J Biol Chem 274:25801-25806.

Iqbal K, Liu F, Gong C-X, Grundke-Iqbal I (2010) Tau in Alzheimer disease and related tauopathies. Curr Alzheimer Res 7:656-664.

Irobi J *et al*. (2004) Hot-spot residue in small heat-shock protein 22 causes distal motor neuropathy. Nat Genet 36:597-601.

Irobi J, Almeida-Souza L, Asselbergh B, De Winter V, Goethals S, Dierick I, Krishnan J, Timmermans J-P, Robberecht W, De Jonghe P, Van Den Bosch L, Janssens S, Timmerman V (2010) Mutant HSPB8 causes motor neuron-specific neurite degeneration. Hum Mol Genet 19:3254-3265.

Ismailov SM, Fedotov VP, Dadali EL, Polyakov AV, Van Broeckhoven C, Ivanov VI, De Jonghe P, Timmerman V, Evgrafov OV (2001) A new locus for autosomal dominant Charcot-Marie-Tooth disease type 2 (CMT2F) maps to chromosome 7q11-q21. Eur J Hum Genet 9:646-650.

James PA, Rankin J, Talbot K (2008) Asymmetrical late onset motor neuropathy associated with a novel mutation in the small heat shock protein HSPB1 (HSP27). J Neurol Neurosurg Psychiatr 79:461-463.

Jia Z, Agopyan N, Miu P, Xiong Z, Henderson J, Gerlai R, Taverna FA, Velumian A, MacDonald J, Carlen P, Abramow-Newerly W, Roder J (1996) Enhanced LTP in Mice Deficient in the AMPA Receptor GluR2. Neuron 17:945-956.

Jordanova A *et al*. (2006) Disrupted function and axonal distribution of mutant tyrosyl-tRNA synthetase in dominant intermediate Charcot-Marie-Tooth neuropathy. Nat Genet 38:197-202.

Jordanova A, De Jonghe P, Boerkoel CF, Takashima H, De Vriendt E, Ceuterick C, Martin J-J, Butler IJ, Mancias P, Papasozomenos SC, Terespolsky D, Potocki L, Brown CW, Shy M, Rita DA, Tournev I, Kremensky I, Lupski JR, Timmerman V (2003a) Mutations in the neurofilament light chain gene (NEFL) cause early onset severe Charcot-Marie-Tooth disease. Brain 126:590-597.

Kaal EC, Vlug AS, Versleijen MW, Kuilman M, Joosten EA, Bär PR (2000) Chronic mitochondrial inhibition induces selective motoneuron death in vitro: a new model for amyotrophic lateral sclerosis. J Neurochem 74:1158-1165.

Kalaydjieva L *et al*. (1996) Gene mapping in Gypsies identifies a novel demyelinating neuropathy on chromosome 8q24. Nat Genet 14:214-217.

Kalaydjieva L, Nikolova A, Turnev I, Petrova J, Hristova A, Ishpekova B, Petkova I, Shmarov A, Stancheva S, Middleton L, Merlini L, Trogu A, Muddle JR, King RH, Thomas PK (1998) Hereditary motor and sensory neuropathy--Lom, a novel demyelinating neuropathy associated with deafness in gypsies. Clinical, electrophysiological and nerve biopsy findings. Brain 121 (Pt 3):399-408.

Kalmar B, Burnstock G, Vrbová G, Urbanics R, Csermely P, Greensmith L (2002) Upregulation of heat shock proteins rescues motoneurones from axotomy-induced cell death in neonatal rats. Exp Neurol 176:87-97.

Kalmar B, Greensmith L (2009a) Induction of heat shock proteins for protection against oxidative stress. Adv Drug Deliv Rev 61:310-318.

Kalmar B, Greensmith L (2009b) Activation of the heat shock response in a primary cellular model of motoneuron neurodegeneration-evidence for neuroprotective and neurotoxic effects. Cell Mol Biol Lett 14:319-335.

Kamholz J, Awatramani R, Menichella D, Jiang H, Xu W, Shy M (1999) Regulation of myelin-specific gene expression. Relevance to CMT1. Ann N Y Acad Sci 883:91-108.

Kampinga HH, Craig EA (2010) The HSP70 chaperone machinery: J proteins as drivers of functional specificity. Nat Rev Mol Cell Biol 11:579-592.

Kandel ER, Schwartz JH, Jessell TM (2000) Principles of neural science. McGraw-Hill, Health Professions Division.

Kappé G, Franck E, Verschuure P, Boelens WC, Leunissen JAM, de Jong WW (2003) The human genome encodes 10 alpha-crystallin-related small heat shock proteins: HspB1-10. Cell Stress Chaperones 8:53-61.

Kappé G, Verschuure P, Philipsen RL, Staalduinen AA, Van de Boogaart P, Boelens WC, De Jong WW (2001) Characterization of two novel human small heat shock proteins: protein kinase-related HspB8 and testis-specific HspB9. Biochim Biophys Acta 1520:1-6.

Katona I, Zhang X, Bai Y, Shy ME, Guo J, Yan Q, Hatfield J, Kupsky WJ, Li J (2011) Distinct pathogenic processes between Fig4-deficient motor and sensory neurons. Eur J Neurosci 33:1401-1410.

Ke L, Meijering RAM, Hoogstra-Berends F, Mackovicova K, Vos MJ, Van Gelder IC, Henning RH, Kampinga HH, Brundel BJJM (2011) HSPB1, HSPB6, HSPB7 and HSPB8 Protect against RhoA GTPase-Induced Remodeling in Tachypaced Atrial Myocytes. PLoS ONE 6:e20395.

Keller MP, Chance PF (1999) Inherited neuropathies: from gene to disease. Brain Pathol 9:327-341.

Kieran D, Hafezparast M, Bohnert S, Dick JRT, Martin J, Schiavo G, Fisher EMC, Greensmith L (2005) A mutation in dynein rescues axonal transport defects and extends the life span of ALS mice. J Cell Biol 169:561-567.

Kijima K, Numakura C, Goto T, Takahashi T, Otagiri T, Umetsu K, Hayasaka K (2005a) Small heat shock protein 27 mutation in a Japanese patient with distal hereditary motor neuropathy. J Hum Genet 50:473-476.

Kijima K, Numakura C, Izumino H, Umetsu K, Nezu A, Shiiki T, Ogawa M, Ishizaki Y, Kitamura T, Shozawa Y, Hayasaka K (2005b) Mitochondrial GTPase mitofusin 2 mutation in Charcot-Marie-Tooth neuropathy type 2A. Hum Genet 116:23-27.

Kim S-A, Vacratsis PO, Firestein R, Cleary ML, Dixon JE (2003) Regulation of myotubularin-related (MTMR)2 phosphatidylinositol phosphatase by MTMR5, a catalytically inactive phosphatase. Proc Natl Acad Sci USA 100:4492-4497.

King SJ, Schroer TA (2000) Dynactin increases the processivity of the cytoplasmic dynein motor. Nat Cell Biol 2:20-24.

Kirbach BB, Golenhofen N (2011) Differential expression and induction of small heat shock proteins in rat brain and cultured hippocampal neurons. J Neurosci Res 89:162-175.

Kirby J, Ning K, Ferraiuolo L, Heath PR, Ismail A, Kuo S-W, Valori CF, Cox L, Sharrack B, Wharton SB, Ince PG, Shaw PJ, Azzouz M (2011) Phosphatase and tensin homologue/protein kinase B pathway linked to motor neuron survival in human superoxide dismutase 1-related amyotrophic lateral sclerosis. Brain 134:506-517.

Kleopa KA, Scherer SS (2006) Molecular genetics of X-linked Charcot-Marie-Tooth disease. Neuromolecular Med 8:107-122.

Knapinska AM, Gratacós FM, Krause CD, Hernandez K, Jensen AG, Bradley JJ, Wu X, Pestka S, Brewer G (2011) Chaperone Hsp27 modulates AUF1 proteolysis and AU-rich element-mediated mRNA degradation. Mol Cell Biol 31:1419-1431.

Kobayashi N, Mundel P (1998) A role of microtubules during the formation of cell processes in neuronal and non-neuronal cells. Cell Tissue Res 291:163-174.

Kolb SJ, Snyder PJ, Poi EJ, Renard EA, Bartlett A, Gu S, Sutton S, Arnold WD, Freimer ML, Lawson VH, Kissel JT, Prior TW (2010) Mutant small heat shock protein B3 causes motor neuropathy. Neurology 74:502 -506.

Kong X-C, Zhang D, Qian C, Liu G-T, Bao X-Q (2011) FLZ, a novel HSP27 and HSP70 inducer, protects SH-SY5Y cells from apoptosis caused by MPP(+). Brain Res 1383:99-107.

Kostenko S, Johannessen M, Moens U (2009a) PKA-induced F-actin rearrangement requires phosphorylation of Hsp27 by the MAPKAP kinase MK5. Cell Signal 21:712-718.

Kostenko S, Moens U (2009) Heat shock protein 27 phosphorylation: kinases, phosphatases, functions and pathology. Cell Mol Life Sci 66:3289-3307.

Krief S, Faivre JF, Robert P, Le Douarin B, Brument-Larignon N, Lefrère I, Bouzyk MM, Anderson KM, Greller LD, Tobin FL, Souchet M, Bril A (1999) Identification and characterization of cvHsp. A novel human small stress protein selectively expressed in cardiovascular and insulin-sensitive tissues. J Biol Chem 274:36592-36600.

Krishnan J, Vannuvel K, Andries M, Waelkens E, Robberecht W, Van Den Bosch L (2008) Over-expression of Hsp27 does not influence disease in the mutant SOD1(G93A) mouse model of amyotrophic lateral sclerosis. J Neurochem 106:2170-2183.

Kuznetsov SA, Langford GM, Weiss DG (1992) Actin-dependent organelle movement in squid axoplasm. Nature 356:722-725.

Kwon SB, Young C, Kim DS, Choi HO, Kim KH, Chung JH, Eun HC, Park KC, Oh CK, Seo JS (2002) Impaired repair ability of hsp70.1 KO mouse after UVB irradiation. J Dermatol Sci 28:144-151.

de Laat SW, van der Saag PT, Shinitzky M (1977) Microviscosity modulation during the cell cycle of neuroblastoma cells. Proc Natl Acad Sci USA 74:4458-4461.

Lafreniere RG *et al*. (2004) Identification of a novel gene (HSN2) causing hereditary sensory and autonomic neuropathy type II through the Study of Canadian Genetic Isolates. Am J Hum Genet 74:1064-1073.

Lai C, Lin X, Chandran J, Shim H, Yang W-J, Cai H (2007) The G59S mutation in p150(glued) causes dysfunction of dynactin in mice. J Neurosci 27:13982-13990.

Lai CW, Aronson DE, Snapp EL (2010) BiP Availability Distinguishes States of Homeostasis and Stress in the Endoplasmic Reticulum of Living Cells. Mol Biol Cell 21:1909-1921.

Lambert H, Charette SJ, Bernier AF, Guimond A, Landry J (1999) HSP27 multimerization mediated by phosphorylation-sensitive intermolecular interactions at the amino terminus. J Biol Chem 274:9378-9385.

Lambowitz AM, Kobayashi GS, Painter A, Medoff G (1983) Possible relationship of morphogenesis in pathogenic fungus, Histoplasma capsulatum, to heat shock response. Nature 303:806-808.

Landouré G *et al*. (2010) Mutations in TRPV4 cause Charcot-Marie-Tooth disease type 2C. Nat Genet 42:170-174.

Landry J, Lambert H, Zhou M, Lavoie JN, Hickey E, Weber LA, Anderson CW (1992) Human HSP27 is phosphorylated at serines 78 and 82 by heat shock and mitogen-activated kinases that recognize the same amino acid motif as S6 kinase II. J Biol Chem 267:794-803.

Langford GM (2002) Myosin-V, a versatile motor for short-range vesicle transport. Traffic 3:859-865.

Lasek RJ, Garner JA, Brady ST (1984) Axonal transport of the cytoplasmic matrix. J Cell Biol 99:212s-221s.

Laskowska E, Matuszewska E, Kuczyńska-Wiśnik D (2010) Small heat shock proteins and protein-misfolding diseases. Curr Pharm Biotechnol 11:146-157.

Latchman DS (2005) HSP27 and cell survival in neurones. Int J Hyperthermia 21:393-402.

Latour P, Thauvin-Robinet C, Baudelet-Méry C, Soichot P, Cusin V, Faivre L, Locatelli M-C, Mayençon M, Sarcey A, Broussolle E, Camu W, David A, Rousson R (2010) A major determinant for binding and aminoacylation of tRNA(Ala) in cytoplasmic Alanyl-tRNA synthetase is mutated in dominant axonal Charcot-Marie-Tooth disease. Am J Hum Genet 86:77-82.

Laughlin SB, de Ruyter van Steveninck RR, Anderson JC (1998) The metabolic cost of neural information. Nat Neurosci 1:36-41.

Lavoie JN, Gingras-Breton G, Tanguay RM, Landry J (1993a) Induction of Chinese hamster HSP27 gene expression in mouse cells confers resistance to heat shock. HSP27 stabilization of the microfilament organization. J Biol Chem 268:3420-3429.

Lavoie JN, Hickey E, Weber LA, Landry J (1993b) Modulation of actin microfilament dynamics and fluid phase pinocytosis by phosphorylation of heat shock protein 27. J Biol Chem 268:24210-24214.

Lavoie JN, Lambert H, Hickey E, Weber LA, Landry J (1995) Modulation of cellular thermoresistance and actin filament stability accompanies phosphorylation-induced changes in the oligomeric structure of heat shock protein 27. Mol Cell Biol 15:505-516.

Lee SH, Kim M, Yoon BW, Kim YJ, Ma SJ, Roh JK, Lee JS, Seo JS (2001) Targeted hsp70.1 disruption increases infarction volume after focal cerebral ischemia in mice. Stroke 32:2905-2912.

Lefebvre S, Bürglen L, Reboullet S, Clermont O, Burlet P, Viollet L, Benichou B, Cruaud C, Millasseau P, Zeviani M (1995) Identification and characterization of a spinal muscular atrophy-determining gene. Cell 80:155-165.

Lewinski F von, Keller BU (2005) Ca2+, mitochondria and selective motoneuron vulnerability: implications for ALS. Trends in Neurosciences 28:494-500.

Lewis RA, Sumner AJ (1982) The electrodiagnostic distinctions between chronic familial and acquired demyelinative neuropathies. Neurology 32:592-596.

Li F-F, Yang M, Ma X, Zhang Q, Zhang M, Wang S-Z, Zhu S-Q (2010) Autosomal dominant congenital nuclear cataracts caused by a CRYAA gene mutation. Curr Eye Res 35:492-498.

Li Y-C, Zhai X-Y, Ohsato K, Futamata H, Shimada O, Atsumi S (2004) Mitochondrial accumulation in the distal part of the initial segment of chicken spinal motoneurons. Brain Research 1026:235-243.

Li Z-W, Li X, Yu Q-Y, Xiang Z-H, Kishino H, Zhang Z (2009) The small heat shock protein (sHSP) genes in the silkworm, Bombyx mori, and comparative analysis with other insect sHSP genes. BMC Evol Biol 9:215.

Licciardo P, Amente S, Ruggiero L, Monti M, Pucci P, Lania L, Majello B (2003) The FCP1 phosphatase interacts with RNA polymerase II and with MEP50 a component of the methylosome complex involved in the assembly of snRNP. Nucleic Acids Res 31:999-1005.

Ligon LA, Steward O (2000) Role of microtubules and actin filaments in the movement of mitochondria in the axons and dendrites of cultured hippocampal neurons. J Comp Neurol 427:351-361.

Lindquist S (1986) The heat-shock response. Annu Rev Biochem 55:1151-1191.

Liu JS (2011) Molecular genetics of neuronal migration disorders. Curr Neurol Neurosci Rep 11:171-178.

Lu TZ, Quan Y, Feng Z-P (2010) Multifaceted Role of Heat Shock Protein 70 in Neurons. Mol Neurobiol 42:114-123.

Luigetti M, Fabrizi GM, Madia F, Ferrarini M, Conte A, Del Grande A, Tasca G, Tonali PA, Sabatelli M (2010) A novel HSPB1 mutation in an Italian patient with CMT2/dHMN phenotype. J Neurol Sci 298:114-117.

Lunn MPT, Willison HJ (2009) Diagnosis and treatment in inflammatory neuropathies. J Neurol Neurosurg Psychiatr 80:249-258.

Ma CH, Omura T, Cobos EJ, Latremoliere A, Ghasemlou N, Brenner CJ, van Veen E, Barrett L, Sawada T, Gao F, Coppola G, Gertler F, Costigan M, Geschwind D, Woolf CJ (2011) Accelerating axonal growth promotes motor recovery after peripheral nerve injury in mice. J Clin Invest 121(11):4332-47.

Magen D, Georgopoulos C, Bross P, Ang D, Segev Y, Goldsher D, Nemirovski A, Shahar E, Ravid S, Luder A, Heno B, Gershoni-Baruch R, Skorecki K, Mandel H (2008) Mitochondrial hsp60 chaperonopathy causes an autosomal-recessive neurodegenerative disorder linked to brain hypomyelination and leukodystrophy. Am J Hum Genet 83:30-42.

Mandal AK, Gibney PA, Nillegoda NB, Theodoraki MA, Caplan AJ, Morano KA (2010) Hsp110 chaperones control client fate determination in the hsp70-Hsp90 chaperone system. Mol Biol Cell 21:1439-1448.

Mandich P, Grandis M, Varese A, Geroldi A, Acquaviva M, Ciotti P, Gulli R, Doria-Lamba L, Fabrizi GM, Giribaldi G, Pizzuti A, Schenone A, Bellone E (2010) Severe neuropathy after diphtheria-tetanus-pertussis vaccination in a child carrying a novel frame-shift mutation in the small heat-shock protein 27 gene. J Child Neurol 25:107-109.

Marchesi C, Milani M, Morbin M, Cesani M, Lauria G, Scaioli V, Piccolo G, Fabrizi GM, Cavallaro T, Taroni F, Pareyson D (2010) Four novel cases of periaxin-related neuropathy and review of the literature. Neurology 75:1830-1838.

Martyn CN, Hughes RA (1997) Epidemiology of peripheral neuropathy. J Neurol Neurosurg Psychiatr 62:310-318.

Matsunami N, Smith B, Ballard L, Lensch MW, Robertson M, Albertsen H, Hanemann CO, Müller HW, Bird TD, White R (1992) Peripheral myelin protein-22

gene maps in the duplication in chromosome 17p11.2 associated with Charcot-Marie-Tooth 1A. Nat Genet 1:176-179.

Mayer MP, Bukau B (2005) Hsp70 chaperones: cellular functions and molecular mechanism. Cell Mol Life Sci 62:670-684.

McLaughlin HM *et al*. (2010) Compound heterozygosity for loss-of-function lysyl-tRNA synthetase mutations in a patient with peripheral neuropathy. Am J Hum Genet 87:560-566.

McMillan HJ, Santagata S, Shapiro F, Batish SD, Couchon L, Donnelly S, Kang PB (2010) Novel MPZ mutations and congenital hypomyelinating neuropathy. Neuromuscul Disord 20:725-729.

McPhedran AM, Wuerker RB, Henneman E (1965) Propterties of motor units in a homogeneous red muscle (Soleus) of the cat. J Neurophysiol 28:71-84.

McQuarrie IG, Brady ST, Lasek RJ (1986) Diversity in the axonal transport of structural proteins: major differences between optic and spinal axons in the rat. J Neurosci 6:1593-1605.

McQuarrie IG, Brady ST, Lasek RJ (1989) Retardation in the slow axonal transport of cytoskeletal elements during maturation and aging. Neurobiol Aging 10:359-365.

Mehlen P, Hickey E, Weber LA, Arrigo AP (1997) Large unphosphorylated aggregates as the active form of hsp27 which controls intracellular reactive oxygen species and glutathione levels and generates a protection against TNFalpha in NIH-3T3-ras cells. Biochem Biophys Res Commun 241:187-192.

Mersiyanova IV, Perepelov AV, Polyakov AV, Sitnikov VF, Dadali EL, Oparin RB, Petrin AN, Evgrafov OV (2000) A new variant of Charcot-Marie-Tooth disease type 2 is probably the result of a mutation in the neurofilament-light gene. Am J Hum Genet 67:37-46.

Miki H, Setou M, Kaneshiro K, Hirokawa N (2001) All kinesin superfamily protein, KIF, genes in mouse and human. Proc Natl Acad Sci USA 98:7004-7011.

Miller KE, Heidemann SR (2008) What is slow axonal transport? Experimental Cell Research 314:1981-1990.

Miltenberger-Miltenyi G, Janecke AR, Wanschitz JV, Timmerman V, Windpassinger C, Auer-Grumbach M, Löscher WN (2007) Clinical and electrophysiological features in Charcot-Marie-Tooth disease with mutations in the NEFL gene. Arch Neurol 64:966-970.

Miron T, Vancompernolle K, Vandekerckhove J, Wilchek M, Geiger B (1991) A 25-kD inhibitor of actin polymerization is a low molecular mass heat shock protein. J Cell Biol 114:255-261.

Morimoto RI (2008) Proteotoxic stress and inducible chaperone networks in neurodegenerative disease and aging. Genes Dev 22:1427-1438.

Morris JR, Lasek RJ (1982) Stable polymers of the axonal cytoskeleton: the axoplasmic ghost. J Cell Biol 92:192-198.

Morse R, Todd AG, Shaw DJ, McConville AL, Robinson IM, Young PJ (2011) Mutations in the survival motor neuron (SMN) protein alter the dynamic nature of nuclear bodies. Neuromolecular Med 13:77-87.

Motley WW, Talbot K, Fischbeck KH (2010) GARS axonopathy: not every neuron's cup of tRNA. Trends Neurosci 33:59-66.

Mounier N, Arrigo A-P (2002) Actin cytoskeleton and small heat shock proteins: how do they interact? Cell Stress Chaperones 7:167-176.

Nagai H, Noguchi T, Takeda K, Ichijo H (2007) Pathophysiological roles of ASK1-MAP kinase signaling pathways. J Biochem Mol Biol 40:1-6.

Nangaku M, Sato-Yoshitake R, Okada Y, Noda Y, Takemura R, Yamazaki H, Hirokawa N (1994) KIF1B, a novel microtubule plus end-directed monomeric motor protein for transport of mitochondria. Cell 79:1209-1220.

Narberhaus F (2002) Alpha-crystallin-type heat shock proteins: socializing minichaperones in the context of a multichaperone network. Microbiol Mol Biol Rev 66:64-93; table of contents.

Neumann M, Sampathu DM, Kwong LK, Truax AC, Micsenyi MC, Chou TT, Bruce J, Schuck T, Grossman M, Clark CM, McCluskey LF, Miller BL, Masliah E, Mackenzie IR, Feldman H, Feiden W, Kretzschmar HA, Trojanowski JQ, Lee VM-Y (2006) Ubiquitinated TDP-43 in frontotemporal lobar degeneration and amyotrophic lateral sclerosis. Science 314:130-133.

Nicholson G, Myers S (2006) Intermediate forms of Charcot-Marie-Tooth neuropathy: a review. Neuromolecular Med 8:123-130.

Nicholson GA, Valentijn LJ, Cherryson AK, Kennerson ML, Bragg TL, DeKroon RM, Ross DA, Pollard JD, McLeod JG, Bolhuis PA (1994) A frame shift mutation in the PMP22 gene in hereditary neuropathy with liability to pressure palsies. Nat Genet 6:263-266.

Nukada H, Dyck PJ (1984) Decreased axon caliber and neurofilaments in hereditary motor and sensory neuropathy, type I. Ann Neurol 16:238-241.

Ojha J, Masilamoni G, Dunlap D, Udoff RA, Cashikar AG (2011) Sequestration of toxic oligomers by HspB1 as a cytoprotective mechanism. Mol Cell Biol 31:3146-3157.

Okado-Matsumoto A, Fridovich I (2002) Amyotrophic lateral sclerosis: a proposed mechanism. Proc Natl Acad Sci USA 99:9010-9014.

Palay SL (1958) The morphology of synapses in the central nervous system. Exp Cell Res 14:275-293.

Pandolfi PP, Sonati F, Rivi R, Mason P, Grosveld F, Luzzatto L (1995) Targeted disruption of the housekeeping gene encoding glucose 6-phosphate dehydrogenase (G6PD): G6PD is dispensable for pentose synthesis but essential for defense against oxidative stress. EMBO J 14:5209-5215.

Pannese E, Ledda M, Arcidiacono G, Rigamonti L, Procacci P (1984a) A comparison of the density of microtubules in the central and peripheral axonal

branches of the pseudounipolar neurons of lizard spinal ganglia. Anat Rec 208:595-605.

Pannese E, Procacci P, Ledda M, Arcidiacono G, Rigamonti L (1984b) A quantitative study of microtubules in motor and sensory axons. Acta Anat (Basel) 118:193-200.

Pareyson D, Marchesi C (2009) Diagnosis, natural history, and management of Charcot-Marie-Tooth disease. Lancet Neurol 8:654-667.

Pareyson D, Marchesi C, Salsano E (2009) Hereditary predominantly motor neuropathies. Curr Opin Neurol 22:451-459.

Pareyson D, Scaioli V, Laurà M (2006) Clinical and electrophysiological aspects of Charcot-Marie-Tooth disease. Neuromolecular Med 8:3-22.

Patel PI, Roa BB, Welcher AA, Schoener-Scott R, Trask BJ, Pentao L, Snipes GJ, Garcia CA, Francke U, Shooter EM, Lupski JR, Suter U (1992) The gene for the peripheral myelin protein PMP-22 is a candidate for Charcot-Marie-Tooth disease type 1A. Nat Genet 1:159-165.

Patriarca EJ, Maresca B (1990) Acquired thermotolerance following heat shock protein synthesis prevents impairment of mitochondrial ATPase activity at elevated temperatures in Saccharomyces cerevisiae. Experimental Cell Research 190:57-64.

Patzkó A, Shy ME (2011) Update on Charcot-Marie-Tooth disease. Curr Neurol Neurosci Rep 11:78-88.

Der Perng M, Quinlan RA (2004) Neuronal diseases: small heat shock proteins calm your nerves. Curr Biol 14:R625-626.

Perng MD, Cairns L, van den IJssel P, Prescott A, Hutcheson AM, Quinlan RA (1999) Intermediate filament interactions can be altered by HSP27 and alphaB-crystallin. Journal of Cell Science 112:2099 -2112.

Pietersma A, Tilly BC, Gaestel M, de Jong N, Lee JC, Koster JF, Sluiter W (1997) p38 mitogen activated protein kinase regulates endothelial VCAM-1 expression at the post-transcriptional level. Biochem Biophys Res Commun 230:44-48.

Pilling AD, Horiuchi D, Lively CM, Saxton WM (2006) Kinesin-1 and Dynein are the primary motors for fast transport of mitochondria in Drosophila motor axons. Mol Biol Cell 17:2057-2068.

Pitt M, Houlden H, Jacobs J, Mok Q, Harding B, Reilly M, Surtees R (2003) Severe infantile neuropathy with diaphragmatic weakness and its relationship to SMARD1. Brain 126:2682-2692.

Pivovarova AV, Chebotareva NA, Chernik IS, Gusev NB, Levitsky DI (2007) Small heat shock protein Hsp27 prevents heat-induced aggregation of F-actin by forming soluble complexes with denatured actin. FEBS J 274:5937-5948.

Pivovarova AV, Mikhailova VV, Chernik IS, Chebotareva NA, Levitsky DI, Gusev NB (2005) Effects of small heat shock proteins on the thermal denaturation and aggregation of F-actin. Biochem Biophys Res Commun 331:1548-1553.

Pratt WB, Toft DO (2003) Regulation of signaling protein function and trafficking by the hsp90/hsp70-based chaperone machinery. Exp Biol Med (Maywood) 228:111-133.

Préville X, Salvemini F, Giraud S, Chaufour S, Paul C, Stepien G, Ursini MV, Arrigo AP (1999) Mammalian small stress proteins protect against oxidative stress through their ability to increase glucose-6-phosphate dehydrogenase activity and by maintaining optimal cellular detoxifying machinery. Exp Cell Res 247:61-78.

Puls I, Jonnakuty C, LaMonte BH, Holzbaur ELF, Tokito M, Mann E, Floeter MK, Bidus K, Drayna D, Oh SJ, Brown RH Jr, Ludlow CL, Fischbeck KH (2003) Mutant dynactin in motor neuron disease. Nat Genet 33:455-456.

Qian W, Iqbal K, Grundke-Iqbal I, Gong C-X, Liu F (2011) Splicing factor SC35 promotes tau expression through stabilization of its mRNA. FEBS Lett 585:875-880.

Rane MJ, Pan Y, Singh S, Powell DW, Wu R, Cummins T, Chen Q, McLeish KR, Klein JB (2003) Heat shock protein 27 controls apoptosis by regulating Akt activation. J Biol Chem 278:27828-27835.

Ransome MI, Turnley AM (2008) Erythropoietin promotes axonal growth in a model of neuronal polarization. Mol Cell Neurosci 38:537-547.

Read DE, Gorman AM (2009) Heat shock protein 27 in neuronal survival and neurite outgrowth. Biochem Biophys Res Commun 382:6-8.

Reid E, Kloos M, Ashley-Koch A, Hughes L, Bevan S, Svenson IK, Graham FL, Gaskell PC, Dearlove A, Pericak-Vance MA, Rubinsztein DC, Marchuk DA (2002) A kinesin heavy chain (KIF5A) mutation in hereditary spastic paraplegia (SPG10). Am J Hum Genet 71:1189-1194.

Reilly MM (2007) Sorting out the inherited neuropathies. Pract Neurol 7:93-105.

Reilly MM, Shy ME (2009) Diagnosis and new treatments in genetic neuropathies. J Neurol Neurosurg Psychiatr 80:1304-1314.

Richter K, Haslbeck M, Buchner J (2010) The heat shock response: life on the verge of death. Mol Cell 40:253-266.

Roberts RC, Peden AA, Buss F, Bright NA, Latouche M, Reilly MM, Kendrick-Jones J, Luzio JP (2010) Mistargeting of SH3TC2 away from the recycling endosome causes Charcot-Marie-Tooth disease type 4C. Hum Mol Genet 19:1009-1018.

Robinson MB, Tidwell JL, Gould T, Taylor AR, Newbern JM, Graves J, Tytell M, Milligan CE (2005) Extracellular heat shock protein 70: a critical component for motoneuron survival. J Neurosci 25:9735-9745.

Rogalla T, Ehrnsperger M, Preville X, Kotlyarov A, Lutsch G, Ducasse C, Paul C, Wieske M, Arrigo A-P, Buchner J, Gaestel M (1999) Regulation of Hsp27 Oligomerization, Chaperone Function, and Protective Activity against Oxidative Stress/Tumor Necrosis Factor α by Phosphorylation. Journal of Biological Chemistry 274:18947 -18956.

Roy S, Coffee P, Smith G, Liem RK, Brady ST, Black MM (2000) Neurofilaments are transported rapidly but intermittently in axons: implications for slow axonal transport. J Neurosci 20:6849-6861.

Russell H. S (2011) Brain aging, Alzheimer's disease, and mitochondria. Biochimica et Biophysica Acta (BBA) - Molecular Basis of Disease Available at: http://www.sciencedirect.com/science/article/pii/S0925443911001943 [Accessed September 20, 2011].

Saito Y, Yamagishi N, Hatayama T (2007) Different localization of Hsp105 family proteins in mammalian cells. Exp Cell Res 313:3707-3717.

Salajegheh M, Pinkus JL, Taylor JP, Amato AA, Nazareno R, Baloh RH, Greenberg SA (2009) Sarcoplasmic redistribution of nuclear TDP-43 in inclusion body myositis. Muscle Nerve 40:19-31.

De Sandre-Giovannoli A, Chaouch M, Kozlov S, Vallat J-M, Tazir M, Kassouri N, Szepetowski P, Hammadouche T, Vandenberghe A, Stewart CL, Grid D, Lévy N (2002) Homozygous defects in LMNA, encoding lamin A/C nuclear-envelope proteins, cause autosomal recessive axonal neuropathy in human (Charcot-Marie-Tooth disorder type 2) and mouse. Am J Hum Genet 70:726-736.

Sau D, Rusmini P, Crippa V, Onesto E, Bolzoni E, Ratti A, Poletti A (2011) Dysregulation of axonal transport and motorneuron diseases. Biol Cell 103:87-107.

Scherer SS, Xu YT, Bannerman PG, Sherman DL, Brophy PJ (1995) Periaxin expression in myelinating Schwann cells: modulation by axon-glial interactions and polarized localization during development. Development 121:4265-4273.

Schröder JM (2006) Neuropathology of Charcot-Marie-Tooth and related disorders. Neuromolecular Med 8:23-42.

Schulz JB, Lindenau J, Seyfried J, Dichgans J (2000) Glutathione, oxidative stress and neurodegeneration. European Journal of Biochemistry 267:4904-4911.

Senderek J *et al*. (2003) Mutations in a gene encoding a novel SH3/TPR domain protein cause autosomal recessive Charcot-Marie-Tooth type 4C neuropathy. Am J Hum Genet 73:1106-1119.

Senderek J, Bergmann C, Quasthoff S, Ramaekers VT, Schröder JM (1998) X-linked dominant Charcot-Marie-Tooth disease: nerve biopsies allow morphological evaluation and detection of connexin32 mutations (Arg15Trp, Arg22Gln). Acta Neuropathol 95:443-449.

Shah JV, Cleveland DW (2002) Slow axonal transport: fast motors in the slow lane. Current Opinion in Cell Biology 14:58-62.

Shamovsky I, Ivannikov M, Kandel ES, Gershon D, Nudler E (2006) RNA-mediated response to heat shock in mammalian cells. Nature 440:556-560.

Shamovsky I, Nudler E (2008) New insights into the mechanism of heat shock response activation. Cell Mol Life Sci 65:855-861.

Sharp PS, Akbar MT, Bouri S, Senda A, Joshi K, Chen H-J, Latchman DS, Wells DJ, de Belleroche J (2008) Protective effects of heat shock protein 27 in a model of ALS occur in the early stages of disease progression. Neurobiol Dis 30:42-55.

Shaw PJ, Eggett CJ (2000) Molecular factors underlying selective vulnerability of motor neurons to neurodegeneration in amyotrophic lateral sclerosis. J Neurol 247 Suppl 1:I17-27.

Shemetov AA, Seit-Nebi AS, Gusev NB (2008) Structure, properties, and functions of the human small heat-shock protein HSP22 (HspB8, H11, E2IG1): a critical review. J Neurosci Res 86:264-269.

Shim E-H, Kim J-I, Bang E-S, Heo J-S, Lee J-S, Kim E-Y, Lee J-E, Park W-Y, Kim S-H, Kim H-S, Smithies O, Jang J-J, Jin D-I, Seo J-S (2002) Targeted disruption of hsp70.1 sensitizes to osmotic stress. EMBO Rep 3:857-861.

Shirk AJ, Anderson SK, Hashemi SH, Chance PF, Bennett CL (2005) SIMPLE interacts with NEDD4 and TSG101: evidence for a role in lysosomal sorting and implications for Charcot-Marie-Tooth disease. J Neurosci Res 82:43-50.

Sinadinos C, Burbidge-King T, Soh D, Thompson LM, Marsh JL, Wyttenbach A, Mudher AK (2009) Live axonal transport disruption by mutant huntingtin fragments in Drosophila motor neuron axons. Neurobiol Dis 34:389-395.

Slaugenhaupt SA, Blumenfeld A, Gill SP, Leyne M, Mull J, Cuajungco MP, Liebert CB, Chadwick B, Idelson M, Reznik L, Robbins C, Makalowska I, Brownstein M, Krappmann D, Scheidereit C, Maayan C, Axelrod FB, Gusella JF (2001) Tissue-specific expression of a splicing mutation in the IKBKAP gene causes familial dysautonomia. Am J Hum Genet 68:598-605.

Slepian MJ, Massia SP, Whitesell L (1996) Pre-conditioning of smooth muscle cells via induction of the heat shock response limits proliferation following mechanical injury. Biochem Biophys Res Commun 225:600-607.

Smith RC, Rosen KM, Pola R, Magrané J (2005) Stress proteins in Alzheimer's disease. Int J Hyperthermia 21:421-431.

Snell RS (2009) Clinical neuroanatomy. Lippincott Williams & Wilkins.

Solla P, Vannelli A, Bolino A, Marrosu G, Coviello S, Murru MR, Tranquilli S, Corongiu D, Benedetti S, Marrosu MG (2010) Heat shock protein 27 R127W mutation: evidence of a continuum between axonal Charcot-Marie-Tooth and distal hereditary motor neuropathy. J Neurol Neurosurg Psychiatr 81:958-962.

Sreedharan J, Blair IP, Tripathi VB, Hu X, Vance C, Rogelj B, Ackerley S, Durnall JC, Williams KL, Buratti E, Baralle F, de Belleroche J, Mitchell JD, Leigh PN, Al-Chalabi A, Miller CC, Nicholson G, Shaw CE (2008) TDP-43 mutations in familial and sporadic amyotrophic lateral sclerosis. Science 319:1668-1672.

Sreedharan R, Riordan M, Thullin G, Van Why S, Siegel NJ, Kashgarian M (2011) The maximal cytoprotective function of the heat shock protein 27 is dependent on heat shock protein 70. Biochim Biophys Acta 1813:129-135.

Stendel C *et al*. (2007) Peripheral nerve demyelination caused by a mutant Rho GTPase guanine nucleotide exchange factor, frabin/FGD4. Am J Hum Genet 81:158-164.

Stendel C, Roos A, Kleine H, Arnaud E, Ozçelik M, Sidiropoulos PNM, Zenker J, Schüpfer F, Lehmann U, Sobota RM, Litchfield DW, Lüscher B, Chrast R, Suter U, Senderek J (2010) SH3TC2, a protein mutant in Charcot-Marie-Tooth neuropathy, links peripheral nerve myelination to endosomal recycling. Brain 133:2462-2474.

Stokoe D, Engel K, Campbell DG, Cohen P, Gaestel M (1992) Identification of MAPKAP kinase 2 as a major enzyme responsible for the phosphorylation of the small mammalian heat shock proteins. FEBS Lett 313:307-313.

Street VA, Bennett CL, Goldy JD, Shirk AJ, Kleopa KA, Tempel BL, Lipe HP, Scherer SS, Bird TD, Chance PF (2003) Mutation of a putative protein degradation gene LITAF/SIMPLE in Charcot-Marie-Tooth disease 1C. Neurology 60:22-26.

Stum M, McLaughlin HM, Kleinbrink EL, Miers KE, Ackerman SL, Seburn KL, Antonellis A, Burgess RW (2011) An assessment of mechanisms underlying peripheral axonal degeneration caused by aminoacyl-tRNA synthetase mutations. Mol Cell Neurosci 46:432-443.

Su Y, Brooks DG, Li L, Lepercq J, Trofatter JA, Ravetch JV, Lebo RV (1993) Myelin protein zero gene mutated in Charcot-Marie-tooth type 1B patients. Proc Natl Acad Sci USA 90:10856-10860.

Sugiyama Y, Suzuki A, Kishikawa M, Akutsu R, Hirose T, Waye MM, Tsui SK, Yoshida S, Ohno S (2000) Muscle develops a specific form of small heat shock protein complex composed of MKBP/HSPB2 and HSPB3 during myogenic differentiation. J Biol Chem 275:1095-1104.

Sun X, Fontaine J-M, Rest JS, Shelden EA, Welsh MJ, Benndorf R (2004) Interaction of human HSP22 (HSPB8) with other small heat shock proteins. J Biol Chem 279:2394-2402.

Sun Y, MacRae TH (2005) Small heat shock proteins: molecular structure and chaperone function. Cell Mol Life Sci 62:2460-2476.

Suzuki A, Sugiyama Y, Hayashi Y, Nyu-i N, Yoshida M, Nonaka I, Ishiura S, Arahata K, Ohno S (1998) MKBP, a novel member of the small heat shock protein family, binds and activates the myotonic dystrophy protein kinase. J Cell Biol 140:1113-1124.

Szigeti K, Garcia CA, Lupski JR (2006) Charcot-Marie-Tooth disease and related hereditary polyneuropathies: molecular diagnostics determine aspects of medical management. Genet Med 8:86-92.

Taipale M, Jarosz DF, Lindquist S (2010) HSP90 at the hub of protein homeostasis: emerging mechanistic insights. Nat Rev Mol Cell Biol 11:515-528.

Tanaka Y, Kanai Y, Okada Y, Nonaka S, Takeda S, Harada A, Hirokawa N (1998) Targeted disruption of mouse conventional kinesin heavy chain, kif5B, results in abnormal perinuclear clustering of mitochondria. Cell 93:1147-1158.

Tang B, Liu X, Zhao G, Luo W, Xia K, Pan Q, Cai F, Hu Z, Zhang C, Chen B, Zhang F, Shen L, Zhang R, Jiang H (2005) Mutation analysis of the small heat shock protein 27 gene in chinese patients with Charcot-Marie-Tooth disease. Arch Neurol 62:1201-1207.

Tang D, Kang R, Livesey KM, Kroemer G, Billiar TR, Van Houten B, Zeh III HJ, Lotze MT (2011) High-Mobility Group Box 1 Is Essential for Mitochondrial Quality Control. Cell Metabolism 13:701-711.

Tang XQ, Wang Y, Han JS, Wan Y (2001) Adenovirus-mediated GDNF protects cultured motoneurons from glutamate injury. Neuroreport 12:3073-3076.

Thomas MG, Loschi M, Desbats MA, Boccaccio GL (2011) RNA granules: the good, the bad and the ugly. Cell Signal 23:324-334.

Thomas PK, Marques W, Davis MB, Sweeney MG, King RH, Bradley JL, Muddle JR, Tyson J, Malcolm S, Harding AE (1997) The phenotypic manifestations of chromosome 17p11.2 duplication. Brain 120:465 -478.

Tidwell JL, Houenou LJ, Tytell M (2004) Administration of Hsp70 in vivo inhibits motor and sensory neuron degeneration. Cell Stress Chaperones 9:88-98.

Timmerman V, Nelis E, Van Hul W, Nieuwenhuijsen BW, Chen KL, Wang S, Ben Othman K, Cullen B, Leach RJ, Hanemann CO (1992) The peripheral myelin protein gene PMP-22 is contained within the Charcot-Marie-Tooth disease type 1A duplication. Nat Genet 1:171-175.

Toivola DM, Strnad P, Habtezion A, Omary MB (2010) Intermediate filaments take the heat as stress proteins. Trends Cell Biol 20:79-91.

Tooth H. (1886) The Peroneal Type of Progressive Muscular Atrophy. HK Lewis, London.

Tradewell ML, Durham HD, Mushynski WE, Gentil BJ (2009) Mitochondrial and axonal abnormalities precede disruption of the neurofilament network in a model of charcot-marie-tooth disease type 2E and are prevented by heat shock proteins in a mutant-specific fashion. J Neuropathol Exp Neurol 68:642-652.

Tsai H-F, Lin SJ, Li C, Hsieh M (2005) Decreased expression of Hsp27 and Hsp70 in transformed lymphoblastoid cells from patients with spinocerebellar ataxia type 7. Biochem Biophys Res Commun 334:1279-1286.

Tucker NR, Ustyugov A, Bryantsev AL, Konkel ME, Shelden EA (2009) Hsp27 is persistently expressed in zebrafish skeletal and cardiac muscle tissues but dispensable for their morphogenesis. Cell Stress Chaperones 14:521-533.

Twig G, Shirihai OS (2011) The interplay between mitochondrial dynamics and mitophagy. Antioxid Redox Signal 14:1939-1951.

Valentijn LJ, Bolhuis PA, Zorn I, Hoogendijk JE, van den Bosch N, Hensels GW, Stanton VP Jr, Housman DE, Fischbeck KH, Ross DA (1992) The peripheral myelin gene PMP-22/GAS-3 is duplicated in Charcot-Marie-Tooth disease type 1A. Nat Genet 1:166-170.

Vande Velde C, McDonald KK, Boukhedimi Y, McAlonis-Downes M, Lobsiger CS, Bel Hadj S, Zandona A, Julien J-P, Shah SB, Cleveland DW (2011) Misfolded SOD1 Associated with Motor Neuron Mitochondria Alters Mitochondrial Shape and Distribution Prior to Clinical Onset. PLoS ONE 6:e22031.

Varon R *et al*. (2003) Partial deficiency of the C-terminal-domain phosphatase of RNA polymerase II is associated with congenital cataracts facial dysmorphism neuropathy syndrome. Nat Genet 35:185-189.

Vembar SS, Brodsky JL (2008) One step at a time: endoplasmic reticulum-associated degradation. Nat Rev Mol Cell Biol 9:944-957.

Verhoeven K, De Jonghe P, Coen K, Verpoorten N, Auer-Grumbach M, Kwon JM, FitzPatrick D, Schmedding E, De Vriendt E, Jacobs A, Van Gerwen V, Wagner K,

Hartung H-P, Timmerman V (2003) Mutations in the small GTP-ase late endosomal protein RAB7 cause Charcot-Marie-Tooth type 2B neuropathy. Am J Hum Genet 72:722-727.

Vicart P, Caron A, Guicheney P, Li Z, Prévost MC, Faure A, Chateau D, Chapon F, Tomé F, Dupret JM, Paulin D, Fardeau M (1998) A missense mutation in the alphaB-crystallin chaperone gene causes a desmin-related myopathy. Nat Genet 20:92-95.

De Vos KJ, Chapman AL, Tennant ME, Manser C, Tudor EL, Lau K-F, Brownlees J, Ackerley S, Shaw PJ, McLoughlin DM, Shaw CE, Leigh PN, Miller CCJ, Grierson AJ (2007) Familial amyotrophic lateral sclerosis-linked SOD1 mutants perturb fast axonal transport to reduce axonal mitochondria content. Hum Mol Genet 16:2720-2728.

Vos MJ, Kanon B, Kampinga HH (2009a) HSPB7 is a SC35 speckle resident small heat shock protein. Biochim Biophys Acta 1793:1343-1353.

Wakerley BR, Harman FE, Altmann DM, Malik O (2011) Charcot-Marie-Tooth disease associated with recurrent optic neuritis. J Clin Neurosci Available at: http://www.ncbi.nlm.nih.gov/pubmed/21764587 [Accessed July 29, 2011].

Warner LE, Mancias P, Butler IJ, McDonald CM, Keppen L, Koob KG, Lupski JR (1998) Mutations in the early growth response 2 (EGR2) gene are associated with hereditary myelinopathies. Nat Genet 18:382-384.

Waterman-Storer CM, Karki SB, Kuznetsov SA, Tabb JS, Weiss DG, Langford GM, Holzbaur EL (1997) The interaction between cytoplasmic dynein and dynactin is required for fast axonal transport. Proc Natl Acad Sci USA 94:12180-12185.

Weedon MN, Hastings R, Caswell R, Xie W, Paszkiewicz K, Antoniadi T, Williams M, King C, Greenhalgh L, Newbury-Ecob R, Ellard S (2011) Exome sequencing identifies a DYNC1H1 mutation in a large pedigree with dominant axonal Charcot-Marie-Tooth disease. Am J Hum Genet 89:308-312.

Welch WJ, Suhan JP (1985) Morphological study of the mammalian stress response: characterization of changes in cytoplasmic organelles, cytoskeleton, and nucleoli, and appearance of intranuclear actin filaments in rat fibroblasts after heat-shock treatment. J Cell Biol 101:1198-1211.

Westhoff B, Chapple JP, van der Spuy J, Höhfeld J, Cheetham ME (2005) HSJ1 is a neuronal shuttling factor for the sorting of chaperone clients to the proteasome. Curr Biol 15:1058-1064.

Widmann C, Gibson S, Jarpe MB, Johnson GL (1999) Mitogen-activated protein kinase: conservation of a three-kinase module from yeast to human. Physiol Rev 79:143-180.

Williams KL, Rahimtula M, Mearow KM (2005) Hsp27 and axonal growth in adult sensory neurons in vitro. BMC Neurosci 6:24.

Williams KL, Rahimtula M, Mearow KM (2006) Heat shock protein 27 is involved in neurite extension and branching of dorsal root ganglion neurons in vitro. J Neurosci Res 84:716-723.

Williamson TL, Cleveland DW (1999) Slowing of axonal transport is a very early event in the toxicity of ALS-linked SOD1 mutants to motor neurons. Nat Neurosci 2:50-56.

Windpassinger C *et al*. (2004) Heterozygous missense mutations in BSCL2 are associated with distal hereditary motor neuropathy and Silver syndrome. Nat Genet 36:271-276.

de Wit NJW, Verschuure P, Kappé G, King SM, de Jong WW, van Muijen GNP, Boelens WC (2004) Testis-specific human small heat shock protein HSPB9 is a cancer/testis antigen, and potentially interacts with the dynein subunit TCTEL1. Eur J Cell Biol 83:337-345.

Wu C (1984) Activating protein factor binds in vitro to upstream control sequences in heat shock gene chromatin. Nature 311:81-84.

Wuerker RB, McPhedran AM, Henneman E (1965) Properties of motor units in a heterogeneous pale muscle (M. Gastrocnemius) of the cat. Journal of Neurophysiology 28:85 -99.

Xia C-H, Roberts EA, Her L-S, Liu X, Williams DS, Cleveland DW, Goldstein LSB (2003) Abnormal neurofilament transport caused by targeted disruption of neuronal kinesin heavy chain KIF5A. J Cell Biol 161:55-66.

Yamagishi N, Fujii H, Saito Y, Hatayama T (2009) Hsp105beta upregulates hsp70 gene expression through signal transducer and activator of transcription-3. FEBS J 276:5870-5880.

d' Ydewalle C, Krishnan J, Chiheb DM, Van Damme P, Irobi J, Kozikowski AP, Berghe PV, Timmerman V, Robberecht W, Van Den Bosch L (2011) HDAC6 inhibitors reverse axonal loss in a mouse model of mutant HSPB1-induced Charcot-Marie-Tooth disease. Nat Med 17:968-974.

Yum SW, Zhang J, Mo K, Li J, Scherer SS (2009) A novel recessive Nefl mutation causes a severe, early-onset axonal neuropathy. Annals of Neurology 66:759-770.

Zanke BW, Rubie EA, Winnett E, Chan J, Randall S, Parsons M, Boudreau K, McInnis M, Yan M, Templeton DJ, Woodgett JR (1996) Mammalian mitogen-activated protein kinase pathways are regulated through formation of specific kinase-activator complexes. J Biol Chem 271:29876-29881.

Zhai J, Lin H, Julien J-P, Schlaepfer WW (2007) Disruption of neurofilament network with aggregation of light neurofilament protein: a common pathway leading to motor neuron degeneration due to Charcot-Marie-Tooth disease-linked mutations in NFL and HSPB1. Hum Mol Genet 16:3103-3116.

Zhang M, Chen L, Wang S, Wang T (2009) Rab7: roles in membrane trafficking and disease. Biosci Rep 29:193-209.

Zhao C, Takita J, Tanaka Y, Setou M, Nakagawa T, Takeda S, Yang HW, Terada S, Nakata T, Takei Y, Saito M, Tsuji S, Hayashi Y, Hirokawa N (2001) Charcot-Marie-Tooth disease type 2A caused by mutation in a microtubule motor KIF1Bbeta. Cell 105:587-597.

Zhao R, Houry WA (2005) Hsp90: a chaperone for protein folding and gene regulation. Biochem Cell Biol 83:703-710.

Zhong M, Orosz A, Wu C (1998) Direct sensing of heat and oxidation by Drosophila heat shock transcription factor. Mol Cell 2:101-108.

Zimarino V, Tsai C, Wu C (1990) Complex modes of heat shock factor activation. Mol Cell Biol 10:752-759.

Zou J, Guo Y, Guettouche T, Smith DF, Voellmy R (1998) Repression of heat shock transcription factor HSF1 activation by HSP90 (HSP90 complex) that forms a stress-sensitive complex with HSF1. Cell 94:471-480.

Züchner S, Noureddine M, Kennerson M, Verhoeven K, Claeys K, De Jonghe P, Merory J, Oliveira SA, Speer MC, Stenger JE, Walizada G, Zhu D, Pericak-Vance MA, Nicholson G, Timmerman V, Vance JM (2005) Mutations in the pleckstrin homology domain of dynamin 2 cause dominant intermediate Charcot-Marie-Tooth disease. Nat Genet 37:289-294.

Åkerfelt M, Morimoto RI, Sistonen L (2010) Heat shock factors: integrators of cell stress, development and lifespan. Nat Rev Mol Cell Biol 11:545-555.